

รายงานการวิจัยฉบับสมบูรณ์

โครงการ การพัฒนาวัสดุโครงร่างกระดูกเทียมสำหรับงานด้านทันตกรรมและสัตวภิบาล

โดย ศาสตราจารย์พิชญ์ ศุภผล และคณะ

สัญญาเลขที่ DBG5280015

รายงานการวิจัยฉบับสมบูรณ์

โครงการ การพัฒนาวัสดุโครงร่างกระดูกเทียมสำหรับงานด้านทันตกรรมและสัตวภิบาล

คณะผู้วิจัย

สังกัด

- 1. ศาสตราจารย์พิชญ์ ศุภผล วิทยาลัยปิโตรเลียมและปิโตรเคมี จุฬาลงกรณ์มหาวิทยาลัย
- 2. ศาสตราจารย์ประสิทธิ์ ภวสันต์ ภาควิชากายวิภาค คณะทันตแพทยศาสตร์ จุฬาลงกรณ์มหาวิทยาลัย
- 3. ศาสตราจารย์มงคล เตชะกำพุ ภาควิชาสูติศาสตร์ เธนุเวชวิทยาและวิทยาการสืบพันธุ์ คณะสัตวแพทยศาสตร์ จุฬาลงกรณ์มหาวิทยาลัย
- 4. ผู้ช่วยศาสตราจารย์กัมปนาท สุนทรวิภาต ภาควิชาศัลยศาสตร์ คณะสัตวแพทยศาสตร์ จุฬาลงกรณ์มหาวิทยาลัย
- 5. ดร.เกศกัญญา สัพพะเลข ภาควิชาศัลยศาสตร์ คณะทันตแพทยศาสตร์ จุฬาลงกรณ์มหาวิทยาลัย
- 6. ผู้ช่วยศาสตราจารย์ธีรวัฒน์ ธาราศานิต ภาควิชาสูติศาสตร์ เธนุเวชวิทยาและวิทยาการสืบพันธุ์ คณะสัตวแพทยศาสตร์ จุฬาลงกรณ์มหาวิทยาลัย

สหับสนุนโดยสำนักงานกองทุนสนับสนุนการวิจัย
(ความเห็นในรายงานนี้เป็นของผู้วิจัย สกว. ไม่จำเป็นต้องเห็นด้วยเสมอไป)

Executive summary

Bone Tissue Engineering is an emerging interdisciplinary field that seeks to address the needs by applying the principles of biology and engineering to the development of viable substitutes that restore and maintain the function of human bone tissues. There are many approaches to bone tissue engineering, but all involve one or more of the following key ingredients: harvested cells, recombinant signaling molecules, and three-dimensional (3D) matrices. One popular approach involves seeding highly porous biodegradable matrices (or scaffolds), in the shape of the desired bone, with cells and signaling molecules (e.g., protein growth factors), then culturing and implanting the scaffolds into the defect to induce and direct the growth of new bone. The goal is for the cells to attach to the scaffold, multiply, differentiate (i.e., transform from a nonspecific or primitive state into cells exhibiting the bone-specific functions), and organize into normal, healthy bone as the scaffold degrades. The signaling molecules can be adhered to the scaffold or incorporated directly into the scaffold material.

Polymer-ceramic (Hydroxyapatite or Silica) composites may be extremely prospective bone substitute material mainly through evidence with its given biocompatibility towards bone and demonstrated continuity between living bone and the composites. The composites are implanted into rectangular bone defect created by operation at the load-bearing area in dog. The changes of surface strain at the composite implantation are measured at week after implantation when the compressive stress was applied in the direction of long axis in order to clarify the mechanical behaviors of composite living bone complex.

The expected results are that the polymer-ceramic composite living bone complex should have been proven to have sufficient flexibility. The strain pattern on the surface of composite implant should develop quite similar to that of natural cortical bone. These characteristics suggest that it achieves normal skeletal function in the points of biomechanical properties in vivo.

Abstract

Development of Bone Scaffolds for Applications in Dentistry and Animal Care

Prof.Pitt Supaphol, Prof.Pavasant, Prof.Mongkol Techakumphu, Assist.Prof.Kumpanart Soontornvipart, Dr.Keskanya Subbalekha, Assist.Prof.Theerawat Tharasanit

Keywords: Tissue engineering, Scaffold, Polycaprolactone, Hydroxyapatite, Mesenchymal stem cells

Recently, organ and tissue loss or failures resulting from an injury or other types of damage become a major human health problem. Tissue engineering has emerged as a promising alternative approach to treat the loss or malfunction of a tissue or organ without the limitations of current therapies. Tissue engineering is an interdisciplinary technology that combines materials engineering, cellular biology and genetic engineering into developing biological substitutes for defected or damaged tissues. One popular approach in bone tissue engineering to the development of viable substitutes that restore and maintain the function of human bone tissues involves seeding highly porous biodegradable scaffolds, in the shape of the desired bone, with cells and signaling molecules then culturing and implanting the scaffolds into the defect to induce and direct the growth of new bone. In this research work, not only the dentistry care is the main application of the scaffolds but also the animal care is the other application of them. Therefore the isolation techniques and differentiation potentials of canine mesenchymal stem cells derived from bone marrow and adipose tissue the specific markers for bone marrow derived MSCs have been compared. The cellular interaction of canine mesenchymal stem cells and polycaprolcatone/hydroxyapatite composite scaffold and the effect of canine mesenchymal stem cells combined with polycaprolcatone/hydroxyapatite(PCL/HA) composite scaffold on the healing of ulnar defects in dogs have been examined for in vitro and in vivo study, respectively. Mesenchymal stem cells (MSCs) have increasingly become an attractive aspect for tissue engineering. However, limitation of cell numbers at isolation and culture has restricted the clinical exploitations. Bone marrow contents were collected from 7 dogs and then submitted to 3 different MSC isolation techniques (direct plating, red blood cell lysis treatment and gradient density). The number of cells, expression of MSC markers and in vitro differentiation obtained

from each technique were examined. In conclusion, this study revealed that MSCs can be derived from bone marrow. The *in vitro* demonstrated a good biocompatibility between canine MSCs and PCL/HA scaffolds. Despite a promising result from an *in vitro* study, neither bone nor callus formation was observed in canine ulnar defects that implanted with PCL/HA and PCL/HA scaffolds. Defects in these two groups were healed with fibrovascular tissue which infiltrated through the pore of the scaffold.

บทคัดย่อ

ชื่อโครงการ : การพัฒนาวัสดุโครงร่างกระดูกเทียมสำหรับงานด้านทันตกรรมและสัตวภิบาล

ผู้ทำงานในโครงการ: ส.คร.พิชญ์ สุภผล, ส.คร.ประสิทธิ์ ภวสันต์, ส.คร.มงคล เตชะกำพุ,

ผศ.คร.กัมปนาท สุนทรวิภาต, คร.เกศกัญญา สัพพะเลข, ผศ.คร.ธีรวัฒน์ ธาราศานิต

คำสำคัญ : วิศวกรรมเนื้อเยื่อ, โครงร่างเนื้อเยื่อเทียม, พอลิคาโพรแลคโตน, เซลล์ต้นกำเนิดมีเซนไคมอล

ในปัจจุบัน ปัญหาที่สำคัญอย่างหนึ่งของมนุษย์คือ การศูนย์เสียอวัยวะหรือเนื้อเยื่อของร่างกายของมนุษย์ จากอุบัติเหตุ วิศวกรรมเนื้อเชื่อ คือ เทค โน โลชีแบบสหวิทยาการที่มีการบูรณนาการความรู้ด้านวิศวกรรม วิศวกรรม วัสด และชีววิทยา เพื่อพัฒนาทดแทน ซ่อมแซม หรือปรับปรงการทำงานของเนื้อเยื่อหรืออวัยวะที่สณเสียหรือ บาคเจ็บ ซึ่งเป็นหนึ่งในวิธีการแก้ปัณหาที่เกิดขึ้น หนึ่งในกระบวนการที่สำคัญของวิศวกรรมเนื้อเยื่อ คือการพัฒนา วัสคุโครงร่างเนื้อเยื่อเทียมที่มีศักยภาพในการกระตุ้นการเกาะ การเพิ่มจำนวน และการสร้างเนื้อเยื่อกระดูก ในการ ถึงแม้ว่าเป้าหมายหลักของงานวิจัยนี้ คือการพัฒนาวัสคุโครงร่างกระดูกเทียมเพื่อสามารถ นำไปใช้งานในค้านทันตกรรม อย่างไรก็ตาม การนำวัสคุโครงร่างกระดูกเทียมไปทคสอบในสัตว์ทคลอง(สุนัข) เพื่อใช้ในการรักษาสนังที่ต้องการการปลกถ่ายเนื้อเยื่อกระคกสามารถเป็นเป้าหมายรองในงานวิจัยนี้ได้อีกทางหนึ่ง ด้วย ดังนั้นในงานวิจัยนี้จึงได้มีการศึกษาการพัฒนาเซลล์ต้นกำเนิดที่ได้จากไขกระดูกและเนื้อเยื่อไขมัน และนำ เพื่อนำมาทดลองเพาะเลี้ยงกับวัสดโครงร่างกระดกเทียมที่ได้มีการพัฒนาขึ้นมาในสภาวะที่ ความรั้มาผสมผสาน สึกษาความเป็นไปได้ในการใช้วัสุโครงร่างเทียมร่วมกับเซลล์ดันกำเนิดจากการทดสอบในจาน ทคลองและทคลองกับสัตว์ทคลอง(สุนัข) จากการทคลองปลูกถ่ายเซลล์ต้นกำเนิดชนิดมีเซนไกมอลที่แยกได้จากไข กระคุกลงบนวัสคุโครงร่างเซลล์ซึ่งใส่อยู่ในตำแหน่งวิการของกระคุกอัลนา เพื่อศึกษาผลของการรักษาภาวะ กระดูกต่อไม่ติดในสุนัข โดยทำการเก็บไขกระดูกในสุนัขจำนวน 7 ตัว ไขกระดูกของสุนัขแต่ละตัวนำมาแบ่งเพื่อ คัดแยกเซลล์ต้นกำเนิดชนิดมีเซนไคมอลเป็น 3 วิธี ได้แก่ density gradient, RBC lysis buffer และ direct plating ทำ การเพาะเลี้ยงในภาวะที่ควบคมเคียวกันและ subculture ในวันที่ 7 เพื่อหาจำนวนเซลล์ทั้งหมดและเปอร์เซ็นต์เซลล์ ที่มีชีวิตที่ได้จากแต่ละวิธี การพิสูจน์คุณสมบัติของเซลล์ตันกำเนิดชนิคมีเซนไคมอลทำได้โดยอาศัยการเกาะบน จานเพาะเลี้ยงพลาสติก การแสดงออกของโปรตีนบนผิวเซลล์และคุณสมบัติในการเปลี่ยนแปลงไปเป็นเซลล์ชนิด อื่น พบว่าเซลล์ตันกำเนิดชนิคมีเซนไคมอลที่กัดแยกได้มีคุณสมบัติในการเปลี่ยนแปลงไปเป็นเซลล์กระคูก ปริมาณ มีเซ็นไคมอลเสต็มเซลล์ที่รอดชีวิตภายในโครงร่างเซลล์พอลิกาโพรแลคโตนไฮตรอกซีอะพาไทต์มีความสำคัญ เนื่องจากเซลล์ที่รอดชีวิตจะสามารถเพิ่มจำนวนและเปลี่ยนแปลงตัวเองไปเป็นเซลล์ที่มีความสามารถในการสร้าง กระคูก ตัวอย่างโครงร่างเซลล์หลังการฉีดเซลล์ตันกำเนิดไม่พบการเปลี่ยนแปลงใดๆที่รอยต่อของกระคูกอัลนากับ วัสดุปลูกถ่ายทั้งทางด้านบนและด้านล่าง รวมทั้งไม่พบการสร้างแคลลัสที่บริเวณวิการของกระคูก เมื่อเปรียบเทียบ ผลการเอกซเรย์หลอดเลือดของขาหน้าบริเวณที่มีโครงร่างเซลล์ก่อนและหลังการฉีดเซลล์ตันกำเนิดเข้าสู่โครงร่าง เซลล์ พบแขนงของเส้นเลือดในบริเวณที่ตรงกับตำแหน่งที่ทำการใส่โครงร่างเซลล์และพบการแตกแขนงของเส้น เลือดในบริเวณที่ตรงกับตำแหน่งที่ทำการใส่โครงร่างเซลล์และพบการแตกแขนงของเส้น เลือดในบริเวณที่ตรงกับตำแหน่งที่มากที่น

สัญญาเลขที่ DBG5280015

โครงการ: การพัฒนาวัสดุโครงร่างกระดูกเทียมสำหรับงานด้านทันตกรรมและสัตวภิบาล รายงานการวิจัยฉบับสมบูรณ์ ของศาสตราจารย์พิชญ์ ศุภผล

- 1. การดำเนินงาน 🕢 ได้ดำเนินงานตามแผนที่วางไว้ทุกประการ
 - θ ได้ดำเนินงานล่าช้ากว่าแผนที่วางไว้
 - θ ได้เปลี่ยนแผนงานที่วางไว้ดังนี้

2. สรุปผลการดำเนินงาน

2.1 Hydroxyapatite/ovalbumin composite particles as model protein carriers for bone tissue engineering: I. Synthesis and characterization

Experimental procedures

1. Materials and material synthesis

The chemical reagents, e.g., nitric acid (HNO3, A.R. grade), phosphoric acid (H3PO4, A.R. grade), 2-amino-2-hydroxymethyl-propane-1,3-diol (tris-base, A.R. grade), and chicken egg white ovalbumin (OVA,grade II), were purchased from Sigma-Aldrich (USA). These were used without further purification. In the synthesis process, calcium oxide(CaO) was first synthesized from discarded egg shells [16]. Briefly, the egg shells were cleaned with distilled water at 80 °C and dried in vacuo. They were then calcined at 1000 °C in a Lindberg LBF799C oven, in two heating stages (i. 25 to 700 °C for 2 h to eliminate organic substances and ii. 700 to 1000 °C for another 2 h to eliminate CO2 to finally obtain CaO powder). Then, 2.5 g of the CaO powder was dissolved in 25 mL of 1 MHNO3 under gentle stirring at 70 °C for 3 h. Subsequently, 3.0 g of conc. H3PO4 (85 wt.-%) was added dropwise into the solution to adjust the Ca/P ratio to 1.67. The pH of the mixed solution was maintained at 2.0 and the whole system was continuously stirred at room temperature. Precisely 2.0 g of OVA was then added into

500 mL of the obtained solution under vigorous stirring for 1 h. Precipitation was achieved after 200 mL of 1, 1.5, or 2 M tris-base had been added into the solution to impart the buffering effect to the solution

at the pH of 7, 8, or 9, respectively. The mixture was vigorously stirred. The precipitates were filtered, washed several times with deionized water, and lyophilized for 48 h. The procedure was repeated to obtain the precipitates that did not contain OVA for comparative purposes.

2. Characterization

A Rigaku D/MAX 2000 X-ray diffractometer (XRD) was used to investigate the crystalline nature of the obtained powdery precipitates, using Cu K α (1.54 Å) radiation over the 20 range of 5–60° with 0.02° scanning step. The crystalline phase of the powder was identified with JCPDS standard (9-432). A Nicolet NEXUS 670 Fourier-transform infrared spectroscope (FT-IR), operating at a resolution of 4 cm-1 over a wavenumber range of 4000 to 400 cm-1, was used to examine the chemical functionalities of the powdery products. A Perkin-Elmer TGA-7 thermogravimetric analyzer (TGA) was used to investigate the thermal degradation behavior of the powder at a heating rate of 10 °C·min-1 in air. Some of the powdery

products, after having been subjected to the thermal treatment in TGA, were reanalyzed by XRD. Microscopic morphology of the powder was observed by a JEOL JEM-2100 transmission electron microscope (TEM), operating at 200 kV. Surface morphology of the obtained products was investigated by a JEOL JSM-5410LV scanning electron microscope (SEM). Particle size distribution (PSD) of the powder was collected by a Mastersizer 2000 Malvern particle size analyzer (PSA). The powder was dispersed ultrasonically in water during the measurement. The pore characteristics and the Bruaauer–Emmett–Teller (BET) specific surface area of the obtained powdery products were determined based on the physisorption of N2 at a temperature of 77 K using a Quantachrome AS-1 autosorb-1 instrument. Lastly,the ζ potentials of the powdery products were measured by electrophoresis, using a Zeta-meter 3.0+ analytical system. Briefly, a suspension of 100 mg of the HAp or the HAp/OVA particles in 20 mL of deionized water was filled in an electrophoresis cell. Once energized, the powder was aroused to move towards one of the electrodes. The unit automatically converted the electrophoretic mobility of the particles into the ζ values using the Smoluchowski equation.

3. Results and discussion

Because of the similarity of the results obtained for the HAp particles that had been obtained at pHs 7, 8, and 9, only those of the particles that had been obtained at pH 9 were extensively reported

and discussed. As shown in Fig. 1, all of the crystalline peaks as observed in the XRD patterns of the precipitated powdery products that had been obtained, both in the absence and the presence of

OVA, at pH 9 could be assigned to those of HAp [i.e., the hexagonal P63/m space group with the lattice constants of a=b=0.9418 nm and c=0.6884 nm (cf. JCPDS No. 09-0432)]. The average crystallite

sizes, as estimated from the width of the (002) reflection peaks using the Scherrer's equation [17], were around 17.3–20.9 nm and 16.8–19.8 nm for the HAp and the HAp–OVA particles, respectively

(see Table 1). In particular, the average value of the crystallite size decreased with an increase in the pH used during the precipitation process. As the pH increased, more tris-base molecules, in their free

form, would be available to nucleate the HAp crystalline entities (cf. the pKa of tris-base=8.06), hence the observed decrease in the crystallite size. At the same pH, the presence of OVA resulted in a

slight reduction in the average value of the size of the obtained HAp crystals. The presence of OVA could retard the influx of Ca^{2+} and PO_4^{3-} into the growth face, as OVA would adsorb readily onto the HAp crystallites during the crystal growth.

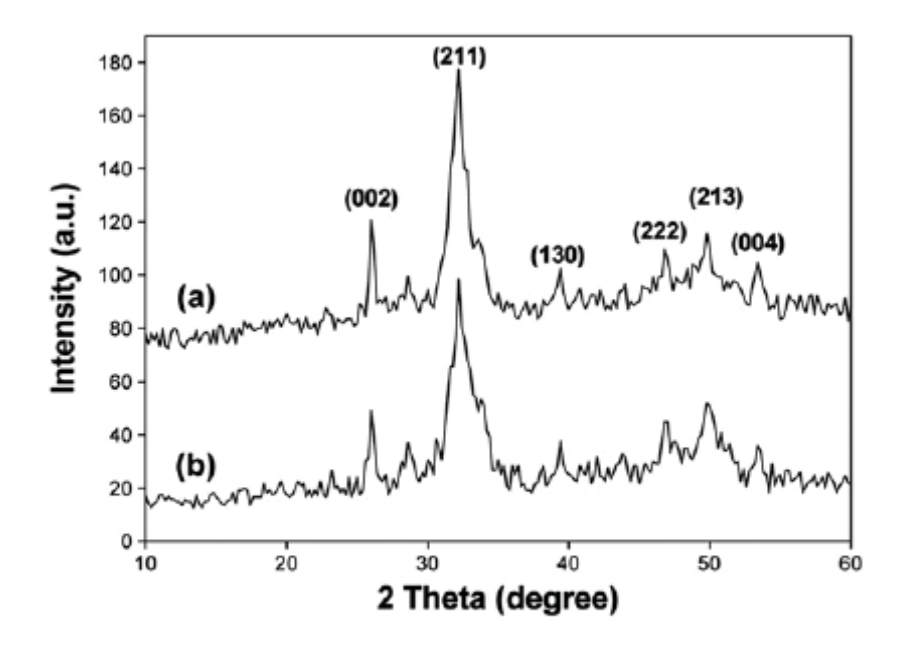


Fig. 1. XRD patterns of (a) pure HAp and (b) HAp-OVA particles that had been obtained at pH 9.

The FT-IR spectra of the HAp and the HAp–OVA particles that had been obtained at pH 9 as well as that of the as-received OVA in its dry state are shown in Fig. 2. For the HAp particles, the adsorption bands centering at 3569 and 1630 cm–1 could be assigned to the OH stretching and the OH vibration of the apatitic group [18]. The bands centering at 1035, 601, and 563 cm–1 should correspond to PO4 3– ions in the HAp structure. However, the band centering at 1384 cm–1 was thought to belong to the carbonate functionality, which might be a result of the contamination from the reaction with CO2 in the atmosphere[11]. As for the as-received OVA, the characteristic absorption peaks at 3299, 1652, 1539, and 1457 cm–1 could be ascribed to the N–H stretching, the carbonyl, the C–N, and the C–H stretching vibrations, respectively [19]. For the HAp–OVA particles, the presence of the absorption bands centering at 1654 and 1539 cm–1 confirmed the presence of OVA within the obtained HAp particles.

The HAp and the HAp-OVA particles that had been obtained at pH 9 were evaluated thermogravimetrically and the results are shown in Fig. 3a. For the HAp particles, three main stages in the loss of their mass were observed. The first stage, over the temperature range of 60–160 °C, should correspond to the loss of adsorbed water. The second stage, with the onset temperature at about 240 °C, should relate to the loss of trisbase from the HAp structure. The last stage at the onset temperature of about 740 °C was thought to relate to the loss of the remaining organic residues within the HAp structure. As for the HAp-OVA particles, all of the three stages were evident. However, the presence of an additional step at the onset temperature of about 330 °C should correspond to the loss of the incorporated OVA. After the TGA analysis, these HAp and the HAp-OVA particles were reanalyzed by XRD (Fig. 3b). Apparently, the crystalline peaks associated with HAp became much sharper (cf. Fig. 1), indicating further crystallization of HAp during the thermal treatment. Additionally, crystalline peaks that belong to other calcium-based chemical species such as CaO and carbonate apatite became much more evident (cf. Fig. 1). This suggests that parts of the imperfectly-formed HAp entities may undergo thermal decomposition or solid state chemical reaction at high temperatures, Notwithstanding, both

the FT-IR and the TGA results confirmed the presence of OVA within the structure of the obtained HAp-OVA particles.

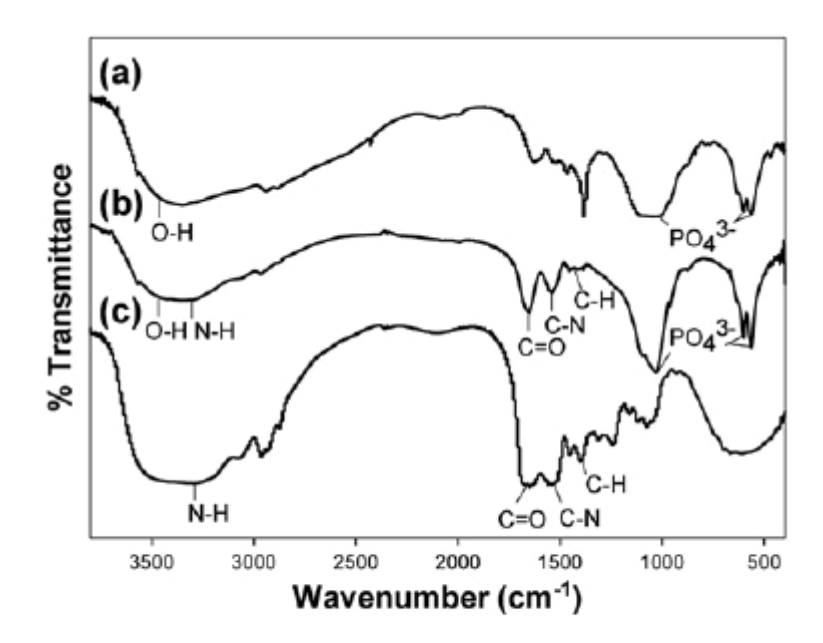


Fig. 2. FT-IR spectra of (a) pure HAp and (b) HAp-OVA particles that had been obtained at pH 9 as well as that of (c) as-received OVA in its dry state.

 Table 1

 Textural parameters of pure HAp and HAp-OVA particles that had been obtained at different pH conditions.

Type of HAp	Crystallite size (nm) $(n=3)$	Average size of primary particles (nm) (n=3)	Pore diameter $(nm) (n=2)$	BET Specific surface area $(m^2 g^{-1})$ (n=2)	Pore volume $(cm^3 \cdot g^{-1})$ $(n=2)$	ζ potential (mV) ($n=10$)
HAp (pH 7)	20.9 ± 0.06	59.3 ± 0.25	8.9 ± 0.2	17.2 ± 0.7	0.079 ± 0.006	-31.6 ± 2.4
HAp (pH 8)	19.2 ± 0.08	57.7 ± 0.43	8.3 ± 0.1	16.1 ± 0.5	0.053 ± 0.003	-32.7 ± 1.6
HAp (pH 9)	17.3 ± 0.11	56.5 ± 0.28	8.1 ± 0.2	15.6 ± 0.3	0.029 ± 0.004	-36.9 ± 2.5
HAp-OVA (pH 7)	19.8 ± 0.09	50.4 ± 0.27	15.5 ± 0.4	21.3 ± 0.3	0.089 ± 0.002	-19.7 ± 1.3
HAp-OVA (pH 8)	18.4 ± 0.05	49.1 ± 0.41	14.4 ± 0.2	19.5 ± 0.4	0.058 ± 0.002	-20.2 ± 0.7
HAp-OVA (pH 9)	16.8 ± 0.06	46.2 ± 0.36	14.1 ± 0.3	16.6 ± 0.7	0.036 ± 0.003	-23.2 ± 1.1

The particle size distribution (PSD) curves of the HAp and the HAp–OVA particles that had been obtained at pH 9 are shown in Fig. 4. Based on the PSD results, the HAp and the HAp–OVA primary particles had the average sizes of around 56–59 nm and 46–50 nm, respectively. The average sizes of the HAp and the HAp–OVA primary particles that had been obtained at all pH levels investigated were measured and summarized in Table 1. Apparently, the presence of OVA resulted in significant reduction in the sizes of the obtained HAp primary particles. On the contrary, the average value of the primary particle size decreased slightly with an increase in the pH used during the precipitation process. Both of these should be a result of the increase in the number of nucleation sites, i.e., owing to the presence of OVA in the former and the more availability of the free trisbase molecules in the latter [20]. As for the effect of tris-base, the greater the amount of trisbase used, the greater the number of nuclei, hence the observed reduction in the sizes of the HAp primary particles.

The nano-crystalline structure of the HAp and the HAp–OVA particles that had been obtained at pH 9 was investigated by TEM (see Fig. 5). The rod-like morphology of the obtained HAp crystals, both in the absence and in the presence of OVA, was evident. The TEM results were consistent with the results obtained from the particle size analyzer (i.e., the PSD results), which revealed that the primary particles were in the nanometer range and the presence of OVA led to the reduction in the size of the primary particles. Despite the nanocrystalline nature of the individual primary particles, representative SEM images of the precipitated HAp and HAp–OVA powder that had been obtained at pH 9 (see Fig. 6) revealed the existence of large agglomerates and the extent of the agglomeration was accented by the presence of OVA. In addition, the HAp particles obtained at higher pH values existed as larger aggregates, owing possibly to the increase in the overall crystallization rate (viz. due to the increase in the nucleation rate, earlier mentioned) [21]. Notwithstanding, the existence of such agglomerates could easily be a result of lyophilization during the drying of the powdery products.

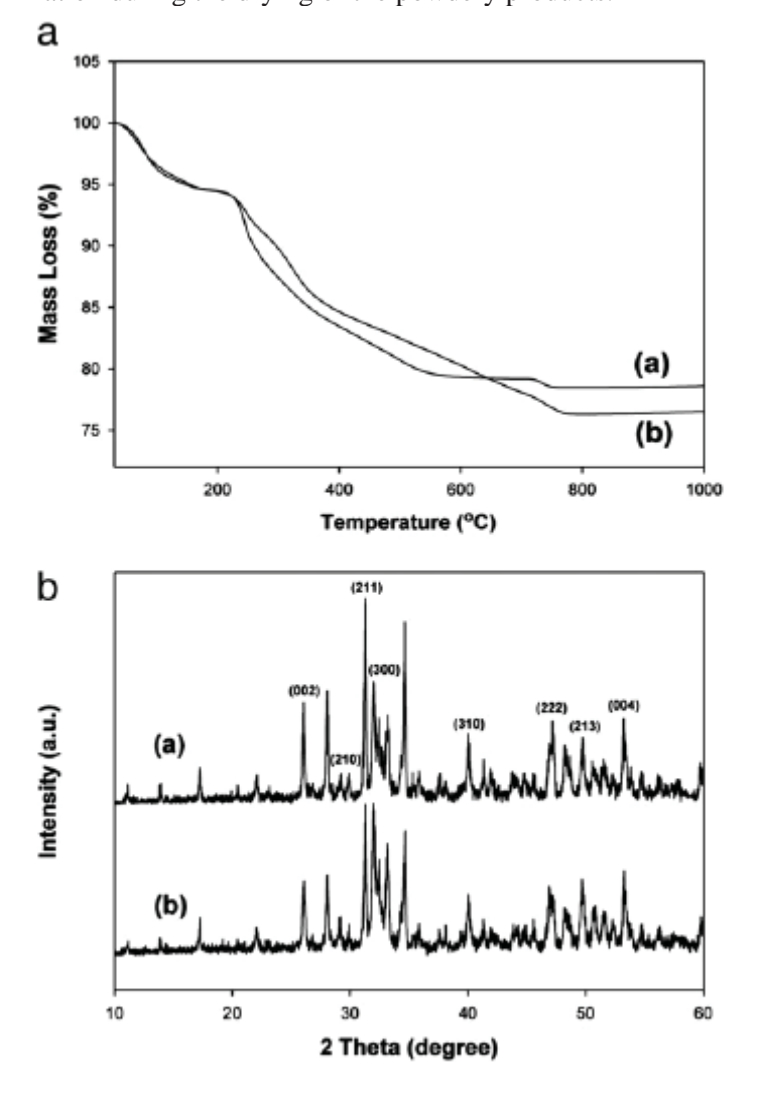


Fig. 3. (a) TGA curves of (a) pure HAp and (b) HAp-OVA particles that had been obtained at pH 9 and (b) XRD patterns of these particles after having been subjected to the TGA analysis.

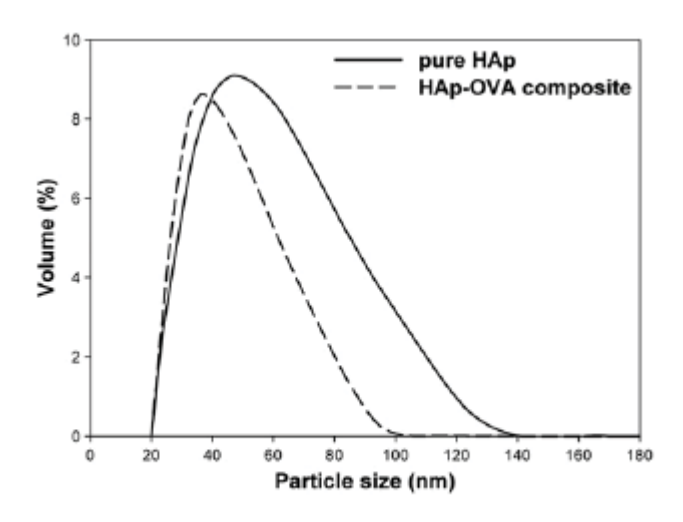


Fig. 4. PSD curves of pure HAp and HAp-OVA particles that had been obtained at pH 9.

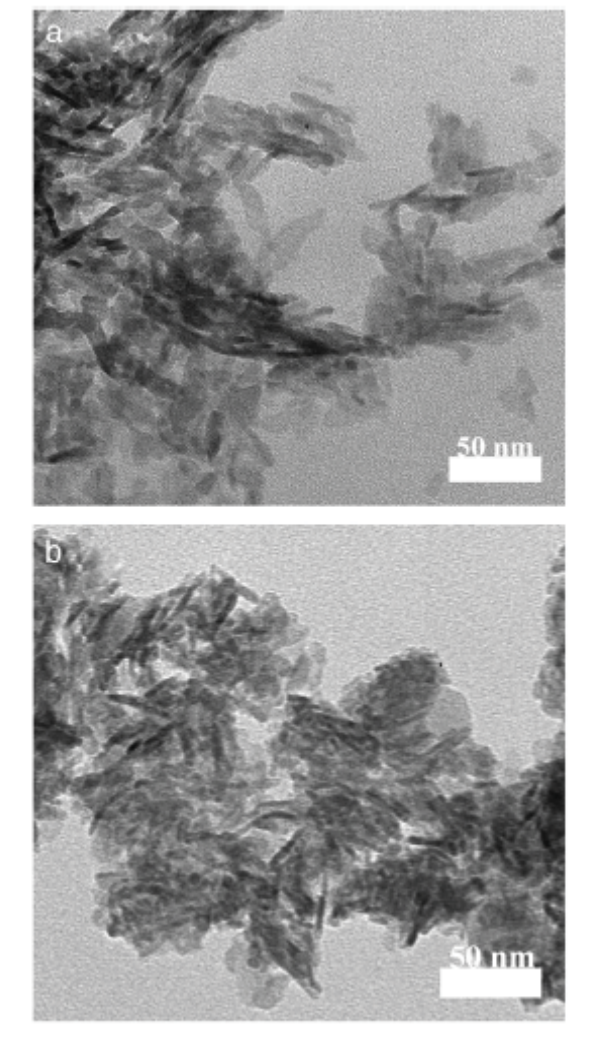


Fig. 5. TEM micrographs of (a) pure HAp and (b) HAp-OVA particles that had been obtained at pH 9.

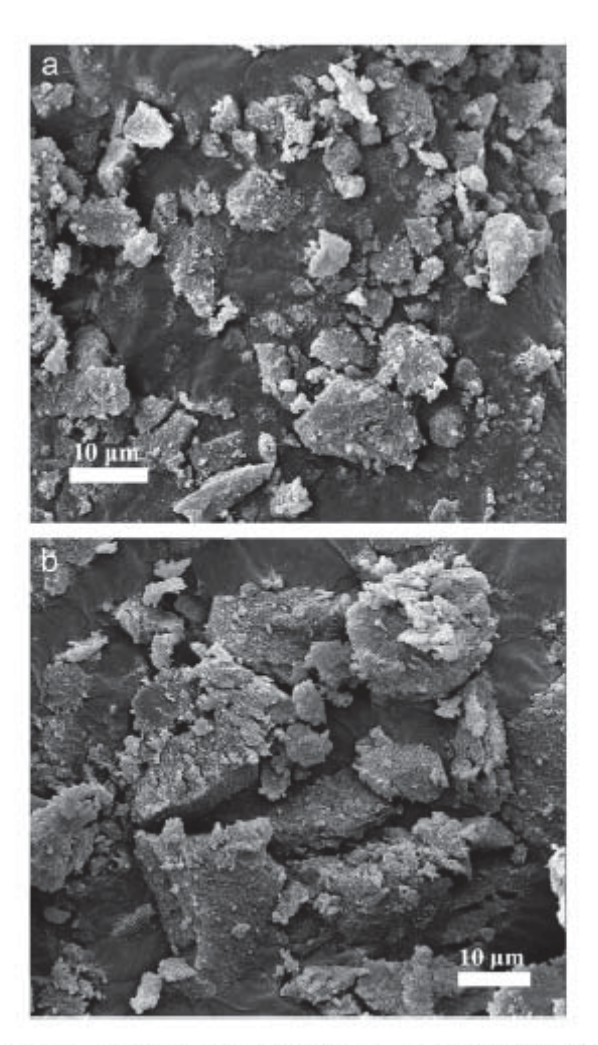


Fig. 6. SEM images of (a) pure HAp and (b) HAp-OVA particles that had been obtained at pH 9.

The N2 adsorption—desorption isotherms and the pore size distribution as calculated from the adsorption branch of the isotherms based on the Bopp-Jancsó-Heinzinger (BJH) model for the Hap and the HAp–OVA particles that had been synthesized at pH 9 are shown in Fig. 7 and in the inset of the figure, respectively. The isotherms can be categorized as type IV, which can be further categorized into H1-hysteresis loops of mesoporous materials [22]. The average pore sizes of the HAp and the HAp-OVA particles were determined to be about 8.1 nm and 14.1 nm, respectively. The isotherms and the pore size distribution of these two cases were slightly different. For the HAp-OVA particles, the isotherm exhibited a slightly steeper slope with a greater pore volume and the pore size distribution was narrower, owing to the more uniform pore sizes. This indicates that the aggregation of OVA within the HAp structure affected slightly the basic pore structure of the obtained mesoporous HAp particles. The pore diameter and the BET specific average surface area for each of the obtained products are summarized in Table 1. In the absence of OVA within the HAp structure, the pore sizes were 8.1–8.9 nm. Larger pore sizes were observed for the OVAincorporated HAp particles (i.e., 14.1–15.5 nm). These correspond to the BET specific average surface area values of 15.6–17.2 and 16.6–21.3 m²·g⁻1, respectively, and the pore volume values of 0.029–0.079 and 0.036–0.089 cm3·g-1, respectively. These pores were thought to be generated upon the sublimation of the ice crystals formed during the lyophilization step [23,24]. The presence of OVA resulted in hypothetical increases in the

values of all of the pore parameters of the resulting HAp particles, while the increase in the pH during the precipitation process led to opposing trends. Furthermore, since the characteristic FT-IR bands associated with both HAp and OVA components were not shifted, it is expected that the mesopores may be present as the voids located at the grain boundaries of the aggregates of the rod-like HAp particles. The ζ potentials of the HAp and the HAp-OVA particles were finally measured based on the electrophoretic mobilities of these particles in deionized water. The average values for the HAp particles were in the range of -31.6 to -36.9 mV, while those for the HAp-OVA particles were in the range of -19.7 to -23.2 mV. Evidently, an increase in the pH during the precipitation process caused the ζ potentials of the HAp and the HAp–OVA particles to become more negative. It was reported that the ζ potentials of commercial Hap particles depended strongly on the pH of the suspending medium[25], in which the values varied from -5 to -37 mV as the pHincreased from 5.0 to 8.0. Over the pH levels of 7.0–8.0 however, the ζ potentials varied within a small range of -35 to -37 mV. Such a value for commercial HAp particles in phosphate buffer solution(pH=7.4) was determined to be -36 mV [26]. Clearly, thevalues of the ζ potentials for the HAp particles, as obtained here, agreed particularly well with those reported in the literature.

Upon the addition of OVA, which is an acidic protein (cf. isoelectricpoint=4.7 [26]) during the precipitation process to obtain the HAp–OVA particles, the ζ potentials decreased by about 12 mV on average. This reduction is a clear indication of the adsorption of the protein on the surface of the Hap crystallites. Marginal reduction in the values of the ζ potentials of the HAp particles was observed when their surfaces were covered with acidic and neutral proteins, while more significant reduction was observed when their surface was covered with basic proteins [25,26].

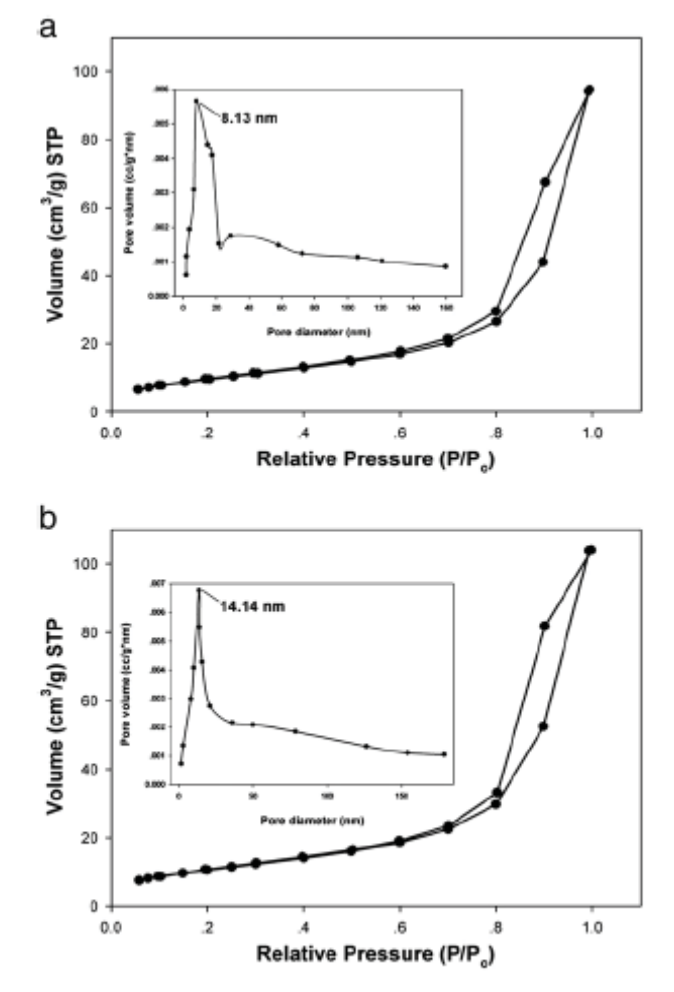


Fig. 7. Adsorption-desorption isotherms of N₂ within the pore structures of (a) pure HAp and (b) HAp-OVA particles that had been obtained at pH 9. The size distribution of the pores as determined based on the Bopp-Jancsó-Heinzinger (BJH) model is shown as the inset.

4. Conclusions

An economical and simple synthetic route for HAp–OVA particles from discarded egg shells and OVA, as the model incorporating protein, by co-precipitation method was proposed. Both XRD and FT-IR results confirmed the formation of HAp, while PSD and TEM results indicated the formation of discrete HAp nanocrystals, which were rod-like in nature. Both the crystallite sizes (as calculated from breadth of the (002) reflection peak) and the sizes of the individual nanocrystalline particles decreased in the presence of OVA. Electrophoretic analysis indicated that OVA adsorbed readily on the surfaces of the HAp nano-crystallites and this was responsible for their agglomeration into larger particles, as revealed by SEM analysis. The knowledge obtained from the preparation of these HAp–OVA materials could be used as a promising archetype for synthesizing composite particles of HAp and another functional protein for biomedical applications or bone tissue engineering purposes in particular.

2.2 Comparative Study of Protein Carriers Based on Hydroxyapatite Particles for Bone Tissue Engineering

Experimental procedure

1. Materials

All chemical reagents including Calcium hydrogen phosphate dihydrate (CaHPO4.2H₂O, A.R. grade, Fluka), Calcium carbonate (CaCO₃, A.R. grade, Carlo Erba), Nitric acid (HNO₃, A.R. grade, Labscan), Phosphoric acid (H₃PO₄, A.R. grade, Labscan), Tris (hydroxymethyl)-aminomethane (tris-base, A.R. grade, Sigma), and Egg albumin (OVA, grade II, Sigma) were used without further purification. CaO from egg shells was prepared following the previous report of Rivera *et al.* [19].

2. Synthesis of hydroxyapatite

HAp was prepared by co-precipitation method. In the typical procedure, 2.00 g of CaHPO4.2H2O (as a phosphorous source) and 0.79 g of CaCO3 (as a calcium source) were dissolved in 1 M HNO3 25 ml under gentle stirring at 70 °C for 2 h and the pH of the solution was kept to 2. OVA, subsequently, was added in the amount of 0, 1, 2, and 3 g/500 ml of the mixed solution at room temperature. 200 ml of 1 M and 2 M tris-base solution were then poured into the mixture generating the precipitation at pH 7 and pH 9, respectively. The precursor solution was stirred vigorously to yield a homogeneous product. The product was then filtered off and washed several times with deionized water. After centrifugation, the resulting material was freeze-dried for 48 h to obtain the fine powder products. The similar process with the use of 1.25 g of CaO and 1.50 g of H₃PO₄ as calcium and phosphorous sources respectively was performed for comparison. With many synthetic conditions above, the sample names were specified as shown in Table 1.

3. Release kinetics of OVA from HAp particles

About 20 mg of HAp-OVA particles were immersed in 10 ml phosphate buffer solution at pH 7.4, in which matches the normal body and blood system of a human being. The controlled release systems were shaken in the water bath with a stirring rate of 70 rpm at 37 °C. The amount of released OVA in the supernatant was measured at various times by UV-VIS spectrophotometer (UV-1800) at the wavelength of 280 nm through the use of a pre-determined standard calibration curve. Furthermore, the gravimetric analysis was used to confirm the amounts of OVA loss again after 21 days.

4. Characterization

The crystallographic phases of the HAp-OVA particles were analyzed by X-ray diffractometer (WDXRD, D/MAX 2000 series Rigaku) with an incident X-ray wavelength of 1.54 Å (Cu Kα line) at the scanning rate of 0.02° per minute over a range of 2θ from 5° to 60° with JCPDS database (9-432). Fourier transform infrared (FT-IR) spectrograph carried out on a Nicolet Nexus spectrometer (NEXUS 670, Nicolet) was performed using the KBr pellet technique, working in the wavelength from 4000 to 400 cm-1. The structural morphology images were recorded on a transmission electron microscope (TEM, JEM-2100, JEOL) with an acceleration voltage of 200 kV. Energy dispersive X-ray (EDX) element analysis of the samples was also investigated with scanning electron microscope (SEM, JSM-5410LV, JEOL) operated at 15 kV. The average pore diameters of the obtained particles were

taken on autosorb-1 instrument (AS-1, Quantachrome) using physisorption of nitrogen at temperature of 77 K. Thermogravimetric analysis (TGA, TGA7, Perkin Elmer) was carried out on the dried samples (5 mg) to examine the relative amount of OVA associated with HAp particles with a heating rate of 10 °C /min under a flowing air atmosphere.

2.5. Statistical Analysis

All quantitative examinations were collected in triplicate and the results were presented as means and standard deviations. Significance between the mean values was determined by ANOVA one-way analysis using Tukey's test for variances at a 95% confidence level.

Results and discussion

1. Material characterization

The formation of HAp particles was ascertained by X-ray diffraction (XRD) analysis. The XRD patterns of the HAp-OVA particles with particular peaks ascribed to the lattice constant of HAp according to the JCPDS database (9-432) were given in the comparative chart of Fig. 1. From these results, the presence of the OVA during the synthesis does not have an influence on the structural development of HAp. Besides, no difference in HAp-OVA characteristic diffraction peaks was perceived for all synthetic cases given above. These XRD data also show poorly-crystallized traces of the powders due to water sublimation in the freeze-drying process [20], resulting in estimated crystallite sizes. Calculations of the crystallite size using the Scherrer equation were performed for the (002) reflection peak corresponding to $2\theta = 26^{\circ}$ because of well resolved characteristics [21]. The mean sizes of crystallites are within the range of 16-20 nm.

Table 1

Experimental conditions of HAp and HAp-OVA particles

Starting materials	Initial amounts of OVA (g)	pH conditions	Sample names
CaCO ₃	-	7	0D-7
+	1	7	1D-7
CaHPO ₄ .2H ₂ O	2	7	2D-7
	3	7	3D-7
	-	9	0D-9
	1	9	1D-9
	2	9	2D-9
	3	9	3D-9
CaO (Egg shells)	-	7	0E-7
+	1	7	1E-7
H_3PO_4	2	7	2E-7
	3	7	3E-7
	-	9	0E-9
	1	9	1E-9
	2	9	2E-9
	3	9	3E-9

Fig. 2 exhibits the FT-IR spectra of the HAp-OVA particles. The IR spectra of pure OVA and HAp are also shown for comparison. The OVA spectrum displayed the typical bands at 3299 cm-1, 1652 cm-1, 1539 cm-1, and 1457 cm-1 represented to the nitrogen-hydrogen stretch (N-H), the carbonyl vibration (C=O), the carbon-nitrogen vibration (C-N), and the stretching vibration of carbon-hydrogen (C-H), respectively [15]. The spectrum of pure HA demonstrates the adsorption bands at 3569 cm-1 assigned to OH stretching, 1630 cm-1 assigned to OH vibration of the apatitic group, 1035 cm-1 assigned to PO₄₃- stretching vibration, as well as 601 cm-1 and 563 cm-1 assigned to PO₄₃- deformation vibration [22,23]. The bands at 1654 cm-1 and 1539 cm-1 of HAp-OVA spectra, therefore, ascertained that OVA was incorporated in HAp particles.

EDX analysis was performed to give further confirmation of a molar Ca/P ratio of the samples. The EDX characteristic peaks indicated the existence of calcium (Ca), phosphorous (P), and oxygen (O) with proportional counts (Fig. 3). The molar Ca/P ratio of all samples revealed that the obtained samples synthesized by using the chemical starting material have the Ca/P ratio of 1.67-1.68 very close to the ideal one of 1.67 for HAp in human bone, while the Ca/P ratio measured for the obtained samples synthesized from the natural starting material are within the range 1.62-1.65. On the other hand, there were not

material are within the range 1.62-1.65. On the other hand, there were not statistically significant differences for the Ca/P ratio of both starting materials (p > 0.05).

The HAp-OVA particles were also examined by transmission electron microscopy (TEM). The TEM micrographs of the samples synthesized from both natural and chemical substances at pH 7 and pH 9 with 1 g OVA show little difference in morphology (Fig. 4). In all obtained specimens, the primary particles have a rod-like shape with dimensions of 3-10 nm in diameter and 15-30 nm in length. However, it was noticed that the sizes of primary particle slightly increase with a higher OVA content and a lower pH condition.

2. Incorporation of OVA into HAp particles

The physi-sorption of nitrogen was performed to collect the average pore diameters of the pure HAp and HAp-OVA particles (see Table 2). The average pore sizes of HAp particles with the presence of OVA are larger than those of the absence ones, suggesting the incorporation of OVA within HAp particles by bond formation. The mechanism was that the carbonyl group and the phosphorous group of OVA have negative dipoles which could chelate the free Ca2+ ions; subsequently, the PO43- ions may bond with OVA-associated calcium to generate HAp-OVA aggregates [18]. OVA, furthermore, could be adsorbed on the HAp surfaces by the crystal surface area available for growth [24]. When considering HAp-OVA particles, their average pore diameters at lower pH are bigger than those at higher pH. At the same pH, the chemical starting material shows the higher values of the average pore diameter compared with the natural one. The average pore diameters, nevertheless, are quite similar in cases of varying initial OVA contents. Therefore, it could be assumed that difference in these initial amounts of added OVA has a little influence on the average pore size. material are within the range 1.62-1.65. On the other hand, there were not statistically significant differences for the Ca/P ratio of both starting materials (p > 0.05).

The HAp-OVA particles were also examined by transmission electron microscopy (TEM). The TEM micrographs of the samples synthesized from both natural and chemical substances at pH 7 and pH 9 with 1 g OVA show little difference in morphology (Fig. 4). In all obtained specimens, the primary particles have a rod-like shape with dimensions of 3-10 nm in diameter and 15-30 nm in length. However, it was noticed that the sizes of primary particle slightly increase with a higher OVA content and a lower pH condition.

Table 2

Physico-chemical characteristics of HAp and HAp-OVA particles

Samples	Average pore	Incorporated OVA		Released OVA	
	diameter (nm)	amounts		amounts	
		(%)*	(mg)*	(%)#	(mg)#
0D-7	9.43 ± 0.02	-	-	-	-
1D-7	16.4 ± 0.15	8.01 ± 0.92	0.40 ± 0.08	57.5 ± 3.71	0.92 ± 0.04
2D-7	16.8 ± 0.11	9.32 ± 0.37	0.47 ± 0.03	60.0 ± 4.10	1.12 ± 0.07
3D-7	16.9 ± 0.07	9.94 ± 0.96	0.49 ± 0.08	62.0 ± 3.82	1.23 ± 0.06
0D-9	8.69 ± 0.14	-	-	-	-
1D-9	13.7 ± 0.18	7.54 ± 0.83	0.38 ± 0.07	42.1 ± 2.73	0.63 ± 0.04
2D-9	14.2 ± 0.06	7.99 ± 0.68	0.40 ± 0.06	43.7 ± 2.90	0.70 ± 0.05
3D-9	14.8 ± 0.03	8.21 ± 0.74	0.41 ± 0.07	44.0 ± 1.95	0.72 ± 0.03
0E-7	8.91 ± 0.19	-	-	-	-
1E-7	15.0 ± 0.14	6.17 ± 0.45	0.31 ± 0.04	50.1 ± 3.06	0.62 ± 0.05
2E-7	15.3 ± 0.27	7.61 ± 0.33	0.38 ± 0.03	52.6 ± 2.81	0.80 ± 0.04
3E-7	15.6 ± 0.29	8.89 ± 0.87	0.44 ± 0.07	54.2 ± 3.66	0.96 ± 0.06
0E-9	8.18 ± 0.03	-	-	-	-
1E-9	13.5 ± 0.22	5.24 ± 0.72	0.26 ± 0.06	38.8 ± 1.13	0.41 ± 0.02
2E-9	13.9 ± 0.26	6.01 ± 0.79	0.30 ± 0.08	40.3 ± 2.09	0.48 ± 0.03
3E-9	14.3 ± 0.15	6.93 ± 0.44	0.35 ± 0.04	40.8 ± 1.84	0.56 ± 0.03

^{*} based on around 5 mg of total weight of the particle analyzed from TGA

based on the incorporated OVA amounts into 20 mg of total weight of the particle 3. Incorporation of OVA into HAp particles

The physi-sorption of nitrogen was performed to collect the average pore diameters of the pure HAp and HAp-OVA particles (see Table 2). The average pore sizes of HAp particles with the presence of OVA are larger than those of the absence ones, suggesting the incorporation of OVA within HAp particles by bond formation. The mechanism was that the carbonyl group and the phosphorous group of OVA have negative dipoles which could chelate the free Ca₂₊ ions; subsequently, the PO₄₃₋ ions may bond with OVA-associated calcium to generate HAp-OVA aggregates [18]. OVA, furthermore, could be adsorbed on the HAp surfaces by the crystal surface area available for growth [24]. When considering HAp-OVA particles, their average pore diameters at lower pH are bigger than those at higher pH. At the same pH, the chemical starting material shows the higher values of the average pore diameter compared with the natural one. The average pore diameters, nevertheless, are quite

similar in cases of varying initial OVA contents. Therefore, it could be assumed that difference in these initial amounts of added OVA has a little influence on the average pore size. with the presence of higher initial OVA amount manifest a little higher OVA-release percentage, depending on the incorportaed OVA content, so the OVA release amount was not significantly dependent on the initial amount of added OVA (p > 0.05).

Conclusions

Protein carriers based on HAp were designed as potential devices for the controlled release system. HAp-OVA particles were obtained by the co-precipitation method with varying the starting material, pH value, and initial amount of OVA. The incorporated and released OVA amounts highly increased with lowering pH value to be neutral and slightly increased with increasing initial OVA content. A greater OVA incorporation and release were also observed in the HAp-OVA particles synthesized from the chemical starting material compared to those prepared from the natural one. All of the release kinetics exhibited a slow release in a sustained manner without initial OVA burst, resulting in prolonged release behavior. Consequently, it may be practicable to use these HAp particles with other protein drugs and growth factors as effective carries to achieve specific targets for bone tissue engineering applications.

3. Polycaprolactone Fibrous Membranes Modified with Gelatin, Bovine Serum Albumin or Crude Bone Protein Extract and Their Potential for Use as Bone Scaffolds.

EXPERIMENTAL SECTION

a. Materials

Materials used in the Fibrous Scaffolds Preparation and Surface Modification

- Poly(ϵ -caprolactone) (PCL) ($M_n = 80,000 \text{ g/mol}$; Aldrich, USA)
- Dichloromethane (DCM; Lab-Scan (Asia), Thailand)
- *N,N'*-dimethylformamide (DMF; Lab-Scan (Asia), Thailand)
- 1,6-hexamethylenediamine (HMD; Aldrich, USA)
- *N*,*N*'-disuccinimidyl carbonate (DSC; Aldrich, USA)
- Ninhydrin (Aldrich, USA)
- Bovine serum albumin (BSA; Sigma, USA)
- Gelatin from porcine skin ,type A (Sigma, USA)
- Gelatin type-B (Sigma, USA)
- Triethylamine (TEA; Sigma, USA)
- Ethanol (J. T. Beaker, USA)

- Isopropanol (IPA; Fisher Sciencific (Asia), Thailand)
- 1,4-dioxane (Fisher Sciencific (Asia), Thailand)
- Dimethylsulfoxide (DMSO; Lab-Scan (Asia), Thailand)
- Phosphate buffer saline (PBS)

Materials used for cell culture

Model Cells

Model cells in this study were mouse calvaria-derived pre-osteoblastic cells (MC3T3-E1).

Medium for MC3T3-E1 cells

Minimum Essential Medium (with Earle's Balanced Salts) (MEM; Hyclone, USA), supplemented by 10% fetal bovine serum (FBS; Sorali, Campo Grande, Brazil), 1% L-glutamine (Invitrogen Corp., USA) and 1% antibiotic and antimycotic formulation [containing penicillin G sodium, streptomycin sulfate, and amphotericin B (Invitrogen Corp., USA)] was used as culture media for MC3T3-E1.

Material for Cell Culture Study

- 3-(4,5-dimethyl-thiazol-2-yl)-2,5-diphenyltetrazolium bromide (MTT; USB Corporation., USA)
- Trypsin-EDTA (GibThai Co.,Ltd.)
- Fetal Bovine Serum (Sorali, Campo Grande, Brazil)
- DMEM without phenol red (GibThai Co.,Ltd.)
- L-Glutamine (GibThai Co.,Ltd.)
- 50% Glutaraldehyde solution (Sigma, USA)
- Hexamethyl disilazane HMDS; Sigma, USA)
- p-nitrophenylphosphate (PNPP; Zymed Laboratories, USA)
- Bicinchoninic acid protein assay (BCA; Pierce Biotechnology, USA)
- L-ascorbic acid (Sigma, USA)
- β-glycerophosphate (Sigma, USA)
- Cetylpyridinium chloride (Sigma, USA)

b. Equipment

Equipment for Electrospinning Process

- High voltage power supply from Gamma High Voltage Research Inc.
 (Ormond Beach, Florida), model D-ES30PN/M692 DC
- Syringe with volume size of 25 ml
- Stainless steel needle with gauge number 20 (or the inner diameter of 0.91 mm)
- The rotating drum which covered with aluminum sheet has the width and OD about 14 and 15 cm, respectively.

Equipment for Characterization of Materials

- UV-Vis spectrophotometer (UV-1800; Shimadzu, Kyoto, Japan)
- quartz tube
- Fourier-transformed infrared spectrometer (FT-IR); attenuated total reflection (ATR-FTIR; Thermo Nicolet Nexus 670; resolution of 4 cm-1 and 128 scans)
- Contact angle goniometer (KRUSS Gmbh Germany; Model: DSA10-Mk2 T1C)
- Scanning electron microscope (SEM; A JEOL JSM 5200)
- X-ray Photoelectron Spectrometer (XPS; Thermo Fisher Scientific Thetaprobe; Monochromatic Al K α X-ray, the analysis area was approximately 400 μ m , while the maximum analysis depth lay in the range of ~4 to 8 nm.)

Equipment for Study of Cell Culture

- A Thermo Spectronic Genesis 10 UV-vis spectrophotometer
- Laminar flow hood

c. Experimental Procedures

Preparation of Polycaprolactone Scaffolds

Preparation and Characterization of Fibrous Scaffolds

Electrospun Polycaprolactone fibrous scaffolds were prepared by electrospinning from a neat 12 % w/v PCL solution in 50:50 v/v DCM/DMF. The as-prepared PCL solution was contained in a glass syringe, the open end of which was connected to a blunt gauge-20 stainless steel hypodermic needle (o.d.0.91 mm) used as the nozzle. An Al sheet wrapped around a rotating cylinder (width and o.d. of the cylinder: 15 cm; rotational speed: 50 rpm) was

used as the collector. The distance from the tip of the needle to the surface of the Al sheet defining the collection distance was fixed at 10 cm. A gamma high-voltage research D-ES30PN/M692 power supply was used to generate a high dc potential (i.e., 21 kV). The spinning time was carried out continuously for 10 hours.

Morphological appearance and size of the individual fibers of the scaffolds were examined by a JEOL JSM-5200 scanning electron microscope (SEM). Fibrous scaffolds were dried in vacuum at 30 °C overnight to remove solvent. Each sample was plated in the stub and coated with a thin layer of gold by using a JEOL JFC-1100E ion sputtering device prior to SEM observation. The average diameters of as-spun fibers were determined by measuring the diameters. At least 100 readings of the fiber diameters from at least five SEM images are statistically analyzed using SemAphore 4.0 software, from which the arithmetic mean values of the individual fibers in the PCL fibrous scaffolds were determined to be 0.93 and 1.26 μm, respectively.

Preparation of Crude Bone Protein.

Crude bone protein (CBP) was extracted from the pork bone. In particular, bone was initially washed and cleaned thoroughly in tap water and then sectioned into small pieces with a high speed motor machine. Pieces of sectioned bones were further crushed into powder in liquid nitrogen. Then, the as-prepared powder was immersed in 0.6 N HCl at 4°C and shaken continuously on an orbital shaker. After three days, the bony solution was centrifuged and the supernatant was collected, dialyzed for 48 h and lyophilized. The dry CBP was kept in desiccators until use.

Surface Modification of PCL Scaffold via Aminolysis and Immobilization of Proteins

The scaffold was cut into disc shape with diameter 1.4 cm and immersed in ethanol/water (1:1, v/v) solution for 2 to 3 hours to clean oily dirt and then washed with a large amount of deionized water. The scaffold was subsequently immersed in various concentrations of 1,6-hexamethylene diamine (HMD) /isopropanol (IPA) solution (0.04, 0.06, 0.08, 0.10, 0.20, and 0.40 g/ml) for 2 hours at 30 °C. The resulting aminolyzed PCL scaffold was rinsed with deionized water for 24 hours at room temperature to remove free 1,6-hexamethylenediamine and dried under vacuum at 30 °C to constant weight. To determine the optimum concentration of HMD used for aminolysis using ninhydrin method, degreadation experiment, water retention experiment and SEM observation.

Aminolyzed PCL scaffold obtained using the optimum condition was immersed in 0.1 M *N,N*'-disuccinimidyl carbonate (DSC)/dimethylsulfoxide (DMSO) solution in the presence of 0.1 M triethylamine (TEA) for 1 hour at ambient temperature

followed by rinsing with large amount of deionized water. The scaffold was then directly transferred to 3 mg/ml of gelatin type-A, gelatin type-B, bovine serum albumin (BSA) or crude bone protein (CBP) in phosphate buffer saline (PBS) solution at ambient temperature for 24 hours. PCL scaffolds immobilized with proteins were rinsed by soaking in deionized water for 24 hours. The samples were dried under vacuum before surface characterization.

Characterization of Fibrous Scaffolds

Density, Porosity and Pore Volume

The density of the scaffolds ($\rho_{scaffolds}$) can be calculated using the following equation

Apparent density
$$(\rho_{\text{scaffold}}, g/\text{cm}^3) = \frac{m}{txA}$$
----(3.1)

where m is the mass of the scaffold (g), t is the thickness of the scaffold (cm) and A is the area of the scaffold (cm²)

The porosity and pore volume of the scaffolds can be calculated using the following equation (Hou *et al.* 2003).

Porosity (%) =
$$\left(1 - \frac{\rho_{scaffold}}{\rho_{polymer}} \right) x 100 \qquad (3.2)$$

Pore volume =
$$\left(\frac{1}{\rho_{scaffold}} - \frac{1}{\rho_{polymer}}\right)$$
 ----(3.3)

where $\rho_{scaffold}$ is the apparent density of the fibrous scaffolds(g/cm³) and $\rho_{polymer}$ is the density of the non-fibrous polymer ($\rho_{polymer}$ of PCL is 1.145 g/cm³).

Water Retention Capacity

The dry scaffolds were weighed and then immersed in 5 mL of 0.1 M PBS solution at 37 °C within 48 hours. At the predetermined time point, scaffold were removed from the solution and carefully placed on glass for 5 seconds to remove the excessive water and weighed immediately. The water retention was calculated by using the following equation (Kothapalli *et al.*, 2005).

Water Retention (%) =
$$\left(\frac{M_{wet} - M_{dry}}{M_{dry}}\right) x 100$$
 ----(3.4)

where M_{dry} and M_{wet} are the weight of the scaffold before and after immersion in 0.1 M PBS solution respectively. Five measurements were performed for the calculation of an average water retention value.

Degradation Study of Fibrous Scaffolds

In degradation study, the disc shape of the fibrous scaffolds with diameter 1.4 cm had been immersed in the 0.1 M PBS pH 7.4 at 37 °C within 48 hours. The fibrous scaffolds were then dried in the vacuum to constant weight.

The rate of degradation can be calculated using the following equation.

Weight loss (%) =
$$\left(\frac{Mf - Mi}{Mi}\right) x 100$$
 ----(3.5)

where M_i is the initial weight of the scaffolds and M_f and is the weight of the scaffold at the given degradation time point, immersed in 0.1 M PBS solution. Five measurements were performed for the calculation of an average water degradation rate value.

<u>Determination of the Amino Groups on PCL Surface after Aminolysis and</u> Protein Immobilization

The ninhydrin analysis method was carried out to quantitatively determine the amount of NH₂ groups on the aminolysed PCL and biomolecule-immobilized PCL scaffolds. The scaffold was immersed in 1 M ninhydrin/ethanol solution for 15 minutes. After the adsorbed ethanol had evaporated, 1,4-dioxane was added to dissolve the scaffold. When the scaffold surface turned blue, isopropanol (IPA) was then added to stabilize the blue compound. This mixture was transfered to quartz tube and measured the absorbance at the wavelength of 538 nm using a UV-vis spectrophotometer. A calibration curve was obtained with known concentration of 1,6-hexamethylenediamine in 1,4-dioxane/IPA (1:1, v/v) solution.

Surface Characterization

Water Contact Angle Measurements

Contact angle goniometer (KRUSS Gmbh Germany; Model: DSA10-Mk2 T1C) were used for the determination of water contact angles. The measurements were carried out by the sessile drop method in air at room temperature. The reported angle was an average of 5 measurements on different area of each sample.

UV-Vis Spectrophotometer

UV-vis spectrophotometer Model Shimadzu, UV-1800 was used for determination of the amount of amino group using ninhydrin method on the modified PCL surface. Ninhydrin will react with a free alpha-amino group, NH₂-C- which is contained in all amino acids, peptides, or proteins, producing Ruhemann's purple colored complex of ninhydrin absorbs the visible light at the wavelength of 538 nm.

Attenuated Total Reflectance-Fourier Transform Infrared Spectrometer (ATR-FTIR)

All spectra are collected at resolution of 4 cm⁻¹ and 128 scans using Nicolet Magna 750 FT-IR spectrometer equipped with a liquid-nitrogen-cooled mercury-cadmium-telluride (MCT) detector. A single attenuated total reflection accessory with 45° germanium (Ge) IRE (spectra Tech, USA) and a varible angle reflection accessory (SeagullTM, Harrick Scientific, USA) with a hemispherial Ge IRE are employed for all ATR spectral acquisitions. Chemical functional groups that were present on the surfaces of both the neat and the surface-modified fibrous scaffolds were analyzed by ATR-FTIR spectrometer.

X-ray Photoelectron Spectrometer (XPS)

XPS was used to estimate the elemental composition and chemical state of the elements on the surface. The analysis of the samples was carried out using a Thermo Fisher Scientific Thetaprobe XPS. Monochromatic Al K_{α} X-ray was employed for analysis of one spot on each sample with photoelectron take-off angle of 50° (with respect to surface plane). The analysis area was approximately 400 μ m, while the maximum analysis depth lay in the range of ~4 to 8 nm. A special designed electron flood gun with a few eV Ar⁺ ion was used for the charge compensation. Electron beam and ion beam were focused and steered towards the analysis position. Further correction was made based on adventitious C 1s at 285.0 eV using the manufacturer's standard software. Survey spectra were acquired for surface composition analysis with Scofield sensitivity factors.

Scanning Electron Microscope

The morphology of cells on the materials was examined by using a JEOL JSM 5200 scanning electron microscope (SEM). Each sample was coated with a thin layer of gold using JEOL JFC 1100E ion sputtering device prior to SEM observation.

Cell Culture Studies

Osteoblast (MC3T3-E1) cell lines are used. MC3T3-E1 cells are cultured in α -MEM medium supplemented with 10 % FBS, 1 % L-glutamine and 1 % antibiotic and antimycotic

formulation (containing penicillin G sodium, streptomycin sulfate, and amphotericin B). The medium was replaced every 2 days and the cultured cells were maintained at 37 °C in a humidified atmosphere containing 5% CO₂.

Cytotoxicity Evaluation

Direct Cytotoxicity

This test was used to evaluate the potential for use of protein directly to the cell. 4×10^4 MC3T3-E1 cells/well were cultured in 24-well plate to allow cell attachment on the plate. After incubation under 5 % CO₂ at 37 °C at least 4 hours, the cells were starved with a 2 % culture media (2 % MEM; containing MEM, 2 % FBS, 1 % L-glutamine, 1 % lactabumin, and 1 % antibiotic and antimycotic formulation.) for 24 hours. After starvation, the culture medium was removed and replaced with the as-prepared extraction media (2 % culture media with appropriate amount of proteins ; gelatin type-A , gelatin type-B, bovine serum albumin, and crude bone protein) and later incubated for 1, 2, and 3 days. The number of living cells was finally quantified with MTT assay.

Indirect Cytotoxicity

The indirect cytotoxicity evaluation was conducted on modified and unmodified PCL scaffolds in adaptation from the ISO10993-5 standard test method. The samples are prewashed with 70 % ethanol in water for 30 minutes, washed twice with PBS solution and deionized water and immerged in a 2% MEM culture medium (2 % MEM; containing MEM, 2 % FBS, 1 % L-glutamine, 1 % lactabumin, and 1 % antibiotic and antimycotic formulation.) under 5 % CO₂ at 37 °C in 24-well plate for 24 hours to prepare the extraction media. 4×10⁴ MC3T3-E1 cells/well were separately cultured in other 24-well plate to allow cell attachment on the plate at least 4 hours. The cells were further starved with a 2 % MEM and replaced in 2 hours for 3 times. After incubation under 5 % CO₂ at 37 °C, the culture medium was removed and replaced with the as-prepared extraction media and later incubated for another 1, 2 and 3 days. The number of living cells was finally quantified with MTT assay.

Cell Adhesion and Proliferation

Both modified and unmodified PCL scaffolds (diameter 1.4 cm) are sterilized by soaking in 70 % ethanol in water for 30 minutes, washed twice with PBS solution and deionized water and immerged in a 10 % MEM culture medium under 5 % CO₂ at 37 °C in 24-well plate for 24 hours. After removing of culture media, approximately 4×10⁴ MC3T3-E1 cells and 0.5 mL culture medium were pipetted into each well containing as-prepared scaffolds as well as into the bottom of tissue culture polystyrene plates (TCPS) as a control and then incubated under 5 % CO₂ at 37 °C. Cell adhesion was studied on 2, 4, 6 hours culture period

while cell proliferation was investigated on 1, 2 and 3 days culture period. The number of living cells was finally quantified with MTT assay.

MTT Assay

The MTT assay is based on the reduction of the yellow tetrazolium salt to purple formazan crystals by dehydrogenase enzymes secreted from the mitochondria of metabolically active cells. The amount of the purple formazan crystal formed is proportional to the number of viable cells. After desirable culture period, the culture medium was removed to discard the unattached cell and incubated at 37 °C for 30 minutes with 300 μ l/well of MTT solution at 0.5 mg/ml culture medium without phenol red. After incubation, MTT solution was removed. A buffer solution containing dimethylsulfoxide (DMSO : 900 μ l/well) and glycine buffer (pH = 10 : 125 μ l/well) was added into the wells to dissolve the formazan crystals. After 10 minutes of rotary agitation, the solutions were then transferred into a cuvette and placed in a spectrophotometer (Thermospectronic Genesis10 UV-visible spectrophotometer) to measure the number of viable cells at absorbance 540 nm .

Morphological Observation of Cultured Cells

After removal of the culture medium, the cell-cultured scaffold samples were rinsed with PBS twice and the cells were then fixed with 3% glutaraldehyde solution (diluted from 50 % glutaraldehyde solution with PBS), at 500 µl/well. After 30 minutes, they were rinsed again with PBS. After cell fixation, the samples were dehydrated in an ethanol solution of varying concentration (i.e. 30, 50, 70, 90, and 100 %, respectively) for about 2 minutes at each concentration. The samples were then dried in 100 % hexamethyldisilazane (HMDS) for 5 minutes and later let dry in air after removal of HMDS. After completely dried, the samples were mounted on an SEM stub, coated with gold, and observed by a JEOL JSM 5200 scanning electron microscope (SEM).

Production of Alkaline Phosphatase of Cultured Cells

ALP is considered as a relatively early marker of osteoblast differentiation. Cells were cultured on scaffold samples for 3, and 7 days to observe the production of alkaline phosphatase (ALP). The samples were rinsed with PBS after removal of culture medium. Alkaline lysis buffer (10 mM Tris-HCl, 2 mM MgCl₂, 0.1 % Triton-X 100, pH 10) (100 μl/well) was added and the samples were scrapped and then frozen at -20°C for at least 30 minutes prior to the next step. An aqueous solution of 2 mg/ml *p*-nitrophenyl phosphate mixed with 0.1 M amino propanol (10 μl/well) in 2 mM MgCl₂ (100

μl/well) having a pH of 10.5 was prepared and added into the samples. The samples were incubated at 37 °C for 15 minutes. The reaction was stopped by adding 0.9 ml/well of 50 mM NaOH and the extracted solution was transferred to a cuvette and placed in the UV-visible spectrophotometer, from which the absorbance at 410 nm was measured. The amount of ALP was then calculated against a standard curve. In order to calculate for the ALP activity, the amount of ALP had to be normalized by the amount of total protein synthesized. In the protein assay, the samples were treated in the same manner as the ALP assay up to the point was the samples were frozen. After freezing, bicinchoninic acid (BCA; Pierce Biotechnology, USA) solution was added into the samples. The samples were incubated at 37 °C for 15 minutes. The absorbance of the medium solution was then measured at 562 nm by the UV-vis spectrophotometer and the amount of the total protein was calculated against a standard curve.

Mineralization

Mineralization refers to cell-mediated deposition of extracellular calcium and phosphorus salts where anionic matrix molecules take up the Ca²⁺, phosphate ions and serve as nucleation and growth sites leading to calcification. Mineralization was quantified by Alizarin Red-S which is a dye that binds selectively calcium salts and is widely used for mineral staining (the staining product i.e., an Alizarin Red S-calcium chelating product). MC3T3-E1 cells (4×10⁴ cells/well in 24-well plate) were cultured on scaffold samples for 16 days to observe the production of mineralization. The isolated cells were plated in 24-well plate and cultured in the cultured medium. The cultured cells were changed after a 24 hours attachment period with culture medium in the presence of 5 mM β-glycerophosphate and 50 μg/ml ascorbic acid. The media was replaced every 2 days thereafter. After 16, 21 and 30 days, respectively, the cells were washed twice with PBS, fixed with cold methanol for 10 minutes, and stained with 1 % Alizarin red solution (prepared in distillated water and adjusted the pH about 4.1 to 4.3 using 10 % ammonium hydroxide) for 5 minutes. After removing the alizarin red-S solution, the cells were rinsed with deionized water and dried at room temperature. The images of each culture were captured and the strain was extracted with 10 % cetylpyridinium chloride in 10 mM sodium phosphate for 1 hour and the absorbance of collected dye was read at wavelength 570 nm in spectrophotometer (A Thermo Spectronic Genesis10 UV-visible spectrophotometer). In comparison, tissue culture plate without cell was treated with the procedure as previously described.

Statistical analysis

Values are expressed as the mean \pm SD. Experiments are performed at least five times and results of representative experiments are presented except where otherwise indicated. Statistical analysis was performed using One-Way Analysis of Variance (ANOVA) with the Least Square Difference (LSD) test multiple comparisons posttest using SPSS version 17 software. p < 0.05 or p < 0.01 is considered statistically significant.

2. RESULTS AND DISCUSSION

4.1 Preparation of Poly(ε-caprolactone) Electrospun Fibrous Scaffold

Poly(ε -caprolactone) (PCL; $M_n=80,000$ g/mol) electrospun fibrous scaffold was prepared via electrospinning process under fixed conditions as mentioned in the previous chapter. Translucent electrospun PCL fibrous scaffolds with a thickness of (130 ± 5) μ m were obtained. Morphological appearance and size of the individual fibers of the scaffolds were examined by JEOL JSM 5200 scanning electron microscopy (SEM) as shown in Figure 4.1(a). At least 100 readings of the fiber diameters from various SEM images were statistically analyzed using SemAphore 4.0 software, from which the arithmetic mean value of the individual fibers within the PCL fibrous scaffolds was determined to be (0.93 ± 0.30) μ m. After surface modification of PCL electrospun fibrous scaffold via aminolysis with various 1,6-hexamethylenediamine (HMD) concentration treatments, the morphology of the surface-modified scaffolds was also observed [Figure 4.1 (b,c and d)].

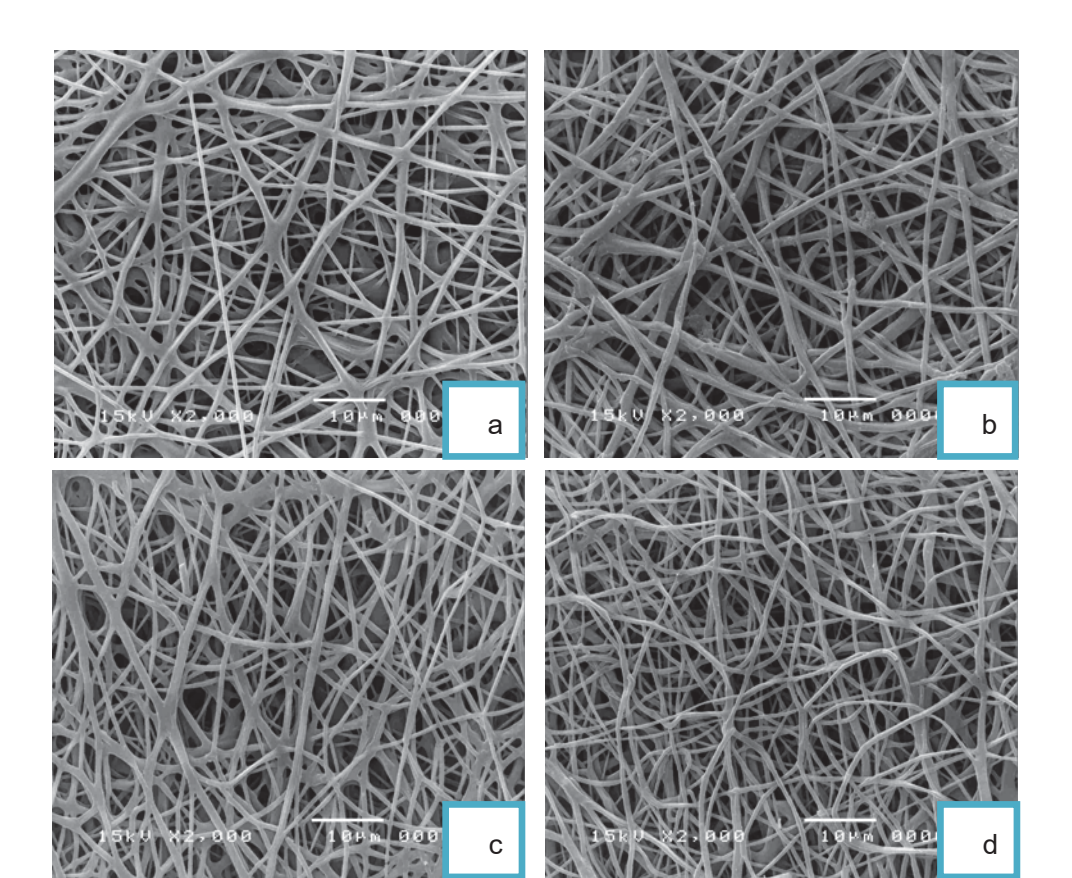


Figure 4.1 Selected SEM image of electrospun PCL fibrous scaffolds (a), aminolyzed PCL fibrous scaffolds which treated with (magnification = 2000x; scale bar = $10 \mu m$) 1,6-hexamethylenediamine at concentration of 0.04 g/ml (b), 0.20 g/ml (c) and 0.40 g/ml (d)

4.2 Characterization of Fibrous Scaffolds

4.2.1 Density, Porosity, and Pore Volume

The density, porosity and pore volume of the unmodified PCL scaffolds and modified PCL scaffolds are shown in Table 4.1. The porosity and pore volume of these scaffolds were in the range of (96 to 97) % and (22 to 29) cm³/g, respectively. Moreover, the density, porosity percentage and pore volume of all type of the surface-modified scaffolds were not significantly different from the unmodified PCL scaffolds.

Material	density $(x10^{-2}g/cm^3)$	porosity (%)	pore volume (cm ³ /g)
PCL pure	4.69 . 0.44	95.91 . 0.38	20.62 . 2.07
aminolyzed PCL	4.25 . 0.97	96.29 . 0.85	23.63 5.28
activated PCL	4.14 0.57	96.39 . 0.50	23.64 3.07
gelatin A immobilized PCL	3.75 . 0.59	96.72 . 0.51	26.33 4.52
gelatin B immobilized PCL	3.59 0.88	96.86 . 0.77	28.15 6.17
BSA immobilized PCL	3.85 . 0.74	96.64 0.65	25.88 4.97
CBP immobilized PCL	4.58 . 0.93	96.00 . 0.81	21.64 4.35

4.2.2 Water Retention Capability

Figure 4.2 demonstrates the water retention capability of these unmodified and modified PCL scaffolds via aminolysis process with different 1,6-hexamethylenediamine (HMD) concentration at 37 °C within 48 hours. In the figure shows the water retention rate increased with increasing HMD concentration treatment.

4.2.3 <u>Degradation Study of PCL Fibrous Scaffolds</u>

In degradation study, the disc shape of the PCL fibrous scaffolds with diameter \sim (100 to 150) μ m had been immersed in the 0.1 M phosphate buffer saline (PBS), pH 7.4 at 37 °C within 48 hours. Figure 4.3 shows the degradation rate of the PCL scaffolds at different HMD concentration treatments. The weight loss increased with time and rapidly increased in

the early 2 hours and steady stable after 18 hours. Furthermore, the weight loss values increased with increasing HMD concentration treatment.

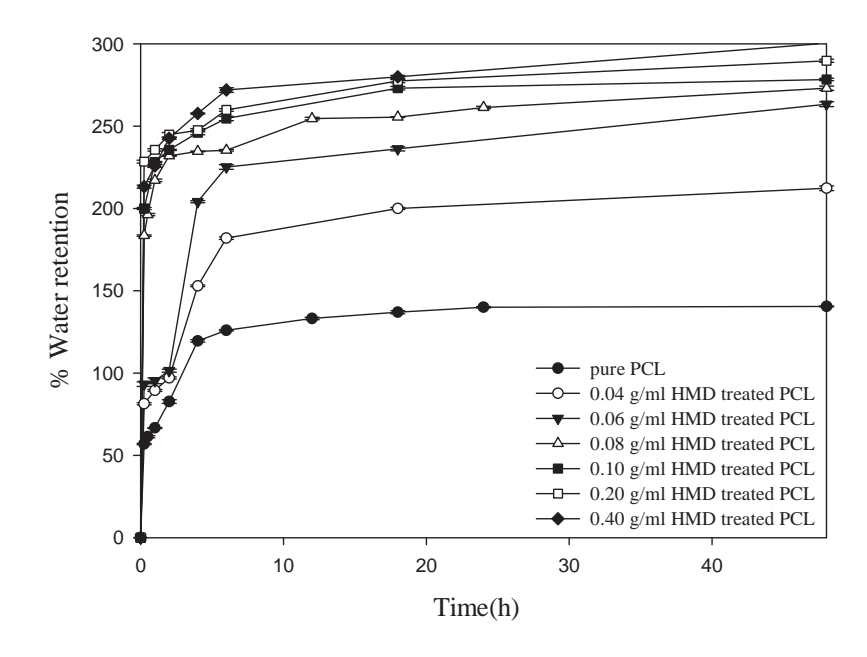


Figure 4.2 Water retention capability of these unmodified and modified PCL scaffolds via aminolysis process with different 1,6-hexamethylenediamine(HMD) concentration at 37 °C within 48 hours.

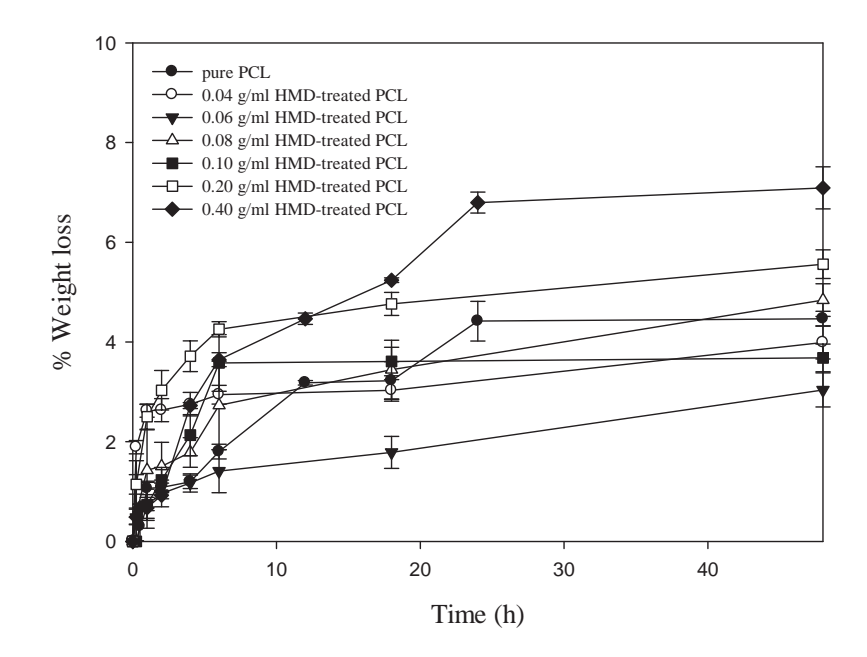


Figure 4.3 The degradation rate of the PCL scaffolds at different HMD concentration treatments.

4.3 Surface Characterization

4.3.1 Quantification of Amino Groups

Amino groups can be covalently introduced onto the surface of the electrospun PCL fibrous scaffolds by reaction with 1,6-hexamethylenediamine (HMD), One amino group (NH₂) of HMD reacts with an ester group (—COO—) of PCL to form the amide linkage (—CONH—), while another amino group which is unreacted and free can be used as active sites through which biomolecules (i.e;proteins) can be bonded to the surface using *N*, *N'*-disuccinimidyl carbonate (DSC) as a coupling agent. However, two-step procedure was carried out to avoid aggregation,. The attached amino groups had been first activated with DSC which *N*-hydroxysuccinimide was lost from the reaction and the as-formed succinimidyl esters were later reacted with respective biomolecules, *N*-hydroxysuccinimide again being cleaved from the reaction. The chemical pathway for the immobilization of biomolecule on the surface of electrospun PCL fibrous scaffolds is summerized in the Figure 4.4.

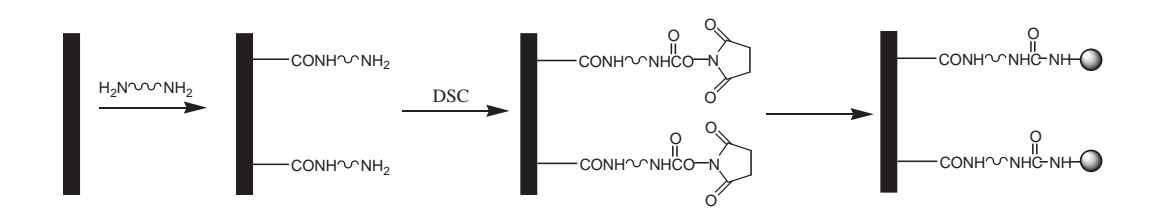


Figure 4.4 The chemical pathway for the immobilization of proteins.

The existence of free amino groups (NH₂) on PCL surface is essential for protein bonding in this modification method. It is important to confirm the existence of amino groups before protein is further introduced. Therefore, ninhydrin is used to confirm and quantify the – NH₂ density on the aminolyzed PCL surface. The NH₂ density on electrospun PCL fibrous scaffold surfaces is relative to the concentration of 1,6-hexamethylenediamine, aminolyzing time, temperature, and so on. Figure 4.5 shows that NH₂ density increased with increasing 1,6-hexamethylenediamine concentration. However, when the concentration of 1,6-hexamethylenediamine is greater than 0.20 g/ml, the structural morphology of the electrospun PCL fiber scaffolds became worse (as shown in Figure 4.1 d). To maintain structural morphology of the electrospun PCL fiber scaffolds for practical applications, PCL electrospun

fibrous scaffolds were aminolyzed in a 0.20 g/ml 1,6-hexamethylenediamine/isopropanol solution at evaluated temperature for 2 hours. According to the calibration curve obtained with 1,4-dioxane–isopropanol (1:1, v/v) solution containing 1,6-hexamethylenediamine of known concentration, the NH₂ density on PCL electrospun fibrous scaffolds aminolyzed under these conditions was $1.37 \times 10^{-7} \text{ mol/cm}^2$.

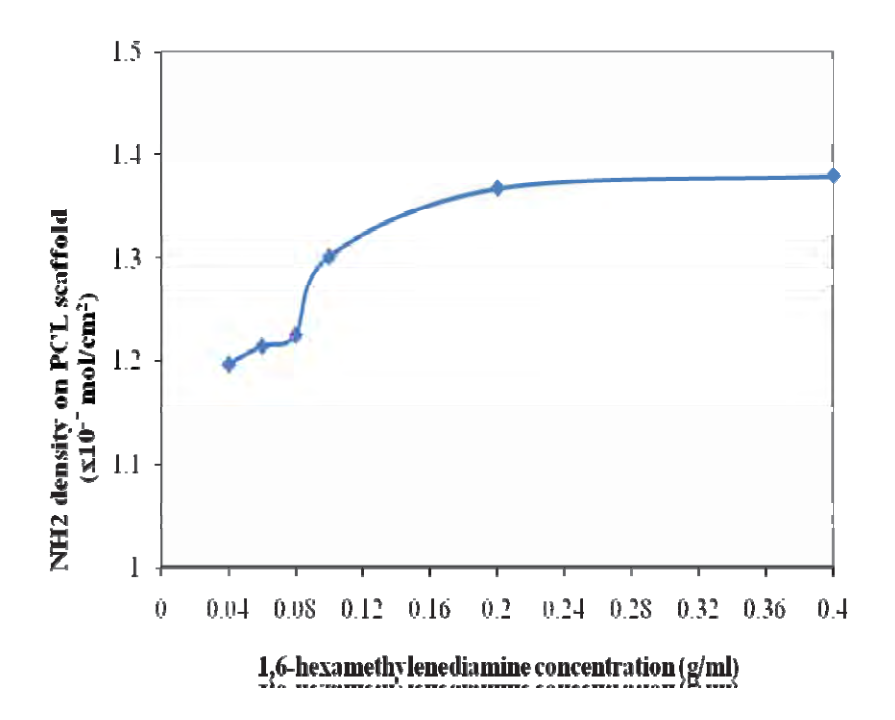


Figure 4.5 NH₂ density on PCL electrospun fibrous scaffolds as a function of concentration of 1,6-hexamethylenediamine/isopropanol solution. The PCL scaffold was aminolyzed for 2 hours.

4.3.2 Surface Wettability

To further evaluate the effect of aminolysis, surface wettability of the modified PCL fibrous scaffolds was measured. Therefore, water contact angle measurement was used to evaluate the surface wettability of the surface modified PCL fibrous scaffolds. Table 4.2 shows the water contact angle measured by the sessile drop method decreased gradually from 123.8° to 118.0° after the scaffolds were aminolyzed with 0.04 g/mL of HMD/IPA solution for 2 hours and slightly decreased with increasing HMD concentration. That is, the introduction of the amino groups on the surface of the PCL fibrous scaffolds improved the hydrophilicity of the surface. Figure 4.6 and 4.7 show that the surface became more hydrophilic after aminolysis and protein immobilization. After the aminolyzed PCL fibrous scaffolds have been activated

with DSC, their surface became more hydrophobic than the neat PCL scaffold and water contact angle also decreased after the proteins were bonded. The water drop appearance on the surface of neat PCL, gelatin type-A immobilized PCL, BSA immobilized PCL and CBP immobilized PCL are shown in Figure 4.7. CBP immobilized PCL scaffold has largest decrease of contact angle as compared with the neat PCL scaffold (control). This means that immobilization of gelatin crude bone protein can most improve the hydrophilicity of the surface.

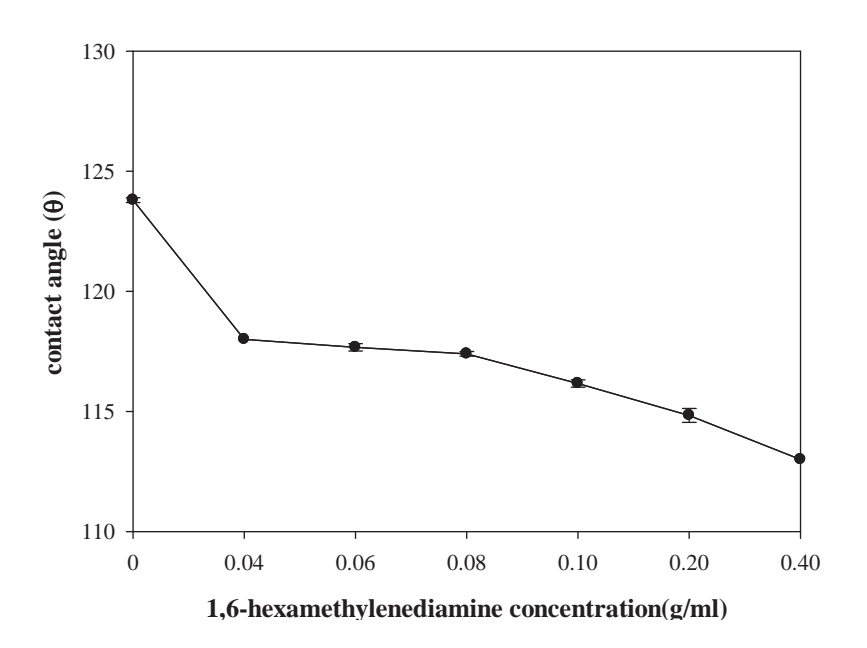


Figure 4.6 Water contact angles of the control and aminolyzed PCL scaffolds at different HMD concentration treatments measured by the sessile drop method.

Table 4.1 The water contact angle of the control and all modified PCL fibrous scaffolds measured by the sessile drop method

Material	Contact angle(θ)
Neat PCL (control)	123.7 ± 0.1
Aminolyzed PCL ^a	115.3 ± 0.2
Activated PCL ^b	118.7 ± 0.3
Gelatin type-A immobilized PCL ^{c1}	95.5 ± 1.1
Gelatin type-Bimmobilized PCL c2	94.4 ± 2.1
BSA immobilized PCL c3	97.5 ± 2.0
CBP immobilized PCL c4	48.5 ± 1.8

 $^{
m a}$ The PCL electrospun fibrous scaffolds was immersed in 0.20 g/ml 1,6-hexamethylenediamine solution at 30 $^{\circ}$ C for 2 hours.

^bThe aminolyzed PCL scaffolds were immersed in 0.1 M DSC solution in the presence of TEA for 1 hour.

c1,c2,c3,c4 The activated PCL scaffolds were immersed in 3.0 mg/mL gelatin type-A, gelatin type-B, BSA, and CBP solutions, respectively, for 24 h followed by the rinsing process.

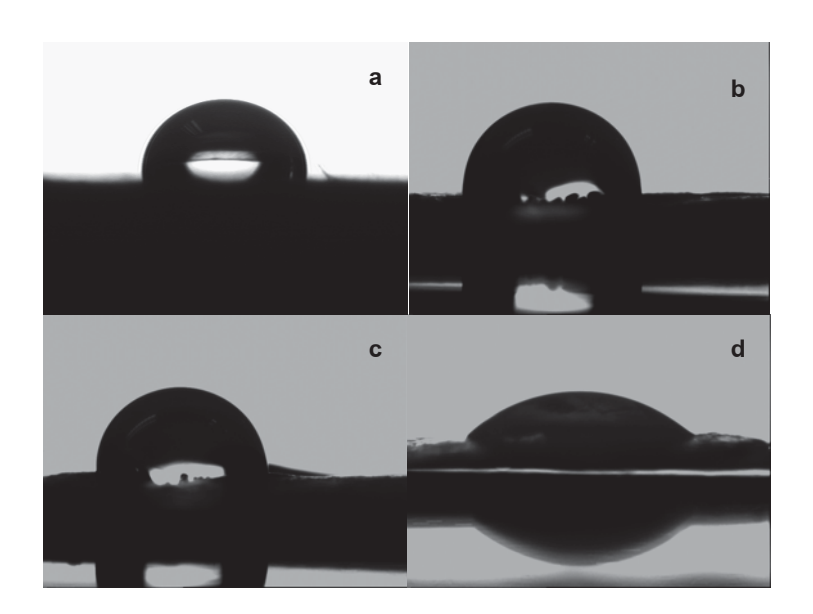


Figure 4.7 Water dropped on the surface of neat PCL fibrous scaffold (a), and PCL fibrous scaffold immobilized with 3.0 mg/ml gelatin type-A (b), 3.0 mg/ml bovine serum albumin (c) and 3.0 mg/ml crude bone protein (d).

4.3.3 Chemical Analysis of Surface

ATR-FTIR spectra of PCL and modified PCL fibrous scaffolds are shown in Figure 4.8 and 4.9 There was a major absorption peak assigned to the ester carbonyl of neat PCL appeared at 1755 cm⁻¹.

The low broad signals from N–H stretching of NH₂ at ~ (3300 to 3500) cm⁻¹ or carbonyl stretching of amide group at 1650 cm⁻¹ were observed on those surface modified PCL. After biomolecule immobilization, C=O stretching peak occurs at 1650 cm⁻¹ (amide I) and N–H bending peak at 1550 cm⁻¹ (amide II) and 1350 cm⁻¹ (amide III) evidently appeared in the spectra of all biomolecule-immobilized PCL scaffolds. Moreover, the higher broad peak in the range of 3000 to 3600 cm⁻¹ corresponding to N–H stretching of NH₂ in gelatin type-A, gelatin type-B, BSA and CBP was observed indicating that gelatin type-A, gelatin type-B,

BSA and CBP have been successfully immobilized on the amino-containing PCL scaffolds. However, the signal of FTIR spectrum were low, resulting from the extremely low concentration of NH₂ present within the sampling depth of ATR-FTIR (1 to 2 μ m).

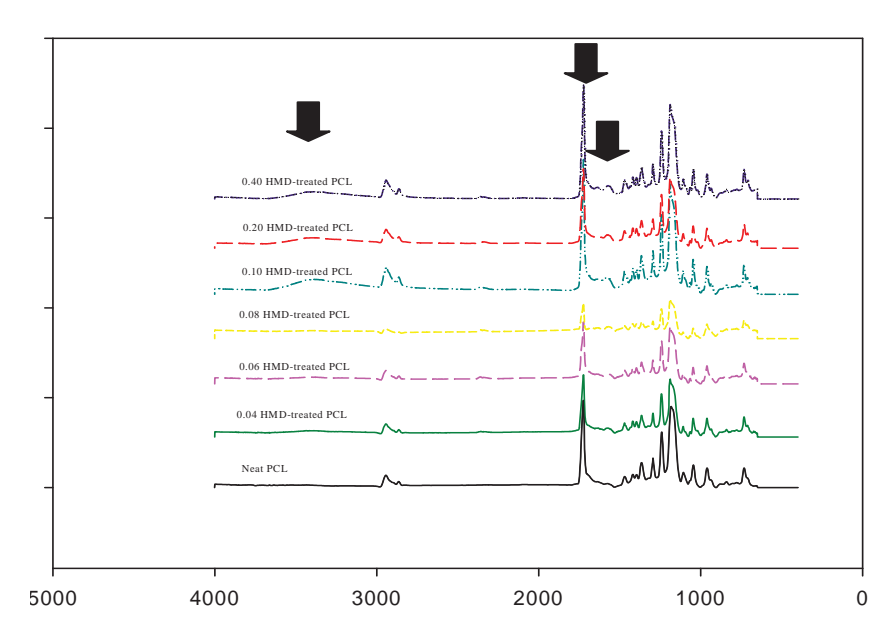


Figure 4.8 ATR-FTIR spectra of neat and aminolyzed PCL fibrous scaffolds with different HMD concentration treatments.

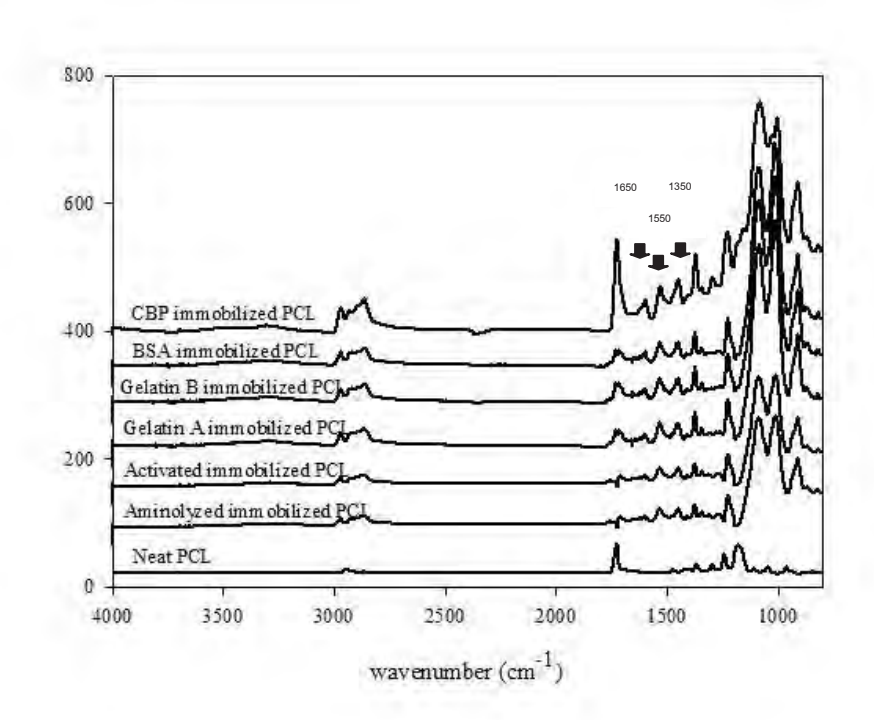


Figure 4.9 ATR-FTIR spectra of neat and modified PCL fibrous scaffolds.

4.3.4 Elemental Composition of the Surface

The surface of modified PCL fibrous scaffolds were further determined the elemental composition by using X-ray Photoelectron Spectrometer (XPS). To study the effect of the aminolysis condition on the surface, N_{1s}/C_{1s} ratios as a function of HMD concentration treatment were evaluated. Table 4.4 shows that the more diamine concentration treated, the more N_{1s}/C_{1s} ratio observed due to the increasing in NH₂ groups. After aminolysis, the N_{1s}/C_{1s} ratio was increased from 0 to 0.0168 because NH₂ groups were introduced on the PCL surface. Figure 4.10 demonstrated that N_{1s} peak appeared after immobilization with proteins (gelatin type-A , gelatin type-B , bovine serum albumin, and crude bone protein) due to the large amount of nitrogen atom in proteins structure was introduced.

Table 4.2 N_{1s}/C_{1s} ratios as a function of 1,6-hexanediamine concentration

1,6-hexamethylenediamine concentration (g/ml)	N _{1s} /C _{1s} ratio
0.04	0.0063
0.06	0.0079
0.08	0.0163
0.10	0.0169
0.20	0.0170
0.40	0.0170

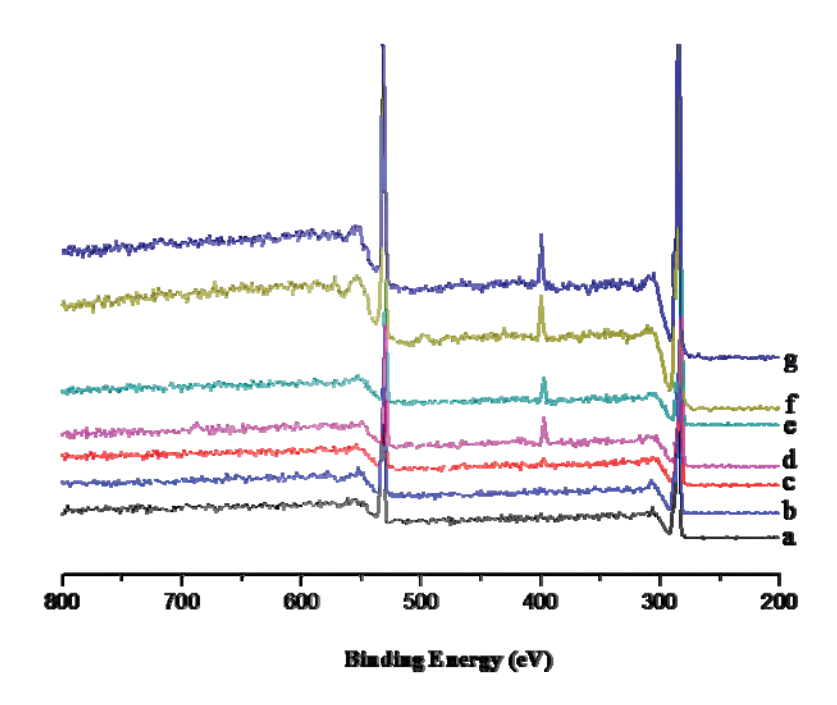


Figure 4.10 The survey XPS spectra of (a) neat PCL, (b) aminolyzed PCL with 0.20 g/ml HMD treatment, (c) activated PCL, (d) PCL immobilized with 3 mg/ml gelatin type-A solution, (e) 3 mg/ml gelatin type-B solution, (f) 3 mg/ml bovine serum albumin solution, and (g) 3 mg/ml crude bone protein solution.

4.4 Biological Characterizations

4.4.1 Cytotoxicity

4.4.1.1 Direct Cytotoxicity

Direct cytotoxicity test is a method to evaluate the toxic effect of proteins directly to cells. The effect was investigated with mouse calvaria-derived pre-osteoblastic cells (MC3T3-E1), based on the initial 40,000 cells/well seeded. MC3T3-E1 were cultured in 24-well culture plate to allow cell growth. The test was conducted by adding gelatin type-A, gelatin type-B, BSA protein and crude bone protein extracts in 2% serum-containing MEM diluted with 7-day extraction medium in seeded cells as mentioned above and cultured for 1, 2, and 3 d. Figure 4.11 shows that the viability of MC3T3-E1, cultured with 2% serum-containing MEM extraction media adding with all types of proteins for 1, 2 and 3 days, was increased with increasing the culturing time in the respective media. The viability of cells

(relative with control TCP) of all material is more than 80 %. All of the obtained results clearly suggested that all types of proteins, released no substances at levels that were harmful to cells.

4.4.1.2 Indirect Cytotoxicity

The potential use of these fibrous scaffolds as bone scaffolds was first evaluated by an indirect cytotoxicity test with mouse calvaria-derived pre-osteoblastic cells (MC3T3-E1), based on the initial 40,000 cells/well seeded. The test was carried out on TCP (control), the neat PCL, aminolyzed PCL, activated PCL, gelatin type-A, gelatin type-B, BSA and CBP immobilized PCL fibrous scaffolds. MC3T3-E1 were cultured in a 24-well culture plate in 2 % serum-containing MEM extraction medium from all type of fibrous scaffolds for 1, 2, and 3 days. Figure 4.12 shows that the viability of MC3T3-E1, cultured with 2 % serum-containing MEM diluted with 1-day extraction media prepared by all types of modified scaffolds, was increased with increasing the culturing time in the respective media and the viability of cells on all types of material measured by MTT assay was more than 80 %. All of the obtained results clearly suggested that all types of the PCL fibrous scaffolds, released no substances at levels that were harmful to cells.

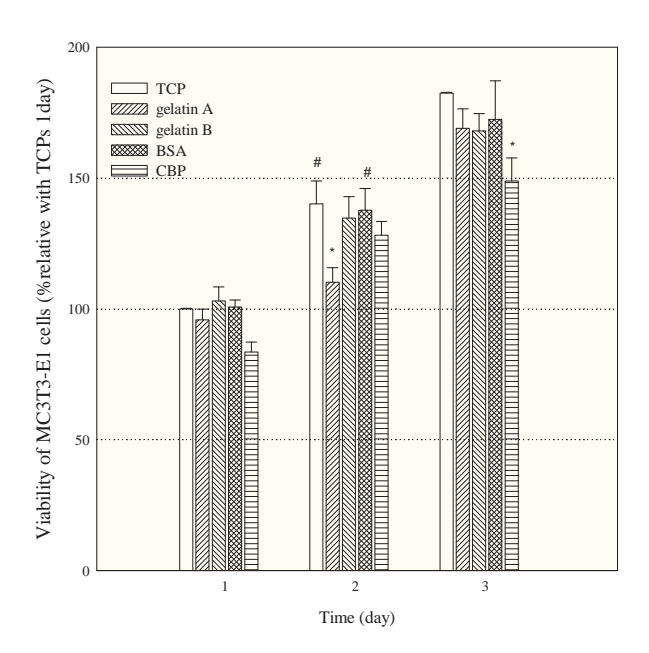


Figure 4.11The viability of MC3T3-E1, cultured with 2% serum-containing MEM extraction media adding with all types of proteins for 1, 2 and 3 days. Statistical significance: *p < 0.05 compared with control and *p < 0.05 compared to the neat PCL fibrous scaffolds at any given time point.

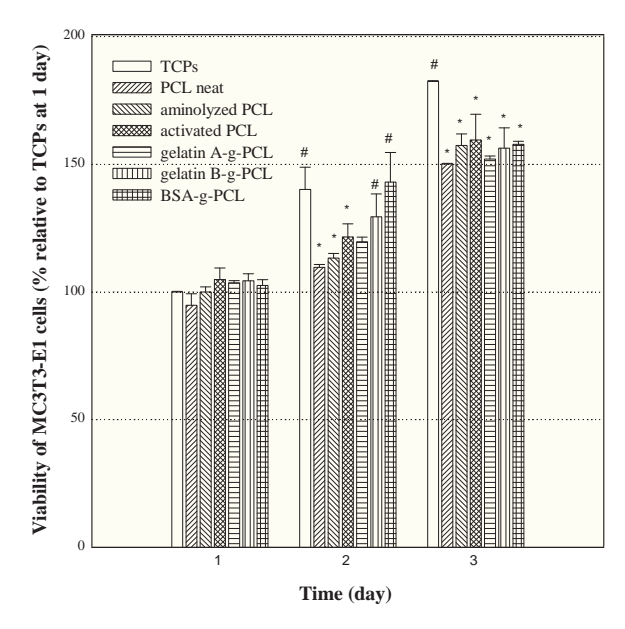


Figure 4.12 The viability of MC3T3-E1, cultured with 2% serum-containing MEM extraction media from all type of PCL fibrous scaffolds for 1, 2, and 3 days relative to TCPS at 1 day Statistical significance: *p < 0.05 compared with control and *p < 0.05 compared to the neat PCL fibrous scaffolds at any given time point.

4.4.2 Cell Attachment and Proliferation

The potential for use of the neat and the modified PCL fibrous scaffolds was further evaluated by determination their ability to support both the adhesion and the proliferation of MC3T3-E1. The viability of the cells that had been cultured on the surface of TCPS for 2 h was taken as the basis to arrive at the relative viability shown in a Figure. Figure 4.13 shows the attachment of MC3T3-E1 on the surfaces of TCPS, neat PCL, aminolyzed PCL, activated PCL, and protein-immobilized PCL at 2, 4, and 6 h after cell seeding in terms of viability. On TCPS, the number of the attached cells increased rapidly from ~100% at 2 h after cell seeding to ~257% at 6 h after cell seeding, based on the initial number of cells seeded (40,000 cells/well). While, the number of cells attached on these fibrous scaffolds was lower in comparison with that on TCPS at any given time point. There was the most viability of cells on crude bone protein-immobilized PCL fibrous scaffold among various types of the modified fibrous scaffolds. This obtained result suggested that the cells prefer to adhere on CBP-immobilized PCL fibrous scaffold rather than other modified scaffolds. However, The lesser viability of cells in the attachment period on various types of the fibrous scaffolds in comparison with that on TCPS could be due to the lesser number of cells that were able to

attach on the rough surface of the fibrous scaffolds in comparison with the smoother and hydrophilic surface of TCPS.

Figure 4.14 shows the proliferation of MC3T3-E1 on the surfaces of TCPS, neat PCL, aminolyzed PCL, activated PCL and protein-immobilized PCL on day 1, 2, and 3 after cell culture in terms of viability (%relative to TCPS at day1). On TCPS, the number of cells increased from ~100% at 1 day after cell culture to ~133 % at 3 days after cell culture, based on the initial 40,000 cells/well seeded. In comparison with that on TCPS, the viability of the cells cultured on various types of PCL fibrous scaffolds were significantly higher at any given time point. The viability of cells proliferated on these fibrous scaffolds, at day 3, was higher than TCPS of about (3 to 4) fold for neat PCL, aminolyzed PCL, and activated PCL and about 8 fold for all type of protein-immobilized PCL. The improvement was achieved with the protein-immobilized PCL fibrous scaffolds on day 3 after cell culture. The greater number of cells in the proliferation period on all types of fibrous scaffolds could be because of high surface area to volume and high porosity of the electrospun fibrous scaffolds through which the cells were able to penetrate into the scaffolds. Among the various modified PCL fibrous scaffolds, the BSA-immobilized PCL fibrous scaffolds provided the most significant improvement in the ability to support the proliferation of the cells which could be due to the protein-containing and more hydrophilic surface of the substrate.

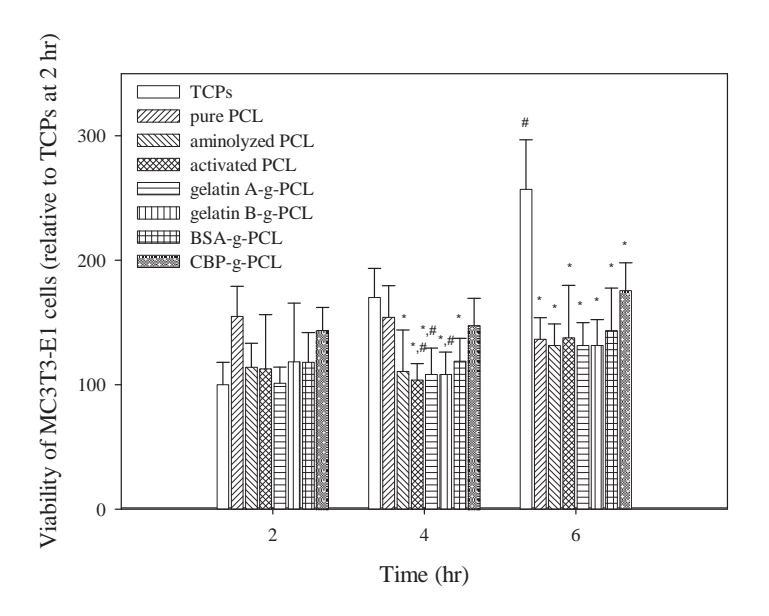


Figure 4.13 Attachment of MC3T3-E1 that had been seeded or cultured on the surfaces of TCPS and the neat and the modified PCL fibrous scaffolds for 2, 4, and 6 h. Statistical

significance: *p < 0.05 compared with control and *p < 0.05 compared to the neat PCL fibrous scaffolds at any given time point.

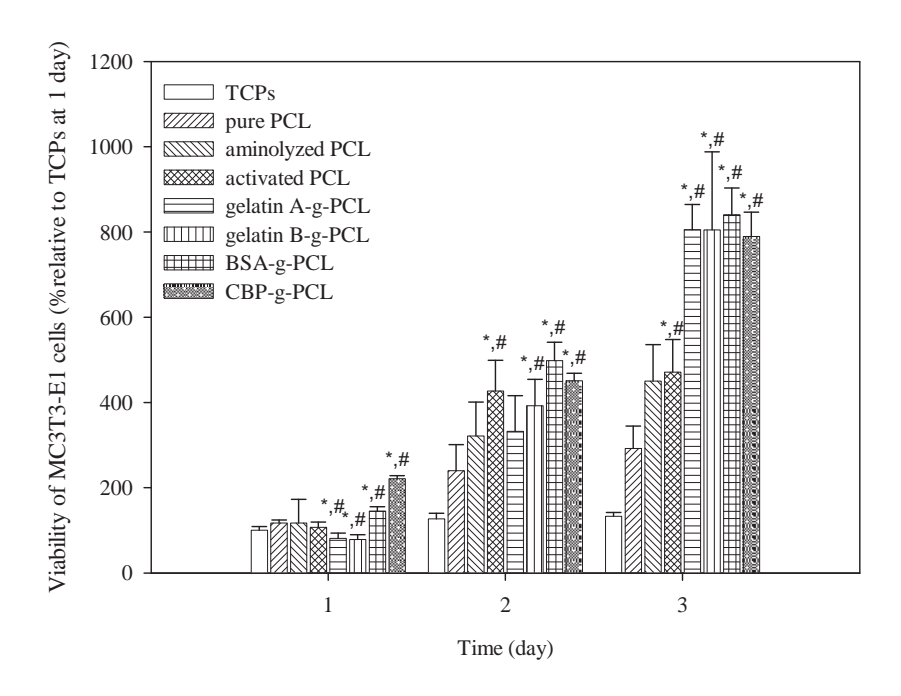


Figure 4.14Proliferation of MC3T3-E1 that had been seeded or cultured on the surfaces of TCPS and the neat and the modified PCL fibrous scaffolds for 1, 2, and 3 days. Statistical significance: *p < 0.05 compared with control and *p < 0.05 compared to the neat PCL fibrous scaffolds at any given time point.

4.4.3 Cell Morphology

Table 4.6 and 4.7 show selected SEM image (magnification = 2000X; scale bar = 10 μm) of MC3T3-E1 that were cultured on the surfaces of neat PCL, activated PCL and gelatin type-A, gelatin type-B, bovine serum albumin, and crude bone-immobilized PCL at different time points. These images provided snap shots in time that revealed the morphology of the cells and interaction between the cells and the tested surfaces. At 2 hours after cell seeding, based on the initial 40,000 cells/well seeded, the morphology of cells on almost all types of the modified PCL scaffolds became round. Exceptionally, the morphology of cells on BSA-immobilized and CBP-immobilized started to extend their cytoplasm and became ellipse. At 4 h after cell seeding, the majority of the cells on all types of modified PCL scaffolds extended their cytoplasm, an evidence of the ability of the cells to attach on the modified surface. At 6 h after cell seeding, expansion of the cytoplasm of the majority of the cells was evident. The majority of MC3T3-E1 that had been seeded on the surfaces of unmodified PCL

fibrous scaffolds for 4 h was remained round, but a closer examination around the edge of the cells revealed an evidence of filopodia. The majority of the cells were evidently expanded after 6 h of cell seeding. On the other hand, the majority of the cells seeded on the surfaces of various types of modified PCL fibrous scaffolds showed an evidence of the extension of their cytoplasm on the fibrous surface even at 4 h after cell seeding. These results suggested that the cells prefer the fibrous surfaces of modified PCL over that of the unmodified. At 1,2, and 3 days after cell seeding, the majority of the cells seeded on the surfaces of all types of modified PCL fibrous scaffolds expanded over the area of the scaffolds which was the most expansion on the surface of BSA-immobilized and CBP-immobilized PCL fibrous scaffolds. From the attachment, proliferation and cell morphology results, we can suggest that the cell prefer to grow and expand on BSA-immobilized and CBP-immobilized PCL fibrous scaffolds over other materials.

Table 4.3 Selected SEM images of cultured specimens, i.e., glass (i.e., control), neat PCL, aminolyzed PCL, activated PCL, and protein-immobilized PCL fibrous scaffolds at various time points after MC3T3-E1 were seeded on their surfaces (magnification = 2,000X; scale bar = $10 \mu m$)

Material	2 h	4 h	6 h
Glass (control)	- 3-2-2-2-2-100 Three 0000000	1500 21-00	15kU 32,000 100n 000000
Neat PCL			
Aminolyzed PCL			
Activated PCL			
Gelatin A immobilized PCL			
Gelatin B immobilized PCL			
BSA immobilized PCL			

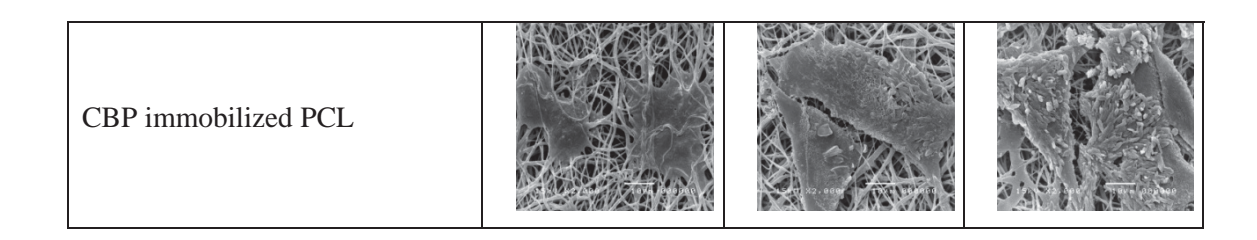
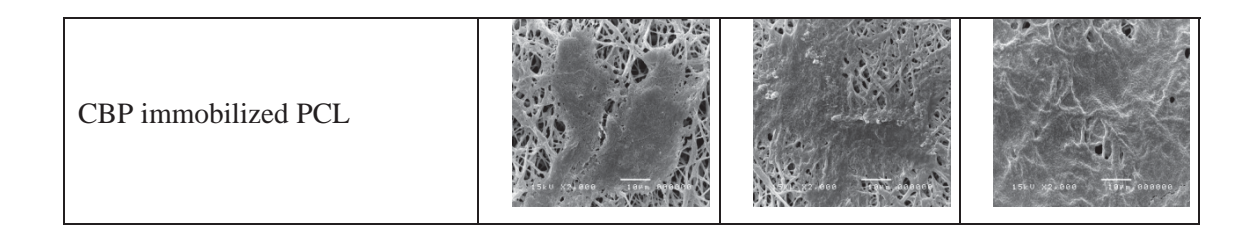


Table 4.4 Selected SEM images of cultured specimens, i.e., glass (i.e., control), neat PCL, aminolyzed PCL, activated PCL, and protein-immobilized PCL fibrous scaffolds at various time points after MC3T3-E1 were seeded on their surfaces (magnification = 2,000X; scale bar = $10 \mu m$)

Material	1 day	2 day	3 day
Waterial	2000x	2000x	2000x
Glass(control)	1510 92 000 100- 000000	1510 (2) 000 Torn 900000	15k0 x20000 10rm 000000
Neat PCL			
Aminolyzed PCL			
Activated PCL			
Gelatin A immobilized PCL			
Gelatin B immobilized PCL			
BSA immobilized PCL			



4.4.4 Alkaline Phosphatase Activity (ALP)

The ability for these PCL fibrous scaffolds to support differentiation, in addition to attachment and proliferation, of cultured cells is another important purpose suggesting potential for use of the scaffold. Alkaline phosphatase is used as an osteoblastic differentiation marker, as it is produced only by cells showing mineralized ECM. The ALP activity of MC3T3-E1 on TCPS (i.e. controls), neat PCL, aminolyzed PCL, activated PCL, and protein-immobilized PCL were evaluated at 3 and 7 days in culture. Figure 4.15 apparently shows the amount of ALP synthesized by the cells that were cultured on TCPS and all of the fibrous scaffolds increased with the initial increase in time in culture. In comparison with other substrates, BSA immobilized PCL fibrous scaffolds exhibited the highest ALP activity of MC3T3-E1 which is close to that of the activated PCL and TCPS at day 7 of cell culturing time. From the obtained results, it was suggested that BSA-immobilized PCL fibrous scaffold was the best among the fibrous scaffolds that promoted both proliferation and differentiation of MC3T3-E1. However, additional long term experiments in order to clarify the effect of scaffolds on the differentiation of osteoblasts are currently determined.

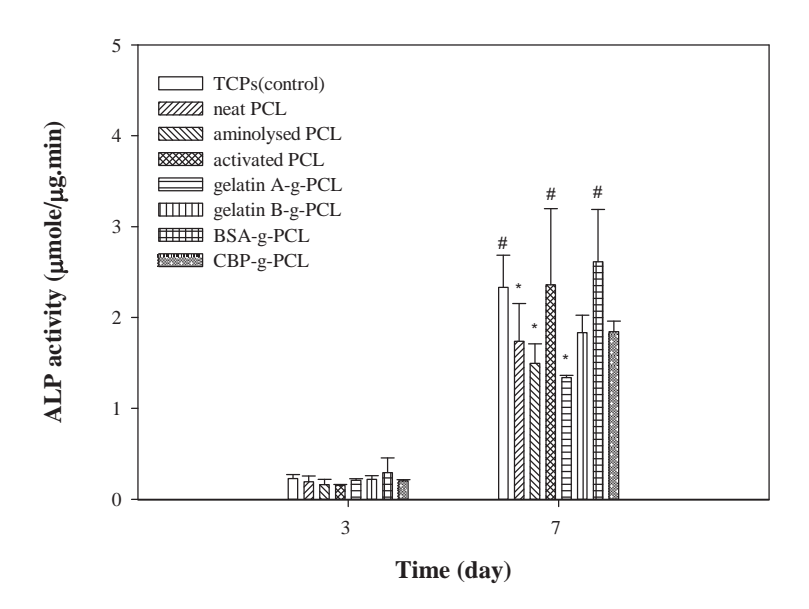


Figure 4.15Alkaline phosphatase activity (ALP) of MC3T3-E1 that were cultured on the surfaces of TCPS and the neat and the modified PCL fibrous scaffolds for 3 and 7 d. Statistical significance: *p < 0.05 compared with control and *p < 0.05 compared to the neat PCL fibrous scaffolds at any given time point

4.4.5 Mineralization

Mineralization was quantified by Alizarin Red-S which is a dye that binds selectively calcium salts. The strain was extracted with 10 % cetylpyridinium chloride in 10 mM sodium phosphate for 1 hour and the absorbance of collected dye was read at wavelength 570 nm in spectrophotometer (A Thermo Spectronic Genesis10 UV-visible spectrophotometer). The absorbance is relative to the quantity of deposited minerals on the materials as shown in Figure 4.16. The images of scaffolds seeded with MC3T3-E1 for 21 days and stained with Alizarin Red-S illustrated in Figure 4.17 confirmed that the above data where high intensity of stained minerals were observed on all type of immobilized PCL scaffolds. and. The CBP-immobilized PCL scaffolds showed the highest mineral deposition compared with control, neat PCL, and other modified materials. This result can be used to support that the crude bone protein immobilization is an attractive method to be used for fabrication of further developed fibrous scaffolds for bone tissue engineering.

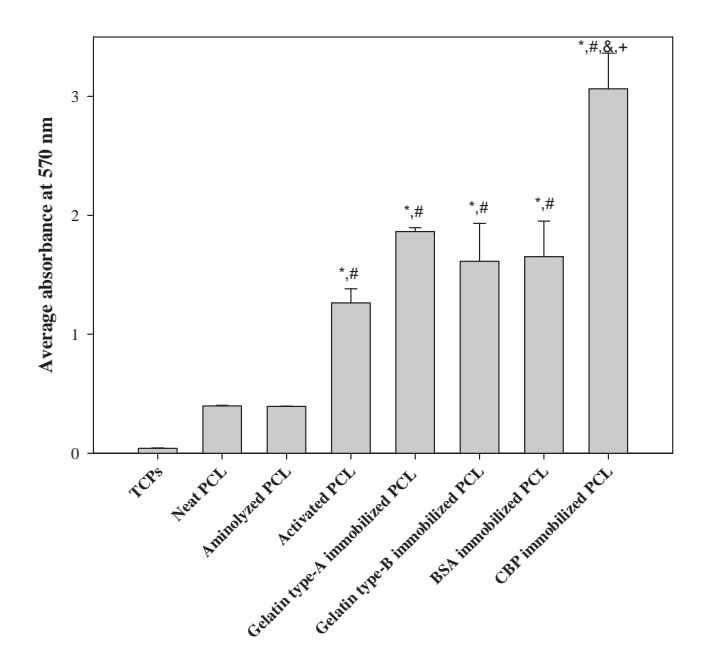


Figure 4.16 Quantification of mineral deposition in MC3T3-E1 at 21 d by the method of Alizarin Red-S staining measured the absorbance by UV-vis spectrometer at 570 nm. Statistical significance: *p < 0.01 compared with control, *p < 0.01 compared to the neat PCL, *p < 0.01 compared with gelatin type-A immobilized PCL, and *p < 0.01 compared with gelatin type-B immobilized PCL fibrous scaffolds at any given time point.

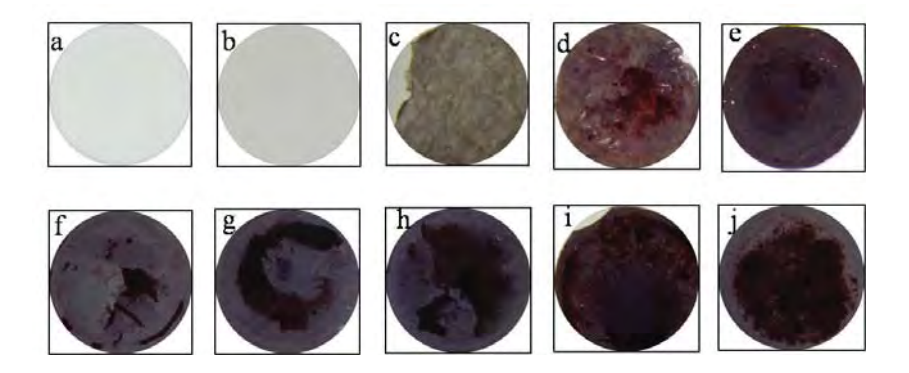


Figure 4.17Image of Alizarin Red-S staining for the mineralization in MC3T3-E1 cells for 21 d: TCPS without (a) and with (b) cells , neat PCL without (c) and with (d) cells, aminolyzed (e) and activated PCL (f), and gelatin type-A (g), gelatin type-B (h), bovine serum albumin (i) and crude bone protein (j) immobilized PCL fibrous scaffold

3. Conclusions

Polycaprolactone fibrous scaffolds were prepared by electrospinning process from a neat 12 % w/v PCL solution in 50:50 v/v DCM/DMF. The PCL electrospun fibrous scaffolds with a thickness of (130 \pm 5) µm were obtained. The scaffold was subsequently immersed in various concentrations of 1,6hexamethylene diamine (HMD) / isopropanol (IPA) solution (0.04, 0.06, 0.08, 0.10, 0.20, and 0.40 g/ml) for 2 hours at 30 °C. To determine the optimum concentration of HMD used in the step of aminolysis, ninhydrin method, degradation experiment, water retention experiment and SEM observation were used. The results show that the optimum condition for aminolysis are 0.20 g/ml HMD treatment for 2 hours at 30 °C. Density, porosity, and pore volume were evaluated to characterize the electrospun scaffolds. The NH₂ density on the aminolyzed PCL surface was confirmed and quantified using ninhydrin method. The NH₂ density increased with increasing 1,6-hexamethylenediamine concentration. However, when the concentration of 1,6-hexamethylenediamine is greater than 0.20 g/ml, the structural morphology of the electrospun PCL fiber scaffolds became worse. In the other word, water contact angle slightly decreased with increasing HMD concentration. This means that aminolysis can improve the hydrophilicity of the surface. Macromolecules i.e. gelatin type-A, gelatin type-B, bovine serum albumin, and crude bone protein were further immobilized using N,N'-disuccinimidyl carbonate (DSC) as a coupling agent. Various techniques; Attenuated Total Reflectance-Fourier Transform Infrared Spectrometer (ATR-FTIR), X-ray Photospectroscopy (XPS), Scaning Electron Microscopy (SEM), and water contact angle measurement were used to monitor the scaffold surfaces after each modification step. In XPS experiment, The N_{1s}/C_{1s} ratio was increased after immobilization with proteins (gelatin type-A, gelatin type-B, bovine serum albumin and crude bone protein) due to the large amount of nitrogen atom in protein structure was introduced. The potential use of the surface-modified PCL scaffolds as bone scaffolds was evaluated with a murine pre-osteoblastic cell line (MC3T3-E1). The cytotoxicity test showed all types of proteins and PCL fibrous scaffolds released no substances at levels that were harmful to cells. The number of cells attached on these fibrous scaffolds was lower in comparison with that on TCPS at any given time point. There was the most viability of cells on crude bone protein-immobilized PCL fibrous scaffold among various types of the modified fibrous scaffolds. MC3T3-E1 proliferation was improved remarkably on the modified surface, with the cells growing on the bovine serum albumin-immobilized PCL fibrous scaffolds showing the greatest proliferation after cell culture as well as the highest ALP activity. In long term experiments, the image of scaffolds seeded with MC3T3-E1 for 21 days and stained with Alizarin Red-S and quantification of deposited minerals measured by UV-vis spectrometer confirmed that high intensity of stained minerals were observed on all type of immobilized PCL scaffolds. The CBP-immobilized PCL scaffold showed the

highest mineral deposition compared with control, neat PCL, and other modified materials. This result supported that the crude bone protein immobilization was able to induce the cell differentiation to bone the most. All the obtained results suggested that bovine serum albumin and crude bone protein immobilization are an attractive method to fabricate of further developed fibrous scaffolds for bone tissue engineering.

4. DEVELOPMENT OF POROUS HYDROXYAPATITE PARTICLES AS CARRIERS OF PROTEINS FOR BONE TISSUE ENGINEERING

Experimental section

4.1 Materials

- Dicalcium phosphate dihydrate (DCPD; Fluka, Germany)
- Calcium carbonate (CaCO₃; Carlo Erba, Italy)
- Tris-base (Tris[hydroxymethyl]amino methane) (Sigma-Aldrich, USA)
- Nitric acid (ACS reagent 69%; J.T.Baker, USA)
- Ovalbumin (OVA; Sigma-Aldrich, USA)
- Gelatin type B (Sigma-Aldrich, USA)
- Bovine serum albumin (BSA; Sigma-Aldrich, USA)
- Sodium phosphate monobasic (NaH₂PO₄) and sodium phosphate dibasic (Na₂HPO₄; Ajex Finechem, Australia)

4.2 Preparation of Protein-Loaded Hydroxyapatite

Calcium hydrogen phosphate dihydrate (CaHPO₄.H₂O, DCPD) and calcium carbonate (CaCO₃) were used as precursors of Ca and P to prepare protein-loaded hydroxyapatite. The molar ratios of Ca to P were fixed at 1.67 which mixed with nitric acid 1 mol/l at 75 °C for 1 h under stirring. Then, pour distilled water at room temperature following protein. Ovalbumin (Sigma-Aldrich A-5253), Gelatin type B, Bovine serum albumin (BSA, Aldrich A-3912) and Crude bone protein from pork bone were selected as candidate proteins in this study. The proteins aqueous solution were prepared by dissolving proteins powder or pellet into distilled water for each synthesis. Regulated pH at a constant value, tris(hydroxymethyl) aminomethane. The aggregates were rinsed with the distilled water until pH=7 (DI water was boiled and decarbonated before use) and further centrifuged at 4500 rpm for 10 mins, freezed at -45 °C and lyophilized at -50 °C. The samples were kept in dessicator until used.

4.3 Crude Bone Protein preparation

CBP was extracted from the pork bone. In particular, bone was initially washed and cleaned thoroughly in tap water and then sectioned into small pieces with a high speed motor machine. Pieces of bones were further crushed into powder in liquid nitrogen. Then, the as-prepared powder was immersed in 0.6 N HCl at 4 °C. After three days, the bony solution was centrifuged and the supernatant was collected, dialyzed for 48 h and lyophilized. The dry CBP was kept in desiccators until use (Hariraksapitak, *et al.*, 2009).

4.4 Characterization

4.4.1 Thermogravimetric Analysis (TGA)

The relative amount of the proteins associated with the HAp was determined using thermogravimetric analysis, TG-DTA (Perkin Elmer) instrument under N_2 flow of 5 ml/min. The heating process was conducted from 30-950 °C at a rate of 10 °C/min.

4.4.2 Fourier-transformed infrared spectrophotometer (FT-IR)

A Thermo Nicolet Nexus[®] 670 Fourier-transformed infrared spectrophotometer (FT-IR) was used to investigate chemical functionalities of hydroxyapatite powder by the KBr disk method. Hydroxyapatite powders were randomly selected from each group of samples and detected for the FT-IR spectra with a resolution of 4 cm⁻¹ in the range of 4000-400 cm⁻¹ and were averaged from 32 scans.

4.3 Autosorb-1

The BET method uses gas with a known adsorption area per 1 g to measure the surface area of samples based on gas quantites adsorbed to the sample surface. Fifty mg of the sample was preheated at 200 °C for 10 min to remove water and gas completely. Surface areas of HAp particles were analyzed by nitrogen adsorption in a Autosorb-1.

4.4 Scanning Electron Microscope (SEM)

For the morphological study, hydroxyapatite were mounted on brass stubs, coated with gold using a JEOL JFC-1100 sputtering device, and observed for their microscopic morphology using JEOL JSM-5200 scanning electron microscopy (SEM). For the morphology of the surface, pore size, distribution and also the interconnectivity.

4.5 Transmission Electron Microscope (TEM)

The microstructural and morphological features of HAp powders were analysed in JEM-2100 operating voltage of 200 kV. Sample for TEM were prepared by air-drying a drop of a sonicated ethanol suspension of particles onto a carbon-coated copper grid and air-dried.

4.6 Energy Dispersive Spectrophotometer (EDS)

The Ca/P ratio of the hydroxyapatite was studied by the X-ray microanalysis, using the method of Energy dispersive X-ray spectroscopy (EDS). EDS is an analytical technique used for the elemental compositions of the HAp.

4.7 X-ray Diffraction (XRD)

The phase compositions, crystal shape and size of HAp powders were characterized by X-ray diffraction (XRD) with copper target. Data were collected over the scanning range (2θ) from 5 ° to 60 ° at a scan speed 2 °/min.

The average crystallite size of the prepared hydroxyapatite samples was determined using the scherrer equation.

$D = K \cdot \lambda / \beta \cdot Cos\theta$

In which D is the average crystallite size (Å), K denotes the shape factor (K=0.9), λ is the X-ray wavelength (for CuK α λ =1.5418 Å), β represents the peak at half width (in rad), and θ is the Bragg angle of the peak (002 reflection of hydroxyapatite at 2θ =26°).

4.8 UV-Visible Spectrophotometer

Determination of protein by UV/Vis spectrophotometry at $215~\mathrm{nm}$ for Gelatin type B, $280~\mathrm{nm}$ for OVA and BSA and $275~\mathrm{nm}$ for CBP.

4.9 Zeta potential (ZP)

Zeta potentials (or electrophoretic mobility) of the hydroxyapatite were determined using Zeta-Meter 3.0+ (Zeta-Meter, Inc., USA). Briefly, the suspension of 100 mg hydroxyapatite in 20 ml of deionized water was filled in an electrophoresis cell. Two electrodes were inserted into the cell and connected to the Zeat-Meter 3.0+ unit. Once the electrodes were energized, microspheres were aroused to move toward one electrode. Particles were observed under a microscope for its movement along a specific distance which was indicated by a built in grid. The zeta potential value was detected at a right time point when the microsphere moved to the end. Measurement was repeated 10 times for each preparative condition and the average values were calculated.

4.10 Particle size distribution

The Malvern Particle size of hydroxyapatite was measured by Mastersizer 2000 a solution of the particles was sonicated in an ultra-sonic bath for 7 min immediately before measurement to ensure separation of particles. A sample of this mixture was injected into the sample cell of the Malvern Mastersizer. The obscuration was between 10 and 30 %, as required by the instrument. The Mastersizer calculates automatically the particle size and distribution from small angle light scattering using Mie theory and Fraunhofer diffraction theory. The measurements were taken with the stirrer in the Mastersizer to ensure even distribution of particles and prevent sedimentation in the sample cell. Shear forces were not a

problem in this case as the goal was to measure the primary particle size. A least 10 measurements were recorded and the average value recorded.

4.11 In vitro protein-HAp release test

Proteins-loaded Hydroxyapatite (20 mg) were dispersed in 10 ml 0.1M phosphate buffer saline (PBS) solution at pH 7.4. All samples were incubated in a shaking water bath (70 rpm) at 37 °C. The releasing medium was withdrawn 1 ml and an equal amount of fresh medium was added to maintain a constant volume of the medium. The amount of protein in the sample solution was determined by UV-visible spectroscopy. Absorbance peaks at 280 nm to determine the ovalbumin and BSA concentration, 215 nm to determine the gelatin type B, and 275 nm to determine the crude bone protein. Concentration through the use of a pre-determined standard concentration—intensity calibration curve. An average value was calculated at each time point. The protein content of the encapsulated particles can be described by two quantities in terms of Encapsulating efficiency of protein-loaded hydroxyapatite (EE) and Loading capacity of hydroxyapatite particle (LC), which were determined according to the following equation (Freiberg and Zhu, 2004).

Encapsulating efficiency (%) = total mg proteins-encapsulated x 100 initial mg proteins-loaded

Loading capacity (%) = total mg proteins-encapsulated x 100 total mg particles

4.4 Results and Discussion

4.4.1 Thermogravimetric Analysis (TGA)

The samples were analyzed by TGA using a Perkin Elmer (TG-DTA) instrument under N_2 flow of 5 ml/min. The heating process was conducted from 30-950 °C at a rate of 10°C/min. To investigate amount of proteins-loaded hydroxyapatite.

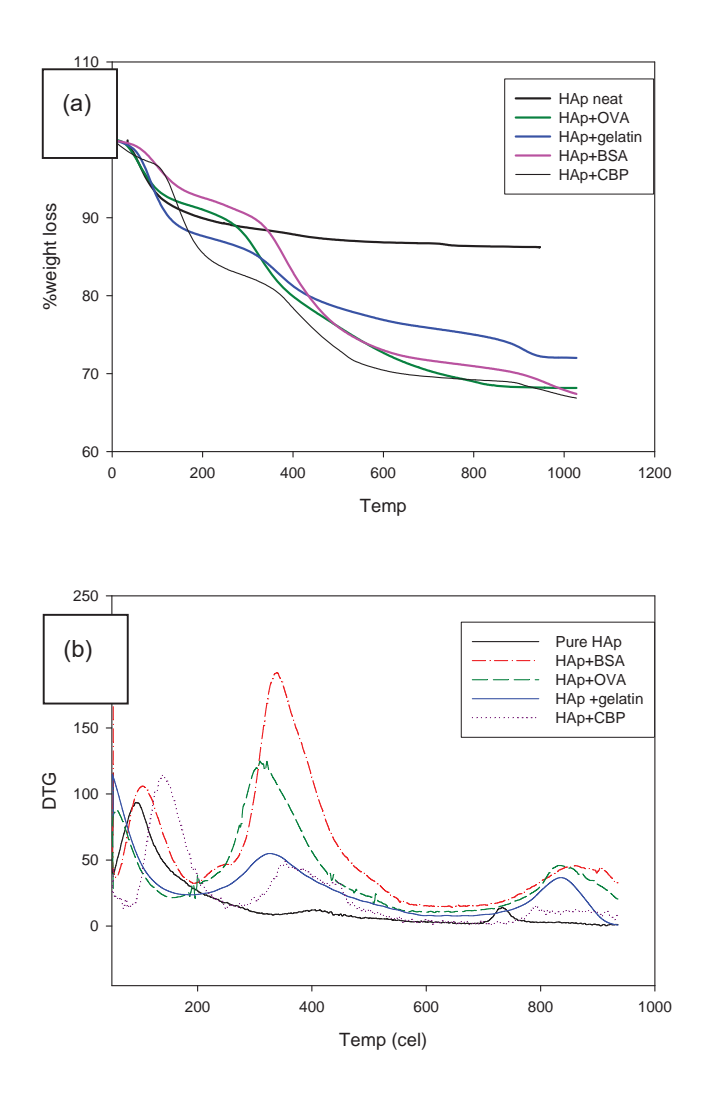


Figure 4.1 TGA-DTG curves (a) TGA, (b) DTG of proteins-loaded hydroxyapatite.

The features of TGA and DTA profiles of proteins-loaded hydroxyapatite were presented in Figure 4.1. The weight loss could be differentiated into three regions in the investigated temperature range such as (i) 25-210 °C, (ii) 210-570 °C, and (iii) 750-950 °C. In the first region of 25-210 °C, the weight loss for all precursors could be attributed to the removal of physically absorbed water. The second region of 210-570 °C is a major weight loss, probably due to the combustion of proteins residuals (organic matter) and with the maximum rate at 350 °C, and decomposition of calcium hydroxide and carbonate to water and carbon dioxide. The third region of 750-950 °C, the weight loss can be assigned to the decomposition of carbonate compounds.

The TGA curves of the samples (Figure 4.1) show differences in the amount of protein weight loss. Weight loss of ovalbumin was 16.8 %, Gelatin type B was 10.22 %, BSA was 20.61 % and CBP from pork bone was 22 %.

4.4.2 <u>UV-Visible Spectrophotometer</u>

Take water after finish synthesis reaction measured by UV-Visible to determine the remaining protein after reaction. OVA and BSA were measured the wavelength with 280 nm, Gelatin type B with 215 nm and CBP from pork bone with 275 nm.

To investigate amount of proteins-loaded hydroxyapatite. Remaining OVA in the DI water is 6.12 %, Gelatin type B is 14.30 %, and BSA is 2.38 %. So, OVA, Gelatin type B, and BSA are entrapped in hydroxyapatite 20.26 %, 12.08 %, and 24% respectively. It is possible that protein may be lost during the washing HAp with DI water about 5-6 times to become neutral.

4.4.3 X-ray Diffraction

In the X-ray diffraction analysis, all synthesized precipitates showed a HAp-like pattern (Figure 4.2). The crystallinity of each precipitate was evaluated from the data of the inverse of half value breadth of the (002) peak of HAp (Figure 4.2). The crystallinity of HAp depends on its synthesized temperature in such a way that HAp synthesized at low temperature has low crystallinity. The solubility of HAp also depended on its synthesized temperature and HAp synthesized at low temperature showed high solubility (Matsumoto, T. *et al.*, 2004).

For HAp powders, the crystallite size in a direction perpendicular to the crystallographic plane is always estimated according to Scherrer's formula as followed:

 $d = (0.9\lambda) / FWHM*Cos\theta$

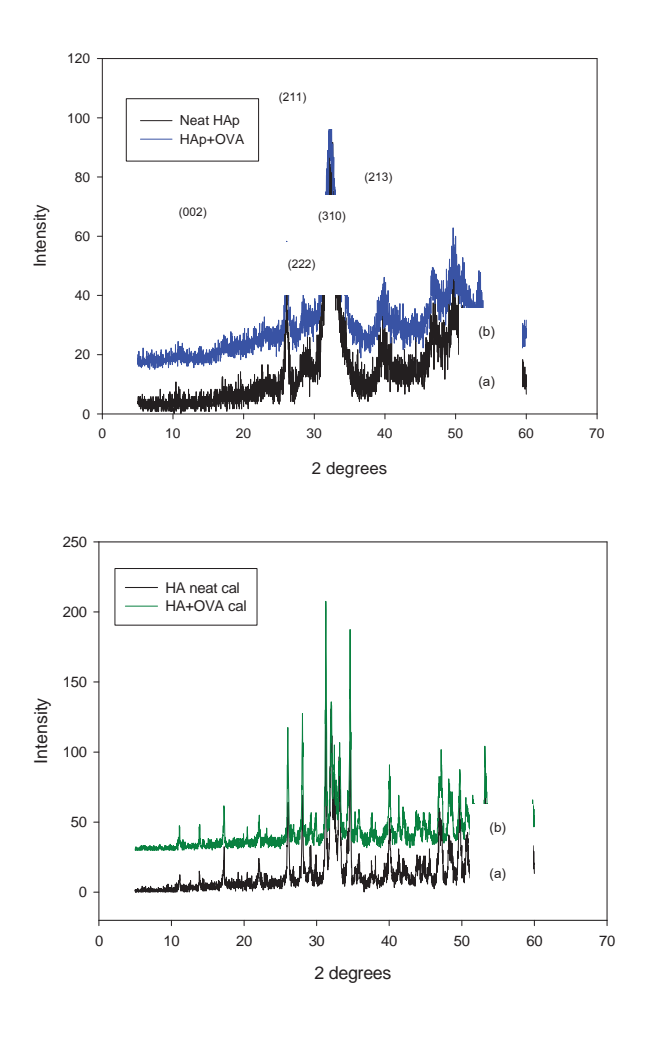


Figure 4.2 XRD pattern of HAp powders: (a) Neat HAp; (b) OVA-loaded HAp.

where d is the crystallite size (nm); λ =0.15406 nm for Cu K α radiation of X-ray beam; FWHM the full width at half maximum for the diffraction peak (rad); and θ is the Bragg angle of the (002) diffraction angle (°). Two major characteristic diffraction peaks could be obtained for all the powdered samples: one closed at 2 θ of ~26° and the other broad one at ~32°. According to PDF no.01-1008, The uncalcined HAp is shown the broad patterns around at (002) and (211). It indicates that the crystallites were very tiny in nature. The (002) peak (2 θ ~26°) from XRD patterns was chosen for calculating the crystallite size as shown in Table 4.1 since it contains the least overlap of the broadened peaks. It could be found that the crystallite size depends on the size of the particle that observed from SEM. Crystallite size of calcined HAp powders was larger than uncalcined powder. Figure 4.2 indicated

(b)

that uncalcined HAp powders were amorphous and did not form CaP crystals, because HAp crystallization is mediated by protein and shown in Figure 4.3.

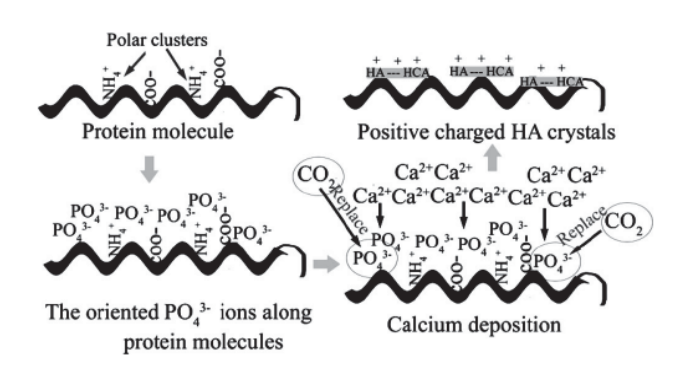


Figure 4.3 Schematic illustration of the protein-medicated crystallization of HAp crystals with positive charges (Zhao, H. *et al.*, 2008).

Table 4.1 The different crystallite size of (a) calcined HAp at 800 °C; (b) uncalcined HAp powder (a)

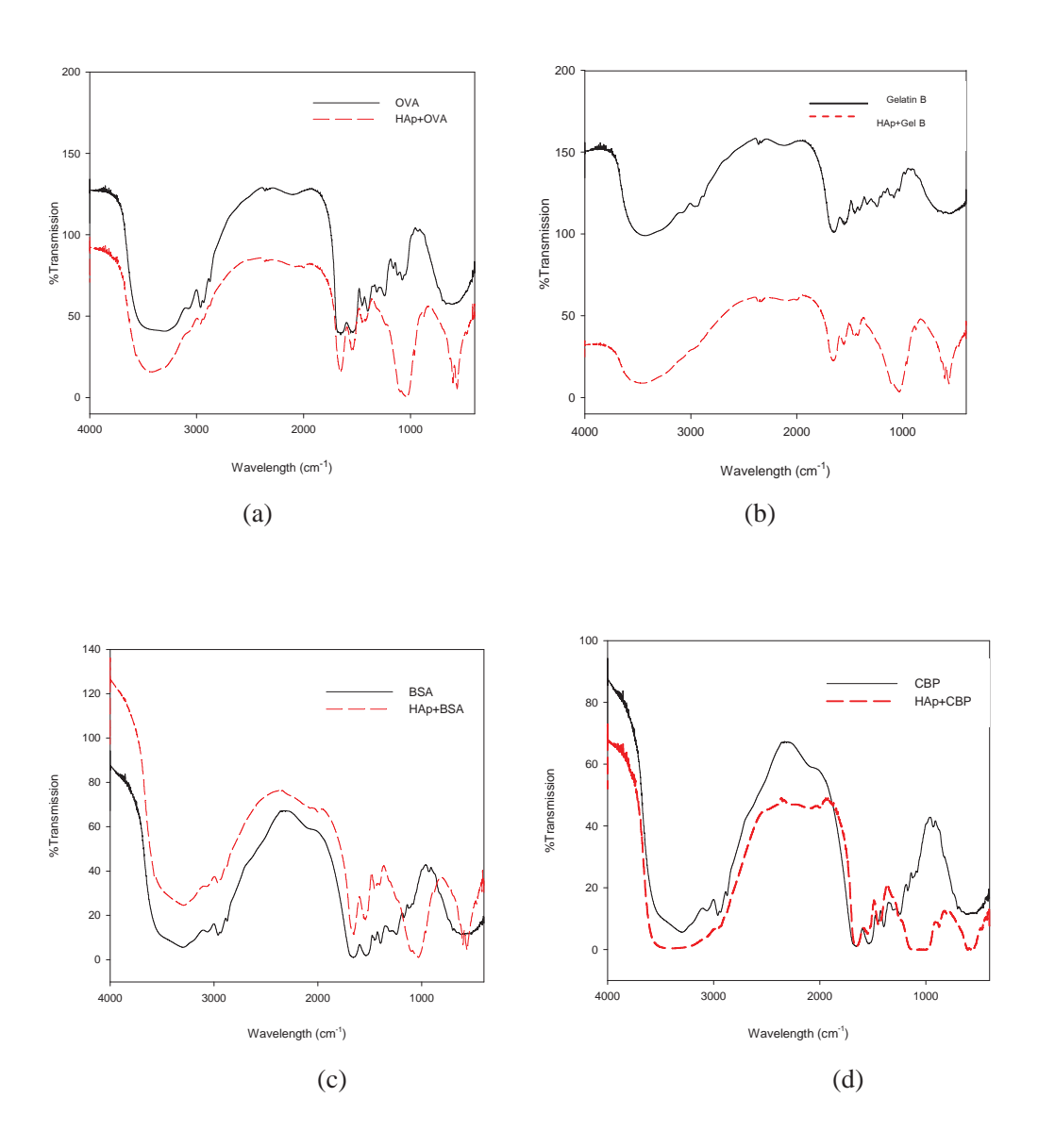
Crystallite size Crystal plane (002) 2θ **FWHM** (nm) Neat HAp calcine 0.22 40.01 26.07 OVA-HAp calcine 26.05 0.15 58.16 Gealtin-HAp calcine 0.23 26.00 38.37 BSA-HAp calcine 25.82 0.23 37.03

Crystal plane (002)	2θ	FWHM	Crystallite size (nm)
Neat HAp uncalcine	26.11	0.44	20.45
OVA-HAp uncalcine	26.12	0.51	17.69
Gelatin-HAp uncalcine	25.80	0.51	19.37
BSA-HAp uncalcine	25.91	0.51	16.88

4.4.4 Fourier-Transformed Infrared Spectrophotometer

Adsorption of protein on HAp particles was detected by FTIR analysis (Figure 4.4). The spectra show the characteristic peaks of absorbed water, hydroxyl, phosphate and carbonate species. The broad peak around 3250 cm⁻¹ to 3500 cm⁻¹ corresponds to the adsorbed water. The spectrum clearly indicates a peak at 1640 cm⁻¹ which is attributed to the presence of water associated with HAp. The

absorption bands at 1460 cm⁻¹ and 875 cm⁻¹ suggest the presence of CO₃²⁻. The absorption bands at 1040, 1093, 962 and 571 cm⁻¹ detected in the spectra are attributed to the PO₄³⁻ ion. The absorption bands at 1210 cm⁻¹ together with one at 1130 cm⁻¹ and clear absorption band at 879 cm⁻¹ are attributed to the HPO₄²⁻. The spectrum of protein exhibited an appearent absorption band at 1654 cm⁻¹ assigned to amide I, C=O stretching mode. The absorption band at 1540 cm⁻¹ assigned to amide II, N-H bending mode and 1384 cm⁻¹ assigned to amide III, C-N stretching mode and N-H bending mode.



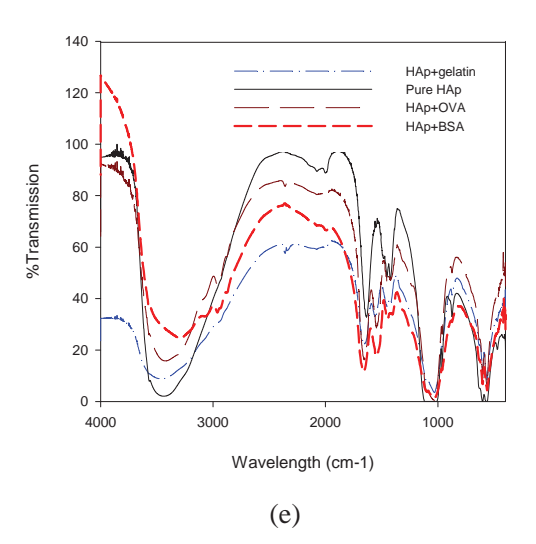


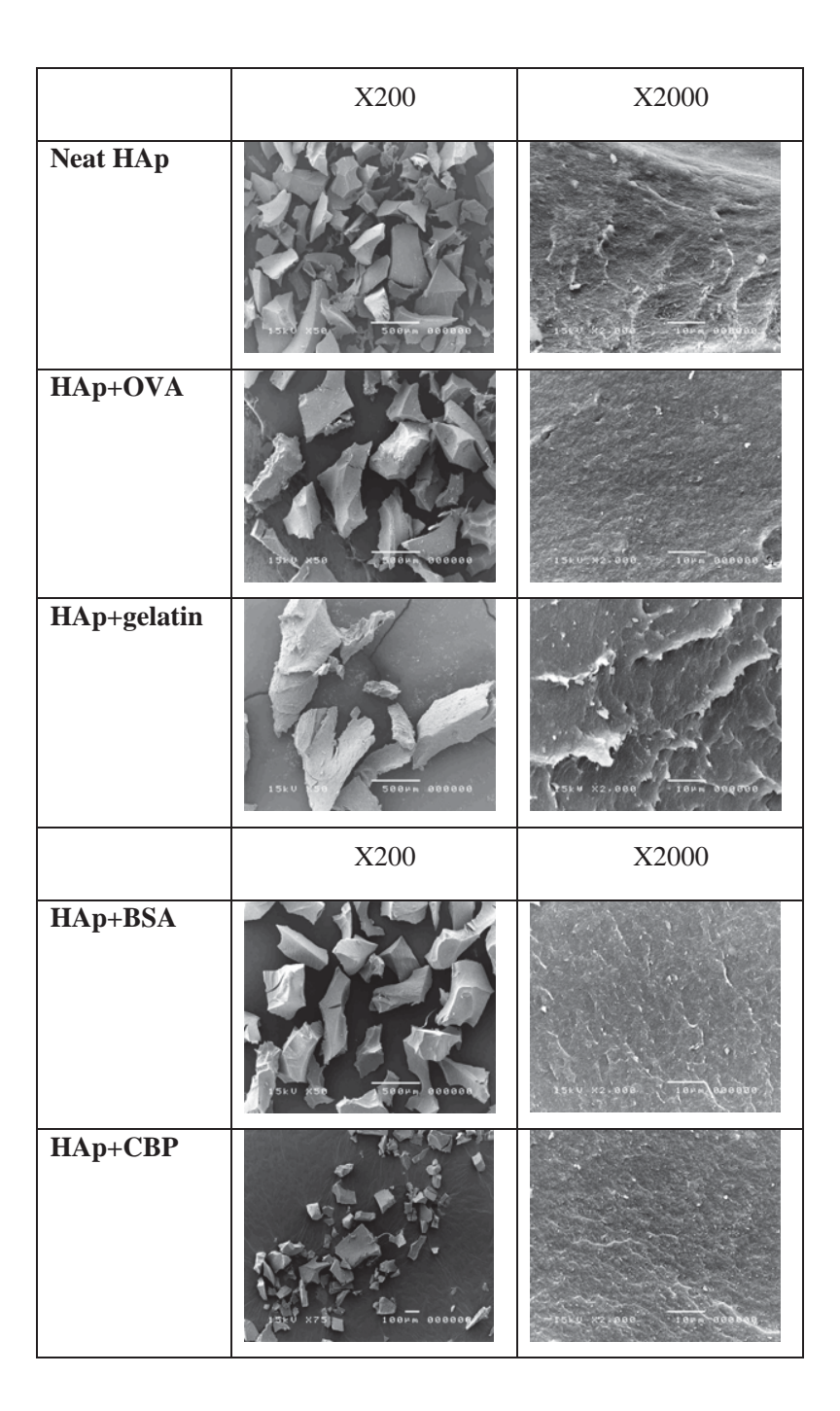
Figure 4.4 The FTIR spectra of HAp powders of : (a) OVA-loaded HAp; (b) Gelatin-loaded HAp; (c) BSA-loaded HAp; (d) CBP-loaded HAp; (e) including protein/HAp.

The possible mechanisms can be adapted to explain the interaction between the HAp and proteins molecules. The mechanism can be operated through the electrostatic interaction between the positive Ca²⁺ and COO⁻ (protein): this has been also reported by Liu who suggested that there is an intermediate complex between COO- and HAp. This complex can be formed via the electrostatic interaction between the negative COO⁻ on protein molecules and positive Ca²⁺ on the C-sites of HAp surface. Kazuhiko K. indicated that the C-sites were located on the crystal planes that are perpendicular to a-axis and b-axis of apatite crystal.

4.4.5 Scanning Electron Microscope (SEM)

To investigate the morphology of HAp powder by using SEM (JEOL, model JEM-5200). It is found that HAps have an arbitrary shape. Some gelatin grafting on the surface of HAp shown in Table 4.2.

Table 4.2 SEM of proteins-loaded HAp powder



4.4.6 <u>Transmission Electron Microscope (TEM)</u>

Figure 4.5 shows the TEM photographs of HAp powders obtained neat HAp and proteins-loaded HAp. The HAp powders contain agglomerated particles consisting of rod-like shaped particle. Neat HAp powders are the short-rod crystal than proteins-loaded HAp. It is found that there are not much differences in morphology and size from the photographs of proteins-load HAp samples.

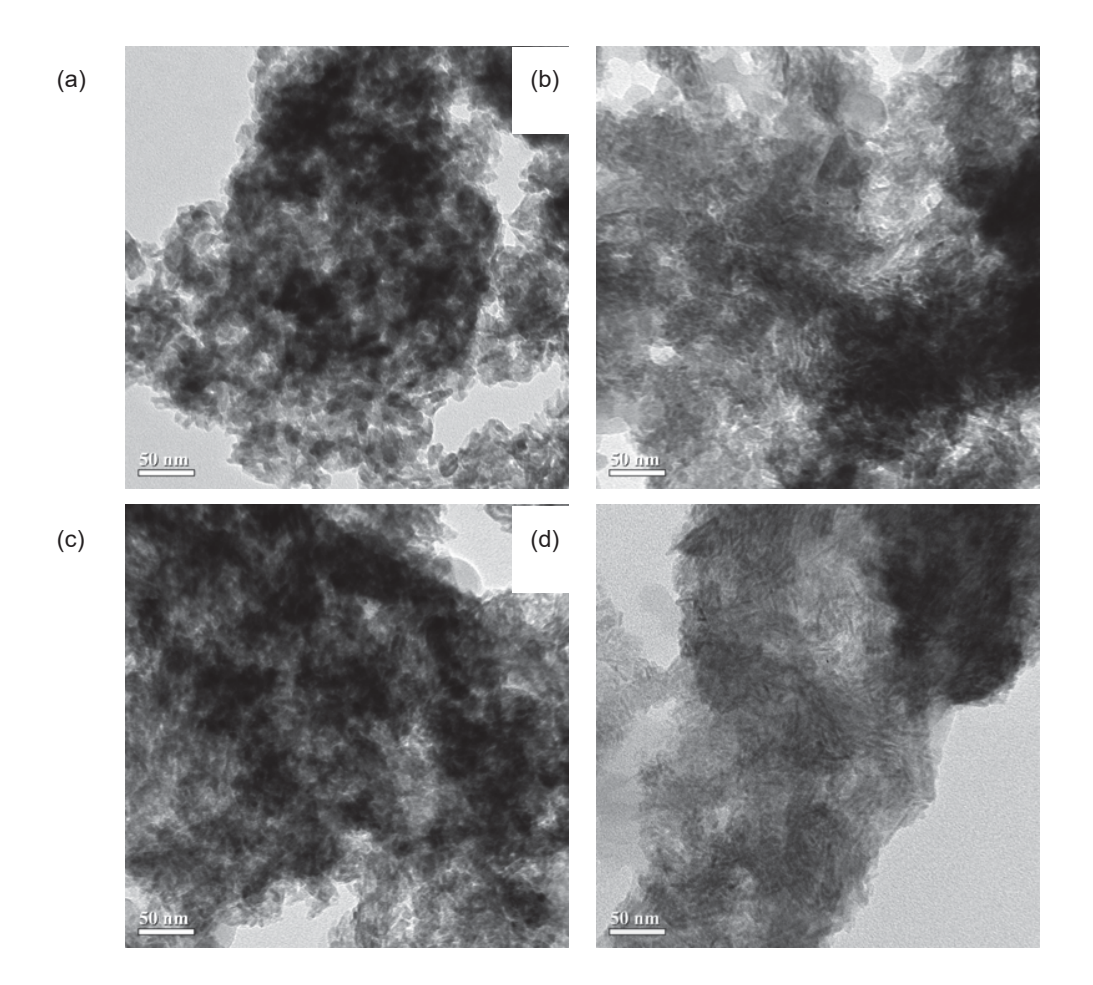


Figure 4.5 TEM micrographs of proteins-loaded HAp powder : (a) Neat HAp; (b) OVA-loaded HAp; (c) Gelatin-loaded HAp; (d) BSA-loaded HAp.

4.4.7 Zeta Potential (ZP).

Twenty mililiter of the suspension was placed in an electrophoresis cup, and the movable images of the particles were recorded by the electrophoresis apparatus. The value would also be beneficial in the study of protein-loaded HAp and releasing through HAp particles. The zeta potentials were measured by appling the electric field in the dispersion and particles in the dispersion will be migrated to electrode of opposite charge. Protein-loaded HAps were dispersed in the DI water pH about 6-7 if protein can releases from HAp, it will be showed negative charge, so zeta potential is the positive. The zeta potentials of all the samples are negative, indicating that the particles themselves have superfluous positive electrical charges. It was indicated that protein entrapped in the HAp particle

The electrical conductivities values were so close as ~ -18, -16, and -20 mV for neat HAp, OVA-loaded HAp, and Gelatin B loaded HAp particle, respectively. Zeta potential is an indicator of charge

density (Brown et al., 1998). Particle size of Gelatin B-loaded HAp is the largest, so it has the highest charge density.

4.4.8 Energy Dispersive Spectrophotometer

The EDS spectrum from HAp particles (Figure 4.6) shows the characteristic peaks of calcium (Ca), phosphorus (P), and oxygen (O). EDS is composed mainly of HAp and exhibits a molar Ca/P ratio of 1.67.

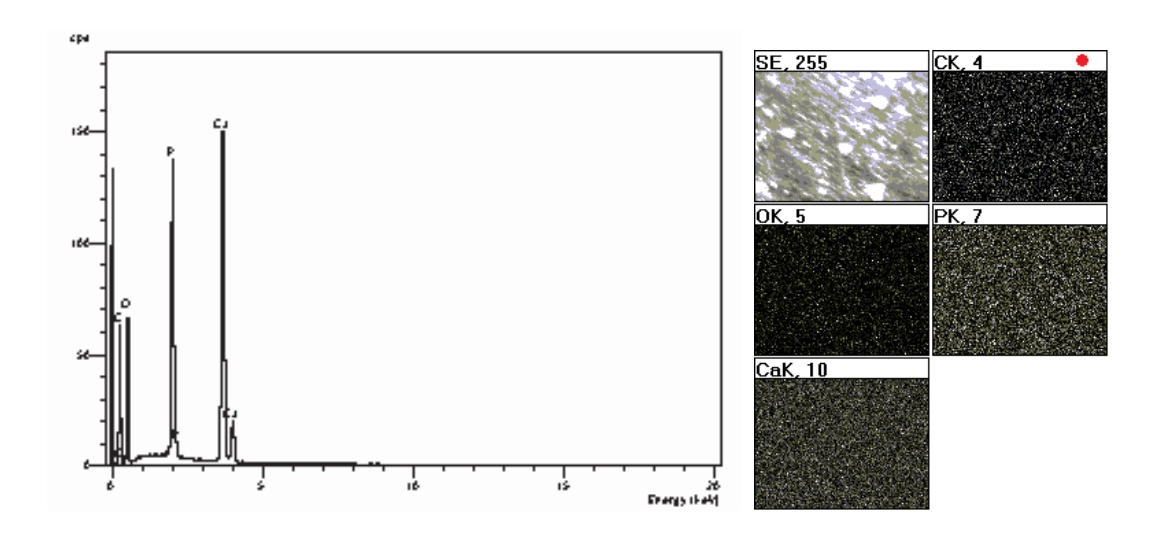


Figure 4.6 EDS spectrum of the biomimetic apatite layer deposited.

4.4.9 <u>The Brunauer—Emmett—Teller (BET)</u>

Surface areas and pore size of the powders were analyzed by nitrogen adsorption in Autosorb-1. The BET surface areas of the calcined samples at 800 °C are summarized in Table 4.3. We found that they are a few differences in surface area and pore size of neat and proteins-loaded HAp. Pore size of proteins-loaded HAp are a few larger than neat HAp due to the existence of pores after the removal of organic materials (proteins) so, surface area of proteins-loaded HAp are a few lower than neat HAp.

Table 4.3 BET surface area and pore size of the calcined samples at 800 °C

	Surface area (m ² /g)	Pore size (nm)
Neat HAp	22.64	8.75
OVA-loaded HAp	19.65	9.35
Gelatin-loaded HAp	20.06	11.42
BSA-loaded HAp	20.99	12.14

4.4.10 Particle size distribution of Hydroxyapatite

We were ground and sieved through a mesh size of 400 micron of protein-loaded HAp particles. About twenty miligrams of HAp were dispersed in water. The size distributions of HAp were measured by light scattering using particle sizer (Malvern, UK). The average particle size distributions of neat HAp and proteins-loaded HAp were about 316 μ m.

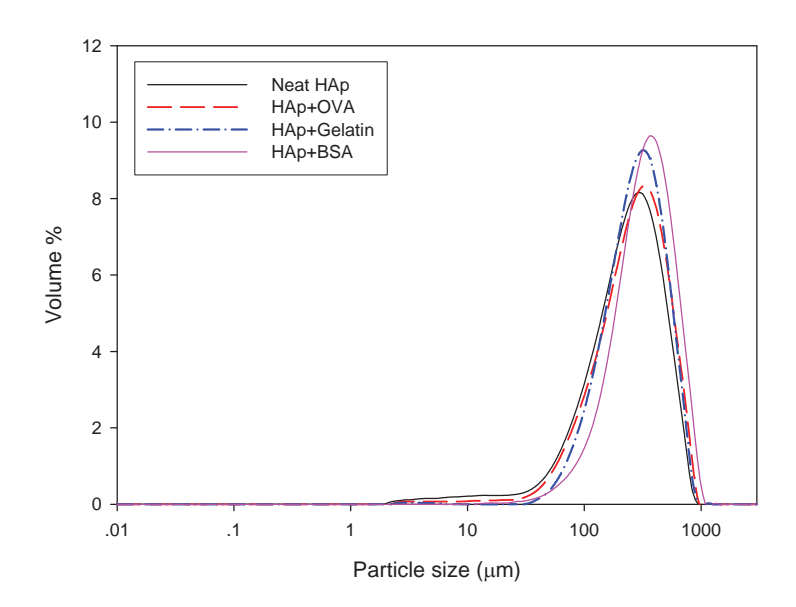


Figure 4.7 Average particle size distribution of Hydroxyapatite.

4.4.11 Controlled Release of Proteins from HAp particles

The protein content of the encapsulated particles can be described by two quantities in terms of encapsulating efficiency of protein-loaded hydroxyapatite (EE) and loading capacity of hydroxyapatite particle (LC). For encapsulating efficiency of protein-loaded hydroxyapatite (EE), the proteins release from hydroxyapatite in phosphate buffer saline solution pH 7.4 was shown in Figure 4.8. The release profile of OVA, BSA and CBP were shown long-term proteins release at least 3 week. The maximum accumulative releases were about 50 % - 60 %. For the release profile of gelatin type B, it was shown the bursting release. The accumulative release was about 12 %. For loading capacity of proteins-loaded hydroxyapatite (LC), the proteins release from hydroxyapatite in phosphate buffer saline pH 7.4 was shown in Figure 4.9. The LC of OVA, BSA, and CBP from HAp particles were shown maximum accumulative releases were about 8-12 %. For the LC of Gelatin type B from HAp particle was shown maximum accumulative releases was about 1 %. Encapsulation of proteins into hydroxyapatite particles in this study was on the basis of polyion complexation. It was expected that a degree of molecular interaction was able to take place between proteins and hydroxyapatite particles of opposite charges (Young *et al.*, 2005); as a consequence, a higher yield of the ionic complexes should result in higher encapsulation efficiency and loading capacity (Tabata and Ikada, 1998; Hoffman, 2002; Young *et al.*, 2005).

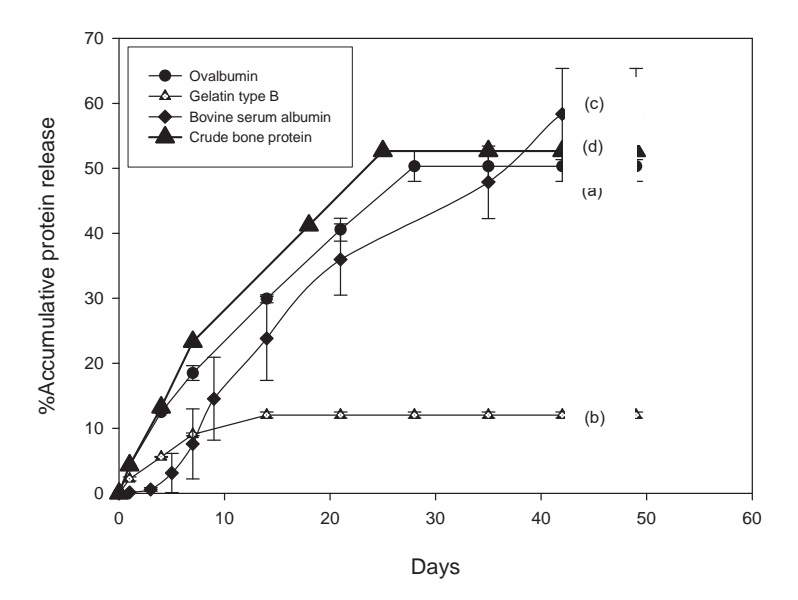


Figure 4.8 Encapsulating efficiency of protein-loaded hydroxyapatite (EE): (a) Ovalbumin (OVA); (b) Gelatin type B; (c) Bovine serum albumin (BSA) and (d) Crude bone protein (CBP) release from HAp in phosphate buffer saline solution.

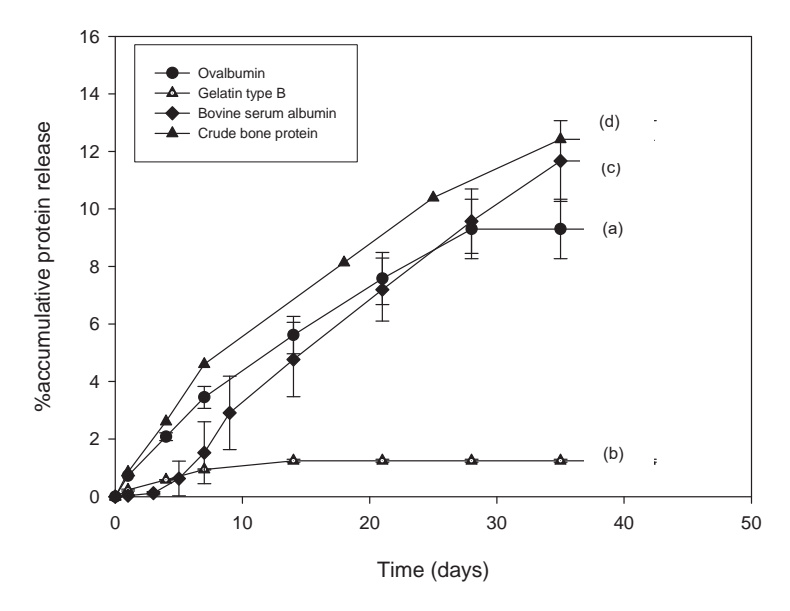


Figure 4.9 Loading capacity of protein-loaded HAp (LC): (a) Ovalbumin (OVA); (b) Gelatin type B; (c) Bovine serum albumin (BSA) and (d) Crude bone protein (CBP) release from HAp in phosphate buffer saline solution.

4.5 Conclusion

The porous hydroxyapatite particle as a controlled release carrier of proteins were successfully synthesized by co-precipitation technique. The precursors were obtained DCPD and CaCO₃. Incorporation of proteins was accomplished during the co-precipitation of the two reactants. Characteristics of the HAp particles were determined by XRD, EDS, FT-IR, TGA, ZP, SEM, TEM, and Autosorb-1. Proteins-loaded HAps were dissolution tested in prolonged PBS solution. Proteins release could be regulated using HAp particles resulting in prolonged release of proteins except gelatin type B. Mechanism of proteins-loaded HAp release was believed to be the combination of diffusion or degradation of the carrier. Many factors play roles and synergistically control on the release of proteins from the hydroxyapatite which were electrostatic interaction between protein and hydroxyapatite.

5. DEVELOPMENT OF POROUS HYDROXYAPATITE PARTICLES AS CARRIERS OF PROTEINS IN A POLYCAPROLACTONE SCAFFOLD FOR BONE TISSUE ENGINEERING

Experimental

5.3.1 Materials

- Polycaprolactone (PCL;80,000 g mol⁻¹; Sigma-Aldrich, USA)
- Sodium chloride (Ajax Finechem, Australia)
- Chloroform (Labscan; Asia, Thailand)
- Modified Eagle's medium (MEM; Thermo Scientific, USA)
- Fetal bovine serum (FBS;Sorali, Campo Grande Brazil)
- 1% L-glutamine (Invitrogen Corp., USA)
- 1% Lactabumin (Invitrogen Corp., USA)
- 1% antibiotic (Invitrogen Corp., USA)
- Bicinchoninic acid (BCA; Thermo Scientific, USA)

5.3.2 Preparation of Polycaprolactone (PCL)-Hydroxyapatite (HAp) Scaffold

A solvent casting and salt particulate leaching was used to prepare the scaffold. Firstly, PCL granules were put into a glass bottle with chloroform to make up a PCL solution in the concentration of 14 percentages of polymer weight by volume of the solution (w/v), then the solution was stirred at room temperature for 2 h. Secondly, protein-loaded HAp were added into the glass bottle and they were stirred together. Thirthly, NaCl salt particles with size of 400 μ m (PCL/NaCl = 1/30) (w/w) were added into the glass bottle and they were mixed together. And finally, the mixture was packed into the petri-dish with the dimension of 10x10 cm. The mold was then left in the hood for 24 h and immersed in the distill water 1 day for taking the mold out. The materials that come out were immersed in DI water for 2 days, during with time the water was changed approximately every 8 h under the room temperature for the leaching out the salt particles. Then the materials were air-dried for 24 h and freeze-dried overnight to obtain porous scaffolds (Prasansuklap *et al.*, 2008).

5.4 Characterization of porous Scaffolds

5.4.1 Porosity, Pore Volume and Pore Size

The density of the scaffolds (ρ scaffold) is determined by using a Sartorius YDK01, Germany density measurement kit (Buoyancy method) which can be calculated using the following equation.

$$\rho_{\text{scaffold}} = W_a \times \rho_{\text{fl}}$$

$$W_a \times W_{\text{fl}}$$

Where W_a is the weight of the scaffold in air, W_{fl} is the weight of the scaffold in water and ρ scaffold is the density of the water (at 25°C, $\rho_{ft} \approx 1$ g/cm³).

The porosity and pore volume of the scaffolds were calculated using the following equation (Hou, Qingpu *et al.*, 2003)

Porosity (%) =
$$\left(\begin{array}{ccc} - \rho_{\text{ scaffold}} & \times \\ \hline \rho_{\text{ polymer}} \end{array}\right) 100$$

Pore volume = 1 - 1
$$\rho_{\text{ scaffold}} & \rho_{\text{ polymer}} \end{array}$$

where ρ scaffold is the apparent density of the porous scaffolds and ρ polymer is the density of the non-porous polymer, compression moulded in the same manner.

Pore size of the scaffold was measured on the SEM micrograph with the UTHSCSA Image Tool version 3.0 software. The average values were calculated from the total 25 pores and accept as the mean pore sizes.

5.4.2 Water Absorption Capability

The dry scaffold scaffolds were weighted and then were immersed in 5 ml of phosphate buffer silane solution (PBS pH 7.4) solution at room temperature for 3 days. Scaffolds were removed from the solution and carefully placed on the glass for 5 seconds to remove the excessive water and weight immediately. The water absorption was calculated using the following equation.

Water absorption (%) =
$$(M_{wet} - M_{dry}) \times 100$$

 M_{dry}

Where M $_{dry}$ and M $_{wet}$ are the weight of the scaffold before and after immersion in water respectively. Five measurements were performed for the calculation of an average water absorption value.

5.4.3 Morphology of Porous Scaffolds

The morphology of the pores size of the porous scaffold were observed by a JEOL JSM-5200 scanning electron microscopy (SEM). The scaffolds were cut with razor blade at the middle of the scaffolds and mounted on stubs. Cross sections of the scaffolds were coated with thin film of gold using JEOL JFC-1100E sputtering devices for 120 second.

5.4.4 *In Vitro* Release of Proteins from Scaffold

The proteins/HAp-PCL were immersed in 1 ml of the minimum essential medium (MEM; Hyclone, Thermoscientific, USA) in 24 well plate. All samples were incubated in a shaking water bath (70 rpm) at 37°C. The amount of proteins releasing from scaffold to the supernatant was measured by BCA protein assay at various times. After the releasing medium (sample solution) was withdrawn 20 µl to mixed with BCA solution, an equal amount of fresh medium was added to maintain a constant volume of the medium. The amount of protein in the sample solution was determined by UV-visible spectroscopy at 562 nm. The MEM used in this study contained plenty of much high molarity inorganic salts comparing with those in PBS such as NaCl 117.24 M, KCl 5.33 M, CaCl₂ 1.8 M, NaH₂PO₄-H₂O 1.01 M (Invitrogen, 2009).

5.5 Cell culture

Mouse calvaria-derived, pre-osteoblastic cells (MC3T3-E1) were cultured as monolayers in minimum essential medium with Earle's Balanced Salts (MEM; Hyclone, Thermoscientific, USA), supplemented with 10% FBS, 1% L-glutamine and 1% antibiotic and antimycotic formulation (containing penicillin G sodium, streptomycin sulfate, and amphopericin B (Invitrogen Corp, USA). Cells were cultivated in 5% CO₂ at 37 °C in a humidified atmosphere.

5.5.1 Indirect Cytotoxic Study.

An indirect cytotoxic test was conducted on the proteins-loaded hydroxyapatite and PCL-HAp scaffold by use MC3T3-E1. First, extraction medias were prepared by immersing powder of each protein-loaded hydroxyapatite and circular shape of each PCL-HAp scaffold specimens about (15 mm in diameter) in wells of a 24-well culture plate in a 2% MEM (containing MEM, 2% FBS, 1% L-glutamine, 1% antibiotic and antimycotic formulation) for 24 h. Each of these extraction media was used to evaluate the cytotoxicity of the HAp powder and scaffold. MC3T3-E1 was separately cultured in wells of a 24-well culture plate in serum-containing MEM for 16 h to allow cell attachment on the plate. The cells were then starved with 2% MEM for 24 h, after which time the medium was replaced with an extraction medium.

After 24, 48, and 72 h of cell culturing in the extraction medium, a 3-(4,5-dimethylthiazol-2-yl)-2,5-diphenyl-tetrazolium bromide (MTT) assay was carried out to quantify the amount of via cells.

The MTT assay is based on the reduction of the yellow tetrazolium salt to purple formazan crystals by dehydrogenase enzymes secreted from the mitochondria of metabolically active cells. The amount of purple formazan crystals formed is proportional to the number of viable cells. First, each of culture medium was aspirated and replaced with 400 µl per well of MTT solution at 0.5 mg/ml for a 24-well culture plate. Secondly, the plate was incubated for 30 mins at 37°C. The solution was then aspired and 900 µl per well of dimethylsulfoxide (DMSO) containing 125 µl per well of glycine buffer (pH=10) is added to dissolve the formazan crystals. Finally, after 10 min of rotary agitation, the absorbance of the DMSO solution at 570 nm was measured using a Thermospectronic Genesis 10 UV-Visible spectrophotometer.

5.5.2 Cell Attachment and Cell Proliferation Study

Mouse calvaria-derived, pre-osteoblastic cells (MC3T3-E1) were allowed to attach on the porous scaffold specimens and empty wells for 2, 4, and 6 h. For the proliferation study, the cells were allowed to attach on the porous scaffold specimens and empty wells for 1, 3, and 5 d. At each time point, a number of the attached and proliferated cells were quantified by MTT assay. Each specimen was rinsed with phosphate buffered saline to remove unattached cells prior to the MTT assay. The morphology of the cells during the attachment and proliferation periods was observed by SEM. At each time point, the culture medium was removed and then the cell-cultured scaffold specimens were rinsed with PBS twice, the cells were then fixed with 3% glutaraldehyde solution, which was dilute from 50% glutaraldehyde solution with PBS 500 μl/well. After 30 min, they were rinsed again with PBS. After cell fixation, the specimens were dehydrated in an ethanol solution of varying concentration (30%, 50%, 70% and 90%, respectively). The specimens were the dried in air. After completely dried, the specimens were mounted on an SEM blass stubs, coated with gold and observed by SEM.

5.5.3 Alkali Phosphate Analysis (ALP)

Mouse calvaria-derived, pre-osteoblastic cells (MC3T3-E1) were cultured on porous scaffolds for 5 and 7 d and in different proteins for 5 and 7 d to observe ALP activity. Each porous specimen was rinsed with PBS after removal of the culture medium. Alkaline lysis buffer (10 mM tris-HCl, 2mM MgCl₂, 0.1% Triton-X100), pH 10) (1000 μl/well) was added, and the specimen was scrapped and then frozen at -20°C for at least 30 min prior to the next step. An aqueous solution of 2 mg ml⁻¹ p-nitrophenyl phosphate (PNPP; Zymed Laboratories) mixed with 0.1 M aminopropanol (10μl/well) in 2 mM MgCl₂ (100μl/well) having a pH of 10.5 was prepared and added into the specimen. It was then incubated at 37°C for 2 min. The reaction was stopped by the addition of 0.9 ml/well of 50 mM NaOH, and the extracted solution was transferred to cuvette and placed in the UV-Vis spectrophotometer, from which the absorbance

at 410 nm was measured. The amount of ALP was then calculated against a BSA standard curve. To determine the ALP activity, the amount of ALP had to be normalized by the amount of total proteins synthesized. In the protein assay, each specimen was treated in the same manner as in the ALP assay up to the point where it was frozen. After freezing, a bicinchoninic acid (BCA; Thermoscientific, USA) solution was into the specimen. It was subsequently incubated at 37°C for 5 min. The absorbance of the medium solution was then measured at 562 nm by the UV-Vis spectrophotometer, and the amount of the total proteins was calculated against a BSA standard curve.

5.5.4 Mineralization Analysis

Calcium deposition was quantified by Alizarin Red S staining. MC3T3-E1 were cultured on the porous scaffolds in 24-well plate for 21 days. The cultures in 24-well plate were rinsed with PBS after that the cells were fixed with cold methanol for 10 min and washed with deionized water prior to immersion for 3 min in 370 µl of 1% Alizarin Red S solution dissolved in 1:100 (v/v) ammonium hydroxide/water mixture for 3 min (pH=3.3). Each stained specimen was washed several times with DI water and air-dried at room temperature. Calcium forms an Alizarin Red S-calcium complex in a chelating process. The stained specimen was photographed and eluted dye with 10% cetylpyridinium chloride for 20 min. The Alizarin Red concentration was determined by measuring the absorbance at 562 nm.

5.6 Results and discussion

5.6.1 Microstructure observation

Figure 5.1 demonstrated the SEM images microstructure of the as-prepared scaffolds when being viewed on the surface and cross sections. For PCL and HAp/PCL scaffold with NaCl: PCL, 30:1 weight ratio. The SEM images of (a) and (c) showed many square units occurring from the shape of NaCl porogens used in the fabricating process. They showed clearly square units due to neat PCL scaffold whereas (b) and (d) exhibited the lost square because HAps embedded in the PCL scaffold.

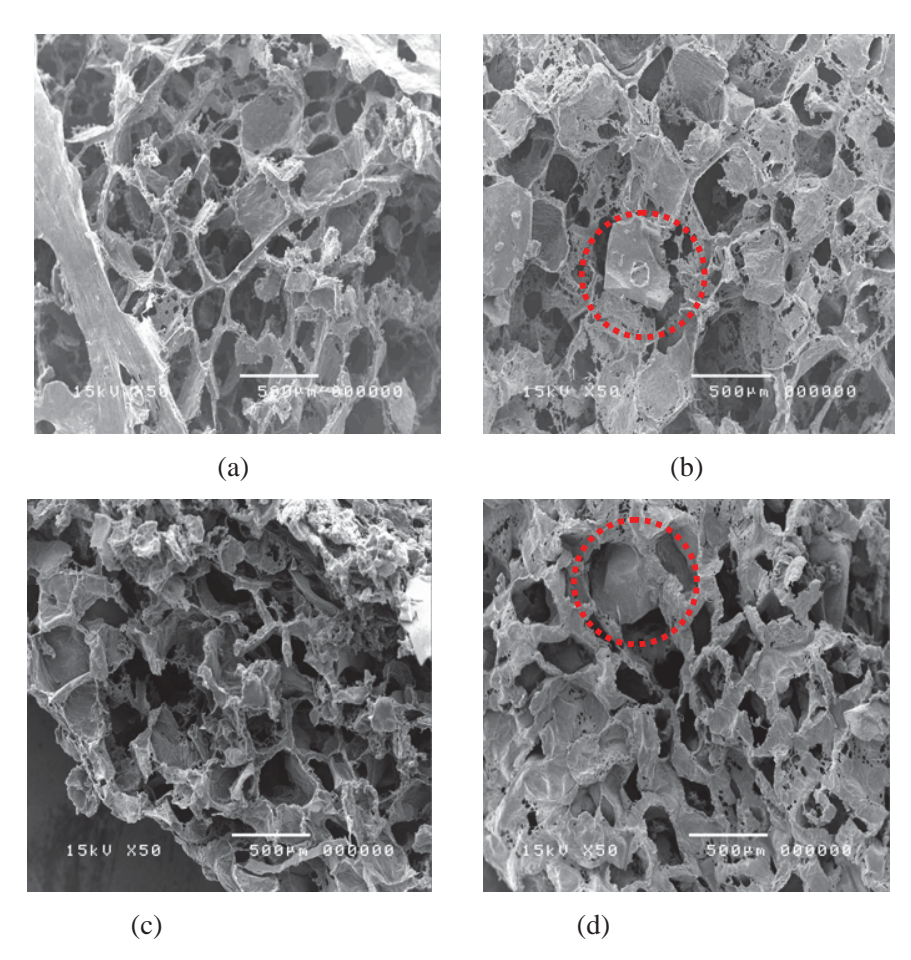


Figure 5.1 SEM images illustrate microstructure of the scaffolds on the surface: (a) PCL, (b) HAp-PCL and on the cross-sections: (c) PCL, (d) HAp-PCL.

5.6.2 Density, Porosity, Pore volume and Pore size

The density, porosity, pore volume and pore size of the scaffold was shown in Table 5.1.

Table 5.1 Density, porosity, pore volume and pore size of PCL scaffold

Scaffolds	Density (g/cm ³)	Porosity (%)	Pore volume (cm ³ /g)	Pore size (μm)
PCL	0.1139	90.05	7.91	347.07 ± 42.19

5.6.3 Water absorption capability and in vitro degradability

Figure 5.2 illustrates the water absorption capabilities of the PCL scaffolds in 0.1 M PBS at room temperature within 3 days (72 h). The water absorption rate was rapidly increased in the early 24 hours and maintained stable.

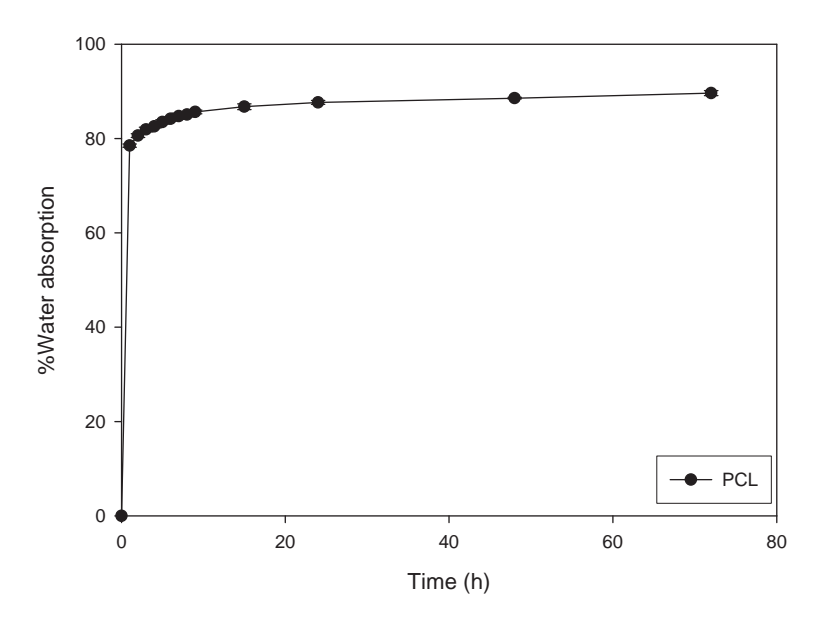


Figure 5.2 Water absorption capability of the PCL scaffolds in 0.1 M PBS at room temperature within 3 days.

5.6.4 In vitro OVA, Gelatin type B, BSA, and CBP Release

The release of proteins from HAp-PCL scaffolds were investigated by immersing HAp-PCL scaffolds into *in vitro* culturing environment, 10% MEM (containing MEM, 10% FBS, 1% L-glutamine, 1% antibiotic). All samples were incubated in a shaking water bath (70 rpm) at 37°C for 21 days. The result shows gelatin and CBP started to before day 7 whereas OVA and BSA release after day 7. The amount of released proteins gradually increased time dependently. This result correspond to the work done by proteins releasing from HAp particles, however, protein release from scaffold spends a longer time due to different media. It is different in ionic strength, in MEM shows higher ionic strength. High ionic strength should promote aggregation of protein and retard release.

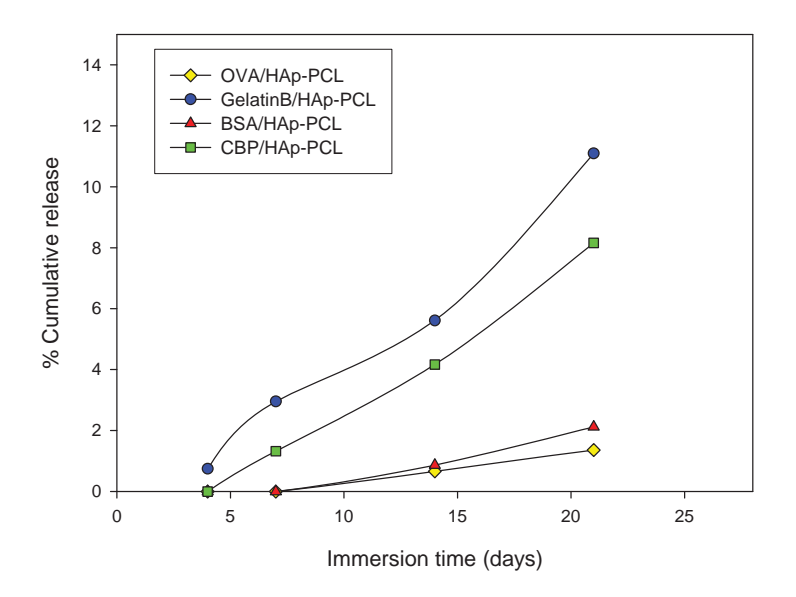


Figure 5.3 Release profile from protein-loaded HAp-PCL scaffold in MEM.

5.7 Cell Culture

5.7.1 Cytotoxicity

Indirect cytotoxicity in this studied can be classified into 3 process are indirect cytotoxicity for protein, HAp, and HAp-PCL scaffold. Firstly, an direct cytotoxicity test of proteins were performed in 4 types which are Ovalbumin (OVA), Gelatin type B, Bovine serum albumin (BSA), and Crude bone protein. MC3T3-E1, pre-osteoblast cell lines, in culture of 40,000 cell/well seeded with 10 μg/ml concentration in 2% MEM for 24, 48, and 72 h. The results are shown in Figure 5.4 with %viability of MC3T3-E1 relative to tissue culture polystyrene (TCPS) in all types of proteins show that increasing with cuturing time. The %viability of MC3T3-E1 is more than 80%, so all types of proteins were no toxicity to cells. Secondly and Thirdly are indirect cytotoxicity test of proteins-loaded HAp and HAp-PCL scaffold. MC3T3-E1 were cultured in 2% MEM extraction media from proteins-loaded HAp (Figure 5.5) and HAp-PCL scaffold (Figure 5.6) for 24, 48, and 72 h. The %viability of MC3T3-E1 in extraction media of each time are more than 80%, so proteins-loaded HAp and HAp-PCL scaffold were no toxicity to cell.

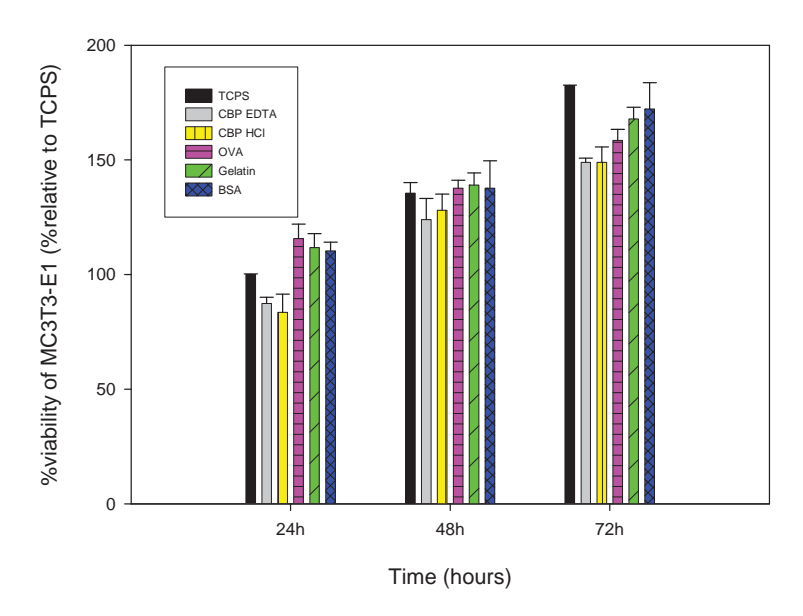


Figure 5.4 Direct cytotoxicity evaluation of proteins based on the viability of MC3T3-E1.

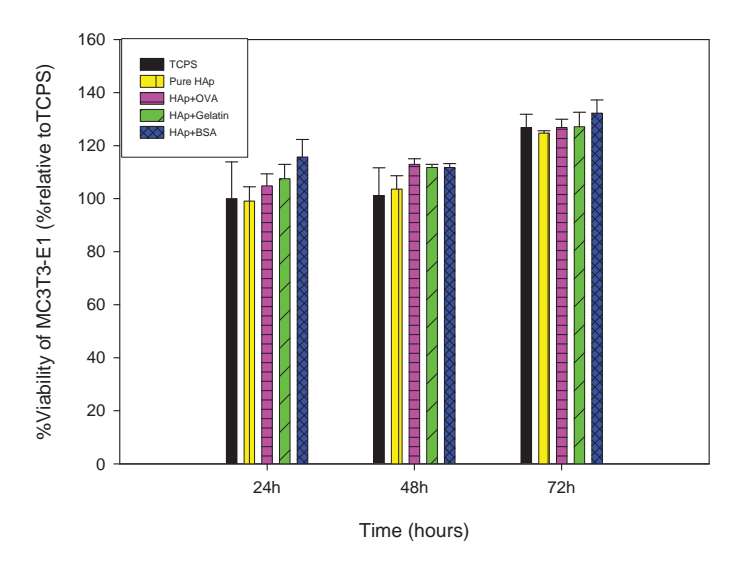


Figure 5.5 Indirect cytotoxicity evaluation of protein-loaded HAp based on the viability of MC3T3-E1.

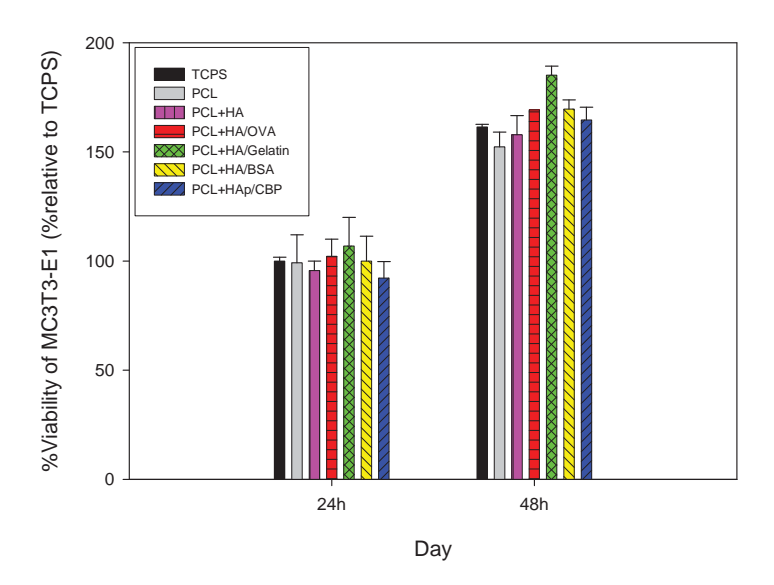


Figure 5.6 Indirect cytotoxicity evaluation of HAp-PCL scaffold based on the viability of MC3T3-E1.

5.7.2 Cell Attachment and Proliferation

Attachment of mouse calvaria-derived, pre-osteoblastic cells (MC3T3-E1) on scaffolding substrate could be quantified by the UV absorbance from MTT assay. Figure 5.7 shows attachment of MC3T3-E1 on the surface of TCPS, PCL, HAp-PCL, OVA/HAp-PCL, Gelatin type B/HAp-PCL, BSA/HAp-PCL, CBP/HAp-PCL at 2, 4, and 6 h after cell seeding. The number of cell attachment on all of the surfaces increase with culturing time. The number of cell attachment on TCPS was the greatest than all of HAp-PCL and proteins-loaded HAp scaffolds at any given time point, in culture of 40,000 cell/well. On TCPS, the number of cell attachment rapidly increased from 100% at 2 h after cell seeding to ~200% at 4 h after cell seeding. Whereas the number of cell attachment on PCL, HAp-PCL and proteins-loaded HAp were lower than TCPS could be because MC3T3-E1 like to attach the smoother surface of TCPS than rough surface of PCL, HAp-PCL and proteins-loaded HAp-PCL scaffold. However, Table 5.2 shows that almost of the formazan crystal still adhere within the scaffolds after using DMSO as eluting agent.

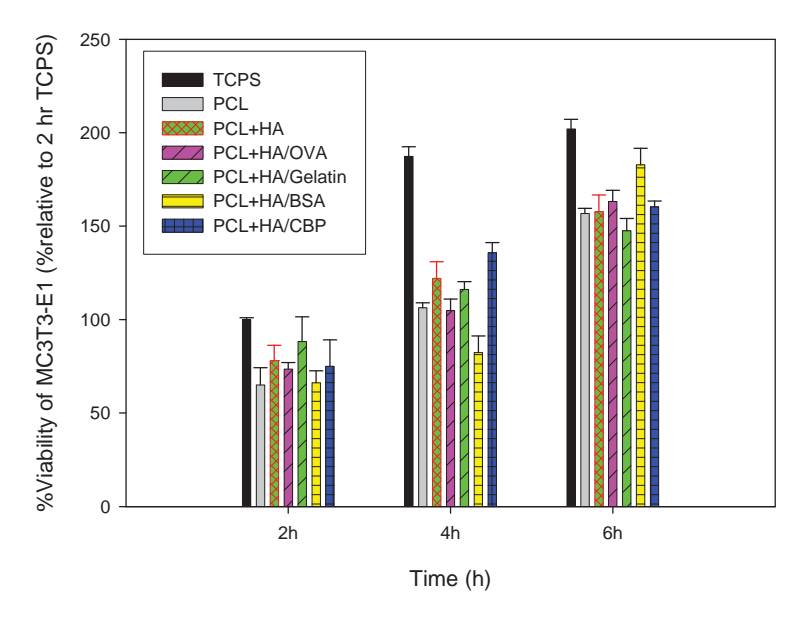
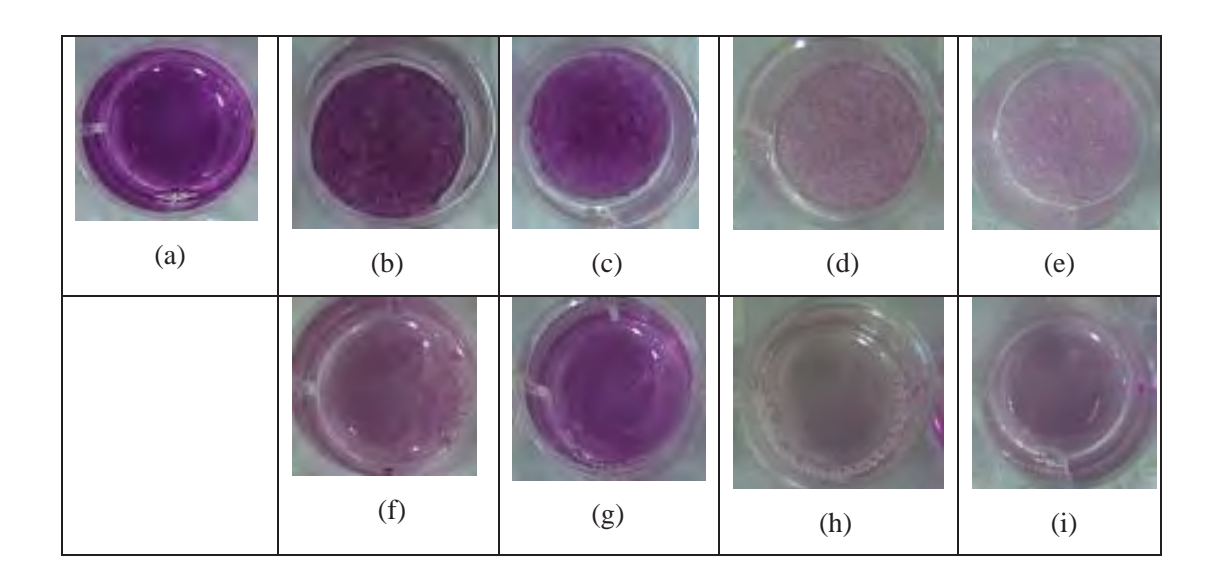


Figure 5.7 Attachment of MC3T3-E1 on control TCPS, PCL, HAp/OVA-PCL, HAp/gelatin B-PCL, and HAp/BSA-PCL

Table 5.2 Formazan crystal within TCPS, PCL, HAp-PCL scaffold were eluted with DMSO after cell seeding 6 h. (a) Eluted formazan from TCPS. (b), (c) Formazan still adhere in scaffold. (f), (g) Eluted formazan from scaffold. (d), (e) scaffold without cells inside. (h), (i) Eluted scaffolds without cells



Proliferation of mouse calvaria-derived, pre-osteoblastic cells (MC3T3-E1) on scaffolding substrate could be quantified by the UV absorbance from MTT assay. Figure 5.8 shows proliferation of MC3T3-E1 on the surface of TCPS, PCL, HAp-PCL, OVA/HAp-PCL, Gelatin type B/HAp-PCL, BSA/HAp-PCL, CBP/HAp-PCL at 1, 2, and 3 d after cell seeding in culture of 40,000 cell/well. The number of cell proliferation on all of the surfaces at any given time point were constant. The number of cell proliferation on TCPS was greater than all of PCL, HAp-PCL, and proteins-loaded HAp-PCL scaffolds at any given time point. On PCL, HAp-PCL and proteins-loaded HAp-PCL scaffold, the number of cell proliferation was only 60%. Whereas the number of cell attachment on HAp-PCL and proteins-loaded HAp were lower than TCPS could be because MC3T3-E1 like to proliferate the smoother surface of TCPS than rough surface of PCL, HAp-PCL and proteins-loaded HAp-PCL scaffold. The difference between the number of cell proliferation to PCL, HAp-PCL, and protein-loaded HAp-PCL scaffold are not clear because of no effect of proteins release from HAp. However, Table 5.3 shows that almost of the formazan crystal still adhere within the scaffolds after using DMSO as eluting agent.

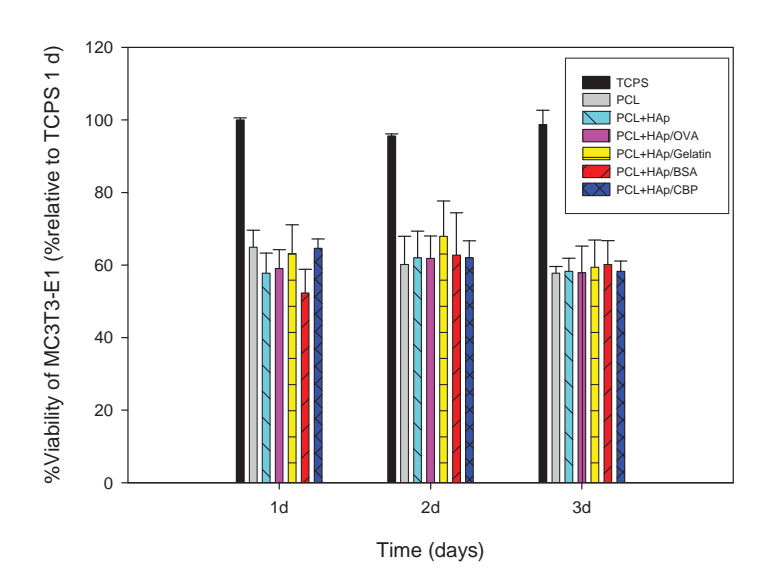
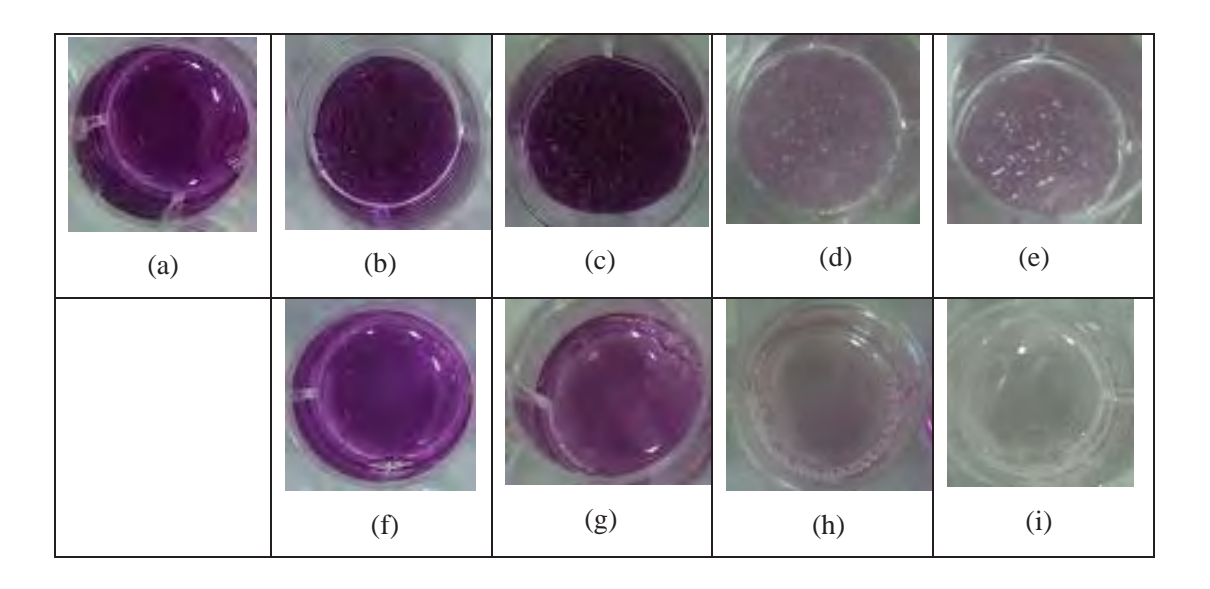


Figure 5.8 Proliferation of MC3T3-E1 that had been seeded or cultured on the surfaces of TCPS, PCL, HAp-PCL and proteins-loaded HAp-PCL scaffolds at 2 and 3 d.

Table 5.3 Formazan crystals within scaffolds after using eluting dye (DMSO) after cell seeding 1 d. (a) Eluted formazan with DMSO from TCPS. (b), (c) Formazan crystal still adhere in scaffolds. (f), (g) eluted formazan crystal with DMSO from scaffolds. (d), (e) scaffold without cells inside. (h), (i) eluted DMSO from scaffolds without cells.



5.7.3 Cell Morphological

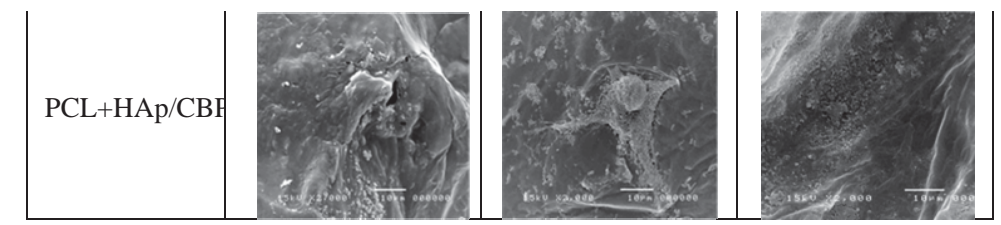
Table 5.4 shows selected the attachment SEM images of MCT3T-E1 (magnification = 2000X; scale bar = 10 μm) at 2, 4, and 6 h. Based on the initial 40,000 cells/well of cells seeded, the majority of the cells on the glass surface and porous scaffolds were still in the round shape at 2 h and started to extend their cytoplasm at 4 h. After cell seeding, expansion of the cytoplasm of the majority of the cells was evident at 6 h. Table 5.5 shows that the selected proliferation SEM images of MC3T3-E1 (magnification = 2000X; scale bar = 10 μm) were cultured on the surfaces of glass, PCL, HAp-PCL, and proteins-loaded HAp scaffolds. The use of glass as the control instead of TCPS was due to the ease of taking the samples to SEM observation. These images provided snap shots in time that revealed the morphology of the cells and interaction between the cells and the tested surfaces. The expansion of the cells was evident with depend on the increasing time at 1, 2, and 3 days. All proteins within the HAp show the same results due to at that time the proteins were no affect to the cells.

Table 5.4 Selected SEM images of MC3T3-E1 after seeding on TCPS, PCL, OVA/HAp-PCL, Gelatin type B/HAp-PCL, BSA/HAp-PCL, and CBP/HAp-PCL scaffolds at 2, 4, and 6 h (magnification = 2,000X; scale bar = $10 \ \mu m$)

	2 h	4 h	6 h
Glass	7517 72100 TOTA 000000	1510 ×1	1510 X2-000 - 157-A COURSE
PCL	1310 22100 -1010 000000		
PCL + HAp			
PCL+HAp/OVA		371 V 37 NO 13-0 10-10-10	
PCL+HAp/Gel B	131 131,000 1010 000000		
PCL+HAp/BSA			
PCL+HAp/CBF		San Service Land confin	

Table 5.5 Selected SEM images of MC3T3-E1 after seeding on TCPS, PCL, HAp-PCL, OVA/HAp-PCL, Gelatin type B/HAp-PCL, and BSA/HAp-PCL scaffolds at 1, 2, and 3 days

X 2000	1 d	2 d	3 d
Glass	1510 12.000 100 00000	1510 H2-000 TOFA 000000	1210 XX 000 107 00000
PCL			
PCL + HAp			
PCL+HAp/OVA			
PCL+HAp/Gel			100 tr. 111 Tue 11111
PCL+HAp/BSA			153/ 72.000 10000



5.7.4 Alkaline phosphatase (ALP) activity

Alkaline phosphatase is an indicator of osteoblast phenotype activity. It was determined after culturing the cells seeded onto the scaffold. The ALP activity of MC3T3-E1 on TCPS, PCL, HAp-PCL, OVA/HAp-PCL, Gelatin type B/HAp-PCL, BSA/HAp-PCL and CBP/HAp-PCL were monitored at 3 and 7 days in culture. In Figure 5.9 at 3 days shows the maximum level of ALP activity and at 7 days, ALP activity was decreased. In actually, ALP activity of PCL, HAp-PCL, OVA/HAp-PCL, Gelatin type B/HAp-PCL, BSA/HAp-PCL and CBP/HAp-PCL scaffold should be the same result of cell proliferation due to at that time the proteins were no effect to the cell, however, they were slightly fluctuated because PCL, HAp-PCL, OVA/HAp-PCL, Gelatin type B/HAp-PCL, BSA/HAp-PCL and CBP/HAp-PCL scaffolds were porous materials, so the cells could go through their scaffolds and could not extract the cells completely. In Figure 5.9, The ALP activity of MC3T3-E1 in OVA, Gelatin type B, BSA, and CBP with 100 μg/ml concentrations in 2%MEM was monitored at 5 and 7 days in culture. At 5 days shows the maximum level of ALP activity and at 7 days, ALP activity was decreased due to cellular process switching to mineralization. This result correspond to the work done by ALP activity of MC3T3-E1 on substrates.

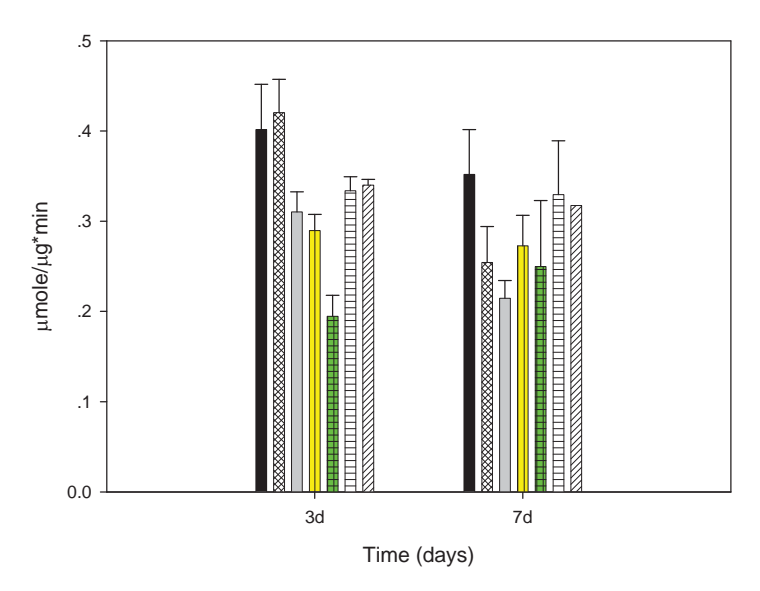


Figure 5.9 ALP activity of MC3T3-E1 cultured on TCP, PCL, HAp-PCL, OVA/HAp-PCL, Gelatin B/HAp-PCL, BSA/HAp-PCL and CBP/HAp-PCL porous scaffolds after 3 and 7days in culture.

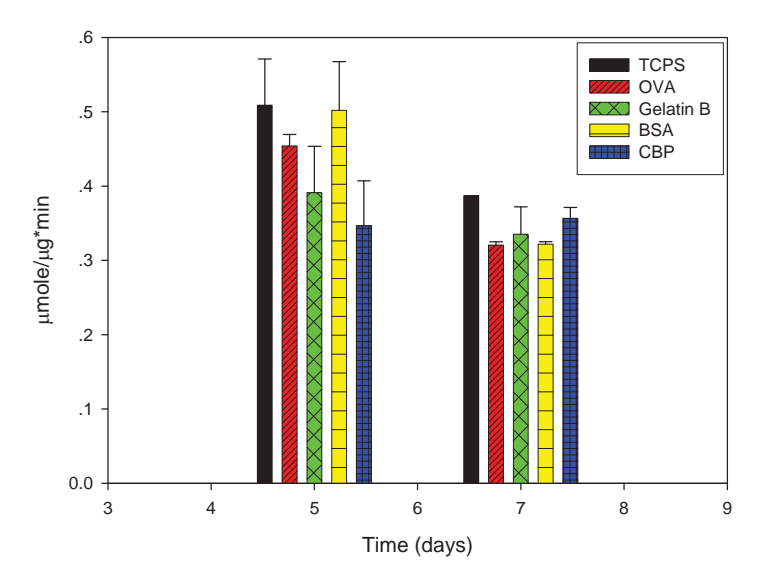


Figure 5.10 ALP activity of MC3T3-E1 cultured with 100 μ g/ml in 2%MEM, OVA, Gelatin type B, BSA and CBP after 5 and 7 days in culture.

5.7.5 Mineralization

Mineralization refers to the process where an organic substrance is converted to an inorganic substrance. Alizalin Red S staining was used to characterize the bone formation of MC3T3-E1. Table 5.6, and Figure 5.11 show photographic images of Alizarin Red S staining of cells cultured on the different surfaces on 21 days. In the presence of calcium, the staining product such as an Alizarin red S-calcium chelating product appeared red. The results showed that PCL, HAp-PCL, and proteins-loaded-HAp scaffold were significantly higher than that on TCPS. Calcium content from MC3T3-E1 culture on CBP/HAp-PCL scaffold was the most positive staining.

Table 5.6 Alizarin Red S staining for mineralization assessment of MC3T3-E1 on 21 days after being cultured on the surfaces of neat PCL, HAp-PCL, HAp/OVA-PCL, HAp/Gelatin-PCL, HAp/BSA-PCL, and HAp/CBP-PCL

Substrate	21 d.		21 d.
TCPS		HAp/OVA-PCL	
Neat PCL		HAp/GelB-PCL	
Control		HAp/BSA-PCL	
HAp-PCL		HAp/CBP-PCL	

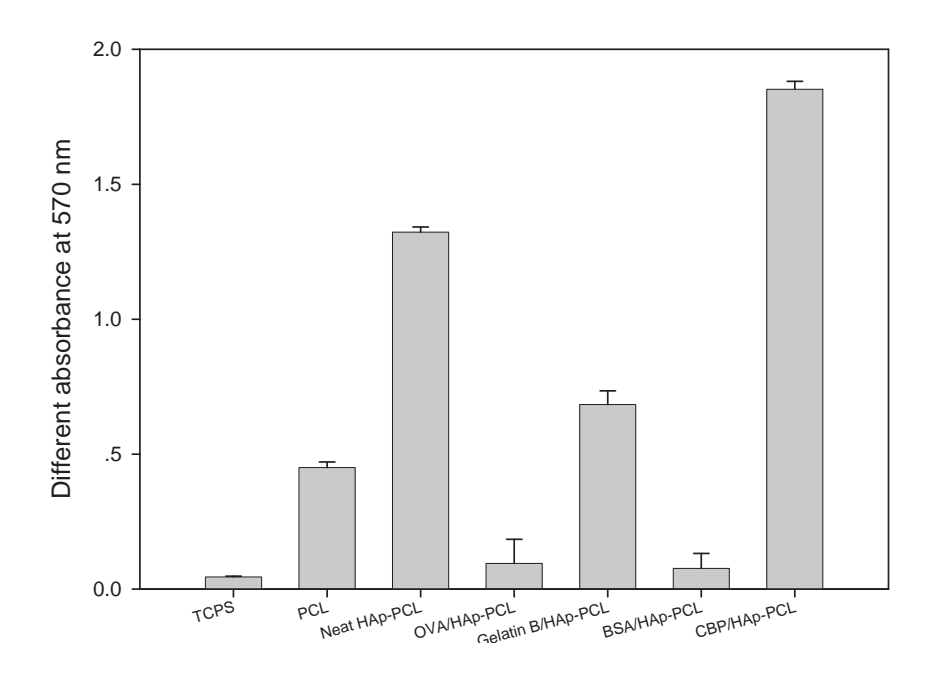


Figure 5.11 Different absorbance of alizalin red S from MC3T3-E1 on TCPS, PCL, HAp-PCL, proteins-loaded HAp-PCL at 21 days.

5.7 Conclusions

The amount of HAp in the PCL scaffold was 40% (w/w, based on the amount of PCL). The direct and indirect cytotoxicity evaluation of the proteins, HAp and protein-loaded HAp-PCL scaffold with MC3T3-E1 indicated that non-toxic. Potential for using of proteins-loaded HAp-PCL scaffolds was assessed in terms of cell attachment, cell proliferation, and ALP activity were no effect of proteins release from HAp. Alkaline phosphatate (ALP) activity at 7 days showed decreasing of the ALP activity due to cellular process switching to mineralization. According to mineralization or calcium deposition of cell for 21 days, the CBP/HAp-PCL scaffold was better than HAp/PCL, PCL, Gelatin/HAp-PCL, OVA/HAp-PCL, BSA/HAp-PCL, TCPS respectively.

6. SURFACE MODIFICATION OF POLY(LACTIC ACID) FIBERS VIA AMINOLYSIS AND COLLAGEN IMMOBILIZATION FOR BONE TISSUE ENGINEERING

Experimental Section

- **1. Materials.** Materials used in the fabrication of the fibrous scaffolds were poly(lactic acid) (PLA; $M_n = 80,000 \text{ g mol}^{-1}$; Aldrich, USA), dichloromethane (DCM; Carlo Erba, Italy), and N,N' dimethylformamide [DMF; Lab-Scan (Asia), Thailand]. Materials used in the surface modification of the PLA fibrous scaffolds were type-I collagen (from calf skin; Sigma, USA), 1,6-hexamethylene-diamine (HMD; Aldrich, USA), and N,N'-disuccinimidylcarbonate (DSC; Aldrich, USA). All other chemicals were of analytical reagent grade and used without further purification.
- 2. Preparation and characterization of e-spun PLA fibrous scaffolds. Electro-spun fiber mats of poly(lactic acid) were prepared by e-spinning from 10% w/v PLA solution in 7:3 v/v dichloromethane/ N,N'-dimethylformamide (DCM/DMF). The as-prepared PLA solutions were continuously stirred until clear solutions were obtained. The solution was fed into a glass syringe fitted with a blunt 20-gauge stainless steel hypodermic needle (OD = 0.91 mm), which used as the nozzle. An aluminum sheet wrapped around a home-made rotating cylinder (width and diameter ≈15 cm; rotational speed ≈ 50 rpm) was used as the collector. The distance from the tip of the needle to the surface of the Al sheet (measured at right angle to the surface) defining the collection distance was fixed at 18 cm. A Gamma High-Voltage Research Inc. (Ormond Beach, Florida), DC power supply was used to generate a high dc potential which was fixed at 20 kV. The emitting electrode of positive polarity was connected to the needle, while the grounding one was to the collector. E-spinning of the as-prepared PLA solution was done continuously for 12 h. The obtained translucent electro-spun PLA fibrous scaffolds were dried in vacuo at room temperature prior to further modification. The thickness of the obtained PLA fiber mats was $\sim 136 \pm 5 \,\mu m$. Morphological appearance and size of the individual fibers of the scaffolds were examined by JEOL JSM 5410LV scanning electron microscopy (SEM) (see Supporting Information). At least 100 readings of the fiber diameters from various SEM images were statistically analyzed using SemAphore 4.0 software, from which the arithmetic mean value of the individual fibers within the PLA fiber mats was determined to be $0.63 \pm 0.1 \, \mu m$.
- **3. Surface modification of PLA fibrous scaffolds.** The PLA fibrous membranes were first immersed in an ethanolic aqueous solution (1:1 v/v) for 2 to 3 h to cleanse the fiber surface and then washed with a large amount of deionized water. The scaffolds were subjected to aminolysis through an immersion in a 1,6-hexamethylene-diamine/isopropanol (HMD/IPA) solution of varying concentration (i.e., 0.02, 0.04, 0.06, 0.08, and 0.1 gml⁻¹) and varying reaction time (i.e., 2, 5, 8, 15, 20, 30 min) at 50°c. The aminolyzed PLA fibrous scaffolds were then rinsed with deionized water for 24 h at room temperature to

remove unreacted HMD and dried *in vacuo* at room temperature to reach a constant weight. Immobilization of type-I collagen on the surface of the PLA fibrous scaffolds was carried out by first activating the aminolyzed PLA fibrous scaffolds in 0.1 M *N,N'*-disuccinimidyl carbonate/dimethylsulfoxide (DSC/DMSO) solution in the presence of 0.1 M triethylamine (TEA) for 3 h at room temperature, followed by rinsing the fiber mats with a large quantity of deionized water. The activated PLA fibrous scaffolds were then immersed in 0.5 or 3 mg·ml⁻¹ of collagen/phosphate buffer saline (PBS) solution at ambient temperature for 24 h. The collagen-immobilized PLA fibrous scaffolds were rinsed by soaking in a large quantity of deionized water for 24 h and finally dried *in vacuo* at room temperature. The chemical pathway for the immobilization of type-I collagen on the surface of e-spun PLA fibrous scaffolds is summarized in the Figure 1.

4. Characterization of neat and modified PLA fibrous scaffolds.

Quantification of free amino groups on the surface. UV-Vis spectroscopy was used for determination the amount of amino (NH₂) groups on the surface of the aminolyzed and the collagen-immobilized PLA fibrous scaffolds using ninhydrin method. First, the fibrous scaffolds were immersed in 1 M ninhydrin/ethanol solution for 1 min in a glass tube, followed by heating at 80°C for 15 min to accelerate the reaction between ninhydrin and the NH₂ groups that might be present on the surface of the scaffolds. As an evidence for the actual presence of the NH₂ groups, the surface of the scaffolds would turn blue. After complete evaporation of absorbed ethanol, 1,4-dioxane was added in the tube to dissolve the scaffolds. IPA was then added to stabilize the blue compound. Absorbance of the obtained compound in the UV-visible range was measured in a spectrophotometer (UV-2550, Shimadzu, Kyoto, Japan) at 538 nm against a predetermined calibration curve that was obtained from HMD solutions in 1,4-dioxane/IPA (1:1 v/v) (see Supporting Information).

Surface Wettability. Water contact angles of the neat and modified PLA fibrous scaffolds were measured at room temperature and, using sessile drop method on a telescopic goniometer (KRUSS Gmbh, DSA10-Mk2 T1C, Germany) equipped with a Gilmont syringe and a 24-gauge flat-tipped needle. The measurements were carried out in pentuplicate on different areas of each sample and the resulting values were averaged.

Elemental composition of the surface. X-ray Photoelectron Spectrometer (XPS; AMICUS, KRATOS, Japan), also known as Electron Spectroscopy for Chemical Analysis (ESCA), was used to investigate the elemental composition and chemical state of the elements on the surface. The XPS N_{1s}/C_{1s} peak-area rations was used as a marker for the analysis of the relative amount of free amino groups and collagen immobilized on the surface.

5. Biological characterization of neat and modified PLA fibrous scaffolds.

Cell culture and cell seeding. Mouse fibroblasts (L929) and mouse calvaria-derived, pre-osteoblastic cells (MC3T3-E1) were used as reference cell lines. L929 were cultured as monolayer in Dulbecco's modified Eagle's medium (DMEM; Sigma-Aldrich, USA), supplemented with 10% fetal bovine serum (FBS; BIOCHROM AG), 1% L-glutamine (Invitrogen Corp.), and a 1% antibiotic and antimycotic formulation [containing penicillin G sodium, streptomycin sulfate, and amphotericin B (Invitrogen Corp., USA)]. MC3T3-E1 were cultured in Minimum Essential Medium (with Earle's Balanced Salts) (MEM; Hyclone, USA), supplemented by 10% fetal bovine serum (FBS; BIOCHROM AG, Germany), 1% L-glutamine (Invitrogen Corp., USA) and 1% antibiotic and antimycotic formulation [containing penicillin G sodium, streptomycin sulfate, and amphotericin B (Invitrogen Corp., USA)]. The medium was replaced every 2 days and the cultures were maintained at 37°C in a humidified atmosphere containing 5% CO₂.

Each scaffold was cut into circular discs (about 15 mm in diameter) and the disc specimens were placed in wells of a 24-well tissue-culture polystyrene plate (TCPS; Biokom Systems, Poland), and were later sterilized in 70% ethanol for 30 min. The specimens were then washed with autoclaved de-ionized water, PBS and subsequently immersed in MEM overnight. To ensure a complete contact between the specimens and the wells, the specimens were pressed with a metal ring (about 12 mm in diameter). MC3T3-E1 from the culture was trypsinized [0.25% trypsin containing 1 mM EDTA (Invitrogen Crop., USA)] and counted by a hemacytometer (Hausser Scientific, USA). MC3T3-E1 were seeded at a density of about 60,000 cells/well for attachment study and 30,000 cells/well for proliferation study, on the scaffold specimens and empty wells of TCPS that were used as control. For indirect cytotoxicity, alkaline phosphatase activity, mineralization evaluations, MC3T3-E1 were seeded at a density of about 40,000 cells/well on the scaffold specimens and empty wells of TCPS. The culture was maintained in an incubator at 37°C in a humidified atmosphere containing 5% CO₂.

Cytotoxicity evaluation. Two types of cells were used: 1) mouse calvaria-derived, pre-osteoblastic cells (MC3T3-E1) and 2) mouse fibroblasts (L929). Indirect cytotoxicity test was conducted on TCPS, neat PLA, aminolyzed PLA, activated PLA, collagen-immobilized PLA, and polycaprolactone/hydroxyapatite (PCL/HA) which used as positive control. First, extraction media were prepared by immersing samples (about 15 mm in diameter) in a serum-free medium (SFM; containing DMEM, 1% L-glutamine, 1 % lactabumin, and 1% antibiotic and antimycotic formulation for L929 and containing MEM, 1% L-glutamine, 1 % lactabumin, and 1% antibiotic and antimycotic formulation for MC3T3-E1) for 1, 3, and 7 days. Each of these extraction media was used to evaluate the cytotoxicity of the scaffolds. L929 or MC3T3-E1 were separately cultured in wells of a 24-well culture plate in 10% serum-containing DMEM and MEM, respectively, for 16 h to allow cell attachment on the plate. Then, the cells were starved with SFM for 24 h, after which time the medium was replaced with an extraction medium. After 24 h of cell culturing in the extraction medium, 3-(4,5-dimethylthiazol-2-yl)-

2,5-diphenyl-tetrazolium bromide (MTT) assay was carried out to quantify the amount of viable cells (see Supporting Information). The experiments were carried out in triplicate.

Another experiment was conducted to confirm the cytocompatibility of the materials on MC3T3-E1. Extraction media were prepared by immersing samples (about 15 mm in diameter) in a serum-free medium (SFM; MEM, 1% L-glutamine, 1 % lactabumin, and 1% antibiotic and antimycotic formulation for MC3T3-E1) for 7 d. The sample was treated in the same manner as the previous experiment up to the point was the cells were starved. After that the SFM was replaced with 2% serum-containing MEM diluted with as-prepared 7-day extraction medium for 1, 2, and 3 d to allow cell growth on the plate. After which time the viability of cell was again quantified by MTT assay in triplicate.

Cell attachment and cell proliferation. Cell behavior such as adhesion and proliferation represent the initial phase of cell–scaffold communication that subsequently effect differentiation and mineralization. For attachment study, MC3T3-E1 was allowed to attach to TCPS, aminolyzed PLA, activated PLA, collagen-immobilized PLA for 2, 4 and 16 h, respectively. At each specified seeding time, the number of the attached cells was quantified by MTT assay. Each sample was rinsed with PBS to remove unattached cells prior to MTT assay. Morphological appearance of the cells during attachment period was observed by SEM. For proliferation study, the viability of cells on the specimens was determined after 1, 2, and 3 day of cell culturing by MTT assay. The experiments were carried out in triplicate.

Morphological observation of cultured cells. After removal of the culture medium, the cell-cultured scaffold specimens were rinsed with PBS twice and the cells were then fixed with 3% glutaraldehyde solution, which was diluted from 50% glutaraldehyde solution (Sigma, USA) with PBS, at 500 μl/well. After 30 min, they were rinsed again with PBS. After cell fixation, the specimens were dehydrated in an ethanol solution of varying concentration (i.e. 30, 50, 70, 90, and 100%, respectively) for about 2 min at each concentration. The specimens were then dried in 100% hexamethyldisilazane (HMDS; Sigma, USA) for 5 min and later let dry in air after removal of HMDS. After completely dried, the specimens were mounted on an SEM stub, coated with gold, and observed by a JEOL JSM-5200 scanning electron microscope (SEM).

Production of Alkaline Phosphatase of Cultured Cells. ALP activity of MC3T3-E1 was measured using Alkaline Phosphate Yellow Liquid. In this reaction, ALP catalyzes the hydrolysis of colorless organic phosphate ester substrate, *p*-nitrophenyl phosphate (pNPP) to a yellow product, p-nitrophenol, and phosphate. MC3T3-E1 was cultured on scaffold specimens for 3, 5, and 7 day to observe the production of alkaline phosphatase (ALP). The specimens were rinsed with PBS 2 times after removal of culture medium. Alkaline lysis buffer (10 mM Tris-HCl, 2 mM MgCl₂, 0.1% Triton-X100, pH 10) (100 μl/well) was added and the samples were scrapped and then frozen at -20°C for at least 30 min prior to the next step. An aqueous solution of 2 mg/ml *p*-nitrophenyl phosphate (pNPP; Zymed Laboratories, USA) mixed with 0.1 M

amino propanol (10 μ l/well) in 2 mM MgCl₂ (100 μ l/well) having a pH of 10.5 was prepared and added into the specimens (110 μ l/well). The specimens were incubated at 37°C for 15 min. The reaction was stopped by adding 900 μ l /well of 50 mM NaOH and the extracted solution was transferred to a cuvette and placed in the UV-visible spectrophotometer, from which the absorbance at 410 nm was measured. The amount of ALP was then calculated against a standard curve. In order to calculate for the ALP activity, the amount of ALP had to be normalized by the amount of total protein synthesized. In the protein assay, the samples were treated in the same manner as the ALP assay up to the point was the specimens were frozen. After freezing, bicinchoninic acid (BCA; Pierce Biotechnology, USA) solution was added into the specimens. The specimens were incubated at 37°C for 15 min. The absorbance of the medium solution was then measured at 562 nm by the UV-visible spectrophotometer and the amount of the total protein was calculated against a standard curve.

Mineralization analysis. Alizarin Red-S is a dye that binds selectively calcium salts and is widely used for mineral staining (the staining product i.e., an Alizarin Red S-calcium chelating product). The isolated osteoblastic cells were plated in 24-well plates at 40,000 cells/well and cultured in the culture medium. After 24 h, the cultures were treated with culture medium, with the supplement of 50 μg/ml ascorbic acid (Sigma, USA), 5 mM β-glycerophosphate (Sigma, USA), and 0.2 μg/ml dexamethasone (Sigma, USA), the medium was replaced every 2 days. After 16 days treatment, cells were washed with PBS and fixed with ice-cold absolute methanol for 10 min. Fixed cells were stained with 1% Alizarin Red in deionized water (Sigma, USA) (pH 4.2) for 2-3 min. After removing alizarin red-S solution, the cells were rinsed with deionized water and dried at room temperature. The images of each culture were captured and the stain was extracted with the use of 10% cetylpyridinium chloride (Sigma, USA) in 10 mM sodium phosphate for 1 h and absorbance of the collected dye was read at 570 nm in spectrophotometer (Thermo Spectronics Genesis10 UV-visible spectrophotometer).

6. Statistical analysis. Values expressed as the mean \pm standard deviation. Statistical analysis of different data groups was performed using One-Way Analysis of Variance (ANOVA) with the least-significant difference (LSD) test using SPSS software version 11.5. The values of p lower 0.05 were considered statistically significant.

Results and Discussion

By reaction with diamine, 1,6-hexanediamine (HMD), amino groups can be covalently introduced onto the surface of the electro-spun PLA fibrous membranes to obtain the aminolyzed PLA fibrous membranes. One amino group (NH₂) of HMD reacts with an ester group (—COO—) of PLA to form the amide linkage (—CONH—), while another amino group is unreacted and free for the further reaction.

These free NH_2 groups can be used as active sites through which proteins like collagen can be bonded to the surface using N,N'-disuccinimidyl carbonate (DSC) as a coupling agent. However, to avoid aggregation, two-step procedure was employed. The attached amino groups had been first activated with DSC with N-hydroxysuccinimide being lost from the reaction and the as-formed succinimidyl esters were later reacted with respective collagen, with N-hydroxysuccinimide again being cleaved from the reaction.

1. Characterization of neat and modified PLA fibrous scaffolds.

Quantification of free amino groups on the surface. The existence of free amino groups (NH₂) on PLA surface is a prerequisite for protein bonding in this modification method. It is important to confirm the existence of amino groups before protein is further introduced. Herein, ninhydrin is used as an indicator to confirm and quantify the -NH2 moiety on the aminolyzed PLA surface. The NH2 density on e-spun PLA fibrous scaffold surface was influenced by the concentration of HMD, aminolyzing time, temperature, and so on. Because the glass transition temperature (T_g) of the present PLA is ~60-70°C, the aminolyzing temperature should be lower than this value to maintain the shape of the material. Hence, 50°C was chosen to perform the following reactions. Table 1 shows that NH₂ density increased with increasing HMD concentration. However, when the concentration of HMD is equal to or greater than 0.1 g/ml, the mechanical integrity of the e-spun PLA fiber mats was affected. Table 2 shows that the surface-bound NH₂ increased with increasing aminolyzing time to reach a maximum value at about 15 min, and then decreased slightly. The decrease at the longer reaction time may be caused by a further reaction of the free amino group on the terminal chain with other ester groups, or by the degradation of the superficial layer²⁷. Both of these situations will reduce the density of the surface amino groups and thus intensity of purple colored complex. To maintain enough mechanical integrity for practical applications, PLA e-spun fiber mats were aminolyzed in a 0.04 g/ml HMD/IPA solution at 50°C for 15 min. According to the calibration curve obtained with 1,4-dioxane/isopropanol (1:1, v/v) solution containing HMD of known concentration, the NH₂ density on PLA e-spun fiber mat aminolyzed under these conditions was $(3.7 \pm 0.02) \times 10^{-7} \text{ mol/cm}^2$ (see Table 3). It also shows that after immobilization with 0.5 mg/ml and 3.0 mg/ml type-I collagen, the average areal density of the amino groups on the surface of the PLA fibrous scaffolds were (4.52 \pm 0.08) x 10^{-9} and $(3.21 \pm 0.2) \times 10^{-8}$, respectively.

Surface Wettability. To further evaluate the effect of aminolysis and collagen immobilization, surface wettability of the modified PLA fibrous scaffolds with respect to that of the neat PLA fibrous scaffolds was measured. Table 4 shows the surface wettability of neat PLA, aminolyzed PLA, activated PLA, collagen-immobilized PLA (without coupling agent; collagen = 0.5 mg/ml), collagen-immobilized PLA (collagen = 0.5 mg/ml), and collagen-immobilized PLA (collagen = 3 mg/ml) fibrous scaffolds. The water contact angle measured by the sessile drop method decreased slightly from 106.8° to 99.5° after the scaffold was aminolyzed with 0.04 g/ml of HMD/IPA solution for 15 min. That is, the introduction of the

amino groups on the surface of the PLA fibrous scaffolds improved the hydrophilicity of the surface. After the aminolyzed PLA fibrous scaffolds has activated with DSC, their surface became more hydrophobic as evidenced by the water contact angle of 112.5°. Water contact angle decreased substantially after the collagen was bonded. Figure 2 shows that the surface became much more hydrophilic after collagen immobilization. Water contact angle was 79.4° for collagen 0.5 mg/ml immersion and was 73.0° for collagen 3 mg/ml immersion. These results show that the more collagen concentration used, the more collagen can be bonded to the PLA surface. It has been known that physisorption processes are virtually always involved in a coating procedure. In our case, we had tried physical coating of collagen on unactivated PLA fibrous scaffolds. Water contact angle measurements showed that water contact angle of physisorbed collagen-coated PLA surfaces was slightly lower than the aminolyzed PLA surface. On the other hand, for collagen-covalently bonded surface, they exhibited much lower water contact angle. That means activation step is an important step in protein grafting process.

Elemental composition of the surface. The surface alteration after the PLA fibrous scaffolds were modified was studied by X-ray Photoelectron Spectrometer (XPS). To study the effect of the aminolysis condition on the surface alteration, N_{1s}/C_{1s} ratios as a function of HMD concentration and aminolyzing time were evaluated. Table 5 shows that the more diamine concentration used, the more N_{1s}/C_{1s} ratio observed which could be due to increasing in introduced NH_2 group concentration. Table 6 shows that the N_{1s}/C_{1s} ratio increased with increasing aminolyzing time to reach a maximum value at about 15 min, and then decreased slightly, which, in addition to the results on ninhydrin analysis method. Figure 3 shows that N_{1s} peaks obviously appeared after immobilization of collagen, which confirmed protein grafting. Table 7 shows N_{1s}/C_{1s} ratio of the neat and the modified PLA fibrous scaffolds. After aminolysis of PLA fibrous scaffold, the N_{1s}/C_{1s} ratio was increased from 0 to 0.0290 because of NH_2 groups introduced on the surface. The N_{1s}/C_{1s} ratio was further increased to 0.0381 by reaction with DSC. It shows that the nitrogen concentration increased when succinimidyl esters was formed. Finally, it was obviously increasing in N_{1s}/C_{1s} ratio after collagen immobilization due to the large amount of nitrogen atom in collagen structure was additionally introduced.

2. Biological evaluation of neat and modified PLA fibrous scaffolds.

Indirect cytotoxicity evaluation. The biocompatibity of these PLA e-spun fiber mats as bone scaffolds was assessed by an indirect cytotoxicity evaluation with mouse fibroblastic cells (L929) and mouse calvaria-derived pre-osteoblastic cells (MC3T3-E1), based on the initial 40,000 cells/well of cells seeded. Indirect cytotoxicity test was conducted on neat, aminolyzed, activated, collagen-immobilized PLA fibrous scaffolds. In this experiment, the PCL/HA that was prepared from particulate leaching technique, was chosen to be the positive control. Even though we were interested in using the obtained modified fiber mats as potential bone scaffolds, it was mandatory to test the materials with L929 just to comply with the

ISO10993-5 standard test method. Figure 4a shows %viability obtained from MTT assay of L929 which were cultured with the 1, 3, 7 day- extraction media in comparison with those cultured with SFM (i.e. control). The viability of the cells that had been cultured with SFM at any given time point was taken as the basis to arrive at the relative viability shown in the figure. Evidently, the viability of L929 for all types of modified PLA fibrous scaffolds exhibited slightly lower, in comparison with that of the control (100%). While the neat PLA fiber and PCL/HA scaffold which used as positive control exhibited comparable viability. In a similar manner was found for MC3T3-E1 (see Figure 4b). However, the viability of cells that were cultured with 7-day extraction media prepared from modified scaffolds were significantly lower, in comparison with that were cultured with 7-day extraction media prepared from the neat PLA scaffold and PCL/HA. Thus, we had to set other experiment to confirm the cytocompatibility of the modified PLA fibrous scaffolds.

MC3T3-E1 was cultured in wells of a 24-well culture plate in 2% serum-containing MEM diluted with 7-day extraction medium for 1, 2, and 3 d to allow cell growth on the plate. Figure 5 shows that the viability of MC3T3-E1, cultured with 2% serum-containing MEM diluted with 7-day extraction media prepared by all types of modified scaffolds, were increased with increasing the culturing time in the respective media. All of the obtained results clearly suggested that all types of the PLA fibrous scaffolds, released no substances at levels that were harmful to both types of cells.

Cell attachment and cell proliferation. The potential for use of the neat and the modified PLA fibrous scaffolds was further evaluated by observing their ability to support both the adhesion and the proliferation of MC3T3-E1. The viability of the cells that had been cultured on the surface of TCPS for 2 h was taken as the basis to arrive at the relative viability shown in a figure. Figure 6 shows the attachment of MC3T3-E1 on the surfaces of TCPS, neat PLA, aminolyzed PLA, activated PLA and collagen-immobilized PLA at 2, 4, and 16 h after cell seeding in terms of viability. On TCPS, the number of the attached cells increased from ~100% at 2 h after cell seeding to ~111% at 16 h after cell seeding, based on the initial number of cells seeded (60,000 cells/well). With regards to MC3T3-E1, the surfaces of all of the PLA fibrous scaffolds were inferior in supporting the attachment of the cells to that of TCPS. Specifically, the number of cells attached on these fibrous scaffolds was only ~50% in comparison with that on TCPS at any given time point. There was not significantly different in the viability among all types of the fibrous scaffolds. Figure 7 shows the proliferation of MC3T3-E1 on the surfaces of TCPS, neat PLA, aminolyzed PLA, activated PLA and collagen-immobilized PLA on day 1, 2, and 3 after cell culture in terms of viability (%relative to TCPS at day1). On TCPS, the number of cells increased from ~100% on day1 after cell culture to ~187% (i.e., an increase of about 2 fold from the initial number of cells seeded) on day 3 after cell culture, based on the initial 30,000 cells/well of cells seeded. In comparison with that on TCPS, the viability of the cells cultured on the modified PLA fibrous scaffolds were significantly higher at any given

time point. The viability of cells proliferated on these fibrous scaffolds, at day 3, was higher than TCPS of about 2 fold for neat PLA, aminolyzed PLA, and activated PLA and about 3.5 fold for collagen-immobilized PLA. Marked improvement was achieved with the collagen-immobilized PLA fibrous scaffolds on day 3 after cell culture.

The lesser viability of cells in the attachment period on various types of the fibrous scaffolds in comparison with that on TCPS could be due to the lesser number of cells that were able to attach on the rougher and more hydrophobic surface of the fibrous scaffolds in comparison with the smoother and hydrophilic surface of TCPS. On the contrary, the greater number of cells in the proliferation period on all types of PLA fibrous scaffolds could be because of high surface area to mass or volume and high porosity of the e-spun fiber mats though which the cells were able to penetrate into the scaffolds. Among the various modified PLA fibrous scaffolds, the collagen-immobilized PLA fibrous scaffolds provided the most significant improvement in the ability to support the proliferation of the cells which could be due to the protein-containing and hydrophilic surface of the substrate.

Cell Morphology. Table 8 shows selected SEM image (magnification = 2000X; scale bar = 10 μm) of MC3T3-E1 that were cultured on the surface of glass, neat PLA, aminolyzed PLA, activated PLA and collagen-immobilized PLA at two different time points, while the SEM images at magnification = 500X are available as Supporting Information. The use of glass as the control instead of TCPS was due to the ease of taking the samples to SEM observation. These images provided snap shots in time that revealed the morphology of the cells and interaction between the cells and the tested surfaces. At 4 h after cell seeding, based on the initial 60,000 cells/well of cells seeded, the majority of the cells on the glass surface started to extend their cytoplasm, an evidence of the ability of the cells to attach on the surface. At 16 h after cell seeding, expansion of the cytoplasm of the majority of the cells was evident. While the majority of MC3T3-E1 that had been seeded on the surfaces of unmodified PLA fibrous scaffolds for 4 h was remained round, but a closer examination around the edge of the cells revealed an evidence of filopodia (i.e., slender cytoplasmic projections extending from the leading edge of the migrating cells that help the cells during their migration over the surface of a scaffolds). The majority of the cells were evidently expanded after 16 h of cell seeding. On the other hand, the majority of the cells seeded on the surfaces of various types of modified PLA fibrous scaffolds showed an evidence of the extension of their cytoplasm on the fibrous surface even at 4 h after cell seeding, with collagen-immobilized PLA surface did so to a greater extent. These results suggested that the cells prefer the fibrous surfaces of modified PLA over that of the unmodified. Specifically, the cells were seemed to prefer the collagen-containing than others.

Alkaline Phosphatase (ALP) Activity. The ability for these PLA fibrous scaffolds to support differentiation, in addition to attachment and proliferation, of cultured cells is another important aspect suggesting actual applicability of the scaffold. Alkaline phosphatase is a membrane bound enzyme and its

activity is used as an osteoblastic differentiation marker, as it is produced only by cells showing mineralized ECM. The ALP activity of MC3T3-E1 on TCPS (i.e. controls), neat PLA, aminolyzed PLA, activated PLA, and collagen-immobilized PLA were monitored at 3, 5 and 7 days in culture (see Figure 8). Apparently, the amount of ALP synthesized by the cells that were cultured on TCPS and all of the fibrous scaffolds increased with the initial increase in time in culture between day 3 and 5, reached a maximum level on day 5, and decreased with a further increase in culture after day 3. In comparison with other substrates, TCPS exhibited the highest ALP activity of MC3T3-E1. According to Figure 8, activated PLA and collagen-immobilized PLA fibrous scaffolds showed the highest ALP activity among the various fibrous scaffolds investigated at day 3 of cell culturing time. And at day 5 and day 7 collagen-immobilized PLA fibrous scaffolds exhibited the highest ALP activity.

The decrease in the ALP activity, after day 5 for the cells grown on both TCPS and PLA fibrous scaffolds, with a further increase in the culturing time can be due to cellular process switching onto further step (i.e. mineralization). Since ALP is not an exclusive protein synthesized by osteoblasts as it is also found in tissues of such organs as kidneys, small intestines, and placenta, the presence of ALP of MC3T3-E1 that were cultured on these substrates could not be used as the sole marker to confirm the osteoblastic phenotype of the cells. From the obtained results, it was suggested that collagen-immobilized PLA fibrous scaffold was the best among the PLA fibrous scaffolds that promoted both proliferation and differentiation of MC3T3-E1.

Mineralization. Mineralization refers to cell-mediated deposition of extracellular calcium and phosphorus salts where anionic matrix molecules take up the Ca^{2+} , phosphate ions and serve as nucleation and growth sites leading to calcification. Mineralization was quantified by Alizarin Red-S studies (see Figure 9), showing degree of mineralization as indicated by extracted stain absorbance obtained on day 16 of cell culture was in the order of collagen-immobilized PLA > aminolyzed PLA > neat PLA > activated PLA > TCPS > glass. The collagen-immobilized PLA scaffold showed 16% higher mineralization than neat PLA scaffold with significant level of p < 0.05 confirming the effectiveness of collagen immobilization of PLA e-spun fibers in mineral formation by MC3T3-E1. The photographic images (see Figure 10) of scaffolds stained with Alizarin Red-S for 16 days supported the above data where high intensity of staining minerals was observed on various type of PLA fibrous scaffolds displaying an overall enhancing effect in mineralization of MC3T3-E1 cells and proving collagen immobilization as an indispensable method for the fabrication of superior fibrous scaffolds for bone tissue engineering.

Conclusion

In the present study, type-I collagen was used to modify PLA in the form of electro-spun fibrous membranes for the purpose of improving cytocompatibility. The XPS confirmed that collagen was immobilized on the surface of PLA fiber mats by the reaction of aminolyzed PLA and type-I collagen employing DSC as a coupling agent. The existence of NH₂ groups on aminolyzed PLA surfaces has been characterized by ninhydrin analysis method, which revealed that the NH₂ density was influenced by the HMD concentration and aminolyzing time. The data of contact angle against water revealed that it had improved the surface hydrophilicity by the aminolysis and the further immobilization of collagen. The cultured MC3T3-E1 *in vitro* proved that the cell proliferation, alkaline phosphatase (ALP) activity and mineralization of modified PLA e-spun fibers were improved compared with the neat PLA fiber. Among the various modified PLA scaffolds, collagen-immobilized PLA showed the greatest ability to support cell proliferation, alkaline ALP activity, and mineralization. Therefore, collagen-immobilized PLA fibrous scaffold is promising material to accelerate bone regeneration.

7. Use of 2-hydroxypropyl-β-cyclodextrin as adjuvant for enhancing encapsulation and release characteristics of asiaticoside within and from cellulose acetate films

Experimental details

Materials

Cellulose acetate (CA; white powder; Mw \approx 30,000 Da; acetyl content = 39.7 wt.%; degree of acetyl substitution \approx 2.4) and 2-hydroxypropyl- β -cyclodextrin (HP β CD; Mw \approx 1,380 Da; average number of substituent per glucopyranose unit \approx 0.6) were purchased from Sigma–Aldrich (Switzerland). Asiaticoside (AC; 90% purity) was purchased from Shanghai Angoal Chemical Co., Ltd.(China). N,N-Dimethylacetamide (DMAc, Lab-Scan Asia, Thailand),glacial acetic acid (Carlo Erba, Italy), anhydrous disodium hydrogen orthophosphate, sodium dihydrogen orthophosphate, and sodium chloride (Ajax Chemicals, Australia) were used as-received. All chemicals were of analytical reagent grades and used without further purification.

Stoichiometry of AC/HP*CD complex in solution state

Phase solubility studies

Phase solubility of AC in HP β CD was studied in distilled water. Briefly, excess amounts of AC were put into aqueous HP β CD solutions(1 mL). The amount of HP β CD in the solutions was varied between 0 and 30mM. The sample solutions were then stirred at room temperature (25%1 °C) for 24 h. It should be noted that the stirring time of 24 h was enough for the solubilization of AC in HP β CD to reach equilibrium. After reaching the equilibrium, unsolubilized AC in the sample solutions was filtered out through a filter membrane (0.45 μ min pore diameter). The filtrates were later quantified for the amounts of the solubilized AC by reversed-phase high performance liquid chromatography (HPLC; see later). The association constant (Ka) was then calculated from the following equation (Higuchi & Connors, 1965):

$$K_a = \frac{m}{s_0(1-m)},\tag{1}$$

where m is the slope of the plot between the solubility of AC in distilled water as a function of the HPβCD concentration and s0 is the solubility of AC in distilled water in the absence of HPβCD. In addition, the complexation efficiency (CE) and the AC:HPβCD molar ratio ([AC]:[CD]) were calculated as follows (Loftsson, Hreindottir, & Musson, 2007):

$$CE = s_0 K_{1:1} = \frac{[AC]/[CD]}{[CD]} = \frac{m}{1-m},$$
 (2)

$$\frac{[AC]}{[CD]} = \frac{1}{1 + (1/CE)},\tag{3}$$

where K_{1:1} is the association constant for the AC:HP CDmolar ratio of 1:1.

The phase solubility of AC in HP_CD was also studied in a 90:10 (v/v) mixture of 80 vol.% acetic acid and DMAc. To ensure the formation of the AC/HP β CD complex in the solvent mixture, the preparation procedure was similar to what had been described above, with an exception to the fact that the mixture of acetic acid and DMAc was used instead of the distilled water.

1H-NMR studies

A Varian UNITYINOVA 1H-nuclear magnetic resonance spectrometer(1H-NMR), operating at 400MHz and 25 °C, was used to determine the stoichiometric ratio of the AC/HP β CD complex. Based on the Job's continuous variation method (Job, 1928), the 1H-NMR spectra were recorded from a mixture of AC (10mM) and HP β CD (10mM) in 10% (v/v) DMSO-d6/D2O mixture at various volumetric ratios between these two solutions at the final concentrations of AC of 1–10mM, prior to being stirred for 24 h.

Preparation of AC/HPβCD complex in solid state

The AC/HP β CD complex was prepared according to the method previously described by Higuchi and Connors (1965), with slight modification. Briefly, a weighed amount of HP_CD was first dissolved in distilled water. A weighed amount of AC was then added to the solution and stirred at room temperature (25±1 °C) for 24 h. The stoichiometric AC:HP β CD molar ratio, as obtained from the studies in Section 2.2, was utilized throughout the rest of the studies. The solution/suspension was filtered through a nylon filter (average pore size = 0.45 μ m) prior to being frozen at -40±2 °C for 24 h. After that, the obtained mass was lyophilized (Labconco FreeZone 6-Liter Benchtop Freeze Dry System). A physical blend of AC and HP β CD at the same molar ratio was also prepared for comparison.

Characterization of solid AC/HPBCD complex

1. X-ray powder diffractometry

X-ray powder diffractograms of the AC/HP_CD complex and the corresponding physical mixture were obtained on a Bruker Model D8 Advance, equipped with a Cu K λ radiation source, over a scattering (2°) range of 5 and 60° at room temperature (25 ± 1 °C). The scan rate, the operating voltage, and the filament current were set at 0.2° min=1, 40 kV, and 30 mA, respectively.

2. Two dimensional 1H-NMR studies

To obtain the 2D 1H-NMR spectrum of the AC/HP β CD complex, the freeze-dried product was dissolved in D2O at room temperature (25 \pm 1 °C) and investigated under the following conditions: acquisition time of 0.205 s, sweep width of 5006.3 Hz, pulse width of 6.3_s, time domain of 2048, Fourier number of 2048 and temperature of 298 K.

Preparation of AC- and AC/HPβCD complex-loaded CA films

CA films containing either AC or AC/HP β CD complex were prepared by solvent casting technique. AC or a AC/HP β CD complex that had been prepared at different mixing molar ratios of HP β CD to AC (i.e., 0.5, 1.0, or 2.0) was incorporated at a concentration of 10%, based on the dry weight of CA powder, in a 90:10 (v/v) mixture of 80 vol.% acetic acid and DMAc. The concentration of CA in the final solutions was 4% w/v. The as-prepared solutions were stirred at room temperature (25±1 °C) for 24 h. Prior to the addition of CA powder, each of the sample solutions was characterized for the particle size of the self-assembling aggregates by a Malvern Zetasizer ZS nanosizer [based on the dynamic light scattering (DLS) principle]. CA powder was then added to the sample solution and subsequently stirred at room temperature (25±1 °C) for 3 h until CA was completely dissolved. The solutions were subsequently poured onto glass Petri dishes and dried under a reduced pressure. The films were dried until of a constant weight and stored in a desiccator in vacuo for at least 24 h, prior to further use. The thicknesses of the as-cast films were $80\pm10_{\rm m}$.

Characterization of AC- and AC/HPBCD complex-loaded CA films

Morphologies of AC- and AC/HPβCD complex-loaded CA films were studied by a JEOL JSM-6400 scanning electron microscope(SEM). All of the specimens were vacuum-coated with a thin layer of gold using a JEOL JFC-1100E sputtering device. The average diameters of the self-assembling aggregates and the pores that were formed after the films had been immersed in a phosphate buffer saline solution (PBS; see later for its preparation) containing 10% (v/v) methanol (hereafter, P/B/M medium) for 24 h were determined by measuring the diameters of the micro-aggregates and the micro-pores at 100 different points on the SEM images of 7500 magnification with SemAphore 4.0 software. For each sample, the diameters were presented as the average Nstandard deviation.

Water retention and weight loss behavior of the AC- and the AC/HP β CD complex-loaded CA films were investigated after their immersion in the P/B/M medium at 37 °C for 24 h. The water retention and the weight loss behavior were calculated as follows:

Water retention (%) =
$$\frac{M - M_d}{M_d} \times 100$$
, (4)

and

Weight loss (%) =
$$\frac{M_i - M_d}{M_d} \times 100$$
, (5)

where M and Md are wet and dry weights of the film specimens after immersion in the buffer solution, respectively, and Mi is the initial, dry weight of the specimens. All measurements were carried out in triplicate.

Release of AC from AC- and AC/HPBCD complex-loaded CA films

1. Preparation of releasing medium

To prepare 1 L of the PBS solution, 6.177 g of anhydrous disodium hydrogen orthophosphate and 1.1014 g of sodium dihydrogen orthophosphate were dissolved under mechanical stirring in distilled water at room temperature (25 ± 1 °C) until the flakes were completely dissolved. Later, 8.7 g of sodium chloride was added into 20mL of the solution. The volumewas adjusted to the required volume with distilled water. The pH of the final solution was 7.4.

2. Actual AC content

The actual amounts of ACin the AC- and the AC/HP β CD complex loaded CA films were quantified by dissolving the samples (circulardisc: about 1.5cm in diameter) in 4mL of 2:1 (v/v) acetone/DMAc. After that, 0.5mL of the solutions were pipetted and diluted into 8mL of the P/B/M medium. Finally, the AC contents in the diluted sample solutions were determined by HPLC (see later) and then back-calculated from the obtained data against a calibration curve for AC.

3. AC release assay

The release characteristics of ACfrom the AC- and the AC/HP β CD complex-loaded CA films were determined by the total immersion method. Each of the specimens (circular disc of about 1.5cm in diameter) was immersed in 25mL of the P/B/M medium at the physiological temperature of 37 °C. At each time point, ranging between 0 and 24 h(1440 min), 1mL of themedium was withdrawn (i.e., sample solution) and an equalamount of the fresh mediumwas refilled. The amounts of AC in the sample solutions were quantified by HPLC (see later) and then back-calculated from the obtained data against the calibration curve for AC.

Determination of AC content

The amount of AC in a given sample solution was determined by HPLC (Shimadzu LC-10 AD). The sample solution was filtered through a nylon filter (average pore size = 0.45_m) and then separated in an Inertsil ODS-3 C18 column (particle size = 5_m; column dimension = 4.6mm²250mm) with an Inertsil ODS-3 guard column (particle size = 5_m; column dimension = 4.0mm¹10mm) at a flow rate of 1mLmin-1. A UV-Visible detector was set a (_max) 204 nm. The mobile phase for the AC separation consisted of acetonitrile, methanol, and distilled water at 26:24:50 (v/v/v) and the retention time was 7.7 min. The calibration curve for AC was obtained over a concentration range of 0.005-0.200mgmL-1.

Statistical analysis

One-way ANOVA was used to analyze the means of different data sets. The significance for all of the tests was accepted at a 0.05 confidence level.

Results and discussion

Stoichiometry of AC/HPβCD complex in solution state

The solubility of AC in the absence or the presence of HP β CD was studied in two types of medium (i.e., distilled water or 90:10 (v/v) of 80% acetic acid and DMAc) and the results are graphically shown in Fig. 2. In the absence of HPBCD, the solubility of AC in any type of the studied medium (i.e., s0) was low (i.e., 0.7mM in distilled water and 48.7mM in 90:10 (v/v) of 80% acetic acid and DMAc). Marked increase in the amounts of solubleACin either mediumwas evident in the presence of HPβCD. At the greatest amount of HPBCD investigated (i.e., 30 mM), the amounts of soluble AC increased to 15.3 and 60.0mM in distilled water and 90:10 (v/v) of 80% acetic acid and DMAc, respectively. Obviously, the amounts of soluble AC in both types of medium exhibited linear relationships with the HPBCD content in the solutions. The association constants, Ka, characterizing the solubility of AC in distilled water and 90:10 (v/v) of 80% acetic acid and DMAc, can be calculated from the slopes of the plots such as those shown in Fig. 2. The slopes of the least-squared lines drawn through both sets of data were less than one, with the values being 0.505 and 0.380, respectively. According to the definition set forth by Higuchi and Connors (1965), these could be categorized as AL type and a 1:1 complex between AC and HPβCD could be assumed. Based on the values of the slopes obtained, the Ka values (or the K1:1 values, for this particular case) can be calculated, based in Eq. (1), to be 11,726.5 and 12.5M-1, respectively. According to Eq. (2), the complexation coefficient values, CE, were determined to be 1.020 and 0.613, respectively, while, according to Eq. (3), the AC:HPβCD molar ratios were 1:2 and 1:3, respectively. This means that, despite the stoichiometric 1:1 molar ratio between AC and HPβCD in the as-formed complex, only 1 in every 2 or 3 molecules of HPβCD underwent the complexation with AC.

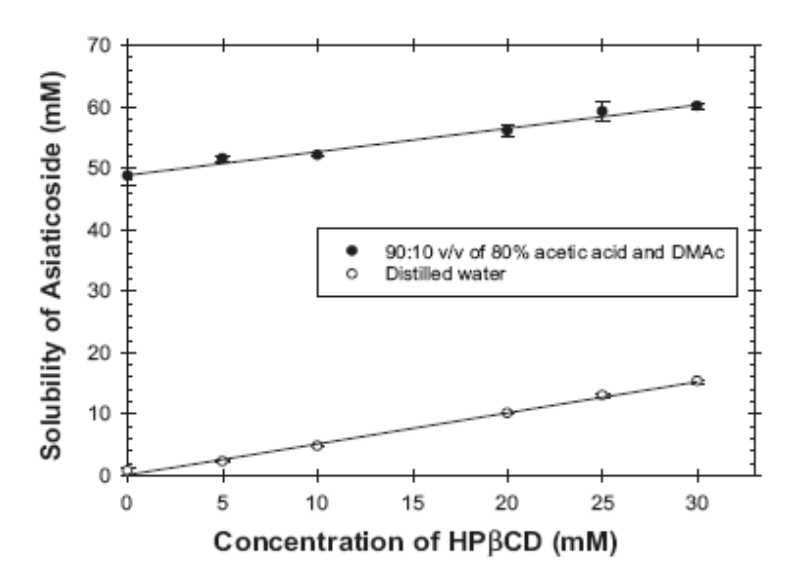


Fig. 2. Phase solubility diagrams of AC in the absence or the presence of 2-hydroxypropyl- β -cyclodextrin (HP β CD) in distilled water and 90:10 (v/v) of 80% acetic acid and DMAc at room temperature.

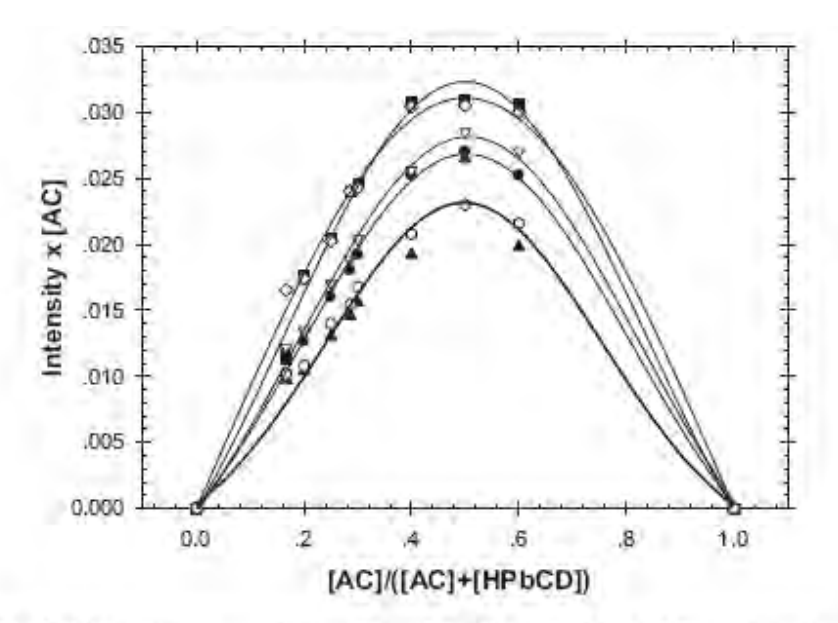


Fig. 3. Job's continuous variation plots of the chemical shifts of the protons, i.e., (∇) H-12, (\diamondsuit) H-18, (\blacktriangle) CH₃-26, (\bullet) CH₃-29, (\blacksquare) Glc-1, and (\bigcirc) Rha-5, of AC, in the presence of different HPBCD concentrations in the 90:10 (v/v) mixture of D₂O and DMSO-d₆.

One dimensional 1H-NMR spectroscopy is useful for studying the inclusion complex of HP β CD with various organic compounds. The variation in the chemical shift of the protons of organic compounds (_1= 1c -10, where 1c and 10 are the chemical shifts of a specific chemical species in the complex and the free forms, respectively), due to the screening environment by magnetic nuclei within the HP β CD cavity, was recorded. In particular, changes in the chemical shifts of protons of the guest molecule(s) within the

CD cavity can be used to quantify the stoichiometry of the complex, simply by plotting them as a function of the mole fraction of the guest molecule(s) or the CD molecule [i.e., Job's continuous variation plots (Job, 1928)]. The mole fraction at the maximum peak(s) is taken as the stoichiometric ratio of the complex. According to Fig. 3, the chemical shifts of CH3-26, CH3-29, H-12, H-18, Rha-5, and Glc-1 protons in the AC/HP β CD mixtures, in 90:10 (v/v) mixture of D2O and DMSO-d6, exhibited the maximum peaks at [AC]/([AC] + [HP β CD]) = 0.5, corresponding to the AC:HP β CD molar ratio of 1:1. In addition, Table 1 shows the chemical shift signals of protons of AC and HP $_{\alpha}$ CD, both in the free and the complex states, inD2Oat equi-molar ratio between AC and HP $_{\alpha}$ CD, along with their differences.

Characterization of AC/HP β CD complex in solid state

X-ray powder diffractometry

The freeze-dried product from the equi-molar mixture of AC and HP β CD was white powder. X-ray powder diffractometry was then used to confirm the formation of the AC/HP β CD complex. Fig. 4 shows the X-ray diffractograms of AC, HP β CD, the AC/HP β CD complex, and the physical mixture of AC and HP β CD. Sharp diffraction peaks were evident for the as-received AC, indicating its crys talline nature. On the other hand, only diffused, scattering peaks were observed for the as-received HP β CD, with the scattering center being observed at the scattering angle, 2_, of about 18°. This indicates the amorphous nature of HP β CD. As for the AC/HP β CD complex, only the scattering peaks similar to those of HP β CD were obtained, indicating the amorphous nature of the material. When AC was physically mixed with HP β CD, however, both the sharp diffraction peaks of AC and the diffused, scattering peaks of HP β CD were evident. These results confirmed the inclusion of AC within the cavity of HP β CD.

Two dimensional 1H-NMR

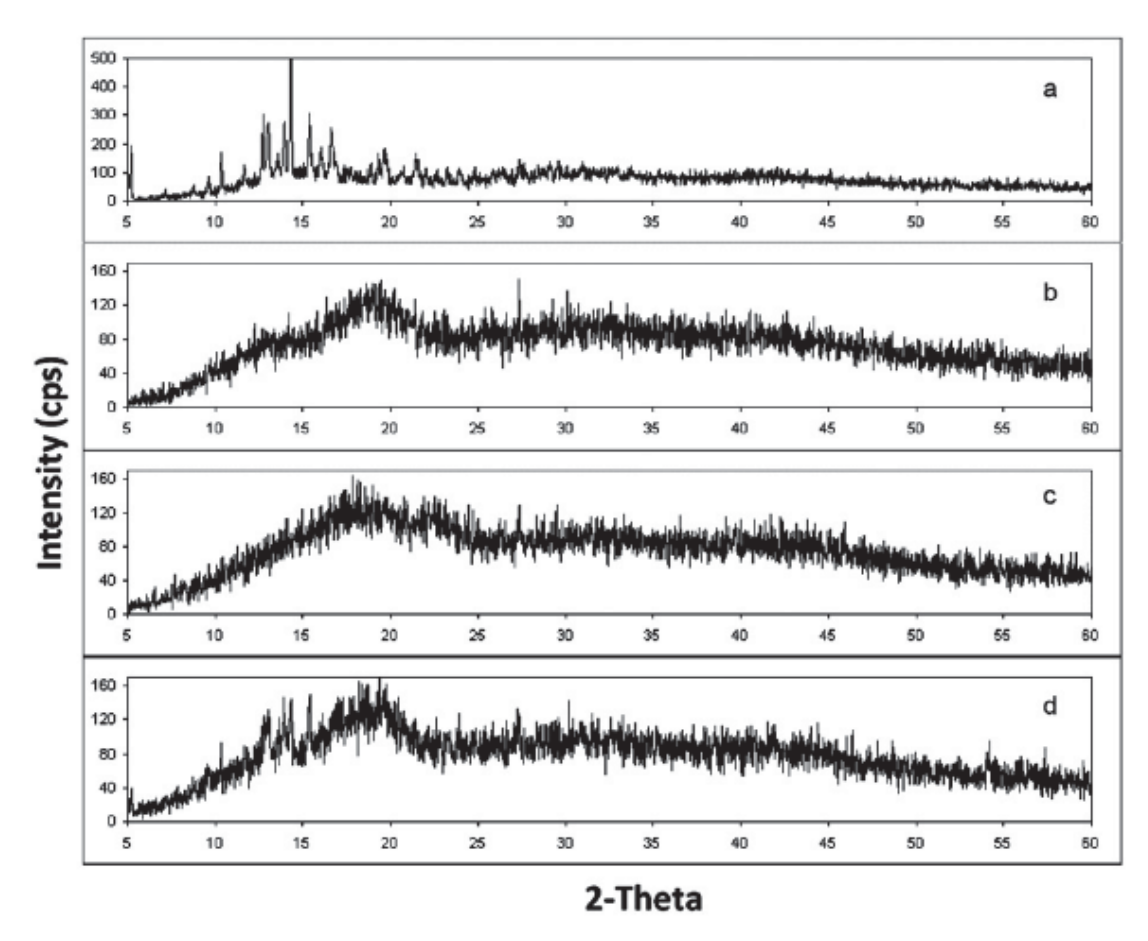
To investigate the spatial arrangement of AC within the HP β CD cavity, Nuclear Overhauser Effect Spectroscopy (NOESY) was applied on the stoichiometric AC/HP_CD complex (1:1 molar ratio) that had been dissolved in D2O and the result is shown in Fig. 5a.Cross-peaks were observed between the CH3-29 and CH3-27 protons of AC and the H-3 inner-cavity proton of HP_CD (located at the wide side of the cavity) and between the CH3-26 and H-6 protons of AC and the H-5 inner-cavity proton of HP_CD (located at the narrow side of the cavity). This indicates that the cyclohexene ring moiety of AC is captivated within the cavity of HP_CD, as depicted in Fig. 5b, hence confirming the stoichiometric 1:1 molar ratio between AC and HP_CD in the solid complex. Notwithstanding, the specific interactions between H-12, H-18, Glc-1, Rha-5, and Rha-Me protons of AC and the H-2, H-4, and H-6 outer-cavity protons of HP_CD are believed to be the probable cause for the self-aggregation of adjacent AC/HP_CD entities.

Characterization of AC- and AC/HP*CD complex-loaded CA films

Physical appearance

Prior to the addition of CA powder into the AC/HP_CD solutions, the diametric dimensions of the self-assembling aggregates of the AC/HP_CD complex that had been prepared at different HP_CD to AC molar ratios of 0.5, 1, and 2 were determined by the nanosizer to be 2.38%1.39, 3.34%0.66, and 3.84%0.53_m, respectively (see Supplementary data). Evidently, the size of the aggregates was an increasing function of the HP_CD proportion in the solution. CDs are known to form into self-assembling aggregates, which is facilitated by their ability to form inter-molecular hydrogen bonding (Coleman & Nicolis, 1992; Gonzulez-Gaitano et al., 2002; Suzuki, Tsutsui, & Ohmori, 1994). In addition, Mele et al. (1998) reported that _-carotene in its complexation with _ and _-CDs in water existed as large aggregates, as revealed by both light scatteringand 1H NMR techniques. Factors that influence the formation of self-assembling aggregates are, for examples, concentration and molecular weight of CDs, pH, and temperature, while high pH, high temperature, and the addition of an electrolyte have been used as

means to prevent the aggregation (Bonini et al., 2006; Das, Mallick, Sarkar, & Chattopadhyay, 2008; He, Fu, Shen, & Gao, 2008).



 $\textbf{Fig. 4.} \ \, \textbf{X-ray diffractograms of (a) AC, (b) HP} \\ \textbf{CD, (c) AC/HP} \\ \textbf{CD complex, and (d) physical mixture of AC and HP} \\ \textbf{BCD.} \\ \textbf{CD.} \\ \textbf$

Table 1 Chemical shift signals of protons (in ppm) of AC and HPβCD in the free (δ_0) and the complexed (δ_c) states in D₂O at the equi-molar ratio between AC and HPβCD of the inclusion complex, along with their differences.

Proton	δ_0	δ_{c}	$\Delta\delta(\delta_c - \delta_0)$
AC			
H-12	5.162	5.216	0.054
H-18	2.033	2.087	0.054
CH ₃ -24	0.644	0.667	0.023
CH₃-26	0.777	0.831	0.054
CH₃-27	1.132	1.134	0.002
CH₃-29	0.844	0.869	0.025
Glc-1	4.385	4.323	-0.062
Rha-CH ₃	1.301	1.321	0.002
Rha-5	3.942	3.988	0.046
HPβCD			
H-1	5.090	5.086	-0.004
H-2	3.542	3.546	0.004
H-3	3.817	3.896	0.079
H-4	3.525	3.526	0.001
H-5	3.600	3.620	0.020
H-6	3.682	3.760	0.078

SEM was used to investigate the morphologies of the obtained AC- and AC/HP CD complex-loaded CA films. Representative images are illustrated in Table 2. Apparently, the surface of the AC-loaded CA film was rough, with no evidence of any specific pattern on it. This should be due to the complete dissolution of AC in the 90:10 (v/v) mixture of 80 vol.% acetic acid and DMAc, prior to the addition of the CA powder, resulting in rather homogeneous distribution of AC throughout the mass of the resulting CA film. On the other hand, specific pattern in the form of spherical aggregates was observed on all of the AC/HP_CD complex-loaded CA films. Specifically, an increase in the HP_CD to AC molar ratio resulted in a monotonous decrease in the sharpness of the boundary of these aggregates. It is believed that these entities were the self-assembling aggregates of the AC/HP CD complex that had been formed in the AC/HP_CD solutions. The diameters of the aggregates that had been formed at the AC:HP_CD molar ratios of 1:0.5 and 1:1 were 0.73 no.13 and 0.84 no.12 m, respectively. However, those of the ones that had been formed at the AC:HP_CD molar ratio of 1:2 could not be precisely measured. Clearly, the dimensions of these self-assembling aggregates of the AC/HP_CD complex were much smaller than those determined by the nanosizer. Such discrepancy could be based on a couple of reasons: (i) the dry or the solvated state of the materials during the measurements by the SEM or the nanosizer, respectively, and (ii) the dependence of diametric projection of the spherical aggregates of the AC/HP_CD complex across the thickness of the AC/HP_CD complex-loaded CA films.

Water retention and weight loss behavior

The CA films containing either AC or the AC/HP_CD complex were further characterized to investigate water retention and weight loss behavior in the P/B/M medium at 37 °C. After the specified immersion time of 24 h had been reached, the weights of the film specimens were recorded and these were calculated to obtain the property values, as reported in Fig. 6. Among the various CA films investigated, the AC-loaded CA films (shown in the figure as the samples with the HP_CD to AC molar ratio of 0) exhibited the lowest water retention (i.e., at about 12%). Such values for the CA films containing either AC or CACE at 40 wt.%, after immersion in the P/B/M medium at 37 °C for 24 h, were reported to be about 39

and 52%, respectively (Suwantong et al., 2008). Compared with the value obtained in the present work, the greater water retention values as reported in the work of Suwantong et al. (2008) could be due to a couple of reasons: (i) the difference in the solvent type used in the fabrication of the films that could affect the physico-chemical properties of the resulting films (Li, Ren, Fane, Li, & Wong, 2006; Romero, Leite, & Goncalves, 2009; Valente, Polishchuk, Burrows, & Lobo, 2005) and (ii) the difference in the as-loaded amounts of the drug within the films that could affect the porosity of the films after the drug molecules had been released into the medium (Suwantong, Opanasopit, Ruktanonchai, & Supaphol, 2007). On the other hand, the water retention of the AC/HP_CD complex-loadedCA films was much greater than those of the AC-loaded CA films, with the average value increasing from about 38% at the HP_CD to AC molar ratio of 0.5 to about 68% at the HP_CD to AC molar ratio of 2.0. The AC-loaded CA films also exhibited the lowest weight loss after immersion in the medium (at about 3%). Slightly greater values at about4or7% were reported bySuwantonget al. (2008) for the CA films that contained either AC or CACE at 40 wt.%, respectively. The reasons for the discrepancy in the property values as reported in the presentwork and those in the work of Suwantong et al. (2008) are similar to those given in the previous paragraph. On the contrary, the loss in the weight of the AC/HP_CD complex-loaded CA films was much greater than those of the AC-loaded CA films, withthe average value increasing from about 19% at the HP CD to ACmolar ratio of 0.5 to about 30% at the HP CD to AC molar ratio of 2.0. The loss in the weight of a drug-loaded material in a medium depends on a number of factors, e.g., the solubility of the drug, the solubility of the carrier material, the diffusion of the drug from the carrier material, and so forth. Due to the low aqueous solubility of both AC and CA in water, the presence of methanol in the medium and of HP_CD in the AC/HP_CD complex-loaded CA films were the obvious reasons for the improvement in the aqueous solubility of both the drug and the matrix materials. Release of AC from AC- and AC/HP CD complex-loaded CA films The effect of HP_CD on the release characteristics of AC from the CA films at different AC:HP_CD molar ratios was evaluated by the total immersion method in the P/B/M medium. They were reported as the percentages of the ratios of the cumulative amounts of AC released to the amounts of the drug actually loaded within the filmsor to the actual weights of the films, as shown in Fig. 7. The actual amounts of AC

within the AC- and the AC/HP_CD complex-loaded CAfilms were a priori determined to be 70.7, 80.3, 69.2, and 83.0% on average (based on the as-loaded amounts of AC within the casting solutions), for the CA films that had been prepared at the AC:HP CDmolar ratios of 1:0, 1:0.5, 1:1, and 1:2, respectively. For the AC-loaded CA films (the content of AC initially loaded in the casting solution was 10 wt.%, denoted in Fig. 7 as the samples with the AC:HP CD molar ratio of 1:0), none of the as-loaded AC, at any given immersion time point, was able to release into the medium. Suwantong et al. (2008) reported that the maximal amounts of AC released from the CA films that had been prepared from the casting solution containing 40 wt.% of the drug were about 11% on average (based on the AC amounts initially loaded within the films). The discrepancy between the amounts of AC released from the CA films in the present work and those reported in the work of Suwantong et al. (2008) should be influenced by the fact that the amounts of AC initially loaded within the films, as reported in the two studies, were different (i.e., 10 versus 40 wt.%), hence the difference in the driving force for diffusion. The different types of the solvent used in the fabrication of the films [i.e., 90:10 (v/v) mixture of 80 vol.% acetic acid and DMAc as in the present work versus 2:1 (v/v) acetone/DMAc as in the work of Suwantong et al. (2008)], which could render different densities to the obtained films, may also contribute to the discrepancy in the results obtained in the two studies.

In comparison with the AC-loaded CA films, the presence of HP_CD in the AC/HP_CD complex-loaded CA films was clearly responsible for the significantly greater amounts of AC released into the medium. Furthermore, the cumulative amounts of AC released from the films, at any given immersion time point, increased with an increase in the HP_CD content. Specifically, about 25% of the AC actually loaded within the AC/HP_CD complex-loaded CA films, a priori prepared at the AC:HP_CD molar ratios of 1:0.5, 1:1, and 1:2, was able to release into the medium within about 1200, 60, and

30 min, respectively. The maximal amounts of AC released from these materials, after having been immersed in the medium for 1440 min, were about 30, 78, and 98% of the amounts of AC actually contained within the CA films, respectively. These values corresponded to about 2.2, 3.9, and 5.8% of the released amounts of AC, when calculated based on the actual weights of the film specimens. As mentioned, as the HP CD content in the films increased, significantly more amounts of AC could be released into the medium. The complexation of a poorly water-soluble drug with a native cyclodextrin (CD) as well as its derivatives improves tremendously the aqueous solubility and the dissolution rate of the drug within an aqueous medium. This phenomenon is especially important for a highly hydrophilic derivative of CD, such as HPβCD. Pose-Vilarnovo et al. (2001) reported that the aqueous solubility of sulfamethizole (i.e., a sulfonamide antibiotic drug) was improved significantly upon forming into an inclusion complex with βCD or HPβCD. The difference as observed in the cumulative amounts of AC released from the AC/HPBCD complex-loaded CA films that had been prepared at various AC:HPβCD molar ratios could be explained based on a couple of reasons. Firstly, the ability of AC to form an inclusion complex with HPBCD disfavored the crystallization of the herb, as evidenced from the X-ray results (see Fig. 4). This allows greater opportunity for the solvent molecules to interact with those of the drug. Secondly, the presence of HPBCDincreased the hydrophilicity of the films, as evidenced by the increase in the water retention of the films with an increase in the HPBCD content (see Fig. 6). Lastly, due to the highly hydrophilic nature of HPβCD, the dissolution of the unassociated HPβCD as well as the AC/HPβCD inclusion complex into the releasing medium could occur easily, which helped facilitate the solubilization of the drug within the medium. This is evidenced by the observed increases in both the weight loss of the films in and the cumulative amounts of AC released from the films into the medium with an increase in the HPβCD content (see Figs. 6 and 7, respectively).

The latter case was accented by the observation of microholes on the AC/HP β CD complex-loaded CA films after having been immersed in the releasing medium (see Table 2). The diametric dimensions of these holes, as measured directly from the SEM images shown in Table 2, were 0.87 \pm 0.14, 1.17 \pm 0.28, and 1.20 \pm 0.19 $_{\rm m}$ m for the films that had been prepared at the AC:HP β CD molar ratios of 1:0.5, 1:1, and 1:2, respectively. These dimensions were essentially similar to the spherical aggregates that had been observed on the films prior to the immersion (see Table 2 and related texts in Section 3.3.1).

Conclusions

Asiaticoside (AC), from the medicinal plant Centella asiatica L., readily forms a complex with 2hydroxypropyl-_-cyclodextrin(HPβCD) at a 1:1 molar ratio both in distilled water and 90:10 (v/v) mixture of 80 vol.% acetic acid and N,N-dimethylacetamide (DMAc). The average diametric dimension of the self-assembling aggregates of the AC/HPBCD complex, in the solvated state, increased from about 2.4_mat the HPβCD to AC molar ratio of 0.5 to about 3.8_m at the HPβCD to AC molar ratio of 2. In the solid state, the AC/HPBCDcomplex that had been prepared at the stoichiometric molar ratio of 1:1 did not show the crystalline nature of the as-received AC. Two-dimensional NMR revealed that the cyclohexene ring moiety of AC is captivated well within the HPβCD cavity. The solvent-castcellulose acetate (CA) films that had been prepared in the presence of amixture of AC/HPβCDof varying molar ratios (i.e., 1:0.5, 1:1, and 1:2) showed evidence of spherical aggregates on their surfaces. The dimensions of these aggregates were lower than those of the selfassembling aggregates of the AC/HPBD complex in the solvated state. While AC could not be released from the AC-loaded CA film into the phosphate buffer saline solution (PBS) containing 10% (v/v)methanol (i.e., P/B/M medium), its cumulative amounts that had been released from the AC/HPBCD complex-loaded CA films were much greater, with values increasing with an increase in the HP βCD content. At 24 h of immersion in the medium at 37 °C, the maximal amounts of AC released from these materials were about 2.2,3.9, and 5.8% (based on the actual weights of the film specimens), respectively.

8. Effect of Degree of Acetylation on in VitroBiocompatibility of Electrospun Cellulose Acetate-Based Fibrous Matrices

EXPERIMENTAL DETAILS

Materials

Cellulose acetate (CA; white powder; M_w = 30,000 Da; degree of acetyl substitution H 2.4; acetyl content = 39.7%) was purchasedfrom Sigma-Aldrich (USA). Sodium hydroxide(NaOH) was purchased from AjaxFinechem (Australia) and hydrochloric acid(HCl) was from J.T. Baker (USA). Acetone(Carlo Erba, Italy), N, N-dimethylacetamide[DMAc, Labscan (Asia), Thailand], andethanol [Labscan (Asia), Thailand] wereused as-received.

Preparation of Electrospun CA FiberMats

The electrospinning of CA was carried out based on the method described in apublished work by some of us and another colleague [26]. Briefly, a weighed amount of CA powder was dissolved in 2:1 v/v acetone/DMAc to obtain a CA solution at a fixed concentration of 17% w/v. Electrospinning of the solution was carried out using a Gamma High Voltage Research ES30P high voltage dc power supply as the power source, a flat-tipped 20-gauge stainless steel needle (OD = 0.91 mm) as the nozzle, and an aluminum foil wrapped around a home-made rotating metal drum (OD = 9 cm) as the fiber collection device. The electric field was 17.5 kV/15 cm, the rotational speed of the rotating drum was 60 \pm 5 rpm, and the feed rate of the solutions was 1 mL h-1. For 9 h of continuous electrospinning, the thicknesses of the CA fiber mats were 20-30 [m.

Thermal Treatment and Alkaline Treatment

The CA fiber mats were peeled off from the aluminum foil, sandwiched between two polytetrafluoroethylene (PTFE) sheets, and put in a hot-air oven at 208°C for 1 h [25]. They were then immersed in 0.1 N NaOH solution in 4:1 v/v water/ethanol mixture at room temperature (25 \pm 1°C) for varying time intervals, ranging from 10 min to 24 h. The alkaline-treated CA fiber mats were then rinsed in deionized (DI) water and kept in a desiccator prior to further uses.

Characterization

Physical characteristics

Morphological appearance of the neat, the heat-treated, and the alkaline-treated CA fiber mats was observed by a JEOL JSM-5200 scanning electron microscope (SEM). They were sputtered with a thin layer of gold using a JEOL JFC-1100E ion sputtering device prior to SEM observation.

Chemical functionalities and degree of deacetylation

Chemical functionalities of the neat and the alkaline-treated CA fiber mats were investigated by a Nicolet Nexus 670 Fouriertransform infrared spectroscope (4 cm-1 resolution with 4 scans over the wavenumber range of 400-4000 cm-1). The degree of deacetylation (%DD) of the alkaline-treated CA fiber mats was evaluated by a titration method. Specifically, weighed samples of the CA fiber mats (2.8 cm in diameter) were immersed in 0.1 N of NaOH solution in 4:1 v/v water/ethanol mixture at the ratio of 1:1 w/v. After 10 min to 24 h of immersion, 5 mL of the NaOH solution was pipettedout and then titrated with 0.1 N HCl aqueous solution, with phenolphthalein being used to indicate the basicity-to-acidity crossover. The amount of the hydroxyl ions participated in the deacetylation reaction of CA could then be calculated from the amount of the titrant, which was used to calculate the %DD, i.e.

$$%DD = \frac{m_{\rm i} - m_{\rm f}}{m_{\rm i}} \times 100$$
, (1)

where m_i and m_f are the moles of the acetyl groups in the CA fiber mats before and

Wide-angle X-ray diffraction studies

The crystalline nature of the neat, the heat-treated, and the alkaline-treated CA fiber mats was examined by a JEOL JDX 3530 wide-angle X-ray diffractometer (30 kV and 40 mA over the 2Theta range of 5 to 50°).

Physico-chemical characteristics

The water retention and the loss in the mass upon submersion in water of the neat and the alkaline-treated CA fiber mats were measured after their submersion in distilled water at 37°C for 24 h. If M_1 denotes the initial mass of each fiber mat sample in its dry state and M and M_d are its masses after submersion in distilled water in its wet and dry states, respectively, the property values can be calculated as follows:

Water retention (%) = $\frac{M - M_d}{M_d} \times 100$, (2)

Water retention (%) =
$$\frac{M - M_d}{M_d} \times 100$$
,
(2)
$$Mass loss (%) = \frac{M_i - M_d}{M_i} \times 100$$
.

Biological Evaluation

The potential for use of the neat and the alkaline-treated CA fiber mats as wound dressing materials was assessed by the indirect cytotoxicity evaluation and the direct cultures of mammalian cellsonto their surfaces. Two types of cells were used: 1) human foreskin fibroblasts(HFF) and 2) immortalized non-tumorigenic human keratinocytes (HaCaT). The experiments were done in adaptation from previously-published protocols [12]. Briefly, either type of cells was first cultured in Dulbecco's modified Eagle's medium (DMEM; Sigma-Aldrich, USA), supplemented with fetal bovine serum (FBS; Biochrom, UK), L-glutamine (Invitrogen, USA), penicillin (Gibco→, Invitrogen, USA) and streptomycin (Gibco-, Invitrogen, USA). When the cells reached 80% confluence, theywere trypsinized and counted by ahemacytometer, prior to further uses. The indirect cytotoxicity of the fibrous materials was assessed based on the method that was adapted from the ISO10993-5standard test method. Briefly, the specimens(~14 mm in diameter), pre-washed with 70% ethanol for 30 min, were washed with autoclaved phosphate buffer saline (PBS)solution twice and once with the culture medium. Either type of cells was seeded in wells of a 24-well tissue-culture polystyrene plate (TCPS; Corning, USA) at 2·104 cells/ well. After 24 h of attachment, the culture medium was replaced with serum-free medium (SFM; DMEM containing penicillinand streptomycin, but without FBS). Each of the specimens was then place into each well and both the cells and the specimen were incubated further for 1, 3, and 5 d. The extraction ratio was fixed at 10 mg mL-1. After each specified time interval was reached, the medium in each well was removed. The viability of the cells was then quantified by 3-(4,5-dimethylthiazol-2-yl)-2,5-diphenyltetrazolium bromide (MTT) assay. The viabilities of the cells that had been cultured with fresh SFM were used as control.

For the direct cell culture studies, the well-washed specimens were placed in wells of 24-well TCPS. A stainless steel metal ring (12 mm in diameter) had been placed on top of each fiber mat specimen and 500 mL of the culture medium had been pipette into each well, prior to the cell culturing. Subsequently, $2\cdot10_4$ cells/well of either type of cells were seeded onto each specimenand allowed to attach and proliferate for 1, 3,and 5 d. After rinsing the specimens withPBS twice to remove unattached cells, the viabilities of the cells were quantified by the MTT assay and the viabilities of the cells that had been cultured on TCPS were used as control. Lastly, the morphology of the cultured cells was investigated. The cellcultured specimens were harvested and washed with PBS twice. After the cells had been fixed with 3% glutaraldehyde aqueous solution and washed with 0.2 M PBS aqueous solution, the specimens were dehydrated through a series of grade ethanol solutions and pure ethanol for 2 minand finally dried in air. Finally, they werobserved by SEM.

Statistical Analysis

All the quantitative values were expressed as means \pm standard deviation values. Statistical comparisons were performed using one-way ANOVA with SPSS 13.0 for Windows software (SPSS, USA). *P* values < 0.05 were considered statistically significant (n = 3).

RESULTS AND DISCUSSION

Morphology

The as-prepared 17% w/v CA solution in 2:1 v/v acetone/DMAc was electrospun under the electric field of 17.5 kV/15 cm for a fixed collection time of about 9 h [26]. A selected SEM image of the obtained fiber mats is shown in Figure 1a. The diameters of these individual fiber segments were determined to be 265 ± 39 nm ($n \approx 50$). Due to the fluffiness of the obtained fibrous matrices, further treatment in an alkaline aqueous solution would become a problem, as the materials could easily lose their physical integrity. Ma et al. [25] suggested that this shortcoming could be solved by thermally-treating the fiber mats at 208° C for 1 h. Figure 1b shows the morphology of the representative heat-treated fiber mat, which is obviously similar to that of the untreated precursor. The thermal treatment not only imparted the ease of handling to the fibrous matrices, but also helped maintain their physical integrity after having been submerged in 0.1 N NaOH solution in 4:1 v/v water/ethanol mixture at $25 \pm 1^{\circ}$ C for periods of up to 24 h. Figure 1c-e shows the morphology of the fiber mats after they had been submerged in the alkaline solution for 10 min, 30 min and 24 h, respectively. Apparently, the fibrous character of the alkaline-treated fiber mats was still intact, with no evidence of the individual fibers being destroyed. On the other hand, Son et al. [24] reported that, after being submerged in a potassium hydroxide (KOH) solution in ethanol for 30 min, obvious destruction of the CA fiber mats was evident.

Chemical Functionalities and %DD

The deacetylation reaction of the alkaline-treated CA fiber mats was followed qualitatively by FT-IR and quantitatively by titration. Figure 2 illustrates representative FT-IR spectra of a neat CA fiber mat and some of the CA fiber mats that had beensubmerged in the alkaline solution for 10 min, 30 min, and 24 h. For the neat CA fiber mat, a strong absorption peak centering at 1750 cm-1, corresponding to the carbonyl groups (C=O) of the acetyl esters of CA, was evident. After 10 min of the alkaline treatment, the intensity of this peak decreased appreciably. Further increasing the alkaline treatment time resulted in a monotonous decrease in the intensity of the peak. The peak disappeared completely after submerging the mat in the NaOH solution for 24 h, thereby confirming the successful formation of RC fiber mats. In a similar manner, the presence of the peak centering at 1232 cm-1, corresponding to the C-O stretching of the ester/ether groups of CA, decreased in its intensity upon submersion in the alkaline solution and even disappeared completely after 24 h of submersion in the alkaline solution. At 24 h of submersion in the NaOH solution, the presence of the peak centering at 1068 cm-1, corresponding to the C-O stretching of the alcohol groups of cellulose, was clearly visible. Strikingly, the peak associated with the O-H stretching, centering at 3480 cm-1, became more intense and broader for the alkaline-treated CA fiber mats, especially for the ones that had been submerged in the alkaline solution for 24 h.

The %DD values of all of the alkalinetreated CA fiber mats were determined by titration and the results are shown in Figure 3. It should be noted that the degree of acetyl substitution and the acetyl content of the as-received CA were 2.4 and 39.7%. The titration procedure was to quantify, in percentage, the amount of the acetyl groups that had been abstracted by the treatment with the NaOH solution. According to the obtained result, the %DD increased sharply from about 40% after 10 min of submersion in the alkaline solution to about 79% after 60 min of submersion. Further increase in the submersion time interval only resulted in a slight increase in the %DD to finally reach plateau values of about 88-90% after the CA fiber mats had been submerged in the alkaline solution for 7 to 24 h.

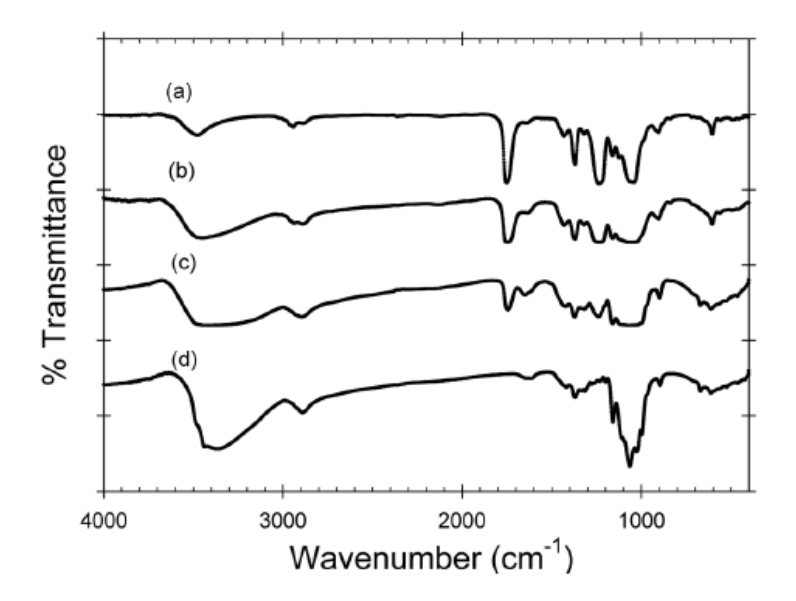


Figure 2. Representative FT-IR spectra of (a) a neat electrospun CA fiber mat and some of the thermally-treated fiber mats that had been submerged in 0.1 N NaOH solution in 4:1 v/v water/ethanol mixture at 25 \pm 1°C for a period of (b) 10 min, (c) 30 min, and (d) 24 h.

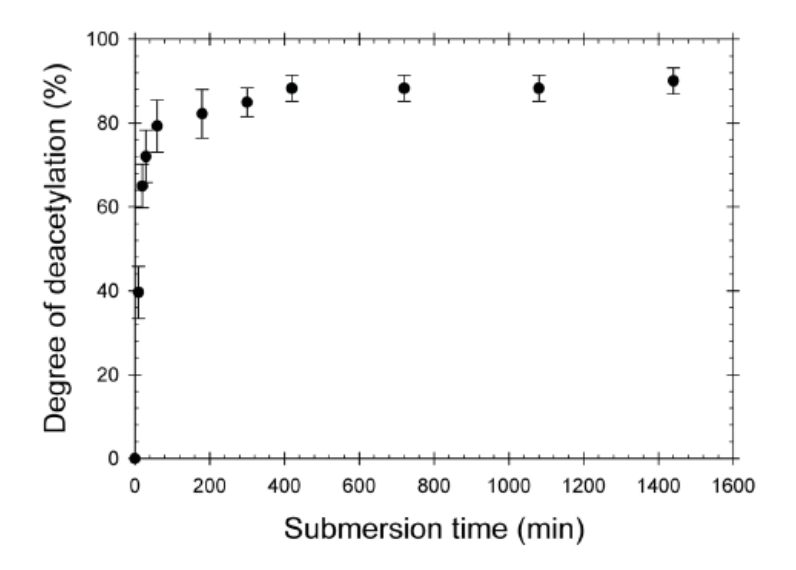


Figure 3. Degrees of deacetylation (%DD) of thermally-treated electrospun CA fiber mats that had been submerged in the NaOH solution as a function of submersion time (n = 5).

X-ray Diffraction

Figure 4 shows the X-ray diffraction patterns of the neat, the heat-treated, and some of the alkaline-treated CA fiber mats. For the neat CA fiber mat, two peaks at the 2Theta values of about 10.0 and 17.4° were observed. These peaks correspond respectively to the crystalline domains of CA and cellulose (ca. the acetyl content of the as-received CA was 39.7%). The intensity of these peaks increased appreciably after the thermal treatment, most likely a result of the increase in the mobility of the CA chains during the thermal treatment, hence the increase in the crystallinity of the crystalline domains. Kamide and Saito [27] reported a relationship between the glass transition temperatures (T_g , °C) and the degrees of acetyl substitution (z, \square [0,3]) of CA, which was given as $T_g = 249.9 - 20.3z$. For z = 2.4, T_g of the as-received CA should be about 201°C. At the treatment temperature of 208°C, CA molecules should, therefore, have enough mobility to form more stablecrystallites, hence the observed increase in the intensity of the crystalline peaks. The increase in the crystallinity of the thermally-treated CA would increase its stiffness and, at the same time, reduce the subservience to penetration by chemicals, hence an improvement of its physical integrity.

As for the alkaline-treated CA fiber mats, while the intensity of the low-angle peak decreased and shifted towards a higher 2Theta value with an increase in the treatment time interval, that of the high-angle peak increased and also shifted towards a higher 2Theta value. As the intensity of the high-angle peak increased with an increase in the alkaline treatment time, it becomes obvious that the decrease in the acetyl content along the CA chains was responsible for the observed increase in the crystallinity of the alkaline-treated CA fiber mats as well as the rearrangement of the crystalline packing into that of cellulose. The reappearance of the-OH groups, hence the occurrence of the hydrogen bonding, should be responsible for the observed increase in the crystallinity of the alkalinet reated CA fiber mats.

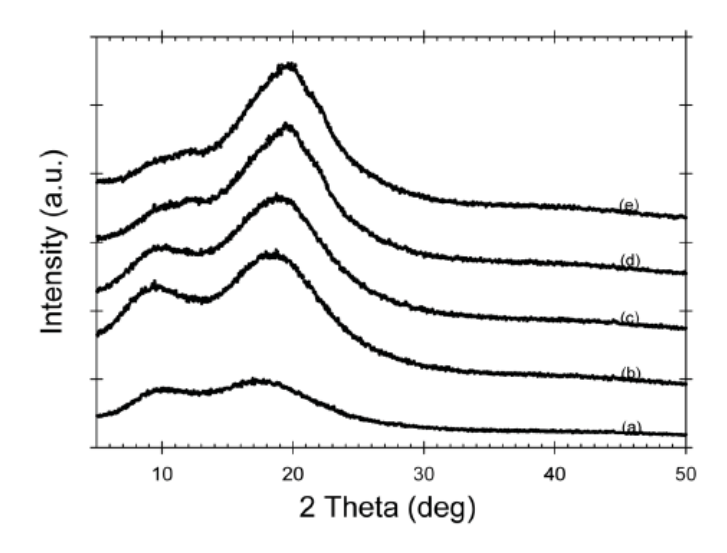


Figure 4. X-ray diffraction patterns of electrospun CA fiber mats (a) before and (b) after thermal treatment at 208°C for 1 h and those of the thermally-treated fiber mats that had been submerged in the NaOH solution for (c) 10 min, (d) 30 min, and (e) 24 h.

Physico-chemical Characteristics

The neat CA fiber mats and the CA fiber mats that had been treated with the alkaline solution for 10 min, 30 min, and 24 h were studied further. Based on Figure 3, the acetyl contents of these fibrous materials were estimated to be about 40, 24, 11, and 4%, respectively. These materials were tested for the water retention and the loss in the mass upon submersion in water for 24 h and the results are summarized in Table 1. The water retention decreased after the CA fiber mats underwent the alkaline treatment and the variation in the submersion time did not have a strong influence on the property values. It should be noted that the retention of water in an ultrafine fibrous material originates from the absorption of water within the mass of the material and from the retention of water between inter-fibrous pores due to the capillary action. While the latter should increase when the CA fiber mats had been treated with the NaOH solution (i.e., due to the increase in the hydrophillicity), the fact that the water retention values of the alkaline-treated CA fiber mats were lower than that of the neat materials should be a result of the decrease in the absorbed amount of water within the mass of the matrix material. This, in turn, resulted from the fact that the CA fiber mats had to be thermally treated prior to being treated with the NaOH solution. The thermal treatment caused the crystallinity of the matrix material to increase, hence less amount of water to be absorbed. On the other hand, after the alkaline treatment, the loss in the mass of the fiber mats increased very slightly. It is well-known that cellulose undergoes alkaline degradation, the degradation occurs from the reducing ends of the molecule and produces watersoluble D-glucoisosaccharinic acid as a byproduct [28].

Table 1. Water retention and the loss in the mass of thermally-treated electrospun CA fiber mats before and after submersion in the NaOH solution for 10 min, 30 min, and 24 h (n = 5).

Sample	Water retention (%)	Mass loss (%)
Neat	420 ± 19	0.6 ± 0.5
10 min of alkaline treatment	335 ± 13	1.0 ± 0.7
30 min of alkaline treatment	326 ± 25	1.1 ± 0.7
24 h of alkaline treatment	336 ± 16	1.4 ± 0.6

^{*} These fiber mat samples had been submerged in distilled water at 37°C for 24 h.

Indirect Cytotoxicity Evaluation

The indirect cytotoxicity of the neat CA fiber mats and the CA fiber mats that had been treated with the alkaline solution for 10 min, 30 min, and 24 h were evaluated against HFF and HaCaT. Here, it is assumed that the viability of the culturedcells was proportional to the MTT absorbance. Figure 5 shows the viabilities of the cells that had been cultured in SFM both in the absence and in the presence of the fiber mat specimens for 1, 3, or 5 d were reported relatively to that of the cells that had been cultured in the absence of the specimens for 1 d. Evidently, the viabilities of both types of cells that had been cultured on the surface of TCPS, without or with the presence of the fiber mat specimens, increased monotonically with an increase in the cell culturing time. In fact, the viabilities of the cells, at any given cell culturing time point, were statistically the same, without or with the presence of the fiber mat specimens. The results indicate clearly that the proliferative ability of the cultured cells was unaffected, despite the presence of the fiber mat specimens in the culture medium of up to 5 d. In other words, these fibrous materials released no substances in the levels that would be harmful or pose any adverse effect to the growth in the number of the cells.

. Cell Culture Studies

As previously mentioned, the acetyl contents of the neat CA fiber mats and the CA fiber mats that had been treated with the alkaline solution for 10 min, 30 min, and 24 h were about 40, 24, 11, and 4%, respectively. These fibrous materials were tested further for *in vitro* biocompatibility with HFF and HaCaT. The cells were directly seeded and cultured on these fibrous matrices for 1, 3, and 5 d and those seeded and cultured on bare wells of TCPS were used as positive control. Again, theviability of the seeded and the cultured cell was proportional to the MTT absorbance. Evidently, both types of cells adhered and proliferated well on the surface of TCPS. On day 1 of cell seeding, the viabilities ofboth types of cells that had been seeded on all of the fibrous matrices were not significantly different from those on TCPS, except for those of HaCaT that had been seeded on the neat CA fiber mats showing significantly lower values. On days 3 and 5, the viabilities of both types of cells that had been cultured on all of the fibrous matrices were inferior to those on TCPS.

For HFF, the variation in the acetyl contents of the CA-based fibrous matrices did not pose strong effect on the viabilities of the cells cultured on them on day 1. Such an effect was seen when the cells had been grown for longer periods of time (i.e., 3 and 5 d). On day 3, only the neat CA fiber mats could support the growth of the cells particularly better than the alkaline-treated counterparts. On day 5, the viabilities of the cells grown on the CA fiber mats that had been treated with the alkaline solution for 30 min increased, while those on the neat CA counterparts decreased, causing the 30 min-alkaline treated CA fiber mats to be the better support for the growth of the cells. For HaCaT, the variation in the acetyl contents of the CA-based fibrous matrices did not affect the viabilities of the cells grown on them on days 1 and 3, despite the slight increase in the viabilities of the cells on day 3, when compared with those on day 1. On day 5, the viabilities of the cells grown on the neat CA fiber mats and the CA fiber mats that had been treated with the alkaline solution for 24 h, which showed equivalent values, increased slightly from day 3, those of the cells grown on the CA fiber mats that had been treated with the alkaline solution for 10 and 30 min decreased slightly.

The morphologies of both HFF and HaCaT that had been seeded and culturedon the surfaces of the CA-based fibrous matrices are shown in Table 2. On day 1, both types of cells extended their cytoplasm over the surfaces of the fibrous matrices particularly well and even appeared in their normal cell shapes (i.e., spindle-like morphology for HFF and cobblestone morphology for HaCaT). On day 3, HFF on the neat CA fiber mat still appeared expanded over the surface, but the extent of the cellular expansion was much decreased, when compared with the cells on day 1. HFF on the surfaces of the alkalinetreated CA fiber mats, on the other hand, were completely round. The change of the cell shape from spindle-like into round morphology, as the cell culturing time increased, suggested that the CAbased fibrous matrices are not supportive of the growth of human fibroblasts. This is in line with the observation reported by Sanchavanakit et al. [29] on bacterial cellulose fibrous membranes. Unlike HFF, HaCaT, on day 3 in their culture on the surfaces of all of the fibrous matrices, still retained their cobblestone morphology. However, the cells appeared to be more aggregated, especially those that had been cultured on the surfaces of the CA fiber mat that had been treated with the alkaline solution for 10 and 30 min. Despite the aggregation of the cells, the numbers of HaCaT on the surfaces of the CA fiber mat and the CA fiber mat that had been treated with the alkaline solution for 24 h increased from those on day 1. As reported by Sanchavanakit et al. [29], bacterial cellulose fibrous membranes showed good support for adhesion and proliferation of human keratinocytes.

CONCLUSIONS

FT-IR, titration, and X-ray diffraction confirmed partial removal of acetyl groups from the thermally-treated (208°C for 1 h) electrospun CA fiber mats upon submersion in 0.1 N NaOH solution in 4:1 v/v water/ethanol mixture at 25 ± 1 °C. For the CA fiber mats that had been treated with the alkaline solution for 10 min, 30 min, and 24 h, the acetyl contents were about 24, 11, and 4%, respectively (cf. the acetyl content of about 40% for the asreceived CA). The indirect cytotoxicity evaluation of the CA and the RC fibrous matrices against human fibroblasts (HFF) and human keratinocytes (HaCaT)

indicated that these materials did not release any substance in the level that would be toxic or suppress the growth of both types of cells. Further evaluation with the direct culture of the cells on the materials revealed that these materials could only support the short term culture of both types of cells (i.e., 1 d) and only the neat CA fiber mats and the CA fiber mats that had been treated with the NaOH solution for 24 h showed marginally good support for the proliferation of the human keratinocytes. These results suggested the potential for use of the fibrous matrices as temporary dressings of skin wounds and this should be evaluated further *in vivo*.

9. PREPARATION CHARACTERIZATION AND STUDY OF CRUDE BONE PROTEIN DELIVERY

FORM GELATIN MICROSPHERES AND GELATIN MICROSPHERES INTEGRATED HYALURONAN GELATIN BLENDED SCAFFOLD FOR BONE TISSUE REGERNATION

EXPERIMENTAL SECTION

1. Materials

Gelatin from porcine skin (type A, Bloom no.170-180) was purchased form Fluka (Switzerland). Gelatin form bovine skin (type B, Bloom no.175-225) was purchased from Sigma Aldrich (USA). Hyaluronan (MW 1.35x10⁶) was purchased from Coach Industries Inc (Japan). Albumin from bovine serum, tetramethylrhodamine conjugate (MW 66,000 Da) was purchased from Molecular Probes Inc (USA). Rhodamine protein label kit was purchased form Pierce (USA). Saturated Glutaraldehyde aqueous solution (5.6 M) was purchased from Fluka (Switzerland). 1-ethy-3-(3-dimethylaminopropyl)carbodiimide (EDC) was purchased form Fluka (Switzerland). Acetone (AR grade) was purchased from Lab-Scan (Thailand). All other chemical agents were of analytical grade and used without further purification.

2. Gelatin microspheres preparation

Gelatin microspheres were prepared by a thermal gelation technique with modification. In detail, 10 ml of 15% w/v gelatin (type A or B) aqueous solution was prepared at 40°C. In addition to the physiologic pH which is 5.2 or 4.95 for the gelatin type A or B respectively, pH of the gelatin solution was adjusted to 7.4 and 10.0 by the addition of 1N HCl or 1M NaOH with an aim to study the effects of pH and type of gelatin on behaviors of the as-prepared microspheres. Then, the solution was added dropwise into 200 ml of Soya oil preheated at 40°C under continuously stirring at 1,000 rpm with a homogenizer to form water-in-oil emulsion. After 10 min, temperature of the emulsion was reduced to be 4°C with an ice bath while stirring was continued for an additional 30 min to allow for physically thermal gelation of the gelatin. Afterward, 200 ml of pre-cooled (4°C) acetone was added and stirred for the next 60 min in order to dehydrate and flocculate the coaceravate droplets. The microspheres were collected by filtration through a

sintered glass filter (1 μ m pores size) under vacuum, washed three times with 100 ml of cool (4°C) acetone to remove residual oil, and dried in air at room temperature over 24 h.

To crosslink the gelatin microspheres, 250 mg of the dry microspheres was suspended in 10 ml of acetone-water (2:1, v/v) containing 1% (w/v,~100mM) Glutaraldehyde solution and stirred at 4°C, 500 rpm for 1 h. The crosslinked microspheres were collected through a sintered glass filter and washed with precooled (4°C) acetone. Then, the crosslinked microspheres were suspended in 20 ml of 10 mM aqueous glycine solution containing Tween 80 (0.1 wt%), shaken at 37 °C, 50 rpm for 1 h to block the residual aldehyde groups of the unreacted glutaraldehyde. The crosslinked microspheres were then washed twice with 60 ml of the cool deionized water (4°C), with cool acetone, filtered, and eventually air-dried at room temperature for over 24 h.

3. Crude Bone Protein preparation

CBP was extracted from the bovine jaws bone. In particular, bone was initially washed and cleaned thoroughly in tap water and then sectioned into small pieces with a diamond disc driven by a rotor. Pieces of bones were further crushed into powder in liquid Nitrogen. Then, the as-prepared powder was immersed in 0.6 N HCl at 4°C and shaken continuously on an orbital shaker. After three days, the bony solution was centrifuged and the supernatant was collected, dialyzed for 48 h and lyophilized. The dry CBP was kept in desiccators until use.

4. Fluorescent labeling of Crude Bone Protein

fluorescent-labeled Crude Bone Protein (CBP) was with the 5-(and 6)carboxytetramethylrhodamine, succinimidyl ester (NHS-Rhodamine). Briefly, 10 mg/ml of CBP solution was prepared with 50mM borate buffer, pH 8.5 and transferred to a reaction tube. Then, 10 mg/ml of NHS-Rhodamine in DMSO was added. The reaction solution was gently mixed well and incubated in the dark at room temperature for 1 hour. To remove the non-reacted NHS-Rhodamine, the reaction solution was filtered through a D-salt dextran desalting column using 10 mM phosphate buffered saline (PBS) with 0.15 M NaCl as a filtrating medium. The effluent solution was collected in 500-µl fraction. All fractions were subsequently detected by measuring the absorbance with spectrophotometer at 280 nm to identify the fraction containing NHS-Rhodamine-labeled CBP (hereafter, CBP-Rhod). The concentration of the CBP-Rhod existing in the selected fraction was further determined using spectrofluorometer (Cary EclipseTM) at 541 and 572 nm for the excitation and emission wavelength respectively, based on a BSA-Rhod (Molecular ProbesTM) standard curve over the concentration range 1-50 μg/ml (r²=0.996). The CBP-Rhod fraction was stored at 4°C and protected from light until ready to use.

5. CBP-Rhod loading into gelatin microspheres

Crosslinked gelatin microspheres were loaded with CBP-Rhod by diffusion method. In particular, the aforementioned CBP-Rhod fraction was diluted with 10 mM PBS, 0.15 M NaCl, pH 7.2 to achieve the concentration ~700 μ g/ml. Gelatin microspheres were immersed in the diluted CBP-Rhod solution to attain the loading dose of 4 μ g CBP-Rhod per mg dried microspheres. The resulting mixture was vortexed for 1 h and incubated at 4°C for 24 h to let the CBP-Rhod infuse. The impregnated microspheres were frozen at -40°C for 24 h, lyophilized, and kept in the dark at 4°C until use.

6. Fabrication of porous composite hyaluronan-gelatin scaffolds

Porous composite hyaluronan (HA)-gelatin scaffolds were fabricated by the solvent casting and freeze-drying technique. Briefly, 2% (w/w) aqueous solution of a HA and gelatin mixture (1:1, w/w) was prepared at 50°C and left to cool down to room temperature. Then, in order to facilitate the blending of HA and gelatin, ionic strength of the mixture was adjusted by adding the equal amount of NaCl to HA (1:1, mole/equ) and being mixed up for 30 min. The resulting mixture became clearer and more translucent. To crosslink the polymers, calculated amount of EDC (1x to HA, mole/equ) was added and reacted under 200 rpm stirring at room temperature for 2 h. Afterward, the neat or the CBP-Rhod labeled microspheres were suspended in HA-gelatin mixture at 1% (w/w) concentration, which equals to 50% (w/w) of the polymer weight. The suspension was continuously stirred until the microspheres were well dispersed in the mixture and the then was cast in polypropylene discs at a constant weight, freezed at -40°C and lyophilized at -50°C. The samples were kept in desiccators until use.

7. Characterization

7.1. Size and morphology of gelatin microspheres and microspheres integrated HA-Gelatin scaffold

Gelatin microspheres were initially inspected under the computer connected Polarizing Optical Microscope (DMRXP, Leica) at 20x magnification. The images were recorded and further used to measure the diameters of the microspheres with the UTHSCSA Image Tool version 3.0 software. One hundred microspheres were measured for each preparative condition and the average values of their sizes were calculated. The data were also used to determine size distribution of the microspheres both before and after crosslinking with 100mM Glutaraldehyde. For the morphological study, gelatin microspheres and the asprepared scaffolds were mounted on brass stubs, coated with gold using a JEOL JFC-1100 sputtering device, and observed for their microscopic morphology using JEOL JSM-5200 scanning electron microscopy (SEM).

7.2. Swelling ability of gelatin microsphere

Swelling ability was determined by the alteration of microspheres' size after water uptake. 20 mg of the dry crosslinked microspheres were incubated in 10 ml of 10 mM PBS with 0.15 M NaCl at 37°C for 24 h. Then, sizes of the swelling microspheres were examined with the same procedure as previously described in 2.7.1. One hundred microspheres of each preparative condition were measured and the average diameters were calculated. The swelling ability was calculated according to the following equation:

Swelling =
$$\mathcal{O}_{swell}/\mathcal{O}_{dry}$$

where \mathcal{O}_{swell} and \mathcal{O}_{dry} are the averaged diameter of the microspheres before and after incubation, respectively.

7.3. Zeta potential determination

Zeta-Meter 3.0+ (Zeta-Meter, Inc., USA). Briefly, the suspension of 25 mg gelatin microspheres in 10 ml of deionized water was filled in an electrophoresis cell. Two electrodes were inserted into the cell and connected to the Zeat-Meter 3.0+ unit. Once the electrodes were energized, microspheres were aroused to move toward one electrode. A microsphere was observed under a microscope for its movement along a specific distance which was indicated by a built in grid. The zeta potential value was detected at a right time point when the microsphere moved to the end. Measurement was repeated 10 times for each preparative condition and the average values were calculated.

7.4. Actual loading of CBP-Rhod in gelatin microspheres

5 mg of Rhodamine-labeled gelatin microspheres were suspended in 1 ml of 10 mM PBS with 0.15 M NaCl in a 1.5 ml microcentrifuge tube. The tube was then placed in cool water and sonicated with the Sonicator (Vibracell™, Sonic, USA) at 20% amplitude. After 1 h, the suspension was centrifuged at 5,000 rpm for 5 min and the supernatant was collected. The actual amount of the CBP-Rhod in supernatant was determined using spectrofluorometer (Cary Eclipse™) by the same procedure done in the step of NHS-Rhodamine labeling (2.4). The experiment was carried out in triplicate and the results were presented in terms of Encapsulating efficiency of CBP-Rhod (EE) and Loading capacity of gelatin microspheres (LC), which were determined according to the following equation [31]:

Encapsulating efficiency (%) = (total μg CBP-Rhod encapsulated / initial μg CBP-Rhod loaded) x 100

Loading capacity (%) = (total mg CBP-Rhod encapsulated / total mg microspheres) x 100

7.5. In vitro CBP-Rhod release

In vitro release of CBP-Rhod from gelatin microspheres and the microspheres integrated HAgelatin scaffold were investigated in buffer solution by a standard sampling-separation method. In the release assay, 5 mg of the CBP-loaded microspheres and one piece of the microspheres integrated HAgelatin scaffold (circular shape with 10 mm in diameter and 2 mm in height), which contained 2.5 mg of gelatin microspheres, were separately immersed in 1 mL of 10 mM PBS with 0.15 M NaCl, and incubated in a shaking water bath (70 rpm) at 37°C. At a given time point, 500 µl of the buffer solution (hereafter, the sample solution) was withdrawn and an equal amount of fresh medium was added in order to maintain a constant volume of the medium. The sample solution was centrifuged at 5000 rpm for 5 min at room temperature and the amount of CBP-Rhod in the sample solution was determined by spectrofluorometry at 541 and 572 nm for the excitation and emission respectively, as previously described. An average value was calculated at each time point. The experiment was done in triplicate.

7.6. Statistical analysis

Data were analyzed using the SPSS software version 14.0 for window. Initially, the normal distribution was assessed by the Shapiro-Wilk test. The normal distribution data, representing the homogeneity of the variances, shown by the Levene's test, were then investigated by the one-way analysis of variance (ANOVA) with the Tukey HSD post hoc multiple comparisons. Otherwise, the Dunnett T3 would be applied if the data did not exhibit the homogeneity of the variances. For the data of which the normal distribution was absent but the variance was homogeneous, the Kruskal-Wallis H was applied. To compare the means between 2 data groups, the students' unpaired t-test was used. The significant level was indicated at p < 0.05 in any case.

RESULTS AND DISCUSSION

1. Morphology of gelatin microspheres and microspheres integrated HA-Gelatin scaffold

The selected SEM images of the uncrosslinked gelatin microspheres are shown in Fig.1. As observed, the microspheres prepared at any given condition presented entirely spherical geometry with a smooth surface, on which the macroscopic pores were not detected. Aggregation of the various sizes microspheres into many small clusters was shown in all cases. In our opinion, such aggregation was caused by the direct contact between the adjacent particles once the solvent was expelled during microspheres preparation. The electrical charge on the surface of particles might be diminished in dry environment so that the electrostatic repulsive force was also weakened; as a consequence, repulsion among particles was unlikely illustrated.

Fig. 2 show the selected SEM images of internal architecture of the composite HA-gelatin scaffold. A well-defined porous structure and the inter-pore connectivity were observed throughout the bulk. The incorporated gelatin microspheres were extensively embedded into the wall of scaffold without deterioration of their geometry. Nevertheless, exceptional for the quite small particles, almost microspheres were not thoroughly submerged in thin walls of scaffold. This manifestation may be responsible for controlled release of the absorbed protein since the releasing medium could transport through the exposed microspheres differently from the one covered with walls of scaffold.

2. Effect of gelatin type and pH on size of the gelatin microspheres

Upon the preparation of gelatin microspheres by thermal gelation technique, the average size of particles depends on several manufacturing parameters, for instance, the type and dimension of stirrer, diameter of the vessel or container, volume ratio between aqueous and oil phases and their respective viscosities, stirring speed, and the surface tension between the two immiscible phases governed by type of the selected oil phase [32]. In this study, all parameters were identically controlled in order to investigate the effect of gelatin type and pH on the microspheres size, and it was found that sizes of the as-prepared microspheres varied from \sim 4 to \sim 40 μ m in which over 85% of the microspheres range between \sim 8 to \sim 25 μ m (Fig. 3). For all given conditions, the size distributions presented a similar pattern of which the curves of normal distribution were observed.

The average sizes of the as-prepared gelatin microspheres at various conditions are presented in Fig. 4. Diameters of the uncrosslinked samples range between ~10 and ~20 µm for gelatin A microspheres, and between ~11 and ~ 23 µm for gelatin B microspheres. Average sizes of the microspheres were apparently in the same dimensional range for any preparative condition. However, when the data were statistically analyzed with the Univariate analysis of variance; test of between-subjects effects, sizes of the as-prepared microspheres were significantly different through the influence of the interaction between type of gelatin and pH. Effect of gelatin type or pH on microspheres size, therefore, can not be individually analyzed. The data were thus reorganized into six discrete groups and analyzed further with one-way ANOVA. The results presented that sizes of both gelatin A and B microspheres prepared at pH 7.4 and 10.0 are statistically the same, in contrast to the microspheres prepared at their physiologic pH at which gelatin A microspheres were significantly smaller than those of gelatin B. The effect of interaction between gelatin type and pH are thus limited at a certain condition, probably only at the physiologic pH.

Considering the crosslinked samples, only gelatin A microspheres prepared at its physiologic pH (5.2) presented a significant reduction in particle size comparing with the others which were ~11 and ~15 μ m respectively. The difference in particle sizes might be due to the difference in crosslinking intensity of gelatin A from the others which was particularly favored at its physiologic pH, resulting in a denser

network and smaller particle sizes [19]. Such observation was also detected in the size of swelling microspheres. Since the CBP was anticipated to be incorporated into gelatin microspheres by diffusion method, swelling ability of the microspheres was required to facilitate absorption of the CBP solution. The as-prepared microspheres illustrated ability to absorb and retain water as the hydrated swelling characteristic was remarkably observed in every study group (Fig. 5). With the crosslinking condition done in this study, the as-prepared microspheres could swell in water significantly at ~1.3 to 1.6 folds over their sizes in the dry state (Table 1). However, the difference of their swelling ability was not noticeably observed at any particular preparative condition.

The type of gelatin used and pH, thus, did not have a clear effect on the resulting size of the microspheres behaving in the uncrosslinked, crosslinked or swelling condition. The result of this study partially corresponded to that of Vandervoort and Ludwig in 2004 [19] which found that type of gelatin did not influence the resulting size of nanoparticle prepared by desolvation method where as the pH did.

3. Zeta potentials

The zeta potentials value of the microspheres was measured at all given conditions with an aim to study the influence driven from gelatin type and pH. The value would also be beneficial in the study of CBP loading and releasing through gelatin microspheres.

The zeta potentials of the microspheres at all given conditions were investigated with an aim to study the influence of gelatin type and pH on zeta potentials of the resulting microspheres. The impact of zeta potentials on CBP loading and releasing was also investigated

Zeta potentials values of the as-prepared microspheres are shown in Fig. 6.. Evidently, both gelatin A and B microspheres presented different zeta potentials values at different pH. In addition, those samples prepared with the same type of gelatin but at different pH also presented different zeta potentials values. Only the pH 10.0 at which statistic analysis was carried out due to the zeta potential values were so close as ~-54 and ~-58 mV for gelatin A and B microspheres, respectively in order to ensure the significance of difference. The analysis revealed their statistically different, therefore, both type of gelatin and pH do have significant influences on the zeta potential value of the microspheres obtained.

Since zeta potential is an indicator of charge density [21], the pH-induced disparity of zeta potential value can be explained with the isoelectric point (IEP), which factually is the pH at which net molecular charge and thus zeta potential is equal to zero. The IEP of gelatin A and B are ~9 and ~5, respectively [19,22], bringing about a different electrical charge of both gelatin types in function of the pH. The electrical charges of gelatin A and B are both positive at their physiologic pH since the pH was under IEP. At pH 7.4, gelatin A has a net positive charge by the under-IEP pH, while gelatin B is charged

negatively by the over-IEP pH. And eventually at pH 10.0 which is over the IEP, they both present negative charge.

Concerning gelatin microspheres, the IEP of type A and B gelatin microspheres located somewhere in between pH 7.4-10.0 and pH 4.95-7.4, respectively (see Fig. 6). The IEP of the obtained microspheres corresponded to the theoretical IEP of gelatin precursor at any given pH. Therefore, the procedure of microspheres preparation used in this study, the thermal gelation in water-in-oil emulsion technique, does not affect the microspheres zeta potentials.

4. Loading of CBP in gelatin microspheres

Encapsulation of CBP into gelatin microspheres in this study was on the basis of polyion complexation. It was expected that a degree of molecular interaction was able to take place between bone proteins and gelatin microspheres of opposite charges [22]; as a consequence, a higher yield of the ionic complexes should result in higher encapsulation efficiency and loading capacity [1,22,23].

In order to overcome either the inactivity of bone protein from those procedures of microspheres preparation or the low loading yield of bone protein which was available in limited quantity, this study designed to incorporate CBP into the preformed empty gelatin microspheres by rehydrating the freeze-dried gelatin microspheres with a solution of the CBP-Rhod at 4°C for 24 h. Such condition should be favorable for the complete absorption [23]. The amount of CBP-Rhod that had been loaded in gelatin microspheres was reported as either the encapsulating efficiency (EE) or the loading capacity (LC) as shown in Table 2.

As observed, the EE of CBP-Rhod ranges highly between ~70 to ~ 90 % for both gelatin types. Comparatively, pH was deemed to influence on the EE with an opposing manner between gelatin A and B microspheres. The EE in groups of gelatin A microspheres was found to be significantly highest at pH 10.0 in which the electrostatic charge was negative; whereas such statistically indifferent highest EE was also found in groups of gelatin B microspheres but at the physiologic pH in which the charge was positive (see also Fig. 6). Basing on the polyion complexation, this observation suggests the existence of both positively and negatively charged protein molecules in the crude bone extracts.

In addition, the encapsulation of CBP was not only influenced by the pH but also the gelatin type. The EE at pH 10.0 was found to be significantly different between gelatin A and B microspheres while the EE at pH 7.4 were insignificantly different. A disparity of zeta potential value due to pH change was not the only answer of the case as shown by the Univariate analysis of variance; test of between-subjects effects (data not shown) that the interaction between gelatin type and pH affect significantly to the EE and LC. As a consequence, both factors could not be separately considered.

Concerning the LC, the result ranges between ~ 280 to $\sim 370~\mu g$ of the CBP-Rhod per 100 mg of microspheres. Reliance of the LC on type of gelatin and pH at any given condition was found to be identical

with the EE. Therefore, the encapsulation of the CBP into microspheres evidently depends on both type of the gelatin and pH.

5. In vitro CBP-Rhod release

5.1. CBP-Rhod release form gelatin microspheres

The CBP-Rhod release form gelatin microspheres and the composite scaffolds were presented in term of CBP-Rhod cumulative releasing percentage from which the actual quantity of CBP-Rhod loaded in gelatin microspheres was calculated, as shown in Fig. 7.

The profiles of CBP-Rhod release form gelatin microspheres are apparently different from the composite scaffolds. Though the release profiles are similar at any given condition of either gelatin microspheres or the composite scaffolds, the amounts of CBP-Rhod release are remarkably different. In particular, the extremely high and low release is observed at the pH 10.0 of gelatin B and A microspheres respectively, where as those of the other conditions are quite the same. However, all profiles astoundingly illustrate the initial burst release of CBP-Rhod within the first hour which was about 73-96 %.

In order to study the CBP release kinetics, the semi-empirical equation based on a power-law expression was introduced as follows [33,34]

 $Mt/M\infty = kt^n$

where $Mt/M\infty$ is the fractional release of the CBP-Rhod, k is a constant concerning the structure and geometry of the releasing device and n is the releasing exponent indicating the mechanism of drug release. By using the least square method, the k and n can be detected from a profile in the plot of log $Mt/M\infty$ as a function of log t (min), as presented in Fig. 8 and Table 3.

From the log Mt/M ∞ - log t plot, The CBP-Rhod release profiles showed biphasic modulation characterized by an initial relatively rapid release period within the first 30 minutes followed by a slower release phase. The phase separation is indicated by the difference of the n value calculated as the slope of a straight line fitted to the profile with a satisfactory high correlation coefficient (see table xxx). The n values of all samples are close to zero particularly in phase 2 which is the slower release phase, leading the factor "t" of the semi-empirical equation close to 1 at any time point. Comparatively, the results are much different form what have been theoretically identified as the n values of the monodispersed sphere are 0.43 and 0.85 for Fickian diffusion and the Case-II transport respectively, or 0.30 and 0.45 respectively for the mixture of multiple sizes microspheres [34,35]. The CBP-Rhod releases from gelatin microspheres, therefore, are constant and hardly depend on the time observed. The fast release implies that the anticipated polyion complexation between the CBP-Rhod and gelatin microspheres did not completely occur. This may be due to the molecule of Rhodamine which from the covalent amide bond to primary amine on the protein restricts the ionic interaction between the molecules of protein and gelatin.

5.2. CBP-Rhod release form composite scaffolds.

Comparing to the gelatin microspheres, the releases of CBP-Rhod from the composite scaffolds are slower and a period of sustained release is illustrated at any preparative condition. The amount of CBP-Rhod release within the first hour was approximately 36-50%. Interestingly, the extremely high and low release is also observed at scaffolds incorporated with pH 10.0 gelatin B and A microspheres respectively.

From the log Mt/M ∞ - log t plot, The CBP-Rhod release profiles showed three phases of release according to the calculated n values (see Fig. 8 and Table 3). Phase 1 correlated to an initial burst release of CBP-Rhod from the scaffolds within the first 30 min. The n values in this phase range from 0.37 to 0.62 which correlate to the theoretical value as mention earlier. Phase 2 corresponded to the sustained release of CBP-Rhod starting from 1 hour to 7 days. The n values of this slow release phase are much lesser than those in phase 1, but are in the same range as the n values of the initial burst CBP-Rhod release form gelatin microspheres. Phase 3, eventually, represented the CBP-Rhod release with an increasing rate from phase 2 but not faster than phase 1.

Considering the mechanism of CBP-Rhod release from the composite scaffolds, the initial burst release may be the combination of diffusion and dissolution release since the n values are in between 0.30 and 0.45[34,35] (except for gelatin B pH 7.4). Such observation is not found in case of CBP-Rhod release from gelatin microspheres. It is believed that CBP-Rhod might partially release into the HA-Gelatin blended solution in which the CBP-Rhod encapsulated gelatin microspheres were dispersed during the process of composite scaffolds fabrication. As a consequence, the releasing CBP-Rhod was also integrated in the mass of HA-Gelatin scaffolds. The initial burst release, therefore, may be the release from the scaffold matrix instead of the incorporated gelatin microspheres.

The mechanism of the sustained release in phase 2 may be the same as that of the initial burst release form gelatin microspheres, but occurs at a slower rate due to their comparable n values and lesser constant (k) values in most samples of the former case. This observation suggests that the sustained release concerns the release of CBP-Rhod from the incorporated gelatin microspheres exposing into porosities within scaffolds.

During phase 3 release, the degradation of HA-Gelatin scaffold might occur, as being observed during sampling, and induce the exposure of the underneath scaffold matrix including the gelatin microspheres which were previously submerged. The rate of CBP-Rhod release is thus higher, but the mechanism can not be truly described regarding the theoretical n values because the mostly n values of phase 3 are lesser than the lower range of the theoretical n values. However, it is believed that phase 3 release is influenced by degradation and diffusive processes.

In this study, the difference in size between the gelatin microspheres was probably not large enough to result in a significantly different CBP-Rhod release rate [33,36]. However, the ongoing mechanism of the CBP controlled release can be the organization of a diffusion-erosion process contributed by the capability of water uptake into the gelatin microspheres and the ability of protein transportation through the scaffold. Microspheres formulation mainly controls the induction time necessary to achieve protein release while the composition of polymeric scaffold controls the release rate [37]. Therefore, a temporal and spatial control of signaling molecules may be obtained by the combination of the appropriated microspheres and scaffold formulations.

CONCLUSION

Type of gelatin and the preparative pH are the two factors that should be considerably controlled in the design of bone protein delivery scaffold which contains gelatin microspheres as an incorporated delivery device. Interaction between those two factors influences significantly on size of the as-prepared microspheres, surface charge or the zeta potential, swelling ability and encapsulation capability of the CBP. This effect, however, is not observed in the drug release studies. The ionic interaction between molecules of bone protein and gelatin in the microspheres was not large enough to provide sustained release of the CBP. Incorporation of the CBP loaded gelatin microspheres into HA-Gelatin blended scaffold create a complex environment and the synergistic functions between gelatin microspheres and scaffold in which controlled release was evidently presented.

10. Development of polycaprolactone porous scaffold by combined solvent casting, particulate leaching and polymer leaching techniques for bone tissue engineering

Experimental Section

Materials. Polycaprolactone (PCL; 80,000 gmol⁻¹) were purchased from Sigma-Aldrich, USA. Polyethylene glycol (PEG; MW = 200, 600, and 1,000 gmol⁻¹) was purchased from Merck, Germany. Chloroform (Labscan; Asia, Thailand) was used as solvent for these polyesters. Sodium chloride (Ajax Finechem, Australia) was used as porogen. All other chemicals were of analytical reagent grade and used without further purification.

Preparation of PCL scaffolds. A solvent casting, polymer leaching and salt particulate leaching was used to prepare the scaffold. Briefly, the polymer solution was prepared by mixing the PCL pellet, PEG and chloroform in the concentration of 28% w/v, then the solution was stirred at room temperature for 2-3 hr, after that NaCl salt particles with size of 400-500 μm (polymer/NaCl = 1/30 w/w) were added. The mixture was then packed into Petri dishes and the cylindrical mold with the dimension of 1.2 mm in diameter and 0.8 mm in thickness. The molds were then placed in the hood overnight for solvent evaporation. After the time, the materials were immersed in deionized(DI) water for 48 hr with repeated change of DI water every 8 hr for leaching out the PEG and salt particles. Scaffolds were air-dried for 24 hr and vacuum-dried overnight. The salt-PEG leached PCL scaffolds have highly interconnectivity pores network. Prior to casting, each of the PCL and PCL-PEG blend solutions was characterized for its viscosity by using a Brookfield DV-III programmable viscometer. The measurement was carried out at room temperature (that is, 25±1 °C).

Characterization of PCL scaffolds.

Microstructure observation. The morphology of the pores, their size, distribution and the interconnectivity between these pores of the porous scaffolds were observed by JEOL JSM-5200 scanning electron microscopy (SEM), Olympus SZH10 stereomicroscope, and Carl Zeiss Mirax desk visual slide microscope. One cylindrical scaffold was randomly selected from each group, cut with razor blade at the middle of the scaffold and mounted onto SEM stub. Cross sections of the scaffolds were coated with thin film of gold using JEOL JFC-1100E sputtering devices for 5 min prior to observation under SEM

Porosity, pore volume, and pore size. Porosity and pore volume of the scaffolds were measured gravimetrically according to the following equations:

Parasity (%) =
$$\left(1 - \frac{\rho \text{ scaffold}}{\rho \text{ polymer}}\right) \times 100$$

Pare valume = $\left(\frac{1}{\rho \text{ scaffold}} - \frac{1}{\rho \text{ polymer}}\right) \times 100$

where $\rho_{polymer}$ is the density of the polymer from which the scaffolds were fabricated and $\rho_{scaffold}$ is the apparent density of the scaffolds which was measured by a Sartorius YDK01 density measurement kit. Here, ρ_{PCL} was taken the value of 1.145 g cm⁻¹. Five specimens were measured for both the porosity and the pore volume and an average value for each property was calculated. On the other hand, pore size of the scaffolds was directly measured from SEM images, using a SemAfore Digital slow scan image recording

system version 5.0 software. At least 30 pores for each of the cross- and the longitudinal sections (i.e., at least 60 pores in total) were measured and the average values for all of the scaffolds investigated were calculated.

Water absorption capability. The scaffold specimens, cut from the moldings that had been cast in the Petri dishes (circular shape with 15 mm in diameter and 3 mm in height), were first dried, weighed, and individually immersed in 10 mL of 10 mM phosphate buffer saline solution (PBS; pH 7.4) at room temperature. At a given time point, the specimens were taken out, carefully placed on the glass for 5 sec to remove the excessive water and weighed immediately. The amount of water retained in the specimens was determined according to the following equation:

$$Water\ absorption (\%) = \frac{(Ww-Wd)}{Ww} \times 100$$

where W_d and W_w are the weight of the specimens before and after submersion in the medium, respectively. The experiment was carried out in pentuplicate and the measurements were carried out at different time intervals within a period of 14 d.

Water permeability. To obtain information about pore interconnection, flow resistance was evaluated by sealing the scaffolds between two rubber rings at the bottom of a measuring tube ending and filled with 10 cm of water. To keep the water level as even as possible during flow, the tube was communicating with a large diameter reservoir. Before each test, samples were preconditioned in water for 24 h. Flow resistance of scaffolds was then evaluated as the time needed for 10 ml of water to flow through the scaffold.

Compressive modulus. Compressive Modulus of the scaffolds were determined with a universal testing machine (Lloyd LRX, UK) using 500 N loaded cell in the dry state at room temperature, the both before and after degraded scaffolds at the different time interval were vertically compressed at the crosshead speed of 3 mm/min. The load was applied until the scaffolds were compressed to approximately 70% of their original thickness. The initial compressive modulus was determined as the slope of the linear portion of the stress strain curve at a compressive strain of 20%.

Biological characterization of PCL scaffolds.

Cell culture and cell seeding. Mouse fibroblasts (L929) and mouse calvaria-derived, pre-osteoblastic cells (MC3T3-E1) were used as reference cell lines. L929 were cultured as monolayer in Dulbecco's modified Eagle's medium (DMEM; Sigma-Aldrich, USA), supplemented with 10% fetal bovine serum (FBS; BIOCHROM AG), 1% L-glutamine (Invitrogen Corp.), and a 1% antibiotic and antimycotic formulation [containing penicillin G sodium, streptomycin sulfate, and amphotericin B (Invitrogen Corp.,

USA)]. MC3T3-E1 were cultured in Minimum Essential Medium (with Earle's Balanced Salts) (MEM; Hyclone, USA), supplemented by 10% fetal bovine serum (FBS; BIOCHROM AG, Germany), 1% L-glutamine (Invitrogen Corp., USA) and 1% antibiotic and antimycotic formulation [containing penicillin G sodium, streptomycin sulfate, and amphotericin B (Invitrogen Corp., USA)]. The medium was replaced every 2 days and the cultures were maintained at 37°C in a humidified atmosphere containing 5% CO₂.

Each scaffold was cut into circular discs (about 15 mm in diameter) and the disc specimens were placed in wells of a 24-well tissue-culture polystyrene plate (TCPS; Biokom Systems, Poland), and were later sterilized in 70% ethanol for 30 min. The specimens were then washed with autoclaved de-ionized water, PBS and subsequently immersed in MEM overnight. To ensure a complete contact between the specimens and the wells, the specimens were pressed with a metal ring (about 12 mm in diameter). MC3T3-E1 from the culture was trypsinized [0.25% trypsin containing 1 mM EDTA (Invitrogen Crop., USA)] and counted by a hemacytometer (Hausser Scientific, USA). MC3T3-E1 were seeded at a density of about 60,000 cells/well for attachment study and 30,000 cells/well for proliferation study, on the scaffold specimens and empty wells of TCPS that were used as control. For indirect cytotoxicity, alkaline phosphatase activity, mineralization evaluations, MC3T3-E1 were seeded at a density of about 40,000 cells/well on the scaffold specimens and empty wells of TCPS. The culture was maintained in an incubator at 37°C in a humidified atmosphere containing 5% CO₂.

Cytotoxicity evaluation. Two types of cells were used: 1) mouse calvaria-derived, pre-osteoblastic cells (MC3T3-E1) and 2) mouse fibroblasts (L929). Indirect cytotoxicity test was conducted on TCPS, salt leached PCL, salt-PEG 200 leached PCL, salt-PEG 600 leached PCL, and salt-PEG 1000 leached PCL. First, extraction media were prepared by immersing samples (about 15 mm in diameter) in a serum-free medium (SFM; containing DMEM, 1% L-glutamine, 1 % lactabumin, and 1% antibiotic and antimycotic formulation for L929 and containing MEM, 1% L-glutamine, 1 % lactabumin, and 1% antibiotic and antimycotic formulation for MC3T3-E1) for 1, 3, and 7 days. Each of these extraction media was used to evaluate the cytotoxicity of the scaffolds. L929 or MC3T3-E1 were separately cultured in wells of a 24-well culture plate in 10% serum-containing DMEM and MEM, respectively, for 16 h to allow cell attachment on the plate. Then, the cells were starved with SFM for 24 h, after which time the medium was replaced with an extraction medium. After 24 h of cell culturing in the extraction medium, 3-(4,5-dimethylthiazol-2-yl)-2,5-diphenyl-tetrazolium bromide (MTT) assay was carried out to quantify the amount of viable cells. The experiments were carried out in triplicate.

MTT Assay. The MTT assay is based on the reduction of the yellow tetrazolium salt to purple formazan crystals by dehydrogenase enzymes secreted from the mitochondria of metabolically active cells. The amount of purple formazan crystals formed is proportional to the number of viable cells. First, each culture medium was aspirated and replaced with 400 mL/well of MTT solution at 0.5 mg mL

for a 24-well culture plate. Secondly, the plate was incubated for 30 minutes at 37 °C. The solution was then aspirated and 1 mL/well of dimethylsulfoxide (DMSO) containing 125 mL/well of glycine buffer (pH 10) was added to dissolve the formazan crystals. Finally, after 5 min of rotary agitation, the absorbance of the DMSO solution at 540 nm was measured using a Thermospectronic Genesis10 UV/Visible spectrophotometer.

Cell attachment and proliferation. Cell behavior such as adhesion and proliferation represent the initial phase of cell–scaffold communication that subsequently effect differentiation and mineralization. For attachment study, MC3T3-E1 was allowed to attach to TCPS, salt leached PCL, salt-PEG 200 leached PCL, salt-PEG 600 leached PCL, and salt-PEG 1000 leached PCL for 2, 4 and 6 h, respectively. Each sample was rinsed with PBS to remove unattached cells prior to morphological observation. Morphological appearance of the cells during attachment period was observed by SEM. For proliferation study, the viability of cells on the specimens was determined after 1, 2, and 3 day of cell culturing by DNA Quantification assay. The experiments were carried out in triplicate.

DNA Quantification Assay. The amount of DNA signifying the number of proliferated cells that had been cultured on each of the scaffolds for 1, 2, and 3 day was quantified by a DNA Quantification Kit (SigmaAldrich, USA). Briefly, the cultured cells were thoroughly washed twice with 400 μ L of PBS. The cells were then lysed with 400 μ L of a cell lysis buffer. The obtained suspension was centrifuged for 10 min to precipitate the cell debris. The supernatant was pipetted out at 20 μ L, which was later mixed with 2mL of 0.1 μ g/mL Bisbenzimide H 33258 solution in 10X Fluorescent Assay Buffer. The fluorescent emission intensity of the obtained solution was then measured at 460 nm, after it had been excited at 360 nm, using the microplate reader.

Morphological observation of cultured cells. After removal of the culture medium, the cell-cultured scaffold specimens were rinsed with PBS twice and the cells were then fixed with 3% glutaraldehyde solution, which was diluted from 50% glutaraldehyde solution (Sigma, USA) with PBS, at 500 μl/well. After 30 min, they were rinsed again with PBS. After cell fixation, the specimens were dehydrated in an ethanol solution of varying concentration (i.e. 30, 50, 70, 90, and 100%, respectively) for about 2 min at each concentration. The specimens were then dried in 100% hexamethyldisilazane (HMDS; Sigma, USA) for 5 min and later let dry in air after removal of HMDS. After completely dried, the specimens were mounted on an SEM stub, coated with gold, and observed by a JEOL JSM-5200 scanning electron microscope (SEM).

Production of Alkaline Phosphatase of Cultured Cells. ALP activity of MC3T3-E1 was measured using Alkaline Phosphate Yellow Liquid. In this reaction, ALP catalyzes the hydrolysis of colorless organic phosphate ester substrate, *p*-nitrophenyl phosphate (pNPP) to a yellow product, p-nitrophenol, and phosphate. MC3T3-E1 was cultured on scaffold specimens for 3, 5, and 7 day to observe the production of

alkaline phosphatase (ALP). The specimens were rinsed with PBS 2 times after removal of culture medium. Alkaline lysis buffer (10 mM Tris-HCl, 2 mM MgCl₂, 0.1% Triton-X100, pH 10) (100 µl/well) was added and the samples were scrapped and then frozen at -20°C for at least 30 min prior to the next step. An aqueous solution of 2 mg/ml *p*-nitrophenyl phosphate (pNPP; Zymed Laboratories, USA) mixed with 0.1 M amino propanol (10 µl/well) in 2 mM MgCl₂ (100 µl/well) having a pH of 10.5 was prepared and added into the specimens (110 µl/well). The specimens were incubated at 37°C for 15 min. The reaction was stopped by adding 900 µl /well of 50 mM NaOH and the extracted solution was transferred to a cuvette and placed in the UV-visible spectrophotometer, from which the absorbance at 410 nm was measured. The amount of ALP was then calculated against a standard curve. In order to calculate for the ALP activity, the amount of ALP had to be normalized by the amount of total protein synthesized. In the protein assay, the samples were treated in the same manner as the ALP assay up to the point was the specimens were frozen. After freezing, bicinchoninic acid (BCA; Pierce Biotechnology, USA) solution was added into the specimens. The specimens were incubated at 37°C for 15 min. The absorbance of the medium solution was then measured at 562 nm by the UV-visible spectrophotometer and the amount of the total protein was calculated against a standard curve.

Mineralization analysis. Alizarin Red-S is a dye that binds selectively calcium salts and is widely used for mineral staining (the staining product i.e., an Alizarin Red S-calcium chelating product). The isolated osteoblastic cells were plated in 24-well plates at 40,000 cells/well and cultured in the culture medium. After 24 h, the cultures were treated with culture medium, with the supplement of 50 μg/ml ascorbic acid (Sigma, USA), 5 mM β-glycerophosphate (Sigma, USA), and 0.2 μg/ml dexamethasone (Sigma, USA), the medium was replaced every 2 days. After 14 days treatment, cells were washed with PBS and fixed with ice-cold absolute methanol for 10 min. Fixed cells were stained with 1% Alizarin Red in deionized water (Sigma, USA) (pH 4.2) for 2-3 min. After removing alizarin red-S solution, the cells were rinsed with deionized water and dried at room temperature. The images of each culture were captured and the stain was extracted with the use of 10% cetylpyridinium chloride (Sigma, USA) in 10 mM sodium phosphate for 1 h and absorbance of the collected dye was read at 570 nm in spectrophotometer (Thermo Spectronics Genesis10 UV-visible spectrophotometer).

Statistical analysis. Values expressed as the mean \pm standard deviation. Statistical analysis of different data groups was performed using One-Way Analysis of Variance (ANOVA) with the least-significant difference (LSD) test using SPSS software version 11.5. The values of p lower 0.05 were considered statistically significant.

Results

Preparetion of PCL scaffolds.

Table 1 show the viscosity of PCL solution and PEG-PCL blend solution in chloroform. The PCL solution was 1064 ± 15 cP on average while the PEG-PCL blend solution were in the range of 989 - 1106 cP on average.

Characterization of PCL scaffolds.

Microstructure Observation.

Figure 1 shows the stereomicroscope images of porous scaffolds formed by PCL, different types of PEG and NaCl salts in chloroform following NaCl and PEG leaching out in deionized water. Figure 2 and 3 show the visual slide microscope images of porous PCL scaffolds.

Fig. 4 and 5 show the SEM micrographs of microporous scaffolds formed by PCL/PEG blends by various types of PEG (PEG, MW = 200, 600, and 1,000) following by leaching in aqueous medium. The highly interconnected pores were formed in scaffolds after PEG was leached out, and corresponded to the transpaprent spots shown in stereomicroscope and visual slide microscope images. The size of pores in scaffolds prepared from PEG leached out were larger than that from no PEG leached out and more interconnected channels were distributed throughout the former ones. Well defined and interconnected pores, detected by optical microscope and SEM analysis of PCL scaffolds, resulted from the use of both salt and PEG. An irregular geometry of pores was obtained for NaCl leached and NaCl-PEG leached scaffolds. The pore dimensions of the obtained scaffolds ranges between 378 and 435 μ m on average (n \geq 30).

Porosity, Pore volume and Pore size.

As shown on table 2., the porosity of scaffold showed the reverse trend with the density value. The porosity values of salt leached PCL scaffolds was 91.6% while the porosity values of the salt-PEG leached PCL scaffold were in the range of 91.2-92.6% on average (n=5). The density of scaffolds were in the range of 0.096-0.101.

Specially, the porosity increased from \sim 91.6% for salt leached scaffold to \sim 91.8% for salt-PEG 600 leached scaffold and 92.6% for salt-PEG 1000 leached scaffold, and pore volume increased from 9.6 cm³g⁻¹ for salt leached scaffold to 9.9 cm³g⁻¹ and 10.9 cm³g⁻¹ for salt-PEG 600 leached and salt-PEG1000 leached PCL scaffold. The pore volume increased with an increased the porosity.

Water absorption capability.

Figure 6 illustrates the water absorption capabilities of the salt leached, salt-PEG 200 leached, salt-PEG 600 leached and salt-PEG 1000 leached PCL scaffolds in 0.1 M PBS at room temperature within 7 days. All salt-PEG leached PCL scaffolds showed a similar profile of the water absorption, the water absorption rate increased rapidly in the early 30 minute and maintained stable in 24 hr. While salt leached PCL scaffold showed a different profile of the water absorption, the water absorption rate slightly increased

in the early 24 hr and maintained stable. Moreover, the water absorption capabilities of the PCL scaffolds were compared at 24 hr; it found that the salt leached PCL scaffold exhibited the lowest level of water absorption compared to the others.

Water permeability

Figure 7 show the flow resistance for the salt leached, salt-PEG 200 leached, salt-PEG 600 leached and salt-PEG 1000 leached PCL scaffolds. The flow resistance of salt leached PCL scaffold was in the range of 14.2-21.6 sec/10 ml (distance ~ 15-50 cm). The flow resistance of salt-PEG 200 leached PCL scaffold was in the range of 11.1-15 sec/10 ml (distance ~ 15-50 cm). The flow resistance of salt-PEG 600 leached PCL scaffold was in the range of 11.7-13.5 sec/10 ml (distance ~ 15-50 cm). The flow resistance of salt-PEG 1000 leached PCL scaffold was in the range of 10.2-13.2 sec/10 ml (distance ~ 15-50 cm).

Compressive modulus.

The increase in the porosity of the scaffolds resulted in an decrease in compressive properties. The compressive modulus decreased from \sim 88 kPa for the salt leached scaffold to 28, 42, and 49 for salt-PEG 200 leached, salt-PEG 600 leached, and salt-PEG 1000 leached PCL scaffold, respectively.

The compressive modulus of the scaffolds was found to decrease as follow:

Salt leached > salt-PEG 1000 leached > salt-PEG 600 leached > salt-PEG 200 leached PCL scaffold.

Biological evaluation of neat and modified PLA fibrous scaffolds.

Indirect cytotoxicity evaluation.

Both mouse calvaria-derived preosteoblastic cells(MC3T3-E1) and mouse fibroblasts cells (L929) were used in the assessment. However we were interested in using the obtained scaffolds as potential bone scaffolds, it was mandatory to test the materials with L929 just to comply with the ISO10993-5 standard test method. For both types of cells, about 40,000 cells/well were seeded in empty wells of TCPS. Indirect cytotoxicity test was conducted on salt leached, salt-PEG 200 leached, salt-PEG 600 leached, and salt-PEG 1000 leached PCL scaffolds. Figure 8 a) and 8 b) show the viability of the cells obtained from MTT assay after the cells had been cultured with the 1, 3, 7 day- extraction media from scaffolds as compared with the fresh SFM(control TCPS). The viability of the cells was reported as the percentage with respect to that of the control. Evidently, the viability ratio of cells that had been cultured with all of extraction media (and with control TCPS) is greater than 80%. This results can be indicated that all types of PCL scaffolds released no substances at levels that were harmful to cells.

Cell attachment and cell proliferation.

The biocompatility of PCL scaffolds was evaluated in the terms of their ability to promote the proliferation of the cells that had been allowed to attach on their surfaces. Figure 9 shows the proliferation of MC3T3-E1 on the surface of TCPS and the PCL scaffolds on day 1-3 after cell culturing in terms of the

viability of cells. The viability of cells on a scaffold could be quantified by Fluorescent emission intensity from the DNA Quantification test.

On day 1, the viability of cells on the salt-PEG leached scaffold was equivalent to that on TCPS while the viability of cell on the salt-PEG 200 leached, salt-PEG 600 leached, salt leached PCL scaffold was slightly lower than that on TCPS. On day 2, the viability of cell on the salt-PEG 1000 leached was equivalent to that on salt leached PCL scaffold. In comparison with TCPS the salt-PEG 200 leached scaffold was significantly lower. The proliferation of cells on salt-PEG 600 leached and salt-PEG 1000 leached PCL scaffold was significantly greater than that on TCPS and salt leached PCL scaffold on day 3.

Cell Morphology.

Table 2 and 3 show selected SEM images (magnification = 3500X; scale bar = $5 \mu m$) of MC3T3-E1 that were either seeded or cultured on the surfaces of glass, salt leached, salt-PEG 200 leached, salt-PEG 600 leached, salt-PEG 1000 leached PCL scaffolds at different time points.

According to these images, cell morphology and interaction between cells and the scaffolds can be visualized. At 2 h after cells seeding, the majority of cells on the glass surface was stilled rounded. At 4 h after cells seeding, the majority of cells on the glass surface started to extend their cytoplasm. At 6 h after cells seeding, the majority of cells showed evidence of the extension of their cytoplasm on the surface. For the cells that were seeded on the surface of various types of scaffolds, at 2 h after cells seeding, the majority of cells on surface was rounded. At 4 h after cells seeding, the majority of cells was remained round, but a closer examination around the edge of the cells revealed an evidence of filopodia. At 6 h after cells seeding, the majority of cells on the scaffolds were evidently expanded.

At 1, 2, and 3 days after cells seeding, the majority of the cells seeded on the surfaces of all types of scaffolds expanded over the area of the scaffolds which were the most expansion on the surface of salt-PEG 600 leached and salt-PEG 1000 leached PCL scaffolds.

Alkaline Phosphatase (ALP) Activity.

Among the various biological functions of osteoblasts, secretion of alkaline phosphatase (ALP) is an important indicator determining the activity of the cells on a scaffold. The ALP activity of MC3T3-E1 that were cultured on PCL scaffolds, in comparison with that of TCPS, for 3, 5, and 7 days. The ALP activity of MC3T3-E1 on TCPS (i.e. controls), salt leached, salt-PEG 200 leached, salt-PEG 600 leached, salt-PEG 1000 leached PCL scaffolds were monitored at 3, 5 and 7 days in culture (see Figure 10). For all of PCL scaffolds investigated, the ALP activity on day 3 was lower than TCPS, while the ALP activity on day 5 was quite similar to TCPS. On day 7, the highest ALP activity of MC3T3-E1 was observed on the salt-PEG 1000 leached scaffold compared to TCPS, while the ALP activity of MC3T3-E1 on salt leached scaffold was lower than on TCPS.

Mineralization.

Alizarin Red S staining was used to quantify the mineral deposition of MC3T3-E1 that were cultured on the surfaces of TCPS, salt leached, salt-PEG 200 leached, salt-PEG 600 leached, and salt-PEG 1000 leached PCL scaffolds for 14 days.

Figure 11. shows photographic images of the stained specimens. The appearance of red on the stained product shows the presence of calcium. The quantitative analysis of the results shown in Figure 12. was carried out by elution of calcium deposition with cetylpyridinium chloride and spectrophotometically read at 570 nm. The results revealed that the mineral deposition of cells cultured in the (salt-PEG 600 leached and) salt-PEG 1000 leached PCL scaffold were significantly greater than that of the cells cultured on the salt leached PCL scaffolds and TCPS.

Discussion

The polarities of PCL and PEG were quite different, when mixing of both, PEG phase spontaneously and spherically dispersed in PCL phase in order to diminish the surface energy on the PCL-PEG interface. ¹⁶ Resulting that after the spherical PEG were leaching out, the interconnected pores network were formed in the salt-PEG leached PCL scaffolds.

A stereomicroscope, visual slide microscope and SEM were used to observe the pores, pores distribution and the interconnected pores network of the scaffolds. The effect of PEG leached out scaffolds is illustrated in Figure 1-5. Figure 1 is the stereomicroscope images of the PCL scaffolds. Highly porous PCL scaffold were obtained for all salt and salt-PEG leached PCL scaffolds. Figure 2 and 3 show the inner morphology of the scaffolds; the salt-PEG leached PCL scaffold show the highly porous with high interconnected network.

The PCL-PEG 1000 blend solution has the highest viscosity compared to PCL-PEG 200 and PCL-PEG 600 blend solution. On the other hand, base on Kamide's theory about particle growth during membrane formation, ¹⁵ since the molecular size of PEG MW = 200 and 600 g/mol would move with a larger diffusion velocity and higher collision frequency than PEG MW = 1000 g/mol would. This resulted in creating more uniform pore and interconnected pores by leaching PEG MW = 1000 g/mol out rather than leaching out PEG MW = 200 and 600 g/mol. Salt-PEG 600 leached and salt-PEG 1000 leached PCL scaffolds have better pores and interconnected pore distribution than salt-PEG 200 leached PCL scaffold. The distribution of pores in scaffolds prepared from PEG MW. 1000 g/mol was greatest and more interconnected networks were distributed throughout the scaffolds.

The salt-PEG leached PCL scaffolds show highly interconnectivity pores network in the scaffolds, which is not in case of the salt leached PCL scaffold. The pores of the salt-PEG leached scaffolds are interconnected and the inner surface of pores looks quite coarse. The developed interconnected pore network is likely to facilitate transporting nutrients and wastes for a facile cell growth and blood vessel

invasion. The interconnected pores network and coarse surface are beneficial for all coherence and quick propagating of cell.

The interconnectivity and dimensions of the pores of the scaffolds affect not only the transport of nutrients into and wastes out of the cells through the pore structure of the scaffolds, but also other properties of the scaffolds. The porosity increased with increased the interconnectivity. According to the results in table 2, the greatest porosity, pore volume, and pore size values and the highest interconnectivity observed for salt-PEG 1000 leached PCL scaffolds are the obvious reasons for their greatest water absorption capability. The water absorption capability is an important property of a functional scaffold, as it allows the absorption and retention of wound exudates. In addition, the passage of exudates through the pore structure provides a possibility for certain proteins which is one steps required for bone regeneration to be absorbed on the scaffold surface. ¹⁹⁻²¹

At any distance, the flow resistance was significantly higher for salt leached PCL scaffold compared to salt-PEG 200 leached, salt-PEG 600 leached, and salt-PEG 1000 leached PCL scaffolds. Standard deviation of flow resistance was higher for salt-PEG 200 leached and salt-PEG 600 leached PCL scaffolds, to indicate a more irregular structure with non uniform distribution of interconnections between pores compared to salt-PEG 1000 leached PCL scaffold. The higher percentage of closed cells account for the higher flow resistance observed for the salt leached PCL scaffold.

The higher porosity (92.6% as opposed to 91.6%) of the scaffolds decreased compressive modulus from 88 to 49 kPa. The porosity is an important parameter of scaffolds, playing a significant role for cell proliferation and growth. The higher porosities can provide cells spacious surrounding for their propagation, but if porosities are too high, ²² it is very difficult for the scaffolds to maintain enough mechanical rigidity. ²³ Although increased porosity facilitate bone ingrowth, the result is a reduction in meachanical properties, since this compromises the structural integrity of the scaffold, since this compromises the structural integrity of the scaffold. ²⁴

The biocompatibity of these PCL scaffolds as bone scaffolds was assessed by an indirect cytotoxicity evaluation with mouse fibroblastic cells (L929) and mouse calvaria-derived pre-osteoblastic cells (MC3T3-E1), based on the initial 40,000 cells/well of cells seeded. Even though we were interested in using the obtained scaffolds as potential bone scaffolds, it was mandatory to test the materials with L929 just to comply with the ISO10993-5 standard test method. The viability ratio of cells that had been cultured with all of extraction media (and with control TCPS) is greater than 80%. All of the obtained results clearly suggested that all types of the PLA fibrous scaffolds, released no substances at levels that were harmful to both types of cells. Similar to our results, Jie et al.²⁵ showed that the cytotoxicity of poly(D,L-lactide)/nano-hydroxyapatite composites was 79.6-82.6% and the cytotoxicity of these scaffolds was in grade I according to ISO10993-1, that means these kind of materials have very good cytocompatibility.

In comparison with TCPS, the viability of cell on the salt-PEG 200 leached, salt-PEG 600 leached, salt leached PCL scaffold was slightly lower on day 1 and the proliferation of cells on salt-PEG 600 leached and salt-PEG 1000 leached PCL scaffold was significantly greater on day 3. The lesser viability of cells in the attachment period on various types of the scaffolds in comparison with that on TCPS In contrast, the greater number of cells in the proliferation period on PCL scaffolds could be because of high porosity and high interconnectivity network of the PCL scaffolds though which the cells were able to penetrate into the scaffolds. As a result, higher porosity did not affect cell attachment, but resulted in increased cell proliferation, due to pore space increased with porosity and facilitated transport of oxygen and nutrients.^{24,26}

ALP activity was measured to compare the effects of the scaffolds on osteoblastic differentiation by culturing MC3T3-E1 cells for 3, 5, and 7 days on PCL scaffolds. As shown in Figure 10, the ALP activities of the MC3T3-E1 cells cultured on the salt-PEG 1000 leached PCL scaffold was significantly higher than that on TCPS on day 7. When the culture was maintained up to 14 days, significantly greater amount of calcium deposition was observed in the salt-PEG 1000 leached PCL scaffolds compared to the TCPS and salt leached PCL scaffolds, as determined by the alizarin red-S staining and the quantification of calcium deposition. Base on all results, the good in biocompatibility of the salt-PEG 1000 leached PCL scaffolds could be result from the high porosity and high interconnectivity network of PCL scaffolds that can permit cell intrusion, and permeation.

Conclusion

Three-dimensional PCL scaffolds with highly porous, and highly interconnectivity network can be prepared by our modified solvent casting, particulate leaching, and polymer leaching techniques using sodium chloride and polyethylene glycol(PEG) as a porogen. Scanning electron microscopic (SEM) and optical microscope images confirm that the scaffolds fabricated using this method have highly interconnected network, equal distribution, and uniform size of 400-500 µm pores. The greatest porosity, pore volume, and pore size values and the highest interconnectivity observed for salt-PEG 1000 leached PCL scaffolds are the obvious reasons for their greatest water absorption capability. The potential of use these scaffolds in bone tissue engineering application was evaluated in vitro with mouse calvaria-derived, pre-osteoblastic cells (MC3T3-E1). Indirect cytotoxicity evaluation revealed that scaffolds fabricated using this method released no substances at levels that were harmful to cells. Scanning electron microscopy observation showed the majority of the cells seeded on the surfaces of scaffolds at 3 days expanded over the area of the scaffolds which was the most expansion on the surface of scaffolds fabricated using this method. For mineralization, cells cultured on surfaces of PCL scaffolds fabricated using this method showed the highest mineral deposition. All of obtained results can be implied their potential for utilization as bone-scaffolding materials.

11. Preparation and Properties of a-Chitin-Whisker-Reinforced Hyaluronan-Gelatin Nanocomposite Scaffolds

Materials

Chitin powder (crab shells, a form, weight-average molecular weight = 4×10^5 g/mol) was purchased from Fluka (St. Gallen, Switzerland). Gel (porcine skin, type A, 170–180 bloom) was purchased form Fluka. HA (weight-average molecular weight = 1.4×10^6 g/mol) was purchased from Coach Industries (Osaka, Japan). 1-Ethyl-3-(3-dimethylaminopropyl)carbodiimide (EDC) was purchased form Fluka. HCl [37% (w/w), analytical-reagent grade] was purchased from Labscan Asia (Bangkok, Thailand). All other chemicals were analytical-reagent grade and were used without further purification.

Preparation of the CWs CWs were prepared by the acid hydrolysis of chitin powder with 3N HCl at 120 °C for 6 h under vigorous stirring and refluxing. The ratio of HCl to chitin powder was 30 mL/g. After acid hydrolysis, the obtained CW suspensions were diluted with distilled water and were then centrifuged at 10000 rpm for 5 min and decanted in triplicate. The suspensions were then transferred to dialysis bags and dialyzed in running water for 2 h and later in distilled water for 2 days. The dispersion of CWs was completed by a 5-min ultrasonification treatment for every 40 mL aliquot. The solid fraction of the asprepared CW suspensions was gravimetrically determined to be 1.43 wt % on average. The CW suspensions were stored at 4 °C before further use.

Preparation of the neat HA-Gel scaffolds and the CW-reinforced HA-Gel scaffolds

An equal mass of HA and Gel powder was first mixed and dissolved in deionized (DI) water at 50 °C to obtain a blend solution of the polymers (i.e., HA–Gel) at a fixed concentration of 2 wt %. The blend solution was left to cool to room temperature before various amounts of the as-prepared CW suspensions were added to the solution. The six different mass ratios between the CWs and HA–Gel were 0, 2, 5, 10, 20, and 30% (w/w). The mixtures were continuously stirred until they were fully homogenized. To crosslink HA–Gel, 1 mmol of EDC was added, and the mixtures were further stirred for 2 h at room temperature.

Volumes of the mixtures were poured into polypropylene dishes to obtain molding specimens of two different shapes and dimensions (i.e., cylindrical and disc shapes), frozen at 40°C for 24 h, and lyophilized at 50°C for another 24 h. The obtained cylindrical scaffolds were about 10 mm in diameter and 2 mm in height, whereas the disc-shaped scaffolds were about 1 mm in thickness; these were later cut into a desired shape and size for the mechanical property assessment. The as-prepared scaffold specimens were kept in a desiccator before further use.

Characterization Microstructure observation and pore size determination

One cylindrical scaffold was randomly selected fromeach group of the scaffolds. It was cut into pieces along both the longitudinal and the transverse directions. The cut pieces were mounted on copper stubs, coated with gold with a JEOL JFC-1100 sputtering device (Tokyo, Japan) and observed for their microscopic structure with a JEOL JSM-5200 scanning electron microscope. To determine the dimensions of the pores, 50 pores for each of the cross sections and the longitudinal sections (i.e., 100 pores in total) were directly measured from the scanning electron microscopy (SEM) images with The University of Texas Health Science Center at San Antonio (UTHSCSA) Image Tool version 3.0 software. The average values for all of the specimens investigated were calculated and reported.

Mechanical properties For the tensile mechanical integrity, specimens (50 x 5 x 1 mm³) were cut from the disc-shaped scaffolds. The mechanical integrity of the specimens, measured in their dry state, in terms of the tensile strength, Young's modulus, and elongation at break was assessed with a Lloyd LRX-Plus universal testing machine (West Sussex, UK) with a 10-N load cell at room temperature (26 \pm 2°C). The gauge length was 30 mm, and the crosshead speed was 10 mm/min. The measurements were carried out in pentuplicate for each group of the scaffolds.

Water-retention capacity

Cylindrical scaffolds, in their dry state, were weighed and then individually immersed in DI water at room temperature. At a given time point, the specimens were taken out, blotted on a glass plate, which was set at

about 45° from a horizontal baseline for 5 s to remove excessive water, and immediately weighed. The amount of water retained in the specimens was determined according to the following equation:

$$Water\ absorption(\%) = \frac{(Ww - Wd)}{Ww} \times 100$$

where W_d and W_w are the weight of the specimens before and after submersion in the medium, respectively. The experiment was carried out in pentuplicate and the measurements were carried out at different time intervals within a period of 24 h

In vitro degradation

The in vitro degradation study of the scaffolds was carried under three conditions. In the first, cylindrical scaffolds were individually immersed in a 10 mM phosphate buffer saline (PBS) solution (pH 7.4) at room temperature without shaking for 24 h. Under the other two conditions, they were individually immersed in either PBS or bacterial collagenase at a concentration of 373 ng/mL at 37°C undershaking(70rpm) for 24 h. After the specified time, the specimens were removed from the media, frozen at 40°C for 24 h, and lyophilized at 50 °C for another 24 h. The degradability of the specimens was then quantified according to the following equation:

Degradability(%) =
$$W_t/W_i \times 100$$
;

where Wi is the initial dry weight of the specimens and W t is the dry weight of the specimens after each respective in vitro degradation assay. The measurements for each group of the scaffolds were carried out in triplicate.

Infrared (IR) spectroscopy and thermal analyses

A Thermo Nicolet Nexus 670 Fourier transform infrared (FTIR) spectrophotometer (Madison, WI) was used to investigate the chemical functionalities of the as-prepared scaffolds by the KBr disk method. One

cylindrical scaffold was randomly selected from each group of scaffolds and subsequently subjected to FTIR scanning over 32 scans at a resolution of 4 cm⁻¹. The thermal stability of the selected cylindrical scaffold specimens was assessed in terms of their degradation temperature with a PerkinElmer TGA-7 thermogravimetric analyzer (Waltham, MA) over a temperature range of 30–600 °C at a heating rate of 10 °C/min under a nitrogen atmosphere. The weights of the specimens ranged between 3 and 5 mg. A PerkinElmer DSC-7 differential scanning calorimeter (Waltham, MA) was used to determine the glass transition temperature (T g) of the scaffold specimens over a temperature range of 25–80°C at a heating rate of 10 °C/min. The specimens, weighing around 5–6 mg, were subjected to a preheating run to erase their thermal history before the test.

Biological evaluation Cell culture

Human osteosarcoma cells (SaOS-2) were cultured as a monolayer in a-minimum essential medium (a-MEM; Sigma–Aldrich, St. Louis, MO), supplemented by 10% fetal bovine serum (Biochrom, Cambridge, UK), 1% Lglutamine (Invitrogen, Carlsbad, CA), and a 1% antibiotic and antimycotic formulation containing penicillin G sodium, streptomycin sulfate, and amphotericin B (Invitrogen). The cells were maintained at 37°C in a 95% humidified atmosphere containing 5% CO2 and passaged once every 3–4 days.

Cytotoxicity evaluation

Only the cylindrical scaffolds containing 0 and 30% CWs were used in these studies. The cytotoxicity of the scaffolds was evaluated by the indirect method with SaOS-2 as the reference cells. First, the extraction media were prepared by immersion of the scaffold specimens in 500 μ L of serum-free medium (SFM; containing MEM, 1% L-glutamine, 1% lactabumin, and a 1% antibiotic and antimycotic formulation) for 24 h. Each of these extraction media was later used in the indirect cytotoxicity evaluation. SaOS-2 were cultured in wells of a 24-well culture plate at 4 x10⁴ cells/well in serum-containing MEM for 16 h to allow attachment of the cells to the plate. The cells were then starved with SFM for 24 h, after which time, the

medium was replaced with an extraction medium. After 24 h of cell culturing in the extraction medium, a 3-(4,5-dimethylthiazol-2-yl)2,5-diphenyl tetrazolium bromide (MTT) assay (see details in the Supporting Information) was carried out to determine the viability of the cells. The experiment was carried out in quadruplicate.

Cell attachment and cell proliferation

A primary evaluation for cell attachment was carried out by a direct morphological observation of SaOS-2 cells that had been seeded on the surface of the scaffold specimens. Only the cylindrical scaffolds containing 30% CWs were used in the study. Specifically, the cylindrical scaffold specimens were put in wells of a 24-well culture plate and sterilized with 1 mL of 70% ethanol for 30 min. They were then washed with sterilized DI water twice and later immersed in a-MEM overnight. SaOS-2 cells were then seeded on the surfaces of the specimens at 4 x 10^4 cells/specimen in a minimum volume of the culture medium and were allowed to attach on the surfaces for 3 h before the addition of 1.5 mL/well of the culture medium. The cells were cultivated at 37 °C in a humidified atmosphere containing 5% CO2

for 1 and 7 days, after which time, the morphology of the cultured cells was observed by SEM. After the removal of the culture medium, the cell-cultured scaffold specimens were rinsed with PBS twice, and the cells were fixed with a 3% glutaraldehyde solution, which was diluted from a 50% glutaraldehyde solution (Electron Microscopy Science, Hatfield, PA) with PBS for 30 min. The specimens were then dehydrated in graded ethanolic solutions (i.e., 30, 50, 70, and 90%) and in pure ethanol for about 2 min each. They were further dried in 100% hexamethyldisilazane (Sigma-Aldrich) for 5 min, dried in air after the removal of hexamethyldisilazane, mounted on SEM stubs, coated with gold, and finally, observed by SEM. The examinations were performed on three randomly selected scaffold specimens.

To quantify the viability of the attached and the proliferated cells, SaOS-2 cells had first been seeded or cultured on each of the four randomly selected specimens from each group of the scaffolds for 1, 24, 48, and 72 h before they were evaluated by the MTT assay at each time point. Only the cylindrical scaffolds were used in this study.

Statistical analysis

Data were analyzed with SPSS software version 14.0 for Windows (SPSS, Chicago, IL). Initially, the normal distribution was assessed by the Shapiro–Wilk test. The normal distribution data, representing the homogeneity of the variances, shown by the Levene's test, were then investigated by a one-way analysis of variance (ANOVA) with the Tukey HSD post hoc multiple comparisons. Otherwise, the Dunnett T3 was applied if the data did not exhibit the homogeneity of the variances. For the data of which the normal distribution was absent but the variance was homogeneous, the Kruskal–Wallis H was applied. To compare the means between two data groups, the Student unpaired t test was used. The significant level was indicated at p < 0.05 in any case.

RESULTS AND DISCUSSION

Characterization of the CWs

The dialyzed CWs exhibited colloidal behavior in water. Protonation of the amino groups of chitin under acidic conditions induced positive charges (NH3) on the surface of the CWs, which generated electrostatic repulsion among the nanocrystallites.30 However, protonation of amino groups was not complete on all of the CW particles; hence, the hydrogen bonding associated with the free amino groups on the CWs caused them to aggregate. The representative TEM image of the as-prepared CWs, which were prepared from a dilute suspension, is illustrated in Figure 1. It was evident that the CWs were present as individual and partially aggregated entities. The aggregation of the CWs was facilitated by the increase in the pH of the suspension during dialysis, hence, the deprotonation of some of the protonated amino groups that occurred during the acid hydrolysis to prepare the CWs. According to the TEM results, the as-prepared CWs were present as slender rods with sharp points on both ends. The lengths (L's) and widths (d's) of these rods were 255 6 56 and 31 6 6 nm, respectively, with an L/d ratio of about 8. The histograms illustrating the distribution of the lengths and the widths of the asprepared CWs, as shown in the Supporting Information, indicated that over 50% of the CWs exhibited lengths and the widths in the range 203–277 and 27–35 nm, respectively. These dimensions compared well with the reported values for CWs obtained from crab shells (L N 50-300 nm and d N 6-8 nm, 30 L N 100–600 nm and d N 4–40 nm, 35 and L N 100–650 nm and d N 10–80 nm 36).

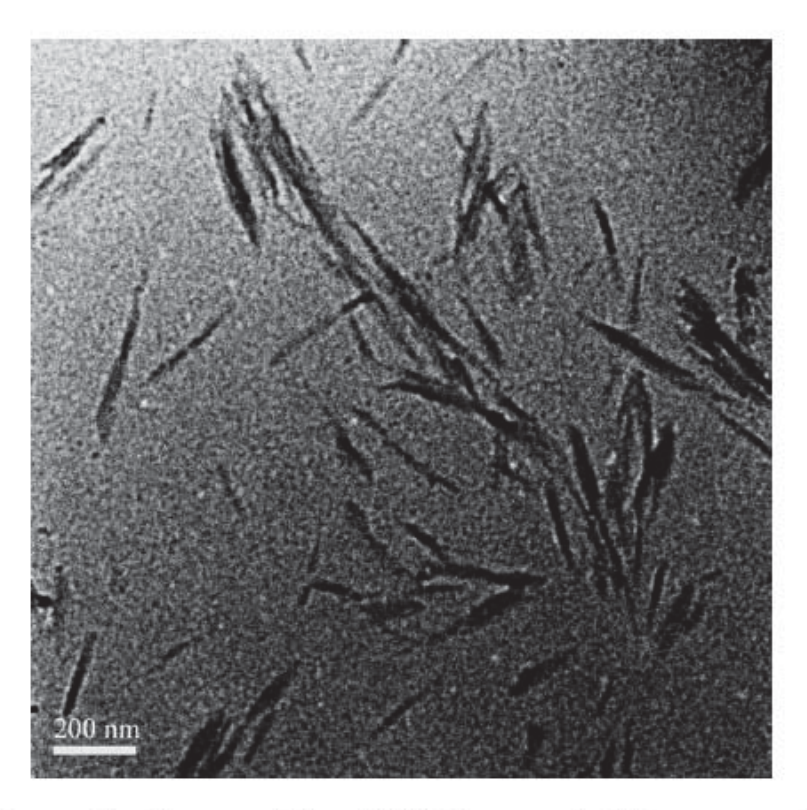


Figure 1 Representative TEM image of CWs prepared from a diluted suspension of acid-hydrolyzed chitin powder from crab shells.

Characterization of the CW-reinforced HA–Gel scaffolds
Physical characteristics

Representative photographic images of the as-prepared cylindrical scaffolds are shown in the Supporting Information. These scaffolds were extremely light in weight because of their highly porous nature. The color of these scaffolds ranged from the pure white of the neat HA-Gel scaffolds to the light brown of the 30% (w/w) CW-reinforced HA-Gel scaffolds. The brown color resulted from the presence of the CWs dispersing within the mass of the scaffolds. Representative SEM images illustrating the microstructure of the as-prepared scaffolds viewed on the surface perpendicular to the transverse direction (i.e., the surface of the transverse sections) are shown in Figure 2, whereas those illustrating the microstructure of the scaffolds viewed on the surface perpendicular to the longitudinal direction (i.e., the surface of the longitudinal sections) are shown in the Supporting Information. All of the scaffolds exhibited a well-defined porous structure, and regardless of the surface under consideration, the interpore connectivity was discernible throughout the bulk of the scaffolds. For a given group of the scaffolds, no significant difference in terms of the morphology of the pore structure was observed between the two sections. This was in exception to the one that contained 30% CWs, which showed a disruption in its microstructure when viewed on the surface of the longitudinal sections. The dimensions of the pores observed in these SEM images were determined and analyzed and are reported in Table I. The size of the pores for all of the scaffolds in both the transverse and the longitudinal sections ranged between 92 and 230 lm, with the average value ranging between 139 and 166 lm. An increase in the content of the CWs

did not have a significant effect on the pore dimensions. A comparison of the pore dimensions that were observed in the two sections for each group of the scaffolds was evaluated statistically, and there was no difference, except for those observed for the neat HA–Gel sample group. With an average pore size smaller than 200 lm, the transportation of nutrients and oxygen and the ingrowth of new blood vessels into the inner pores of the scaffolds were somewhat restricted. The lack of ample oxygen supply leads to a medical condition known as hypoxia, which is suitable for the regeneration of cartilage but certainly not bone.37,38 To obtain scaffolds with larger pore dimensions, the cooling rate associated with the freezing of the HA–Gel solution or the HA–Gel/CWs suspensions before the subsequent sublimation of the ice crystals needs to be decreased further because it is a known fact that a fast cooling rate induces the formation of tiny ice crystals, hence, the small pore dimensions.39,40

TABLE I

Dimensions of the Pores of the Neat HA-Gel Scaffolds and the CW-Reinforced HA-Gel Scaffolds Observed on the
Surfaces of Both Transverse and Longitudinal Sections

	Pore size (µm)					
	Transve	erse sections	Longitudinal sections			
Specimen	Range	Average	Range	Average		
	(Minimum – Maximum)	(Mean ± Standard deviation)	(Minimum – Maximum)	(Mean ± Standard deviation)		
0% CW	92.3–208.8	140.9 ± 21.8^{a}	112.8–231.4	165.8 ± 27.7^{a} 145.4 ± 15.3^{b} 142.7 ± 13.8^{c} 162.8 ± 23.6^{d} 143.9 ± 17.2^{e} 149.0 ± 25.1^{f}		
2% CW	114.4–182.0	139.4 ± 16.0^{b}	108.4–182.1			
5% CW	104.1–224.5	153.2 ± 23.9^{c}	110.6–171.1			
10% CW	118.0–202.3	158.9 ± 19.1^{d}	104.3–205.4			
20% CW	113.5–200.5	151.4 ± 19.3^{e}	105.8–181.0			
30% CW	108.5–184.4	155.4 ± 15.7^{f}	97.2–231.3			

Superscript letters indicate comparisons only between sections of a given group of specimens at p < 0.05 (one-way ANOVA with Tukey HSD, n = 50).

Mechanical properties

Mechanical properties, expressed in terms of the modulus of elasticity, elongation at break, and tensile strength, of the as-prepared scaffolds were evaluated, and the results are summarized in Table II. Statistical analysis indicated that inclusion of the CWs in amounts of 2–30% in the HA–Gel scaffolds resulted in a significant increase in the modulus of elasticity from that of the neat scaffolds. Nevertheless, the property values among the various groups of the CW-reinforced HA–Gel scaffolds were not statistically different, except for the one containing 20% CWs, which showed significantly lower values. For the elongation at break, the neat HA–Gel scaffolds exhibited significantly greater values over all of the reinforced samples, which statistically showed equivalent values among themselves. With regard to the tensile strength, it was obvious that the HA–Gel scaffolds that contained 2% CWs exhibited the property values that were significantly greater than those of the other groups of samples, which, among themselves, showed equivalent values. The result agreed well with the report of Sriupayo et al.,34 who found that the greatest tensile strength of CW-reinforced chitosan films was observed at a CW content of 2.96% and an increase in the CW content resulted in a reduction in the property values. To put it into perspective, the modulus of elasticity and the tensile strength values of the scaffolds containing 2% CWs were much lower than those of bone, which are 16.4 GPa and 117.4 MPa, respectively, on average.4

TABLE II
Mechanical Properties of the Neat HA-Gel Scaffolds and the CW-Reinforced HA-Gel Scaffolds

Specimen	Modulus of elasticity (MPa)	Elongation at break (%)	Tensile strength (MPa)
0% CW 2% CW 5% CW 10% CW 20% CW 30% CW	0.99 ± 0.10^{a} 14.10 ± 2.23^{b} 19.96 ± 3.64^{b} 12.46 ± 2.00^{b} 07.10 ± 0.93^{c} 11.96 ± 0.47^{b}	53.48 ± 10.69^{a} 28.35 ± 6.16^{b} 06.36 ± 1.42^{c} $11.63 \pm 4.15^{c,d}$ $16.07 \pm 0.96^{b,d}$ $16.03 \pm 3.40^{b,d}$	0.52 ± 0.06^{a} 1.03 ± 0.09^{b} $0.53 \pm 0.15^{a,c}$ $0.48 \pm 0.19^{a,c}$ 0.47 ± 0.06^{a} 0.72 ± 0.08^{c}

Superscript letters indicate comparisons between groups of specimens for a single property at p < 0.05 (one-way ANOVA with Dunnett T3, n = 5).

Water absorption and in vitro degradability

The ability of the neat and CW-reinforced HA-Gel scaffolds to absorb water at room temperature within 24 h is graphically shown in Figure 3. All groups of the scaffolds demonstrated comparable water absorption within the first 60 min, which accounted for more than about 95% of their total wet weights. The values were as high as that of a superabsorbent.42 The results were similar to those reported by Park et al.43 on collagen-HA sponges. Such a great tendency to absorb a great amount of water is characteristic of a hydrogel material, such as HA and Gel, which are very hydrophilic in nature. 9 With the absorbed water, the interior of a scaffold becomes a hydrated environment, which facilitates the process of tissue regeneration by protecting cells and their products, such as secreted ECM. Furthermore, the hydrated environment facilitates the transportation of nutrients into and wastes out of the cells.24 According to Figure 3, all groups of the scaffolds exhibited similar water absorption values and equivalent profiles; that is, the property values decreased gradually with increasing submersion time. The absorption of water in a given group of the scaffolds reached a maximum only after having been submerged in DI water for 15 min, and the inclusion of the CWs within the scaffolds did not strongly influence the water absorption. This was due to the inherent hydrophilicity of all of the compositions, the interconnectivity of the pore structures, and the similarity in the pore dimensions of all of the scaffolds, which facilitated the capillary action and, hence, the rapid adsorption of water.42 The observed decrease in the amounts of water absorbed as the immersion time increased might have been due to the fact that the scaffolds began to disintegrate or partially dissolve, which diminished their capacity to imbibe both free and bound water.24,43

Despite the many benefits of the high water absorption of a scaffold, certain drawbacks should also be considered, such as weakening and acceleration due the to degradation of the scaffold.24 The degradation of a scaffold occurs mainly by either a physical or chemical pathway. The physical pathway involves dissolution and hydrolysis, whereas the chemical pathway involves enzymatic cleavage in the presence of a suitable enzyme.9 Here, we investigated the dissolution and hydrolytic degradation of the scaffolds in PBS over a submersion period of 24 h under both static conditions at room temperature and dynamic conditions, that is, by means of a shaking water bath at 70 rpm and 37_C. The enzymatic

degradation of the scaffolds was also investigated in 373 ng/mL of bacterial collagenase, which represented a model concentration of tissue collagenase in the synovial fluid of the patients with osteoarthritis.44,45 The investigation was carried out in the shaking water bath at 70 rpm and 37_C for 24 h. The results of thesstudies are graphically shown in Figure 4. Figure 4 shows the remaining weights of the scaffolds after submersion in PBS or collagenase (COL) solution for 24 h. Upon submersion in PBS under the static conditions at room temperature, the remaining weights of the scaffolds were about 58-76% of their original dry weights, with no significant difference among all groups of the scaffolds. Under the dynamic conditions, on the other hand, the remaining weights, for a given group of the scaffolds, were significantly lower than those observed under the static conditions. The enhancement in the weight loss was obviously due to the added energy from the agitation, which increased the kinetic energy of the system. In addition, the thermal degradation of the HA molecules could occur to a certain extent at 37 C.18 These could have been factors contributing to the observed values of the remaining weights of the scaffolds at 33-60% of the original dry weights of the scaffolds. The incorporation of CWs in the amounts of 20–30% in the HA-Gel scaffolds enhanced the resistance to degradation under the dynamic conditions compared with the neat scaffolds. Although a trend was observed for the relationship between the remaining weights of the scaffolds and the CW content, statistical analysis among the scaffolds that contained 5-30% CWs did not show a significant difference in their property values. In the collagenase medium, the degradation of the scaffolds was noticeably enhanced as the remaining weights, for a given group of the scaffolds, were the lowest. Regardless of the CW content, the values were in the range 11-52% of the original dry weights of the scaffolds. In addition to the agitation and the hypothetical thermal degradation of HA, the scission of Gel peptide bonds at glycine subunits by the enzyme was the main contributing factor.43 The presence of the CWs at levels of 5% or more significantly enhanced the stability to degradation of the scaffolds in the presence of the enzyme. Such an enhancement could have been due to the interaction between the CWs and the HA-Gel matrix molecules, which reduced the enzyme accessibility.46

IR spectroscopy analysis

Figure 5 illustrates FTIR spectra of the neat and CW reinforced HA-Gel scaffolds over the wave-number range 3500–500 cm_1. Those of the constituting materials are also shown for comparison. The absorption peaks at 1656, 1547, 1450, and 1237 cm 1, characteristic of amide bonds (COANH), were observed in the spectrum of Gel,43,47,48 whereas those at 1412 and 1076 cm_1, corresponding to carboxylate salts (symmetric stretching) and ester bonds, respectively, were observed in the spectrum of HA, of which repeating units comprised glucuronic acid and acetylglucosamine. The spectrum of the CWs should have been similar to that of HA because both of them were polysaccharides. Being crystalline entities, however, the CWs presented sharper and more intense signals at certain positions, 49 particularly at 1076 (ester bonds), 1378 (carboxylate salts), and 3267 and 3446 cm_1 (hydroxyl groups).48 Additionally, the CWs exhibited characteristic amide I peaks at 1621 and 1656 cm_1 and the amide II peak at 1556 cm_1.35,47 The peak at 1621 cm_1 was only specific to CWs, whereas that at 1656 cm_1, representing the stretching of hydrogen bonds between carbonyl groups and the neighboring amine groups of intrachains, could also be found for the amide bonds of a protein.49 For the neat HA-Gel scaffolds, the peaks at 1650, 1550, 1412, and 1076 cm_1 were discernible. Crosslinking with EDC generated both the amide and the ester linkages in the structure of the blends.50 The amide bonds were formed between the carboxyl groups of Gel and/or of the glucuronic acid in HA and the amino groups of Gel. The ester bonds, on the other hand, were formed between the carboxyl groups and the hydroxyl groups of Gel and/or of HA.51,52 For the scaffolds that contained CWs, the presence of the CWs were confirmed by the presence of characteristic peaks at 1378 and 1076 cm_1 and the absorption shoulder at 3267 cm 1, and the intensities of these peaks and the shoulder were found to increase with an increase in the content of the CWs.

Thermal characteristics

Figure 6 shows thermogravimetric analysis thermograms of the as-prepared scaffolds. All samples

exhibited similar profiles of weight change. Table III summarizes the values of the temperatures at which the losses in the weight of the scaffolds reached 5, 25, and 50% (on the basis of their original weights). Apparently, at temperatures lower than 200_C, the loss in the weight of all of the scaffolds, except for the ones containing 5% CWs, was less than 5%, with no particular relationship with the CW content. At temperatures around 210–230_C, the loss in the weight increased abruptly to reach maximum values at temperatures around 245–250_C, as indicated by the positions of the peaks of the corresponding derivative curves (not shown). As the temperatures increased to around 260–360_C, the loss in the weight of the different groups of the scaffolds became most noticeably different and inversely related to the CW content within the scaffolds. Careful consideration of the results revealed that the temperatures required for the scaffolds that contained 10–30% CWs to reach 25 and 50% of the weight loss were significantly greater than those of the neat scaffolds and the ones containing 2 and 5% CWs. This demonstrated that reinforcing the scaffolds with 10–30% CWs enhanced the thermal stability of the resulting scaffolds. Notwithstanding, such enhancement was only reflected in a limited temperature range, that is, 260–360_C, as the residual weights of all of the scaffolds at 550_C were comparable.

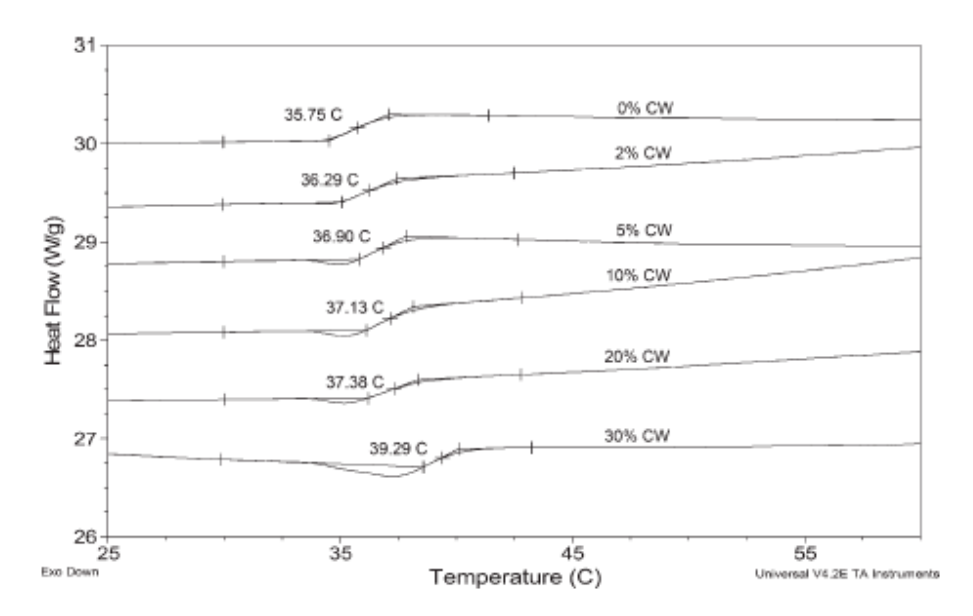


Figure 7 Differential scanning calorimetry thermograms (10°C/min) in a nitrogen atmosphere) of the neat HA–Gel scaffolds and the CW-reinforced HA–Gel scaffolds. Their T_g 's are illustrated.

Figure 7 shows the differential scanning calorimetry thermograms of the as-prepared scaffolds. The range of the temperature was chosen such that it revealed the glass transitions of the materials. Apparently,the neat HA–Gel scaffolds exhibited the Tg at about 35.8_C. With the addition and increasing amount of the CWs, Tg was found to increase from that of the neat materials to 36.3_C at 2% CWs and finally to 39.3_C at 30% CWs. With the Tg values of the HA–Gel scaffolds that contained 5–30% CWs in the range 36.9–39.3_C, the enhancement in the resistance to biodegradation of the corresponding scaffolds by collagenase, as previously shown, could have been, at least partly, due to the observed increase in the Tg values from that of the neat materials. The increased Tg values that were close to or greater than the physiological temperature of 37_C should have resulted in less mobility of the matrix molecules and, thus, the lower tendency for conformational change. However, because the Tg values of these scaffolds were measured in their dry state, the actual values in the physiological environment (i.e., wet conditions) should be much less because of the plasticizing effect from absorbed water molecules.

Nevertheless, the marked increase in the Tg values for the scaffolds that contained 5–30% CWs coincided with the observed improvement in the resistance to enzymatic degradation of these scaffolds.

Cytotoxicity and in vitro response of bone cells

We first investigated the cytotoxicity of the as-prepared scaffolds. The assessment was carried out on the basis of the indirect cytotoxicity assay, in which the extraction media from the neat and the 30% CWreinforced HA–Gel scaffolds were used to incubate SaOS-2 osteosarcoma cells for 24 h. The viability of the cells, determined spectrophotometrically at 570 nm, was compared with that of the cells that had been incubated with SFM for the same period of time. The results are shown in Table IV. Evidently, the viability of the cells that were cultured with either the extraction media from the neat scaffolds or the SFM was statistically the same, a result indicating that the neat HA–Gel scaffolds were biocompatible with the bone cells. Nevertheless, the viability of the cells decreased significantly when they were cultured with the extraction media form the scaffolds that contained 30% CWs. This result suggests that the presence of the CWs (at 30%) had an adverse effect on cell viability. Further evaluation by the direct culturing of the cells onto the scaffolds was then carried out to confirm whether they were toxic to the cells.

Figure 8 shows representative SEM images in various magnifications of SaOS-2 cells that were cultured on the surfaces of the 30% CW-reinforced HA–Gel scaffolds for 1 or 7 days. On day 1, the cells attached well to the surfaces of the scaffolds. The majority of the cells exhibited evidence of cytoplasmic process in the form of filopodia over the surfaces [see Fig. 8(b,c), as indicated by arrows]. The observation of cytoplasmic expansion indicated a good initial response of the cells to the as-prepared scaffolds, which influenced the subsequent cellular processes of proliferation and differentiation.53 On day 7, the morphology of the cells changed from the rather well-defined round shape observed on day 1 to fully expanded and even fused to the underlying surfaces of the scaffolds [see Fig. 8(d–f), as indicated by arrows]. Such an observation confirmed the preference of the cells to the surfaces, as they adhered and spread well over the surfaces. Despite the fact that the indirect cytotoxicity evaluation of the studied scaffolds produced a poor result, the observation of the bone cells that appeared to attach and expanded well over their surfaces indicated the applicability of the scaffolds for bone cell culture.

To investigate the effect of CW content on the proliferation of bone cells, the viability of SaOS-2 cells that were cultured on the neat and CW-reinforced HA-Gel scaffolds for 1, 24, 48, and 72 h was evaluated by the MTT assay. The results are graphically shown in Figure 9. At 1 h after cell seeding, the viability of the adherent cells on the surfaces of the scaffolds was either as good as or better than that on the tissue culture plate. At 24 h after cell culturing, only the cells that had been cultured on the surfaces of the 10% CW-reinforced HA-Gel scaffolds showed viability greater than the other groups of the scaffolds and the tissue culture plate. At 48 and 72 h after cell culturing, the viability of the cells on the tissue culture plate was significantly greater than that of those cultured on the surfaces of the scaffolds. Among the various groups of the scaffolds, the ones containing 10% CWs, again, exhibited the greatest viability of the cultured bone cells. It has been suggested that the presence of HA is not always positive in regulating the functions of cells.54 Liu et al.27 reported that HA-Gel-chitosan ternary blend films with a weight content of HA of 0.31% significantly promoted the attachment, migration, and proliferation of fibroblasts better than those with weight contents of HA of 1.56 and 3.11%. On the basis of these negative reports, the composition of HA within the scaffolds could be reduced to establish a much better positive environment for cell culture. Notwithstanding, among the various groups of the scaffolds, the ones that contained 10% CWs showed the most promising results for the attachment and proliferation of the bone cells.

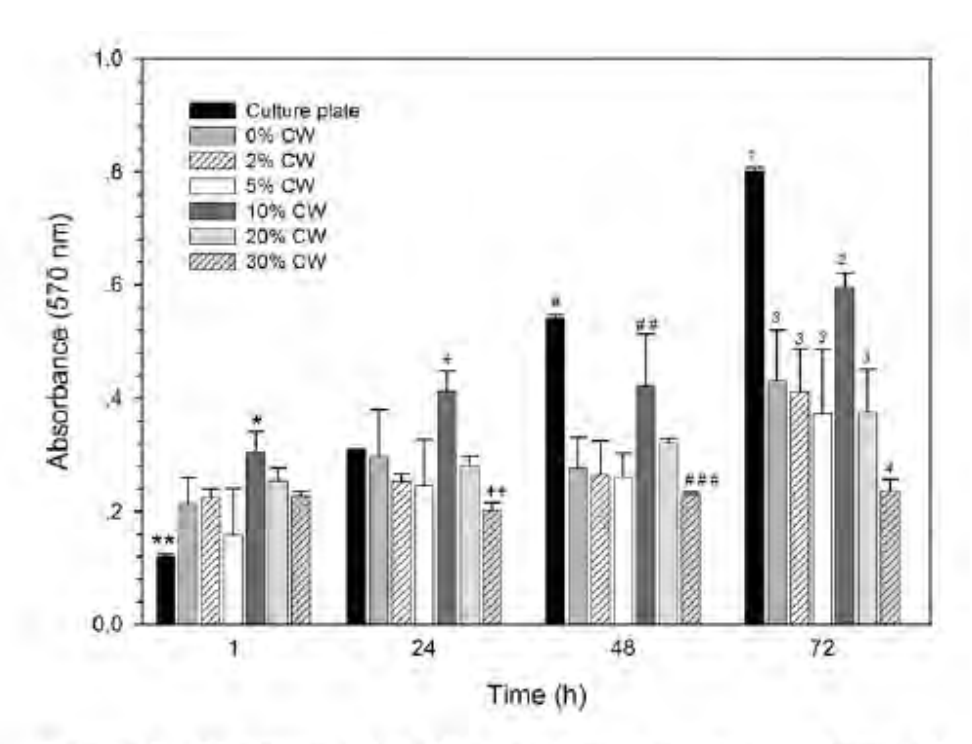


Figure 9 Viability of SaOS-2 cultured on the surfaces of the neat HA–Gel scaffolds and the CW-reinforced HA–Gel scaffolds. *,*-,**,**,**p < 0.05 (one-way ANOVA with Tukey HSD, n = 4).

CONCLUSIONS

CW-reinforced HA–Gel nanocomposite scaffolds were successfully fabricated by the freeze-drying method. The variation in the amount of the incorporated CWs did not have an obvious effect on the morphology of the internal structure of the scaffolds. Nevertheless, the characteristics of the as-prepared scaffolds could be regulated through the variation in the amount of the incorporated CWs so that the optimal balance among their physicochemical, mechanical, and biological properties could be achieved. A high proportion of incorporated CWs was found to enhance the thermal stability and the resistance to biodegradation, whereas a rather lo proportion of the CWs increased the tensile strength and enhanced the biocompatibility in terms of the attachment and proliferation of the cultured human osteosarcoma cells of the resulting scaffolds. Although the scaffolds that contained 10% CWs showed great promise as substrates for bone cell culture, their actual utilization could be limited to a low-stressbearing area, such as the socket of a dental root.

12. Preparation and Characterization of Caffeic Acid-Grafted Electrospun Poly(L-Lactic Acid) Fiber Mats for Biomedical Applications

EXPERIMENTAL SECTION

Materials. PLLA (Mn = 80 000 g mol-1), CA, HMD, EDC, and NHS were purchased from Sigma-Aldrich (USA). DCM (Carlo Erba, Italy), DMF [Lab-Scan (Asia), Thailand], and ethanol [Lab-Scan (Asia), Thailand] were of analytical reagent grade and used withoutfurther purification.

Preparation of Electrospun PLLA Fiber Mats. Electrospinning

of PLLA was carried out based on a previously published method.14 Briefly, 10% w/v PLLA solution in 7:3 v/v DCM/DMF was fed into a glass syringe fitted with a blunt 20-gauge stainless steel hypodermic needle (OD = 0.91 mm), used as the nozzle. An aluminum sheet wrapped around a homemade rotating cylinder (width and diameter ≈ 15 cm; rotational speed ≈ 50 rpm) was used as the collector. The solution was charged with a Gamma High Voltage Research DES30PN/M692 at a fixed electric field of 20 kV/18 cm. After the solution had been electrospun continuously for 18 h, the thicknesses of the obtained fiber mats were measured to be $120 \pm 15 \mu m$. Surface Modification of Electrospun PLLA Fiber Mats. Aminolysis of the PLLA fiber mats was carried out based on a previously published method,22 with slight modification. Specifically, the fiber mats had been washed in an ethanolic aqueous solution (1:1 v/v) for 2 to 3 h, prior to being washed with a large quantity of deionized (DI) water. The aminolysis was then carried out by immersing the fiber mats in a HMD/isopropanol (IPA) solution of varying concentrations (i.e., 0.02, 0.04, 0.06, and 0.08 g mL-1) for varying periods of the reaction time (i.e., 5, 10, 15, 20, and 30 min) at 50 °C. The aminolyzed PLLA fiber mats (hereafter, a-ePLLA) had been rinsed in DI water for 24 h at room temperature to remove unreacted HMD, prior to being dried in vacuo at room temperature until of a constant mass. Activation of CA was done based on a previously published method,23 with slight modification. Specifically, 250 mg of CA, a priori dissolved in 10 mL of ethanolic aqueous solution (1:1 v/v), was reacted with 169 mg of EDC and later with 102 mg of NHS. The mixture was stirred in an ice-water bath for 1 h to finally obtain a solution of the activated CA. The aminolyzed PLLA fiber mats were subsequently immersed into the activated CA solution and stirred in the ice-water bath for 30 min. After 24 h of the reaction time at room temperature, the CA-grafted PLLA fiber mats (CA-gePLLA) were washed thoroughly with ethanol several times and finally dried in vacuo at room temperature.

Materials Characterization.

The free amino (NH2) groups on the surfaces of the neat and the modified PLLA fiber mats were quantified by ninhydrin or 2,2-dihydroxyindane-1,3-dione assay.22 The fiber mat samples were first immersed in 1 M ninhydrin/ethanol solution for 1 min, transferred into a glass tube, and then heated at 80 °C for 15 min to accelerate the reaction between ninhydrin and the NH2 groups that might be present on the surfaces of the fiber mat samples. If there were enough NH2 groups on the surfaces, they would turn blue. Upon complete evaporation of the adsorbed ethanol, 1,4-dioxane was added to dissolve the fiber mat samples. IPA was subsequently added to stabilize the blue compound. The absorbance of the obtained solutions were read at 538 nm using a Shimadzu UV-2550 ultraviolet–visible (UV–vis) spectrophotometer and the concentrations of the NH2 groups in the sample solutions were calculated from a standard calibration curve of HMD solutions in 1,4-dioxane/IPA (1:1 v/v) (see Figure I in the Supporting Information). Surface elemental chemistry of the neat and the modified PLLA fiber mats was analyzed by a Thermo Fisher Scientific Thetaprobe Xray photoelectron spectroscope (XPS).24 Monochromatic Al $K\alpha$ X-ray was employed for the analysis of one spot on each sample with a photoelectron emission angle of 50° (with respect to the surface

normal). The analytical area was approximately 400 μ m \times 400 μ m, and the maximal analytical depth was

in the range of ~4-8 nm. A few eV Ar+ ions, generated by an electron flood gun, were used for charge

compensation. Electron and ion beams were focused and steered toward the analytical area. Further correction was made based on adventitious C 1s at 285 eV, using the manufacturer's standard software. Survey spectra were acquired for surface composition analysis with sensitivity factors from Scofield library. The amounts of the immobilized CA on the surfaces of the CA-gePLLA

specimens were also investigated. Specimens (circular disk; ~2.8 cm in diameter; cut from randomly

selected areas of three different fiber mats) were individually dissolved in 10 mL of 7:3 v/v DCM/DMF solution. The absorbance of the sample solutions was spectrophotometrically read at 243 nm and the concentrations of the immobilized CA were calculated from a standard calibration curve of CA solutions in 7:3 v/v DCM/DMF (see Figure II in the Supporting Information).

Static water contact angles of the neat and the modified PLLA fiber mats were measured at room

temperature using a Krüss DSA 100 drop shape analyzer,25 equipped with a Gilmont syringe and a 24-

gauge flat tipped needle. Five droplets of distilled water (10 μ L) were placed randomly at different positions on each sample. The projected images of the droplets, after they had been settled on the surfaces until of no noticeable change in their shapes, were analyzed for the contact angles.

Morphological appearance and size of the individual fibers of the neat and the modified PLLA fiber mats were examined by a JEOL JSM 5410LV scanning electron microscope (SEM). At least 100 readings of the fiber diameters from various SEM images were analyzed using SemAphore 4.0 software. Mechanical properties in terms of stress at maximum load, strain at maximum load, Young's modulus, and elongation at break of the neat and the modified PLLA fiber mats were tested on a Lloyd LRX universal testing machine (gauge length = mm and crosshead speed = 100 mm min $^{-1}$). The specimens were cut into a rectangular shape (10 mm \times 100 mm). The measurements were carried out on ten different specimens.

Biological Evaluation. Murine dermal fibroblasts (L929) and human dermal fibroblasts (HDFa) were used as reference cells. L929 and HDFa were cultured as monolayer in Dulbecco's modified Eagle's medium (DMEM; Sigma-Aldrich, USA), supplemented with 10% fetal bovine serum (FBS; Biochrom, UK), 1% L-glutamine (Invitrogen, USA), and a 1% antibiotic and antimycotic formulation [containing penicillin G sodium, streptomycin sulfate, and amphotericin B Invitrogen, USA)]. The medium was replaced on every other day and the cultures were maintained at 37 °C in a humidified atmosphere containing 5% CO2.

In the indirect cytotoxicity evaluation, the fiber mat specimens were assessed using a procedure adapted from the ISO10993–5 standard test method. First, extraction media were prepared by immersing

the fiber mat specimens (~15 mm in diameter) in a serum-free medium (SFM; containing DMEM, 1% L-

glutamine, 1% lactabumin, and 1% antibiotic and antimycotic formulation) for 1, 2, or 3 d in an incubator

at the extraction ratio of 20 mg/mL. L929 or HDFa (~40 000 cells/ well) were separately cultured in

wells of a 24-well tissue-culture polystyrene plate (TCPS; Biokom, Poland) in 10% serum-containing DMEM for 16 h to allow cell attachment onto the well surface. After starving the cells with SFM for 24 h, the medium was replaced with 0.5 mL of an extraction medium and the cells were reincubated for another 24 h. The viability of the cells cultured with each of the extraction media and the fresh SFM that had been preincubated for an equivalent time interval (i.e., control) was determined with 3-(4,5-dimethylthiazol-2-yl)-2,5-diphenyl-tetrazolium bromide (MTT) assay. The MTT assay is based on the reduction of the yellow tetrazolium salt to purple formazan crystals by dehydrogenase enzymes secreted from the mitochondria of metabolically active cells. The amount of formazan crystals is supposedly proportional to the number of viable cells. First, each specimen was incubated at 37 °C with 300 μ L/well of MTT solution at 0.5 mg mL-1, without phenol red. After 30 min of incubation, the MTT solution was removed. A buffer solution containing dimethylsulfoxide (DMSO; 900 μ L/well) and glycine buffer (pH 10; 125 μ L/well) was added into the wells to dissolve the formazan crystals. After 10 min of agitation, the solutions were measured for their absorbance at 540 nm, using a Thermospectronic Genesis10 UV-visible spectrophotometer.

In the cell attachment and the cell proliferation studies, only HDFa were used. Specimens (~15

mm in diameter) were placed in wells of a 24-well TCPS and subsequently sterilized in 70% ethanol for 1 h. The specimens, after having been washed successively with autoclaved deionized water and phosphate

saline solution (PBS), were immersed in DMEM overnight. A stainless steel ring (~12 mm in diameter)

was placed on top of each specimen to ensure its complete contact to the bottom of the well. HDFa

(~40,000 cells/well) were seeded on the fiber mat specimens and empty wells of TCPS (i.e., control) and

incubated at 37 °C in a humidified atmosphere containing 5% CO2. In the attachment study, the cells had been allowed to attach onto the substrates for 2, 4, or 18 h, prior to being quantified for their viability by the MTT assay. Prior to the measurement, each cell-plated specimen had to be rinsed with PBS to remove unattached cells. In the proliferation study, the cells had been allowed to attach onto the substrates for 16 h, prior to being quantified for their viability by the MTT assay on days 1, 2, and 3 after cell culturing. The morphology of the cells at some time points was observed by SEM. After removal of the culture medium, each cell-cultured specimen was rinsed twice with PBS and the cells were fixed with 3% glutaraldehyde solution [diluted from 50% glutaraldehyde solution (Sigma-Aldrich, USA) with PBS] at 500 μ L/well. After 30 min, the specimen was rinsed again with PBS and underwent dehydration with

ethanolic aqueous solutions of varying concentrations (i.e., 30, 50, 70, and 90 vol %) and pure ethanol for

~2 min each. It was then dried in hexamethyldisilazane (HMDS; Sigma-Aldrich, USA) for 5 min and

finally in air. The specimens were then observed by a JEOL JSM-5200 scanning electron microscope (SEM). The morphology of the cells that had been seeded or cultured on glass substrates (12 mm in diameter; Menzel, Germany) was used as positive control.

Protein Adsorption. Specimens (~15 mm in diameter) were placed in wells of a 24-well TCPS.

A stainless steel ring (~12 mm in diameter) was placed on top of each specimen to ensure its complete

contact to the bottom of the well. A solution of type I collagen in PBS (0.1 mg·mL $^-$ 1 for 0.5 mL) was then added to each well. After 2, 4, 24, 48, and 72 h of immersion, each specimen was thoroughly rinse with DI water to remove excess collagen. The amount of adsorbed collagen on each specimen was carried out by first immersing the specimen in 2 mL of 1% w/v sodium dodecyl sulfate (SDS) aqueous solution for 30 min. The concentration of the dissolved collagen was then quantified by BCA protein assay kit (Thermo Fisher Scientific, USA). Specifically, 25 μ L of each of the dissolved collagen sample solutions had been pipetted into a 96-well TCPS, before the BCA working solution of 200 μ L was added. The plate was sealed and incubated at 60 °C for 30 min. The absorbance measurements were taken at 562 nm at room temperature. The collagen concentration was calculated from a standard calibration curve (see Figure III in the Supporting Information).

Antioxidant Activity. The antioxidative activity of CA after it had been grafted onto the surfaces of the PLLA fiber mats was assessed by the DPPH assay. The procedure was carried out based on a

previously published method,14,26 with slight modification. Specifically, each specimen (~2.8 cm in

diameter) was dissolved in 10 mL of 7:3 v/v DCM/DMF solution. The sample solution was then diluted with 10 mL methanol. After that, 3 mL of an ethanolic solution of DPPH (100 μ M) was added into 1 mL of the sample solution. The mixture had been incubated at room temperature in darkness for 30 min, prior to being spectrophotometrically read at 517 nm. The neat fiber mat specimens were used as internal control and the amount of the immobilized CA participated in scavenging activity of the DPPH radical species could be quantified against a standard curve of CA (see Figure IV in the Supporting Information). The antioxidant activity (% AA) was then expressed as the percentage of the absorbance value of the DPPH radical species that was decreased in comparison with that of the control condition (i.e., the testing solution without the addition of the dissolved specimens), according to the following equation

$$\%AA = \frac{(A_{\text{control}} - A_{\text{sample}})}{A_{\text{control}}} \times 100 \tag{1}$$

where Acontrol and Asample represent the absorbance values of the blank and the sample solutions, respectively.

Statistical Analysis. All values were presented as the means \pm standard deviations. Statistical analysis between two data sets was performed using One-Way Analysis of Variance (ANOVA) and Scheffe's post hoc test in SPSS (SPSS, USA). The values of p lower than 0.05 were considered statistically significant.

RESULTS AND DISCUSSION

The purpose of chemical immobilization of CA onto the surfaces of the individual electrospun PLLA fibers is 2-fold. The first is to increase the hydrophilicity of the surfaces, as the hydroxyl moieties of CA are more hydrophilic than the ester linkages indigenous to PLLA. Second, it is aimed at impartingthe antioxidant activity to the modified PLLA fibrous matrices, as this activity is deemed important for an active wound dressing. According to the reaction schemes shown in Figures 1 and 2, the grafting of CA onto the surfaces of the individual electrospun PLLA fibers can be done in two sequential steps. In the first step, amino groups were covalently introduced onto the surfaces of the individual electrospun PLLA fibers through the reaction with HMD to obtain the aminolyzed PLLA fiber mats (a-ePLLA). Here, an amino moiety (-NH2) of HMD would react with an ester linkage (-COO-) of PLLA to from the amide linkage (-CONH-), whereas the other amino moiety would be left available for further reaction. In the second step, the CA-grafted PLLA fiber mats (CA-g-ePLLA) were obtained through the reaction between CA, the carboxylic acid moiety (-COOH) of which had been activated sequentially with EDC and NHS, and the other amino moiety of HMD, which had been introduced on the surfaces of the aePLLA in the first step.

Characterization of Neat and Modified PLLA Fibrous

Matrices. Quantification of Free Amino Groups. Quantification of the amino moieties that had been introduced on the surface of the a-ePLLA was evaluated with the ninhydrin assay. A number of factors would influence the amounts of the amino groups that would be introduced on the surface of the a-ePLLA. Some of these are the initial concentration of HMD, the reaction time, and the reaction temperature. Here, only the effects of the HMD concentration (see Table 1) and the reaction time (see Table 2) were studied.

Table 1. Surface Density of -NH₂ Groups on the a-ePLLA as a Function of HMD Concentration at a Fixed Reaction Time of 10 Min^a

HMD concentration (g mL-1)	surface density of -NH $_2$ (\times 10 $^{-7}$ mol cm $^{-2}$)
0.02	0.82 ± 0.06
0.04	1.20 ± 0.03
0.06	1.65 ± 0.05
0.08	1.96 ± 0.04

Table 2. Surface Density of $-{\rm NH_2}$ Groups on the a-ePLLA as a Function of Reaction Time at a Fixed HMD Concentration of 0.04 g ${\rm mL^{-1}}^a$

"The reaction temperature was fixed at 50 °C.

reaction time (min)	surface density of $-NH_2~(\times10^{-7}~mol~cm^{-2})$			
5	0.76 ± 0.04			
10	1.20 ± 0.03			
15	1.77 ± 0.07			
20	1.82 ± 0.06			
30	3.10 ± 0.04			
^a The reaction temperature was fixed at 50 °C.				

Within the investigated ranges of the HMD concentrations and the reaction times, the density of the amino groups was an increasing function of both independent parameters. Nevertheless, treating the neat

PLLA fibrous membranes at a high HMD concentration and/or a long reaction time would jeopardize both the physical and the mechanical integrity of the modified fibrous membranes. As the aminolytic condition becomes harsher (i.e., a result of the increased HMD concentration, increased reaction time, etc.), increasing numbers of ester linkages would be cleaved and the carboxylic acid chain ends would react with HMD, resulting in greater numbers of shorter PLLA chains and this occurs from the surface in. Here, the optimized aminolytic condition that resulted in the a-ePLLA that did not disintegrate while undergoing further reaction and/or evaluation is $0.04~{\rm g~mL}-1$ of HMD/IPA solution at $50~{\rm °C}$ for $10~{\rm min}$. At this condition, the surface density of the introduced amino groups was $0.120 \pm 0.003~{\rm \mu mol~cm}-2$.

Elemental Composition of Surfaces and Quantification of Immobilized CA. XPS was used to examine the chemical composition at the surfaces of the neat and the modified PLLA fibrous matrices. Quantitative analysis of the obtained results is shown in Table 3.

Table 3. Percentages of Area under the Peaks of High-Resolution C 1s, O 1s, and N 1s XPS Spectra, Including the Ratios of the Percentages of the Area under the Peaks O 1s/ C 1s, N 1S/C 1s, and N 1s/O 1s, of the Neat and the Modified PLLA Fibrous Matrices

	sample	C 1s	O 1s	N 1s	O 1s/C 1s	N 1s/C 1s	N 1s/O 1s
e)	PLLA	61.1	38.9	0	0.6367	0	0
a-	-ePLLA	64.4	34.8	0.8	0.5404	0.0125	0.0230
C	A-g-ePLLA	60.6	39.0	0.4	0.6436	0.0066	0.0103

As expected, no nitrogen-based moieties were observed on the surfaces of the neat PLLA fibrous membranes (i.e., the ePLLA). This was evidenced by the nonexistence of the N 1s spectra. In addition, the ratio between the surface oxygen atoms and the surface carbon atoms (i.e., O 1s/C 1s) was about 0.64. For the a-ePLLA, this ratio decreased to about 0.54 and, at the same time, surface nitrogen atoms could then be detected. This is because aminolysis introduced both the carbon and the nitrogen atoms on the fiber surfaces. For the CA-g-ePLLA, the O 1s/C 1s ratio increased again to about 0.64. This is because the grafting of CA introduced both the carbon and the oxygen atoms on the fiber surfaces. This resulted in the simultaneous decrease in the number of surface nitrogen atoms, as evidenced by the decrease in the N 1s/C 1s and the N 1s/O 1s ratios from those of the a-ePLLA. The surface density of the immobilized CA on the CA-gePLLA was quantified spectrophotometrically to be $6.2 \pm 0.2~\mu g$ cm-2 or $0.034 \pm 0.003~\mu mol$ cm-2 (based on the projection area of the specimens and note that Mw of CA = 180.16 g·mol-1) (n = 5). This implies that about 28% of the amino groups on the surface of the a-ePLLA participated in the immobilization reaction with CA. When calculated based on the actual weights of the specimens, the amount of the immobilized CA on the CA-g-ePLLA was $1.13 \pm 0.03~\mu g$ mg-1 or $0.0063 \pm 0.0006~\mu mol$ mg-1. To see whether the as-grafted CA could be released from the CA-g-ePLLA or not, a separate

experiment was carried out. Here, the CA-g-ePLLA specimens (~2.8 mm in diameter) were immersed in

PBS at 37 °C for periods of 1, 3, and 7 days. After each time point, a sample solution was withdrawn and spectrophotometrically read at 243 nm. The obtained results confirmed nonexistence of CA in the sample solutions. This clearly implies that there was no physical adsorption of CA on the surfaces of a-ePLLA and that the cleavage of the amide linkages could not occur in PBS.

Wettability and Morphology.

Static contact angles of water droplets on the surfaces of the neat and the modified PLLA fibrous membranes were used to assess the hydrophilicity of these surfaces. Such values for the neat PLLA

fibrous matrices were $104.8^{\circ} \pm 0.3^{\circ}$. The surfaces became much more hydrophilic after the aminolytic treatment in 0.04 g mL $^{-1}$ of HMD/IPA solution at 50 °C for 10 min (i.e., the water contact angles = $83.3^{\circ} \pm 0.4^{\circ}$). The hydrophilicity of the surfaces increased even more after CA having been grafted onto the surfaces of the a-ePLLA (i.e., the water contact angles = $55.5^{\circ} \pm 0.5^{\circ}$). The wettability of a surface depends not only on the chemical modification of the surface, but on the typographical nature of it as well. For an electrospun fibrous membrane, the wettability of its surface depends on the topography, the size, the arrangement,25 and the surface chemistry of the individual, underlying fibers.22 To ascertain that the increase in the hydrophilicity of the modified PLLA fibrous membranes over that of the neat ones was not due to any change in their surface topography, the morphology of the neat and the modified PLLA fibrous membranes was investigated (see Figure 3). Evidently, there is no obvious discrepancy in the morphology of the modified fibers from that of the neat ones, as the surface of all of these individual

fibers was smooth. Nonetheless, the diameters of the modified fibers (i.e., ~850 and ~920 nm on

average after the aminolysis and the grafting of CA, respectively) were generally greater than those of the

neat ones (i.e., ~620 nm on average). The increase in the electrospun fiber diameters after a surface

modification was also reported on electrospun poly(D,L-lactic acid) (PDLLA) fibers that had been grafted with chitosan.27 Recently, It has been demonstrated that an increase in the size of the individual fibers increased the hydrophobicity of the electrospun fibrous membranes.25 Thus, the increase in the hydrophilicity of the modified PLLA fibrous membranes over that of the neat materials was certainly not due to the change in the size of these individual fibers.

Mechanical Integrity.

The mechanical properties of the ePLLA and the CA-g-ePLLA were investigated. The stress at maximum load and the Young's modulus of the ePLLA were 3.6 ± 0.2 and 351 ± 5 MPa, respectively, whereas the strain at maximum load and the strain at break of the materials were 75.6 ± 4.6 and $87.7 \pm 4.6\%$, respectively. On the other hand, the stress at maximum load and the Young's modulus of the CA-g-ePLLA were 0.89 ± 0.29 and 154 ± 14 MPa, respectively, whereas the strain at maximum load and the strain at break of the materials were 2.2 ± 0.2 and $5.8 \pm 0.5\%$, respectively. Upon ePLLA surfaces, both the stiffness and the extensibility of the CA-g-ePLLA decreased significantly.

Biological Evaluation of Neat and Modified PLLA Fibrous Matrices.

Indirect Cytotoxicity Evaluation.

The potential for use of the neat and the modified PLLA fibrous membranes in biomedical applications was first assessed by the indirect cytotoxicity evaluation assay, using L929 and HDFa as reference cells. In the assessment, the extraction media were prepared by immersing each fiber mat sample in SFM for different periods of up to 3 days. The viability of the cells that had been cultured with each of these media, in comparison with that of the cells that had been cultured with the fresh SFM that had been preincubated for similar periods of time, for 1 day isshown in Figure 4. The viability of the cells that had been cultured with the fresh SFM that had been preincubated for 1 d was used as the basis to obtain the relative viabilities shown in the figure. For both cell types, the viability of the cells that had been cultured with the fresh SFM was found to decrease with an increase in the preincubation period, which may be due to the increase in the dissolved CO2 level upon the prolonged incubation. Notwithstanding, the viabilities

of either cell type were greater than \sim 80% on average. For L929 that had been cultured with the extraction media from both the neat and the modified PLLA fibrous matrices, the viabilities of the cells showed increasing trends, with the values ranging from \sim 92 to \sim 109% on average. For HDFa on the

other hand, decreasing trends were observed, with the values ranging from ~82 to ~95% on average.

Because the viabilities were greater than ~80%, the obtained results indicated nontoxicity of all of the

fibrous matrices, as none of the materials released substances in the levels that were detrimental to the cells.

Cell attachment and Cell Proliferation.

All of the fibrous matrices were evaluated further for their potential for use as wound dressing materials. For this, HDFa were directly seeded or cultured on their surfaces in order to assess the ability of the materials in supporting the attachment and the proliferation of the cells. The viabilities of the cells that had been grown on the surfaces of TCPS at 2 h after cell seeding (for the attachment assay) and on day 1 after cell culturing (for the proliferation assay) were used as the bases to obtain the relative viabilities shown in Figure 5.

For the attachment assay, the viability of the attached cells on the surface of TCPS at 4 h was lower than that at 2 h, whereas that of the attached cells at 16 h was greater. At any given time point, the viabilities of the attached cells on all of the fibrous matrices were lower than that on the control surface. At 2 and 4 h after cell seeding, the ability to support the attachment of the cells for a given type of the fibrous matrices was not of statistical difference. At 16 h, however, the viabilities of the cells attached on all types of the fibrous matrices increased tremendously to approach that of the cells that could adhere onto the control surface. Noticeably, the CA-g-ePLLA were better than the a-ePLLA in supporting the attachment of HDFa at any given time point. On day 1 after cell culturing, the viabilities of the cells on all of the fibrous matrices were still inferior to that of the cells on TCPS. Interestingly, the profiling of viabilities was similar to that observed at 16 h after cell seeding. This result could be interpreted that at least 24 h was

required for HDFa to completely adhere to these surfaces. Significant increase in the proliferation of the cultured cells on all types of the fibrous matrices was observed on days 2 and 3 after cell culturing. Though not statistically significant, the ability of the CA-g-ePLLA in supporting the proliferation of HDFa was better than that of the a-ePLLA, which in turn was better than that of the ePLLA. The inferiority of all of the fibrous matrices to TCPS in supporting the attachment of HDFa could be due to the lesser numbers of cells that were able to attach on the rougher and more hydrophobic surfaces of the fibrous matrices in comparison with the smoother and more hydrophilic surface of TCPS. Surfaces of different degrees of hydrophilicity (orhydrophobicity) would influence different types and amounts of proteins to adsorb. Even though a rough surface of the fibrous matrices possesses a greater specific surface area than asmoother surface of TCPS, the types and amounts of the proteins that are adsorbed on the smooth and hydrophilic surface of TCPS may mediate the adherence of the cells much better than do those adsorbed on the rough and hydrophobic surface of the fibrous matrices. The flat surface of TCPS also ensures that the adsorbed proteins are readily accessible to the cells. Unlike the flat surface of TCPS, only a limited part of the adsorbed proteins on the rough surface is accessible to the cells. Furthermore, the kinetics of the protein adsorption on the surfaces of different characters (i.e., different surface topographies, different effective surface areas, different surface wetting phenomena, etc.) play important roles in regulating the different time intervals for which the proteins require to adsorb in the amounts that are effective for mediating cellular behavior. Here, it is logical to hypothesize that a much longer time is needed for a much greater amount of proteins required to adsorb on the surfaces of the fibers to have a mediating effect to the cultured cells. Hence, on days 2 and 3, we see much greater increase in the proliferation of the cells grown on all types of the fibrous matrices and such an increase should be a result of the greater surface areas of the fibrous substrates. Among the three types of the fibrous matrices, the CA-g-ePLLA were the best in supporting the attachment and the proliferation of HDFa (i.e., based on the average values of the viabilities shown in Figure 5). Because the surface of the CA-g-ePLLA was more hydrophilic than those of the ePLLA and the a-ePLLA, the greater adsorption of proteins on their surface should be the main reason.

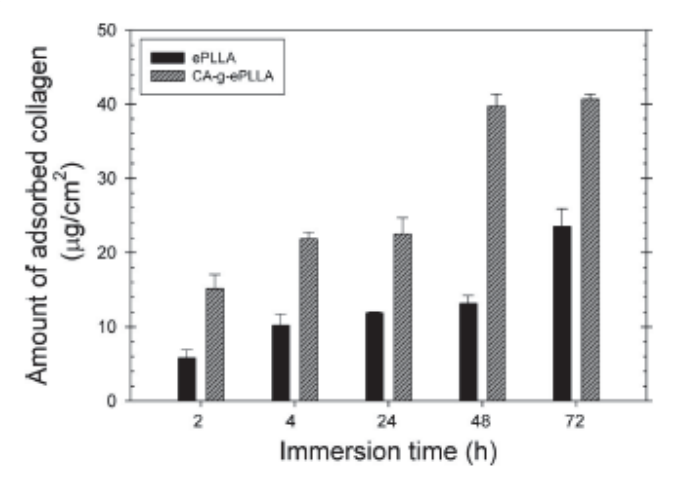


Figure 6. Areal amounts of type I collagen adsorbed on the surfaces of ePLLA and CA-g-ePLLA (i.e., the adsorbed amounts divided by the projection area of the specimens) at various immersion time points. All data sets at any given time point were significantly different (*p < 0.05).

Here, a separate experiment was carried out to quantify the amounts of a model protein that were able to adsorb onto the surfaces of the ePLLA and the CA-g-ePLLA. Type I collagen was used as the model protein. The amounts of the adsorbed proteins were reported at various immersion time points and the results are shown in Figure 6. Obviously, increasing the immersion time in the protein solution caused the amount of the absorbed protein to increase, except for the CA-g-ePLLA at 48 and 72

h that showed equivalent values (suggesting that the maximal adsorption was already reached at these time points). Regardless of the time points investigated, the adsorption of CA-g-ePLLA should be responsible for the greater amounts of type I collagen adsorbed on their surfaces.

Table 4. Representative SEM Images (magnification = $1500 \times$; scale bar = $10 \mu m$) of Cultured HDFa on Glass, ePLLA, a-ePLLA, and CA-g-ePLLA at Four Different Time Points after Cell Seeding or Cell Culturing

Cell Morphology.

The morphology of HDFa that had been seeded or cultured on the surfaces of the neat and the modified PLLA fibrous membranes was also investigated. Here, glass was used as the control substrate instead of TCPS because of the ease of taking the specimens for SEM observation. Representative SEM images are shown in Table 4. At 2 h after cell seeding, the majority of the cells on the glass surface was still round, while, at 4 h, the evidence of cytoplasmic process was already observed. The full cytoplasmic expansion of the cells on the glass substrate was realized after they had been cultured on the surface for 1 and 3 d. At 4 h after cell seeding, the majority of the cells on the surfaces of the ePLLA and the aePLLA was rather round, whereas that on the surface of the CA-g-ePLLA was more expanded. The full cytoplasmic expansion of the cells grown on these fibrous substrates was observed at 4 h after cel seeding, particularly for that of the cells grown on the CA-g-ePLLA. On day 1 after cell culturing, HDFa, in their fully expanded form, covered about 80% or more on the surfaces of all of the fibrous substrates. On day 3, the cell-covered areas were evidently increased, especially for that observed on the CA-g-ePLLA. The obtained results clearly confirmed the preference of HDFa toward the CA-g-ePLLA surface.

Antioxidant Activity of CA-g-ePLLA.

The antioxidant activity of the CA-g-ePLLA was determined by the DPPH assay. DPPH• is a stable free radical, exhibiting a characteristic UV absorption at 517 nm, and has been extensively used to evaluate the antioxidant activity of a variety of substances. 14,28–30 CA, which can act as a donor of an H-atom or electron in a similar manner to gallic acid, can transform DPPH• into its reduced form DPPH•-H.31 The antioxidant activity of CA, as the grafted species on the surface of the PLLA fibers, was determined to be

 $88.4 \pm 1.3\%$ (n = 5). The result confirmed that CA still retains its free radical scavenging ability, even though its mobility was limited because of its chemical immobilization onto the surface of the PLLA fibers. Interestingly, the amount of the as-grafted CA on the surfaces of the individual fibers of the CA-g-ePLLA that participated the scavenging activity of the DPPH radical species was determined to be $2.73 \pm 0.10 \ \mu g \cdot cm - 2$ (based on the projection area of the specimens) or $0.49 \pm 0.17 \ \mu g \ mg - 1$ (based on the actual weights of the specimens) or about 44% (based on the amount of the immobilized CA).

CONCLUSION

Electrospun PLLA fiber mats, with the average fiber diameter about 620 nm, were prepared from 10% w/v PLLA solution 7:3 v/v DCM/DMF. The surfaces of the individual PLLA fibers were successfully modified by CA via a two-step grafting procedure and the reactions were confirmed by the ninhydrin assay and XPS. Amino groups were introduced first on the fiber surface and the optimal condition was 0.04 g mL $^-$ 1 of HMD/ IPA solution at 50 °C for 10 min, resulting in the surface density of the introduced amino groups of (1.20 \pm 0.03) 10 $^-$ 7 mol cm $^-$ 2. After this step, the wettability of the fiber mat surface improved significantly, as the water contact angles reduced from those of the neat PLLA fiber mats (i.e., 104.8° 0.3°) to 83.3° \pm 0.4°. The wettability of the fiber mat surface improved even further after the chemical immobilization of CA (with the water contact angles being 55.5° \pm 0.5°). Such the

chemical modifications caused the fiber diameters to increase to ~850 and ~920 nm on average after the

aminolysis and the grafting of CA, respectively. In the indirect cytotoxicity assay, none of the fibrous materials released substances in the levels that were detrimental to the cells. In the direct cell culturing assay, all of the fibrous matrices showed very good support for the proliferation of HDFa on days 2 and 3 after cell culturing, with the CA-modified fibrous substrates being the best. Lastly, the antioxidant activity of the grafted CA moieties on the PLLA fibers was determined to be $88.4 \pm 1.3\%$.

13. Effect of the Surface Topography of Electrospun Poly(ϵ -caprolactone)/ Poly(3-hydroxybuterate-co-3-hydroxyvalerate) Fibrous Substrates on Cultured Bone Cell Behavior

Experimental part

1. Preparation of Fibrous Substrates.

Blend solutions of 50/50 w/w PCL/PHBV of varying concentrations ranging from 4 to 14 wt % were prepared in 80/20 v/v chloroform/DMF at roomtemperature (25 (1 C). PCL solution at 12 wt % was prepared in 50/50 v/v DCM/DMF at room temperature, and PHBV solution at 14 wt % was prepared in chloroform at 50 °C.

The electrospinning of these solutions was carried out using a typical method. Briefly, each of the solutions was contained in a glass syringe, the open end of which was connected to a gauge-20 stainless steel needle (o.d. = 0.91 mm), used as the nozzle. An aluminum (Al) sheet wrapped around a rotating

drum (width and o.d. of the drum ~15 cm; rotational speed ~50rpm)wasemployedasa collector. The

distance from the tip of the needle to the outer surface of the Al sheet was set at 10 cm. A Gamma High-Voltage Research D-ES30PN/M692 power supply was used to generate a high dc potential (i.e., 21 kV for the blend and PCL solutions and 12 kV for the PHBV solution). The emitting electrode (+) of the power supply was attached to the needle, and the grounding electrode was attached to the collector. A Kd

Scientific syringe pump was used to maintain the feed rate of the solution at ~1mL/h. The solutions were

electrospun consecutively for ~ 10 h.

2. Characterization.

The viscosities of the polymer solutions were measured by a Brookfield DVIII Ultra rheometer at room temperature and 20 rpm rotational speed of the spindle (n = 5).

The surface topographies and sizes of the individual fibers as well as those of the beads (in the case of the beaded fibers) of the obtained fibrous substrates were analyzed by a JEOL JSM-5410LV scanning electron microscope (SEM). For each sample, the sizes of the individual fibers (and beads, where

applicable) were measured from various positions of at least five different SEM images by SemAphore

4.0 software (n g50). Additionally, the thicknesses of the fibrous substrates were measured by a Mitutoyo digital micrometer (n = 5).

The chemical integrity of the obtained fibers was identified by a Nicolet NEXUS407 Fourier transform infrared spectrometer in attenuated total reflection mode (ATR-FTIR), at a resolution of 4 cm over a wavenumber range of 4000 to 400 cm⁻¹.

Static water contact angles of the obtained fibrous substrates were measured with a Kr€uss DSA 100 drop shape analysis system. Ten droplets of distilled water (10 µL) were placed randomly at different positions on each sample. The projected images of the droplets, after

they had been allowed to stay on the substrates until no further change in their shapes was observed, were analyzed for the contact angles, and the data were averaged.

The mechanical integrity, in terms of the tensile strength and Young's modulus, of the obtained fibrous substrates (rectangular shape, $10 \text{ mm} \ 100 \text{ mm}$) was assessed using a Lloyd LRX universal testing machine (gauge length = 50 mm and crosshead speed = 20 mm/min)(n = 5).

The true densities of the obtained fibrous substrates (ρ scaffold) were measured on \sim 1 g samples using a

Quantachrome Ultrapycnometer-1000 gas pycnometer (n = 5). On the basis of the obtained data, the porosities and pore volumes of the matrices can be calculated from the following expressions, respectively:

(1 - (pscaffold /ppolymer)) x 100 and (1/ pscaffold - 1/ppolymer), where pscaffold represents the bulk

density of the polymeric constituent(s). Here, ρ PCL, ρ PHBV ,and ρ PCL/PHBV(50/50 w/w), were taken as 1.145, 1.250, and 1.198 g.cm⁻³ respectively.

Cell Culturing. Mouse-calvaria-derived preosteoblastic cells (MC3T3E1; ATCC CRL-2593) were cultured in minimum essential medium with Earle's Balanced Salts (MEM; HyClone, USA), supplemented by 10% fetal bovine serum (FBS; Biochrom, U.K.), 1% L-glutamine (Invitrogen, USA), and a 1% antibiotic and antimycotic formulation (containing penicillin G sodium, streptomycin sulfate, and amphotericin B; Invitrogen, USA). The medium was replaced every other day, and the cultures were maintained at 37 °C in a humidified atmosphere containing 5% CO₂

. Fibrous substrate specimens (circular discs, ~15 mm in diameter) were placed in wells of a 24-well

tissue-culture polystyrene plate (TCPS; Corning, USA) and subsequently sterilized in 70% ethanol for 90 min. The specimens were then washed with autoclaved deionized water and then immersed in MEM

overnight. A metal ring (~12 mm in diameter) was placed on top of each specimen to ensure good contact

of the specimen with the bottom of each well.

MC3T3-E1 from the cultures were trypsinized (0.25% trypsin containing 1 mMethylenediaminetetraacetic

acid (EDTA); Invitrogen, USA), counted by a Hausser Scientific hemacytometer, and seeded at ~40 000

cells cm $^{-2}$ on each of the specimens and the empty wells of a TCPS (i.e., positive control). In the attachment and the proliferation studies, cells were cultured in the same media as mentioned above. For other studies, cells were cultured in MEM supplemented by 2% FBS, 1% L-glutamine, and 1% antibiotic and antimycotic during the first 3 days, after which they were cultured in the same medium but with the addition of an osteogenic supplement (i.e., 5 mM glycerol-2-phosphate disodium salt hydrate (β -glycerophosphate; Sigma-Aldrich, USA) and 50 μ g . L-ascorbic acid (Sigma-Aldrich, USA)).

Cell Attachment and Cell Proliferation. The cells were allowed to attach to the fibrous substrate specimens and empty wells of a TCPS for 2, 4, and 6 h in the attachment study (n = 4). At each time point, the number of attached cells was quantified by a 3-(4,5-dimethylthiazol-2-yl)2,5-diphenyl-tetrazolium bromide (MTT; Sigma-Aldrich, USA) assay. Additionally, the cells were first allowed to attach to the specimens and empty wells of a TCPS for 16 h and then were measured at 24 h. The number of proliferated cells was also determined by MTT assay on days 1, 2, and 3 after cell culturing (n = 4). The appearance of the cells during the attachment and proliferation periods was characterized by SEM (discussed later).

Quantification of Viable Cells (MTT Assay). MTT assay is a cell quantification method that measures the activity of mitochondria in their ability to reduce a tetrazolium-based compound, MTT, to a purplish formazan product. The amount of purplish formazan product is proportional to the number of viable cells. Each cell-cultured specimen was incubated at 37 C for 30 min with MTTsolution, and the formazan product was then dissolved in a mixture of dimethylsulfoxide (DMSO; Carlo Erba, Italy; 900 μ L/well) and glycine buffer (pH 10; 125 μ L/well). The absorbance of the supernatant was evaluated with a Thermospectronic Genesis10 UV visible spectrophotometer at 570 nm. The observed UV absorbance values were converted to the number of cells using predetermined standard calibration curves.

vol %) and in pure ethanol for ~2mineach.Itwasdriedin 100% haxamethyldisilazane (HMDS; Sigma-

Aldrich, USA) for 5 min and subsequently in air. The specimens were then observed by SEM, and the

morphology of the cells that had been cultured on glass substrates (12 mm in diameter; Menzel, Germany) was used as a positive control.

Alkaline Phosphatase (ALP) Analysis. MC3T3-E1 were cultured on the fibrous substrate specimens and the empty wells of a TCPS for 3 and 7 days to determine the ALP activity (n = 4). Each specimen, after the removal of the culture medium, was rinsed with PBS. Alkaline lysis buffer (10 mM Tris-HCl, 2 mM MgCl, 0.1% Triton-X 100, pH 10) (100 μ L/well) was added, and the specimen was scrapped, sonicated,

and then frozen at 20 Cfor~30 min. Anqueous solution of 2 mg/mL. p-nitrophenyl phosphate (PNPP;

Invitrogen, USA) mixed with 0.1 M aminopropanol (10 µL/well) in 2mMMgCl(100 µM/well) was added to the specimen, which washen incubated at 37 °C for 30 min. An aqueous solution of NaOH(50 nM at 0.9 mL/well) was added, and the extracted solution was measured spectrophotometrically at 410 nm. The amount of ALP was calculated against a predetermined standard curve and then normalized by the total protein content. For the protein assay, each specimen was treated in the same manner as in the ALP assay up to the point where it was frozen. A bicinchoninic acid (BCA; Pierce Biotechnology, USA) solution was then added to the specimen and incubated at 37 °C for 30 min. The absorbance of the medium solution was finally measured spectrophotometrically at 562 nm, and the amount of total proteins was calculated against a predetermined standard curve.

Mineralization Analysis. Calcium deposition was investigated by Alizarin Red-S (Sigma-Aldrich, USA) staining. MC3T3-E1 had been cultured on the fibrous substrate specimens and empty wells of a TCPS for 14 days (n = 4), after which the cells were fixed with cold methanol for 10 min, washed with deionized water, and immersed in 1% Alizarin Red-S solution in a mixture of 0.4 mL ammonium hydroxide/40 mL water for 3 min. Each stained specimen was washed several times with deionized water and air dried at room temperature. The stained specimen was photographed, and the redness, signifying the amount of

calcium deposition, was quantified by destaining with 10% cetylpyridinium chloride monohydrate (Sigma-Aldrich, USA) in 10 mM sodium phosphate at room temperature for 15 min and spectrophotometically read at 570 nm.

Statistical Analysis. All values were presented as means (standard deviations. The significance between two data sets was determined by one-way ANOVA analysis using the t test for all analyses, except for the attachment, proliferation, and ALP activity analytical studies. Scheffe's test was applied to the three studies. The statistical significance was accepted at a 0.05 confidence level.

RESULTS AND DISCUSSION

Characterization of Polymer Solutions and Fibrous Substrates.

As previously mentioned, the shear viscosity poses a strong influence on the morphology of the individual electrospun fibers.10 Prior to electrospinning, the PCL/PHBV solutions were measured for the shear viscosities (Table 1). As the total concentration of the blend solutions increased from 4 to 14 wt %,

the shear viscosity increased from \sim 290 to \sim 580 mPa 3 s. Electrospinning of these solutions was carried out under an electric field of 21 kV/10 cm. (See Figure 1 for the representative SEM images of the obtained products.) At 4 wt %, a combination of discrete beads (\sim 16 μ m on average) and smooth fibers

 $(\sim 0.4 \mu m \text{ on average})$ was obtained. At 6 and 8

wt %, a combination of beaded and smooth fibers was evident. At these concentrations, the sizes of the beads were in the range of $2.6_3.4$ µmon average and those of the fibers were in the range of $0.5_0.6$ µm on average. The densities of the beads that were observed on the electrospun products from 4 to 8 wt % PCL/ PHBV solutions were 1420, 3480, and 3020 beads 3mm_2, on average. Between 10 and 14 wt %,

only smooth fibers were generated. The size of these fibers increased from ~0.8 μm on average at 10 wt%

to~1.8 μmon average at 14 wt %. It should be

mentioned at this point that the blend composition of 50/50 w/w between PCL and PHBV was chosen on the basis of preliminary results, which showed that the fibers that had been obtained from other blend

compositions were very nonuniform (results not shown). This may arise from the immiscibility of the two polymers (later discussion). From these SEM images, the individual fibers in all of the fibrous substrates were randomly aligned, and they appeared to conglutinate to one another at touching points. Although the random alignment related directly to the slow rotational speed of the collection device used during fiber collection, the partial conglutination was due to the rather short collection distance and hence incomplete evaporation of the solvent from the jet segments during their flights to the collector.10 Electrospinning of the neat PCL and PHBV solutions was also carried out for comparison (Figure 1). The obtained fibers shared essentially the same features as those obtained from the 10_14 wt % PCL/PHBV solutions. The

sizes of these fibers were~1.0 and~2.2 μm on average, respectively. Upon consecutive spinning for ~10

h, the thicknesses of the blend fibrous substrates ranged between ~90 and ~110 μm on average whereas

those of the PCL and the PHBV counterparts were \sim 120 and \sim 90 μm on average, respectively. The actual

sizes of the fibers and beads, where applicable, are also summarized in Table 1. The chemical integrity of the PCL/PHBV fibers was investigated by ATR-FTIR (Figure 2).

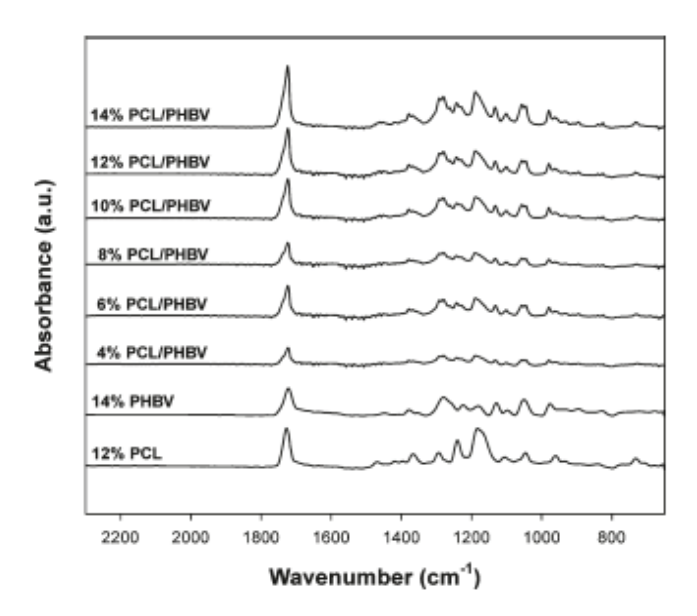


Figure 2. ATR-FTIR spectra of the obtained electrospun fibrous substrates.

Those of the neat PCL and PHBV counterparts are also shown for comparison. The absorption peak, centered at around 1724 cm_1 and belonging to the stretching vibrations associated with the crystalline conformations of the carbonyl ester (CdO),26 was evident in all of the IR spectra. For the blend fibers, the way in which this peak increased in its intensity with an increase in the total

concentration of the solutions is indicative of the increase in the total crystallinity. Referring to Figure 2, because all of the characteristic peaks of the neat polymers can be observed in the IR spectra of the blend fibers, the existence of both PCL and PHBV components within the blend fibers was confirmed. Furthermore, because no peak shifts or new absorption peaks were observed for the blend fibers, it is expected that specific interactions between PCL and PHBV molecules were inexistent. Qiu et al.27 showed that solvent-cast PCL/PHBV blend films exhibited distinctive and unchanged glass-transition and melting temperatures of either component, which is indicative of an immiscible polymer blend.

The physico-chemistry, in terms of static water contact angles, of all of the fibrous substrates was investigated (Table 1). When the size of the plated water droplet is much greater than that of the underlying fibers of a fibrous substrate, both the size and the topography of the underlying individual fibers play important roles in controlling the contact angle of the water droplet.28,29 For the beaded fibers, as the size of the beads decreased

(corresponding to the increase in the solution concentration), the water contact angle was found to increase, hence leading to a decrease in the wettability.28 As the beads disappeared completely (i.e., smooth fibers), a sudden decrease in the water contact angles and hence a sudden increase in the wettability was observed.28 For the smooth fibers, an increase in the sizes of the fibers was responsible for the observed increase in the water

contact angles and hence the decrease in the wettability.29

Here, as the total concentration of the PCL/PHBV solutions increased from 4 to 8 wt %, the average water

contact angle of the obtained beaded fibers decreased from ~ 121 to ~ 106 . A sharp drop in the average

water contact angle was observed when only the smooth fibers were the main products at 10 wt %, but as the concentration of the blend solutions increased from 10 to 14 wt %, the average water contact angle of

the obtained smooth fibersincreased again from ~85 to ~99_. Evidently, the wettability of the fibrous

substrate that had been obtained from the 10 wt %

blend solution was the greatest. On the basis of the SEM images of the PCL/PHBV fibrous substrates in Figure 1, it can be postulated that the smoother the surface of the fibrous substrates, the greater the wettability. For comparison, the average water contact angles of the PCL and PHBV fibrous substrates

were ~ 103 and ~ 115 _, respectively.

The mechanical integrity in terms of the tensile strength, Young's modulus, and elongation at break of the fibrous substrates is also investigated (Table 1). For the blend fibrous substrates, the tensile strength and

the elongation at break values were found to increase (i.e., from ~0.98 to ~1.95 MPa on average for the

tensile strength and from ~1.4 to ~4.9% on average for the elongation at break), whereas that of the

Young's modulus was found to decrease (i.e., from ~ 162 to ~ 103 MPa on average), with an increase in the total concentration of the PCL/PHBV solutions from 4 to 14 wt %. Interestingly, the neat PCL fibrous substrates exhibited the greatest values of the tensile strength and elongation at the break (i.e., ~ 2.41 MPa

and~5.7% on average, respectively,) and at the same time they had the

lowest value of the Young's modulus (i.e., ~82.4 MPa on average). The property values of the neat

PHBV fibrous substrates, on the other hand, were relatively moderate (Table 1). The true densities, porosities, and pore volumes of the obtained fibrous substrates were investigated (Table 2).

Table 2. True Densities, Porosities, and Pore Volumes of the Obtained Electrospun Fibrous Substrates

sample	true density, ρ_{scaffold} (× $10^{-2} \text{ g} \cdot \text{cm}^{-3}$)	porosity (%)	pore volume (cm³·g ⁻¹)
4% PCL/PHBV	2.30 ± 0.26	98.1 ± 0.5	42.6 ± 3.2
6% PCL/PHBV	2.61 ± 0.15	97.8 ± 0.3	33.2 ± 2.5
8% PCL/PHBV	2.86 ± 0.54	97.6 ± 0.7	34.1 ± 3.0
10% PCL/PHBV	3.19 ± 0.23	97.3 ± 0.4	30.5 ± 1.7
12% PCL/PHBV	3.57 ± 0.39	97.0 ± 0.7	27.2 ± 1.7
14% PCL/PHBV	3.93 ± 0.38	96.7 ± 0.6	24.6 ± 2.4
12% PCL	4.69 ± 0.11	95.9 ± 0.4	20.6 ± 2.1
14% PHBV	2.13 ± 0.17	98.3 ± 0.2	46.1 ± 2.6

For the blend fibrous substrates, the true density was found to increase (i.e., from $\sim 2.3 - 10_2$ to $\sim 3.9 - 10_2$ g 3 cm_3 on average), and those of the porosity and the pore volume were found to decrease (i.e.,

from ~98.1 to ~96.7% on average for the porosity and from ~42.6 to ~24.6 cm3 3 g_1 on average for

the pore volume), with an increase in the total concentration of the PCL/PHBV solutions from 4 to 14 wt %. The results imply that as the total concentration of the blend solutions increased the packing of the underlying fibers also increased. Among all of the fibrous substrates investigated, those made of PCL exhibited the lowest porosity and those made of PHBV were the greatest (Table 2).

Cell Attachment and Cell Proliferation.

Quantitative analysis for the adherence of MC3T3-E1 after having been seeded on the surfaces of TCPS and all types of fibrous substrates for 2, 4, and 6 h is shown in Figure 3. For any given type of substrate, the number of cells increased with an increase in the cell seeding time. At 2 h, the numbers of cells on the surfaces of almost all types of fibrous substrates, except for those of the substrates from 4 wt % PCL/PHBV and 14 wt % PHBV solutions that exhibited significantly lower values, were equivalent to that on TCPS. At 4 h, the numbers of cells on the surfaces of the fibrous substrates from 4, 10, and 12 wt % PCL/PHBV and 12 wt % PCL solutions were equivalent to that on TCPS. At 6 h, only the numbers of cells on the surfaces of the fibrous substrates from 10 and 12 wt % PCL/PHBV solutions were equivalent to that on TCPS. Among the various types of fibrous substrates, those from 10 and 12 wt % PCL/PHBV and 12 wt % PCL solutions, regardless of the cell seeding time, appeared to support the attachment of the investigated bone cells slightly better than did the others.

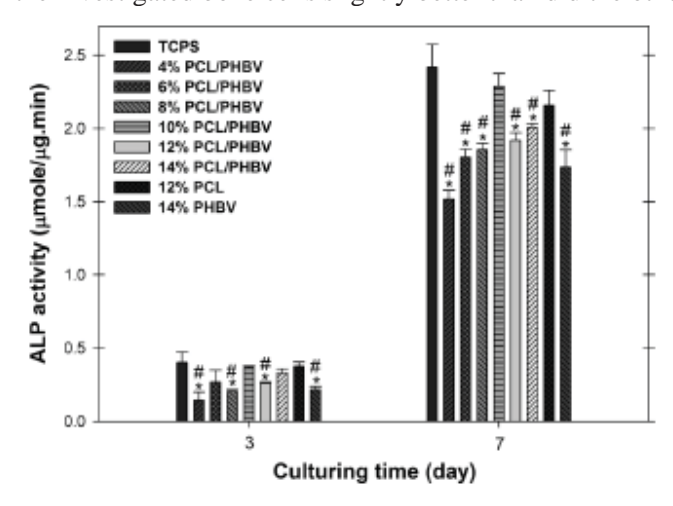


Figure 6. ALP activity of MC3T3-E1 that was cultured on the surfaces of TCPS and various types of fibrous substrates at various given time points after cell culturing, *Significance at p < 0.05 with respect to TCPS. *Significance at p < 0.05 with respect to the fibrous substrate from 12 wt % PCL solution.

A quantitative analysis of the proliferation of MC3T3-E1 after having been cultured on the surfaces of TCPS and all types of fibrous substrates for 1_3 days is shown in Figure 4. For any given type of substrate, the number of cells increased with an increase in the cell culturing time. On day 1, the numbers of cells on the surfaces of fibrous substrates from 6 to 12 wt % PCL/PHBV were equivalent to that on TCPS. On days 2 and 3, the numbers of cells on the surfaces of fibrous substrates from 6, 10, and 14 wt % PCL/PHBV and 12 wt % PCL solutions were equivalent to that on TCPS. Nevertheless, the average number of cells proliferated on the surface of the fibrous substrate from 10 wt % PCL/PHBV solution was greater than those on the surfaces of the other types of fibrous substrates. Particularly on day

3, the average number of cells on the surface of the fibrous substrate from 10 wt % PCL/PHBV solution was significantly greater than that of the fibrous substrate from 12 wt % PCL and slightly greater than that on TCPS.

Though not totally relevant, Kumbar et al.30 demonstrated that the biological response of human skin fibroblasts (hSF) that had been cultured on the surfaces of poly(lactic acid-co-glycolic acid) (PLAGA) fibrous substrates was, in many respects, fibersize- dependent. Specifically, the PLAGA fibrous substrates with the diameters of the underlying fibers ranging from 250 to 1200 nm showed significantly greater support for the proliferation and the expression of collagen III of the cultured hSF than the matrices with lower or larger fiber diameters. However, no particular trends were observed for the production of collagen I and elastin with the variation in fiber diameter.30 Khang et al.31 prepared poly(L-lactide-co-glycolide) (PLGA) films with chemogradient wettability by a corona treatment and found that fibroblasts adhered, spread, and grew particularly better onto positions with moderate

hydrophilicity (i.e., a water contact angle of \sim 55_). On the basis of these studies,30,31 both the size

of the underlying fibers and hence the wettability of a fibrous substrate should play important roles in mediating the cell behavior. Here, the mouse bone cells appeared to attach and proliferatewell on the surface of the fibrous substrate from 10 wt% PCL/PHBV solution, which exhibited the lowest water

contact angle of ~85_ on average.

Because the adsorption of proteins is influenced by the hydrophilicity/hydrophobicity of a surface, a surface with a certain water contact angle would favor the adsorption of certain proteins, which may or may not act as cellular mediators. Additionally, it is hypothesized that both the size and the topography of the underlying fibers of a fibrous substrate may directly influence the organization of organelles within the attached cells. Different organizations of the organelles may result in different chemosignaling pathways that directly influence the cell behavior. Although the effect of different surface topographies on the wettability, adsorption of proteins, and responses of the cultured bone cells should be a subject of thorough investigation, the effect of different organizations of organelles, in response to different surface topographies, on certain behaviors of the cultured bone cells can be rationalized from an existing published report.32 In an attempt to investigate the effect of fiber alignment on the responses of MG63 human osteosarcoma cells that had been cultured on the surfaces of randomly aligned and well-aligned poly(L-lactic acid) (PLLA) fibrous substrates, Wang et al.32 found that the cells on the well aligned fibrous substrate elongated their cytoplasms along the fiber axis but appeared to attach, proliferate, and differentiate better on the randomly aligned fibrous substrate. This exemplifies the importance of the surface topography of a scaffold in cellular behavior.

Selected SEM images illustrating the morphologies of MC3T3-E1 that had been cultured on the surfaces of glass and all types of fibrous substrates for various time intervals are shown in Figure 5. At 2 h after cell seeding, most of the cells on almost all types of the fibrous substrates were still round, except for those on the surfaces of the fibrous substrates from 6 wt%PCL/PHBV, 10 wt % PCL/PHBV, and 12 wt % PCL solutions that showed a slight expansion of their cytoplasms. At this time point, the cells on the control glass substrate were also still round, but a cytoplasmic process in the form of filopodia was clearly visible. At 4 and 6 h after cell seeding, the cells on all types of substrates became more expanded. Interestingly, the cells on the fibrous substrate from 14 wt % PHBV solution were very small, and because of the large size of the individual fibers, the cells appeared to elongate their cytoplasms along the fiber axis. On days 1 and 2 after cell culturing, the cells, in their expanded morphology, proliferated well

to cover~30 to~40% of the surfaces on almost all types of fibrous substrates. On day 3, full expansion of

the cells on all types of substrates was seen. Strikingly, most of the cells expansion was observed for the

cells on the fibrous substrate from 10 wt % PCL/PHBV solution, which proliferated to cover ~70% of the

surface. Noticeably, the cells on the fibrous substrate from 14 wt % PHBV solution grew in size but still exhibited the elongation of their cytoplasms along the fiber axis. On the basis of the results shown in Figure 5, the fibrous substrate from 10 wt % PCL/PHBV solution was clearly the best among the investigated fibrous substrates for supporting the growth of MC3T3-E1.

Alkaline Phosphatase (ALP) Activity.

The expression of ALP from MC3T3-E1 that had been cultured on TCPS and all types of fibrous substrates for 3 and 7 days is shown in Figure 6.On day 3, the ALP activities of the cells that had been grown on the surfaces of TCPS and the fibrous substrates from 6, 10, and 14 wt % PCL/ PHBV and 12 wt % PCL solutions were statistically the same, which appeared to be greater than that of cells on the rest of the fibrous substrates. On day 7, increases in the ALP activity from that observed on day 3 of the cells that had been grown on all types of substrates were evident. Strikingly, only the cells that had been grown on the surfaces of the fibrous substrates from 10 wt % PCL/PHBV and 12 wt % PCL solutions exhibited ALP activity at levels that are statistically equivalent to those that had been grown on TCPS, whereas the cells that had been grown on the surfaces of all other types of fibrous substrates had much lower values. Because ALP is usually secreted from normal bone cells during the early matrix formation and maturation period and is triggered by cellular contacts (when the cells reach confluence) and/or by the expression of ample amounts of early matrix proteins (e.g., type I collagen, fibronectin, and/or TGF-β1),4,33 it is logical to note that the fibrous substrates from 10 wt % PCL/PHBV and 12 wt % PCL solutions were both able to up-regulate the ALP production of MC3T3-E1much better than the rest of the fibrous substrates. Between the two types of the fibrous substrates, the one from 10 wt % PCL/PHBV solution was able to support the ALP production of the cells slightly better than the one from the 12 wt% PCL solution (on the basis of the average values of the obtained results).

Mineralization.

The ability to promote bone formation is the most important characteristic of a bone scaffold. Here, photographic images of Alizarin Red S staining of MC3T3-E1 that had been cultured on TCPS and all types of fibrous substrates for 14 days, along with their quantitative analyses, are shown in Figure 7. Because of the presence of calcium ions in the mineralized tissues, the staining product with Alizarin Red S appeared red. According to the obtained results, the cells that had been cultured on all types of the fibrous substrates stained positively for calcium deposition along with those that had been cultured on the fibrous substrate from 10 wt % PCL/PHBV solution exhibiting the greatest intensity, followed by those that had been cultured on the fibrous substrate from 12 wt % PCL solution. Interestingly, despite the high attachment, high proliferation, and high expression of ALP for the cells that had been grown on TCPS, mineralization of the cells on this control surface on day 14 was the lowest. All of the obtained results emphasize the importance of a thorough investigation for the efficacy of a bone scaffold because themineralization of the bone cells does not rely solely on the ability of the scaffold to promoting the attachment, the proliferation, and/ or the secretion of ALP of the cells. The obtained results also imply that both the topography (i.e., patterning and/or roughness) and the physicochemical characteristic (i.e., hydrophilicity/ hydrophobicity) of the surface of a scaffold are important factors in determining the

efficacy of the scaffolds. To this end, it should also be emphasized that before a scaffold that has been evaluated as positive for promoting infiltration, attachment, proliferation, and differentiation of the target cells in vitro can be used in vivo, it should also be tested for inflammatory reactions because it has recently been demonstrated that the in vitro inflammatory response of a scaffold by macrophages is also surface-topography-dependent.34

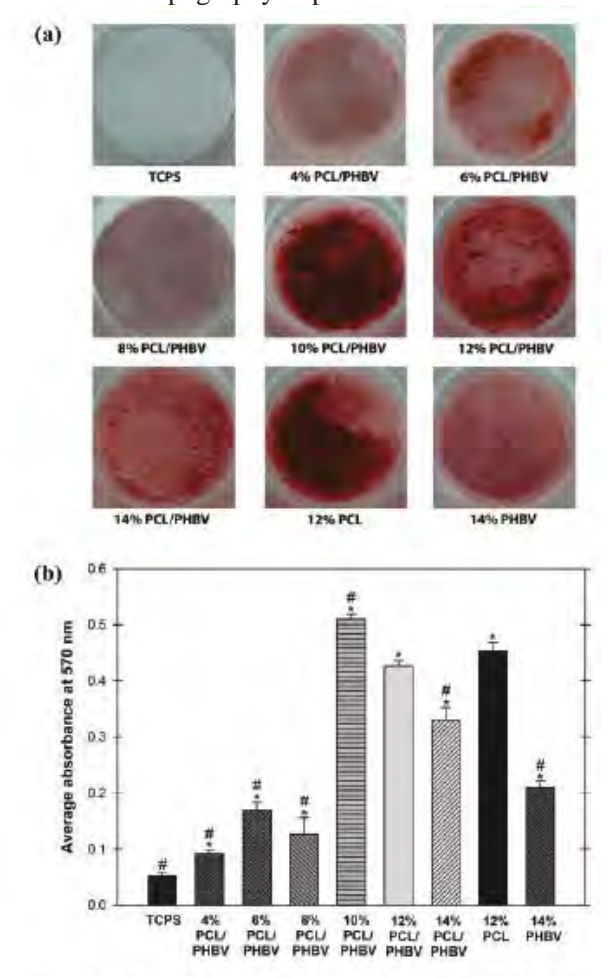


Figure 7. Alizarin Red S staining for the mineralization of MC3T3-E1 on day 14 after being cultured on the surfaces of TCPS and various types of fibrous substrates: (a) photographic images of the stained specimens and (b) the corresponding quantitative analyses. *Significance at p < 0.05 with respect to TCPS. *Significance at p < 0.05 with respect to the fibrous substrate from 12 wt % PCL solution.

CONCLUDING REMARKS

The fibrous substrates with different morphologies of the individual fibers were prepared from solutions of 50/50 w/w PCL/PHBV in 80/20 v/v chloroform/DMF by electrospinning. As the concentration of the solutions increased from 4 to 14 wt %, the topography of the individual fibers changed from discrete beads/smooth fibers to beaded fibers/smooth fibers and finally to smooth fibers, and the size of the

individual fibers increased from ~0.4 to ~1.8 μm on average. Among the various fibrous substrates, the

one prepared from 10 wt % PCL/PHBV solution exhibited the lowest static water contact angles of ~85_

on average. Likely because of the smoothness of the obtained fibrous substrate and the lowest water contact angles of its surface, the fibrous substrate from 10 wt % PCL/PHBV solution, with an average

fiber diameter of $\sim 0.8 \, \mu m$, was the best at promoting the attachment, proliferation, and differentiation

of the cultured mouse bone cells (MC3T3-E1). This type of fibrous matrix could be used as scaffolding substrates for calvarial defects.

14. Comparison of isolation techniques for bone marrow derived canine mesenchymal stem cells (MSCs) and the effects of MSCs loaded onto polycarpolactone hydroxyapatite scaffold on non-union bone healing

Materials and methods

All chemicals used in this study were purchased from Sigma Aldrich, St. Louis, USA, unless otherwise specified.

1 Collection and isolation of canine bone marrow derived mesenchymal stem cells

This study was approved by the Committee for the Ethical Care of Animals of the Chulalongkorn University. Seven mature dogs, mixed breeds, weighed between 10 to 15 kg were enrolled in this study. All dogs were physically examined and remained health entirely the experiment. Routine blood analysis was performed preoperatively. Acepromazine 0.02 mg/kg and morphine 0.5 mg/kg were administered intramuscularly, and the anesthesia was induced with propofol (Fresenius Kabi, Austria GmbH, Graz, Austria) and maintained with isoflurane in 100% oxygen. Cefazolin (25 mg/kg) was administered intravenously as prophylactic antibiotic. Epidural anesthesia using 0.5% bupivacaine (1 mg/kg) combined with morphine (0.1 mg/kg) was additionally performed to relief pain sensation caused by bone marrow aspiration procedure. Fifteen milliliters of bone marrow were harvested from the iliac crest of each dog with a heparinized syringe.

The bone marrow aspirate (15 ml) was equally divided into 3 aliquots, and each aliquot of 5 ml bone marrow was then submitted to one of the following isolation techniques: 1) direct plating, 2) red blood cell lysis treatment and 3) gradient density.

1.1 Direct plating

Direct plating was performed by adding bone marrow aspirate directly into a 10 cm Petri-dish (BD-FalconTM, Franklin Lake, NJ, USA) containing with 7 ml of MSC culture medium. After 24 of culture, the attached cells were washed with Dulbecco's phosphate buffered saline without calcium and magnesium (DPBS, Invitrogen, Carlsbad, CA, USA) for 2-3 times, and the fresh MSC medium was then added.

1.2 Red blood cell lysis treatment

Red blood cell lysis buffer (8.3 g/L ammonium chloride in 0.01 M Tris-HCl buffer, pH 7.5 \pm 0.2) was used to eliminate the contaminated red blood cells (RBC) in the bone marrow aspirate. The RBC lysis buffer was mixed at a ratio of 1: 1 with bone marrow aspirate and then incubated at room temperature (approximately 25-26°C) for 5 min. The mixture was then centrifuged at 1000 rpm for 5 min. After the supernatant was discarded, the pellet was resuspended with MSC medium, and the isolated cells were cultured in MSC culture medium. The non-attached cells were washed out in the following day.

1.3 Gradient density

Bone marrow aspirate (5 ml) was gently layered onto a histopaque® 1077 (density 1.077 ±0.001) in a 15 ml conical tube (BD-FalconTM, Franklin Lake, NJ, USA). The centrifugation was performed at 26°C and 400g for 30 min, and the interface containing mononuclear cells was then collected. The presumptive MSCs were washed with MSC culture medium for two times prior to culture.

2.2 Culture of bone marrow derived mesenchymal stem cells

Following MSC isolation (day 0) as previously described, the isolated cells were allowed to attach to the culture plate for 24 h prior to washing with DPBS. These cultured cells were assigned as primary cells at passage 0 (P₀). MSC culture medium was composed of a low-glucose Dulbecco's modified Eagle's medium (low glucose DMEM) supplemented with 10% (v/v) fetal bovine serum (FBS,

Invitrogen), 2 mM L-glutamine (Invitrogen, Carlsbad, USA), 100 unit/ml penicillin G, 100 μ g/ml streptomycin, 40μ g/ml gentamicin and 5 μ g/ml amphotericin B.

Subculture of MSCs was performed after treating the cells with 0.05% (w/v) trypsin-EDTA (Invitrogen). The disaggregated cells were then centrifuged and split into new Petri-dish at a ratio of 1:3. Putative MSCs at passages 3 (P₃) were used for flow cytometric analysis in order to examine the expression of cell-surface antigens and also for *in vitro* differentiation. In all cases, the culture condition was performed at 37°C in a humidified condition of 5 % CO₂ in air.

3 Assessing the characteristics of canine mesenchymal stem cells

3.1 Flow cytometry

The examination of MSCs was performed as essentially described by Tharasanit et al. (2011). Canine MSCs at the 3rd passages from a total of 5 dogs (Dog no. 1, 4, 6, 7 and 8) were immunologically examined for surface markers. These makers included the positive (CD 44, CD 90) and negative (CD 34) makers. The MSCs were first dissociated from the Petri dishes with Trypsin- EDTA and then centrifuged. A total of 200,000 to 300,000 cells were used for immunolabeling. Rat monoclonal anti-canine CD 90 (AbD serotec, Kidlington, UK) with rabbit anti-rat FITC secondary antibodies and monoclonal anti-canine CD44 antibody conjugated with allophycocyanin (APC) (R&D system, Minneapolis, USA) were used as MSC positive markers. A rat monoclonal anti-canine CD 34 antibody conjugated with fluorescein isothiocyanate (FITC) was used as the negative MSC marker. Fluorescently-labeled MSCs were washed and fixed with 1% (w/v) paraformaldehyde in PBS and stored at 4°C in the dark until analysis. Non-staining MSCs and MSCs labeled with only the secondary antibody were used as controls. At least 20,000 MSCs were analyzed by flow cytometry.

3.2 In vitro bone differentiation of MSCs

Canine bone marrow derived MSCs at passage 3 from four dogs were simultaneously induced to osteogenic lineage (each dog represented one replicate). Osteogenic differentiation was performed as essentially described by Bosch et al. (2006) with minor modifications. The MSCs were first cultured to

reach approximately 80% confluence, the osteogenic medium containing MSC medium supplemented with 0.1 μ M dexamethasone, 50 μ M ascorbic acid, 10 mM β -glycerophosphate (Merck, Darmstadt, Germany) was then added into the culture dish. The *in vitro* bone differentiation was performed for 21 days. Von Kossa staining was used to detect deposition of calcium phosphate indicating *de novo* bone formation.

3.3 Scaffold preparation and MSC transplantation

PCL/HA composite scaffolds were prepared as previously described ²⁸. The scaffold were cut into 10x5x25 millimeters and sterilized with 100% (v/v) absolute ethanol for 1 h. The scaffolds were washed thoroughly with sterilized distilled water and then DPBS to remove the ethanol.

Anesthesia and surgical procedures were performed as similar as previously described. Brachial plexus block using 0.5% bupivacaine (1.3 mg/kg) was additionally performed prior bilateral ulnar osteotomy to reduce pain. A total of 3 dogs were induced bilateral ulnar non-union (n=6) by cutting the mid-shaft of the ulnar bone (2.5 cm) using an oscillating saw. The osteotomized sites were implanted with the PCL/HA composite scaffold to improve bone stability. After the operation, all forelimbs were applied with modified Robert Jone bandages reinforced with thermoplastic splint (Vet-lite, Bangkok, Thailand). All dogs also received 5 mg/kg enrofloxacin (Bayer, Bangkok, Thailand) and 4 mg/kg carprofen (Pfizer, Bangkok, Thailand) orally for 7 days after implantation. All dogs demonstrated for bone non-union during 12 weeks after scaffold implantation. For transplantation, autologous MSCs were subcultured to passage 4 as previously described. After trypsinization, approximately 10x10⁶ cells/ml were loaded into a syringe containing with minimum volume (0.5 ml) of DMEM supplemented with 1% (v/v) FBS. Three MSC transplanted sites (proximal, middle and distal parts of the PCL/HA scaffold implant) were injected via a 23 G indwelling intravenous catheter with MSCs under a fluoroscope (Philips healthcare, Eindhoven, the Netherlands).

4 Examination of bone formation

4.1 Radiography

The lateral radiographs were taken immediately at 2, 4, 6, 8, 10 and 12 weeks post-operation in all dogs. Bone healing was evaluated using radiographic scoring system previously described ²⁹ as shown in

table 1. Bone union was justified grading from 0 to 3 at the proximal and distal of implanted material. In addition, the new bone formation was scored 0 to 4.

4.2 Angiography

Fluoroscopic angiography was performed in two experimental dogs at 12 weeks before MSC injection (dog no. 1, 2) and 16 weeks after MSC injection (dog no.1) in order to observe blood vessels at an implantation site. Anesthesia and surgical procedures were performed as previously described. The 23 G intravenous catheter connected with an extension tube was inserted into the axillary vein and the radiographic contrast medium (iohexol, Omnipaque®, G E healthcare, Buckinghamshire, UK) was slowly administrated in order to observe the presence of the blood vessel at the MSC transplanted site using fluoroscopy.

4.3 Histological examination of MSCs loaded scaffold

The biopsy was performed both before (n=2) and after MSC transplantation (n=2) at 12 and 20 weeks post-transplantation. The biopsy samples were fixed with 10% (v/v) buffered formalin, and the fixed samples were embedded in paraffin and processed following guideline for a routine histological procedure. The sections were stained with hematoxylin & eosin (H&E) and examined for neovascularization and bone formation under a light microscope. Occasionally, Masson's trichrome staining was additionally performed to detect the presence of collagen fibers.

3. Statistical analysis

Values are present as means ± standard deviation (SD). Efficacy for different MSC isolation techniques on the number of isolated MSCs, viability and expression of MSC markers were compared by one-way analysis of variance (ANOVA) and post-hoc analysis with the least significant difference (LSD). Angiographs and histological findings were descriptively analyzed. The differences in radiographic scores at 2, 4, 6 and 8 weeks post MSC transplantation were evaluated using Kruskal-Wallis one way analysis and Mann-Whitney U test. In all cases, statistical analysis was performed using SPSS statistical program (version 17.0). P values <0.05 were considered statistically significant.

Results

Following MSC isolation, putative MSCs were attached onto Petri-dish. These MSCs irrespective the MSC isolation techniques demonstrated a typical MSC morphology (figure 1 A-C). There were several cell types including thin spindle shaped, typical fibroblast-like, and mantle cells. On day 7 after MSC isolation, the total number of MSCs obtained from a 5-ml of bone marrow aspirate was ranged from 0.35×10^6 to 2.8×10^6 , 0.04×10^6 to $1.43\times$, 0.03×10^6 to 0.75×10^6 for gradient density, RBC lysis treatment and direct plating, respectively (Table 2). The gradient density techniques significantly increased the numbers of isolated MSCs when compared with direct plating technique (P<0.05), while cell yields obtained from this gradient density was efficiently comparable to RBC lysis treatment (P>0.05).

Cell-surface antigen profiles of canine MSCs was ascertained after immunolabeling with canine-specific/cross-reacted monoclonal antibodies and examined with a flow cytometer. Ranges and averages of percentage of cells positive for CD 44, CD 90 and CD34 are shown in table 2. Canine MSCs at passage 3 highly expressed CD 44 (95.66-99.89) and rarely expressed CD 34 in all cases (table 2). Furthermore, the cultured MSCs demonstrated to have capability to differentiate into osteogenic lineage as they positively stained with Von Kossa following osteogenic induction (figure 2).

Following MSC transplantation into non-union sites, all three dogs could walk properly within 24 hours after surgery. Neither radiological changes at scaffold-ulna interface nor callus formation was presented at the implant sites of PCL/HA alone (figure 3A) and PCL/HA combined with MSCs (figure 3B) at 2, 4, 6, 8 and 12 weeks post-operatively. The density of the implant grafts was comparable to soft tissue density. The radiographic scores was 0 in all cases.

Fluoroscopic angiography indicated the presence of blood vessels within the PCL/HA scaffolds at 12 weeks after implantation (figure 4A). These blood vessels descriptively appeared to increase when examined at 16 weeks after MSC injection (figure 4B). This result was in an accordance with histology of the host-PCL/HA transplanted sites that neovascularization was observed in PCL/HA both with and without MSC injection. However, no such osteoid formation was observed in the histological sections. The transplanted PCL/HA scaffolds was filled with loose and unorganized connective tissue (figure 5A) but the

thickness of the fibrous tissues and the number of small blood vessels were likely to increase at 20 weeks after MSCs injection (figure 5B). The fibrous tissue was mainly comprised of the spindle cells with extensive collagen deposition which was confirmed by Masson's trichrome staining (Figure 5B). Interestingly, we also found a number of multinucleated gaint cells and lymphocytes within the scaffolds indicating the inflammatory response.

Discussion

In the present study, we demonstrated that bone marrow derived canine MSCs could be enriched by treating the bone marrow aspirate prior to culture, and these harvested cells were highly expressed MSC markers (CD 44 and CD 90) and had a potential to differentiate into osteogenic lineage in vitro. However, the de novo bone formation following transplantation of the MSCs into PCL/HA scaffold was compromised.

Bone marrow was considered as a primary source of MSCs but only 0.001 to 0.01% of bone marrow mononuclear cells in rodents and felines were identified as MSCs ^{13, 14}. In addition, no consensus makers have been defined as conclusive markers for canine MSCs and thus the ability of cells that can adhere onto plastic Petri-dish is often used.³⁰ In the current study, we first examined the different techniques to enrich MSCs from bone marrow aspirate and found that gradient density significantly increased the numbers of isolated MSC on day 7 of culture when compared with direct plating technique (P<0.05, table 2). It had become clear that the presence of RBC in the culture dish negatively affected on the number of harvested MSCs probably because the RBC may compromise the MSCs to settle and adhere to the Petridish.³¹ In addition, excessive RBC lysis during culture may cause the release of free hemoglobin that can induce cellular stress and apoptosis ^{32, 33}. Although the efficacy of the gradient density was similar to that of RBC lysis treatment (P>0.05), the RBC lysis buffer treatment is preferable for clinical use since it requires less time-consuming and inexpensive. This technique may also be beneficial for initial growth of the isolated MSCs due to the platelet derived growth factor secreted from the remaining platelets following RBC lysis. ³⁰ In addition to the effect of isolation techniques on MSC derivation, the numbers of MSCs

isolated were considerably variable among donors, irrespective the isolation techniques used. This result was in an agreement to the facts that the number of bone marrow MSCs significantly decreases with increased age and poor health status ³⁴⁻³⁷, while the cells obtained from young donors grew more rapidly. ³⁸ However, there was no effect of isolation techniques on the expression of MSC makers (CD 40 and CD 90) and also in vitro differentiation, suggesting that MSC properties could be maintained using the current culture system. However, study on the effect of long term culture of these MSCs on MSC proliferation activity and also differentiation capability remains elusive. This aspect is important given that the large numbers of cells would be required for cell/tissue engineering. ⁶

To date, several attempts have been made on transplantation of MSC into long-bone defects. ^{3, 13, 39,} ⁴⁰ However, the de novo bone formation following transplant has been unsuccessful ¹³ especially in dog that has a slower bone turnover rate compared with mouse. 41 Furthermore, the injured bone site often becomes ischemic due to the excessive vascular destruction 42 A combination of osteopotential cell and biolodegradable scaffold is one of the most successful strategies in bone tissue engineering. Our previous data suggested that PLC/HA composite scaffold demonstrated as a promising approach for promoting new bone formation when transplanted to calvarial defect in mouse. ⁴³ In order to minimize the risk of ischemic lesion, we therefore first transplanted the PCL/HA scaffold to the large bone lesion allowing the neovascularization within the scaffold before MSC transplantation. After 12 week of PCL/HA scaffold transplant, no bone formation was found but the fluoroscopy indicated the neovascularization within the scaffold (figure 4A). However, no osteogenic differentiation was observed following MSC transplant into the vascularized scaffolds. From this result, it has become clear that implanted site of scaffold and species employed plays an important role for bone regeneration (i.e. cortical versus cancellous bone) 44. Furthermore, a large size and slow degradable PCL-HA scaffolds may also create an unfavorable environment for bone formation 45-47. In this study, several multinucleated giant cells in the PLC/HA scaffold indicated chronic reactions due to the foreign body response. Similar tissue reaction was previously reported. 48-50. Although the scaffolds used in this study were contaminated with copper (probably from hydroxyapatite ceramic) as we further we analyzed the scaffold using energy dispersive x-ray (SEM/EDX)

analysis (unpublished data), the failure for osteogenesis of transplanted MSCs in the scaffold was probably not caused by the cell cytotoxicity of the contaminated copper. There was a good evidence of fibrovascular tissue infiltration with an extent matrix deposition throughout the entire PCL/HA scaffold, and injection of MSCs into the scaffold seemed to increase the thickening size of the fibroblastic mass and vascularization (figure 5B). In fact, several factors are critical for bone tissue engineering, the main hallmark remains to be the sufficient osteogenic factors to stimulate de novo bone differentiation of the transplanted MSCs. Several growth factors and pathways have been demonstrated to be necessary for bone development. For example, bone morphologic protein-2 (BMP-2) increased osteocalcin release from MSCs promoting and healing response and induced chondrogenic and osteogenic differentiation of human bone marrow MSCs. And also promoted the new bone formation in femoral defects in rats and increased the local population of cells and the connective tissue progenitors in a canine femur defect model with the combination of MSCs. Section 15.

In conclusion, this study revealed that MSCs can be derived from bone marrow. These MSCs could further enrich by treating bone marrow aspirate with gradient density and red blood cell lysis treatment. Although these MSCs highly expressed the MSC markers and also retained the differentiation potentials, the bone differentiation following implantation was compromised. Further novel strategy in particular the combination of tissue engineering and osteogenic substances that can create a proper environment for de novo bone formation remain to be studied.

Table 1 Radiographic scoring system for evaluation of bone healing.³⁹

Score		Description
Bone formation	0	No new bone; graft approximates density of soft tissue
		Minimal new bone composed mostly of noncontiguous
	1	Areas of minimal density
	2	New bone present as mostly contiguous areas of normal

Density and fills approximately 50% of the defect

New bone present as mostly contiguous areas of normal

Density and fills approximately 51-95% of the defect

New bone a solid contiguous mass that fills > 95% of the defect

No contact between new bone and noninvolved adjacent normal bone

Partial bridge (< 50%) from new bone to adjacent normal bone

Partial bridge (> 50%) from new bone to adjacent normal bone

Complete bridge from new bone to adjacent normal bone

Table 2 Mean \pm SD (range) of total number of MSCs on day 7 and the proportion of MSCs (passage 3) positive to cell surface markers. The MSCs were isolated from bone marrow using three different techniques.

	Total cell number			
	$(x10^6)$	Cell surface markers		
	_	CD 44	CD 90	CD 34
Whole aspiration	0.26 ± 0.28^{a}	98.74+1.73	95.84+3.05	0.018+0.03
	(0.03-0.75)	(95.66-99.59)	(91.93-99.15)	(0-0.01)
RBC lysis treatment	$0.94 \pm 0.55^{a,b}$	99.28+0.82	93.48+10.76	0.014+0.03
	(0.04-1.43)	(99.18-99.89)	(74.3-99.21)	(0-0.06)
Gradient	1.08 ± 0.92^{b}	99.2+0.96	93.62+6.65	0.012 + 0.027
	(0.35-2.8)	(99.02-99.89)	(82.53-98.88)	(0-0.06)

Figure 1 Morphology of canine MSCs derived from bone marrow using direct plating (A), RBC lysis treatment (B) and gradient density (C).



Figure 2 An example of canine bone marrow MSCs that were induced to differentiate into osteogenic lineage as they were positive to Von Kossa staining

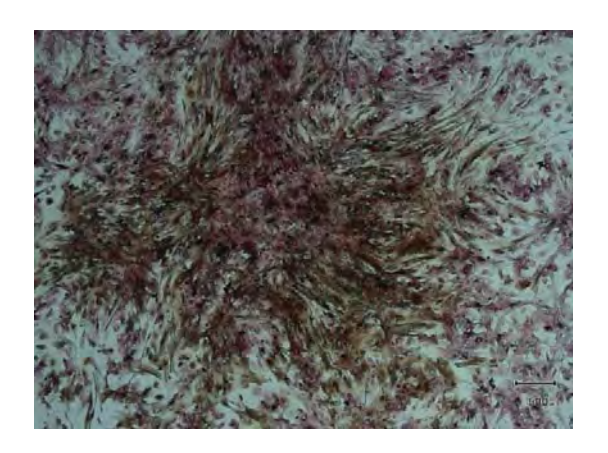


Figure 3 Radiographs demonstrating canine ulnar segment defect with PCL/HA alone (A) or PCL/HA combined with MSCs at 12 weeks (B) postoperatively. Note that no *de novo* bone formation was observed.

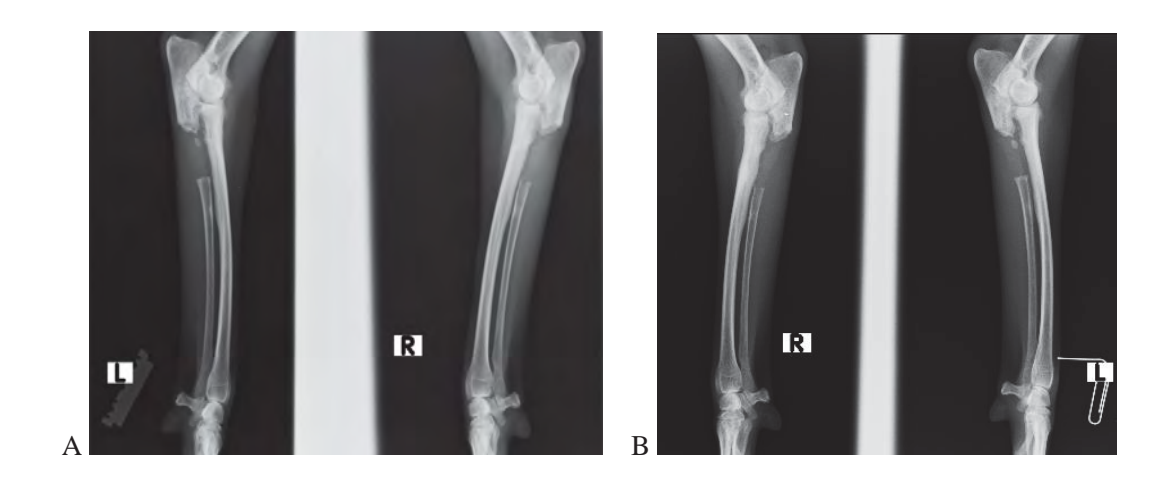
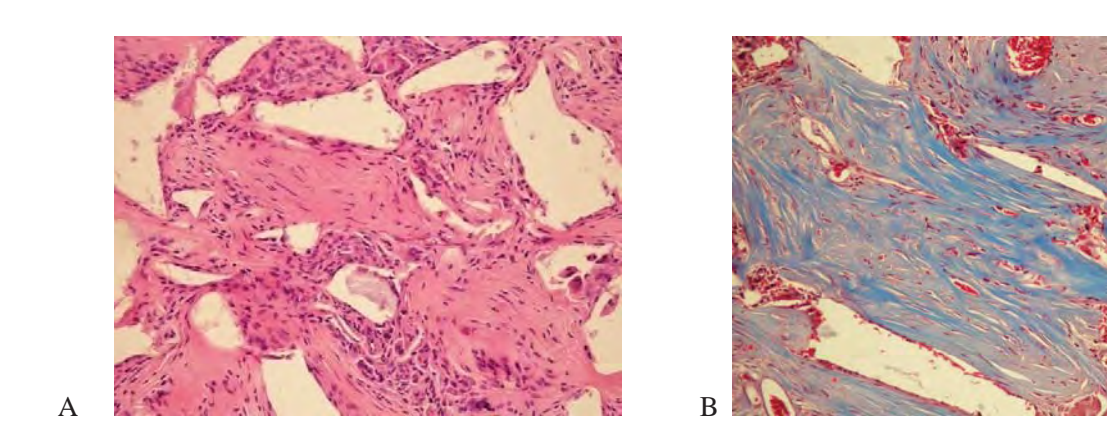


Figure 4 Fluoroscopic angiography at 12 weeks (A) after PCL/HA scaffold implant and at 16 weeks after MSC injection (B). The increased blood vessels were observed at the implantation site after BMSC injection.





Figure 5 Histology of PCL/HA implanted site at 12 weeks after surgery (A) and at 20 weeks after MSC injection (B) indicates the newly formation of capillaries and arterioles. Masson's trichrome staining (B) indicates that the thickening of fibrous tissue mainly constructed by an extensive collagen fibers.



15. The effects of mesenchymal stem cells combined with polycapolactone/hydroxyapatite composite scaffold on the healing of ulnar defect in dogs

Materials and Methods

All chemicals used in this study were purchased from Sigma Aldrich, St. Louis, USA, unless otherwise specified.

1 Scaffolds

PCL/HA composites scaffolds used in this study were prepared as previously described (Wutticharoenmongkol et al., 2006). Scaffolds were prepared from Polycaprolactone (PCL;

Aldrich, USA; $Mw = 80,000 \text{ g·mol}^{-1}$) incorporated with 40% w/w HA powder by solvent casting and particular leaching technique. Sucrose with diameter around 400–500 µm was used as the porogen to create the interconnected network. The scaffold porosity was in the range of 85-87%. PCL/HA composite scaffolds were cut into 5 x 5 x 5 mm and 10 x 5 x 25 mm for *in vitro* and *in vivo* studies, respectively. The scaffolds were sterilized with 100% (v/v) absolute ethanol for 1 hour and washed thoroughly with steriled distilled water and DPBS to remove residual ethanol. The scaffolds were preconditioned in culture medium for 2 hours prior to seeding procedure.

2 Animals

All protocols used in this study were approved by the Committee for the Ethical Care of Animals of the Chulalongkorn University. Seven mongrel dogs were enrolled in this study with various sexes (male=2, female=5), body weights were ranging from 12 to 16 kg. In each dog, a 2.5 cm bilateral ulnar ostectomy was performed to create critical sized defects. One dog had to undergo the second operation in order to get the total of 15 defect sites. Complete blood counts and blood chemical profiles were also examined prior surgery. Acepromazine maleate (0.02 mg/kg) (VetranquilTM, Ceva Sante animal, Libourne, France) combined with morphine sulphate (0.5 mg/kg) (Food and drug administration, Bangkok, Thailand) were used as the premedication drugs which administered intramuscularly. General anesthesia was induced with 4-6 mg/kg propofol (Fresenius Kabi Austria GmbH, Graz, Austria) intravenously and then maintained with an inhalation anesthesia using isoflurane in 100% oxygen via the rebreathing anesthetic circuit. Cefazolin (250 mg/ml) 25 mg/kg was administered intravenously as the prophylactic antibiotic. Additionally, brachial plexus nerve block using 0.5% bupivacaine (1 mg/kg) was performed to minimize pain sensation (Skarda and Tranquilli, 2007) that may occur during ulnar ostectomy.

3 MSCs isolation and culture expansion

The bone marrow contents (5-10 ml) from 4 dogs were collected using a 18 G needle connecting to a 5 ml heparinized syringe. To remove an excessive RBC, 5 ml of red blood cell lysing buffer (8.3 g/L ammonium chloride in 0.01 M Tris-HCl buffer pH 7.5 ± 0.2 ; Sigma-Aldrich, USA) was added into 5 ml aspirated bone marrow in a 15 ml sterile plastic tube (BD FalconTM, Becton Dickinson, Thailand). The solution was gently mixed followed by centrifugation at 1000 rpm for 5 minutes at 26 °C. The supernatant was discarded and the pellet was resuspended with 1 ml of MSC culture medium containing low-glucose Dulbecco's modified Eagle's medium (low glucose DMEM; Sigma, USA.) supplemented with 10% (v/v) fetal bovine serum (FBS) (Invitrogen, Carlsbad, USA), 2 mM L-glutamine, 100 unit/ml penicillin G, 100 μ g/ml streptomycin and 5 μ g/ml amphotericin B. Cells were plated in 100 mm tissue culture dish (BD FalconTM, Thailand) in 6 ml of culture medium. The initial seeding density was approximately between 50-60% confluences. The culture plate was gently mixed before incubated at 37°C in a humidified condition of 5% CO₂.

4 Characterization of canine mesenchymal stem cells

4.1 Flow cytometry

The examination of MSCs was performed as essentially described by Tharasanit et al. (2011). Canine MSCs at the 3rd passages from a total of 4 dogs were immunologically examined for surface markers. These makers included the positive (CD 44, CD 90) and negative (CD 34) makers. The MSCs were first dissociated from the Petri dishes with Trypsin- EDTA and then centrifuged. A total of 200,000 to 300,000 cells were used for immunolabeling. Rat monoclonal anti-canine CD 90 (AbD serotec, Kidlington, UK) with rabbit anti-rat FITC secondary antibodies and monoclonal anti-canine CD44 antibody conjugated with allophycocyanin (APC) (R&D system, Minneapolis, USA) were used as MSC positive markers. A rat monoclonal anti-canine CD

34 antibody conjugated with fluorescein isothiocyanate (FITC) was used as the negative MSC marker. Fluorescently-labeled MSCs were washed and fixed with 1% (w/v) paraformaldehyde in PBS and stored at 4°C in the dark until analysis. Non-staining MSCs and MSCs labeled with only the secondary antibody were used as controls. At least 20,000 MSCs were analyzed by flow cytometry.

4.2 *In vitro* bone differentiation of MSCs

Canine bone marrow derived MSCs at passage 3 from four dogs were simultaneously induced to osteogenic lineage (each dog represented one replicate). Osteogenic differentiation was performed as essentially described by Bosch et al. (2006) with minor modifications. The MSCs were first cultured to reach approximately 80% confluence, the osteogenic medium containing MSC medium supplemented with 0.1 μM dexamethasone, 50 μM ascorbic acid, 10 mM β-glycerophosphate (Merck, Darmstadt, Germany) was then added into the culture dish. The *in vitro* bone differentiation was performed for 21 days. Von Kossa staining was used to detect deposition of calcium phosphate indicating *de novo* bone formation.

5 In vitro assay for MSC and scaffold interaction

For *in vitro* study of biocompatibility of MSC and the scaffold, PCL/HA scaffolds were seeded with canine MSCs at a density of 100,000 cells/scaffold. The loaded scaffolds were incubated at 37°C in a humidified condition of 5% CO₂ in air After 45 min of incubation, a 5-ml of culture medium was added to cover the entire scaffold.

5.1 Scanning electron microscopy

Scanning electron microscope (SEM) was performed to illustrate MSC morphology and the ability to attach on the PCL/HA scaffold on day 1, 3 and 5 after seeding. Briefly, the loaded

PCL/HA scaffolds were washed twice with PBS (pH 7.2) and fixed with ice-cold 3% glutaraldehyde for 30 min. Then, the scaffolds were dehydrated with serial ethanol dilutions (30%, 50%, 70%, 90% and 100% (v/v) ethanol, respectively) for 2 min at each concentration. Finally, the scaffolds were soaked with Hexamethyldisilazane (HMDS) for 5 min and allow to air dried overnight at room temperature, so that HMDS was evaporated from the scaffolds before coating with gold. The SEM was performed using a JSM-5410LV scanning electron microscope (JEOL, Japan).

5.2 MSC viability and proliferative capacity

After 1 day of seeding, MSC-loaded scaffolds were cut into thin sections for evaluation of canine MSC viability. The viability assay was performed by dual fluorescent staining method using calcein AM and ethidium homodimer. A bright green fluorescence from calcein AM demonstrated the presence of active esterase enzyme activity while cell plasma membrane disrupted cells (dead cells) exhibited red fluorescent color. For MSC proliferation evaluation, PCL/HA scaffolds were seeded with canine at a density of 50,000 cells per scaffold. The proliferative capacity was qualitatively analyzed based on the serial fluorescent images of canine MSCs staining with 4', 6-diamidino-2-phenylindole dihydrochloride (DAPI; Roche, Germany) in conjunction with a quantitative analysis of the total protein content by the bicinchoninic acid (BCA) protein assay kit (Pierce Biotechnology, USA). For DAPI fluorescence staining, the loaded PCL/HA scaffolds were fixed at day 1, 2 and 4 of incubation with 3.7% formaldehyde. MSC loaded-PCL/HA scaffold were then stained with DAPI (1:1000) for 10 min and observed under Zeiss Axio Observer fluorescence microscope (Carl Zeiss, Germany) at a wavelength of 380 nm. The total protein quantification of MSC-loaded PCL/HA construct was determined on day 1, 3 and 5 after seeding. The BCA assay is a colorimetric detection and quantification of total protein in the

cell/scaffold construct by measuring the purple water-soluble product resulting from the chelation of BCA and Cu⁺¹. Briefly, the working solution was prepared by mixing Reagent A and reagent B in the ratio of 50:1. Then the loaded PCL/HA scaffolds were washed twice with PBS to eliminate the contaminated protein from the culture medium and chopped with a shaped scissors into small pieces before adding 200 µl of 2% sodium dodecly sulfate in a 1 ml of microcentrifuge tube. Mixed thoroughly by vortexing for 1 min and centrifuged at 5000 rpm for 1 min. A 50 µm of the supernatant was transferred into new 1 ml of microcentrifuge tube then added 1 ml of working solution, mixed thoroughly by vortexing, and incubated at 37°C for 30 min. Finally, 80 µl of the final solution was pipetted into a 24-well plate and measured the absorbance at 562 nm wavelength using an absorbance microplate reader (ELx800TM; Biotek, Vermont). All data were collected and analyzed by microplate data collection and analysis Software (Gen5TM; Biotek, Vermont) with the reference to bovine serum albumin.

Osteogenic differentiation of MSC within PCL/HA scaffold

The ability of canine MSCs to differentiate into an osteoblastic lineage on PCL/HA scaffold was investigated by seeding MSCs at a density of 50,000 cells onto the PCL/HA scaffold size 5 x 5 mm. The MSC loaded PCL/HA scaffold treated with the bone induction medium on day 3 of culture, and differentiation was confirmed by using Alizarin Red staining on day 14 of induction.

6 Effect of PCL/HA and MSCs on bone healing of critical- size ulnar defects

To perform bilateral ulnar ostectomy, dogs were anaesthetized as mentioned above. A 10 cm incision was made through the skin and subcutaneous tissue over the caudolateral aspect of the ulna. The bilateral 2.5 cm ulnar ostectomy was performed using an oscillating saw. No internal fixation was used in this study due to the canine model is mechanically stability without further fixation as the radius is the major load-bearing structure in the canine forelimb. In this study, defects on the left ulnae were implanted with the corticocancellous autografts to serve as a control group (n=7) while defects on the

right ulnae were randomly implanted with PCL/HA composite scaffold alone (n=4) or PCL/HA combined with canine MSCs (n=4). After the operation, all forelimbs were applied with modified Robert Jone bandages reinforced with thermoplastic splints (Vet-lite, BEC, Thailand) for 2 weeks. The dogs were received 5 mg/kg enrofloxacin (Baytril; Bayer, USA) and 4 mg/kg carprofen (Rimadly; Pfizer, USA) orally twice a day for 7 days after implantation.

6.1 Examination of bone healing by Radiographic examination

The craniocaudal (CrCd) radiographs were taken immediately after operation and at 2, 4, 6, 8 weeks postoperatively. Bone healing was evaluated and scored by 3 radiologists in a blinded fashion using the radiographic scoring system described by Jones et al. (2008) (Table 4)

6.2 histological analysis of PCL/HA scaffold implant

At the 8 weeks after implantation, biopsy was performed to verify the formation of bone following transplantation. The sites of biopsy included the middle portion of the implant and the host bone-implant interface. The sample was fixed in 10% (v/v) formalin and processed as a routine histological procedure as described elsewhere. The samples were sectioned and stained with hematoxylin and eosin (H&E).

Table 1 Radiographic scoring system for bone healing evaluation (Jones et al., 2008)

Description	Radiographic	
	score	
No change from immediate postoperative appearance	0	
A slight increase in radiodensity distinguishable from the graft	1	
Recognizable increase in radiodensity, bridging of one cortex with new bone	2	

formation to the graft	
Bridging of at least one cortex with material of nonuniform radiodensity, early	3
incorporation of the graft suggested by obscurity of graft borders	
Defect bridged on both medial and lateral sides with bone of uniform radiodensity,	4
cut ends of the cortex still visible, graft and new bone not easy to differentiate	
Same as grade 3, with at least one of four cortices obscured by new bone	5
Defect bridged by uniform new bone, cut ends of cortex no longer distinguishable,	6
graft no longer visible	

Statistical analysis

For total protein concentrations, Leven test was used to assess the homogeneity of variance among the groups and all data was analyzed using analysis of Variance (ANOVA) to determine the difference in protein concentrations between day 1, 3 and 5 after seeding. Significance was defined when a p value was less than 0.05.

For radiographic scores which were nonparametric data, Kruskal-Wallis one-way analysis of variance was used to determine the difference in healing efficacy of the implants at 2, 4, 6 and 8 weeks postoperatively. Significance was defined as a p value less than or equal to 0.05.

Result

At 24 hours after plating, adherent cells demonstrated heterogeneous morphology including a fibroblastic-like cell, polygonal cell and round cell. Non-adherent cells were removed by changing the culture medium and cells were distributed more homogeneous population of

spindle-shaped cells was mainly observed (Fig. 2). The total number of adherent cells on day 7 of culture was 1.327x10⁶ cells and the percentages viability was 98.64.

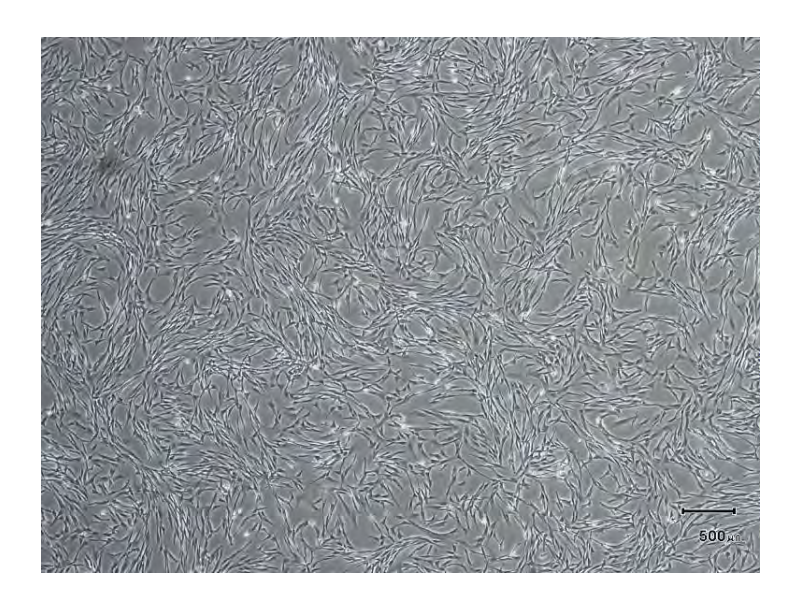


Figure 1 Canine bone marrow derived mesenchymal stem cells at passage 1 on day 3 of culture

(100 X magnification, 500 μm scale bar)

The percentage of cells positive for each CD was demonstrated in table 5. The percentage of CD 44 expressed by canine MSCs at passage 3 was more than 97% while the percentage of CD 90-positive cells was more than 93%. In addition, less than 1% of MSC population expressed CD 34.

Canine MSCs at passage 3 were subjected to demonstrate the mesenchymal differentiation capacity with the specific condition according to the cell type. Histochemical special staining was performed in order to verify each differentiation on day 21 after induction. Von Kossa, Oil Red O and Alcian blue staining were used to confirm osteoblastic, adipogenic and chondrogenic differentiation, respectively. Under an osteogenic condition (Figure 4), the former spindle-shaped

cells gradually transformed into polygonal, cuboidal, osteoblast-like cells extending their long processes connecting to each other to form a cellular network and started to synthesize the extracellular matrix that was positive to Von Kossa (Figure 5A) and Alizarin Red (Figure 5B). For adipogenic differentiation, thin fibroblastic cells became oval to round-shaped cells with large cytoplasm containing lipid vacuoles stained positively with Oil Red O (Figure 6). Finally, chondrogenic differentiation was achieved by culturing canine MSCs in a pellet cultural system combining with a special chondrogenic induction medium. MSCs were slowly aggregated and developed into a small round nodule within the first week of induction. The nodule was positively stained with Alcian blue indicated the presence of glycosaminoglycans at 3 weeks of induction.

Table 2 The percentage of canine MSCs positive for CD 44, CD 90 and CD 34 determined by flow cytometry at passage 3

			Markers	
Dog	Passage	CD34	CD44	CD90
Dog 1	3	0	99.82	99.21
Dog 2	3	0	99.89	98.02
Dog 3	3	0	99.95	93.52
Dog 4	3	0.06	97.91	96.92